Studies on the autophagy gene WIPI4 and its interactor UBR5

Ye Zhu

Supervisor: Prof. David C. Rubinsztein

Cambridge Institute for Medical Research

University of Cambridge

This thesis is submitted for the degree of

Doctor of Philosophy

Hughes Hall College

31/05/2019

Declaration

This thesis is the result of my own work and includes nothing which is the outcome of work done in collaboration except as declared in the Preface and specified in the text. It is not substantially the same as any that I have submitted, or, is being concurrently submitted for a degree or diploma or other qualification at the University of Cambridge or any other University or similar institution except as declared in the Preface and specified in the text. I further state that no substantial part of my thesis has already been submitted, or, is being concurrently submitted for any such degree, diploma or other qualification at the University of Cambridge or any other University or similar institution except as declared in the Preface and specified in the text. It does not exceed the prescribed word limit for the relevant Degree Committee.

Ye Zhu

31/05/2019

Abstract

Autophagy is a tightly regulated process that sequesters and delivers proteins and other cellular substances for degradation in the lysosome. Dysfunction of autophagy has been implicated in many diseases including neurodegenerative diseases, cancer, and infectious diseases. Beta-propeller Protein-Associated Neurodegeneration (BPAN), an early-onset neurodegenerative disease, is caused by mutations in WIPI4, a member of the WD repeat domain phosphoinositide-interacting family. This thesis identifies WIPI4 as a regulator of the closure of autophagosomes. Although many proteins have been found to regulate the late stage of autophagosome formation, the exact mechanism of this process has remained unclear. This thesis explored the regulatory mechanism of GABARAP by WIPI4. GABARAP is a potential closure regulator and is also required for expansion and fusion steps of autophagy. I identified that WIPI4 regulates the stability and trafficking of GABARAP. Further studies identified UBR5, an N-recognin, to be a potential GABARAP-targeting E3 ligase. In WIPI4 depleted HeLa cells, there is an increased interaction between UBR5 and GABARAP. The negative regulatory activity of UBR5 on GABARAP is dependent on its E3 ligase activity. In addition, mutation of the N-degron of GABARAP reduces its ubiquitination by K48-linked chains, suggesting that GABARAP may be an N-end rule pathway substrate. Altogether, this thesis furthers our understanding of the mechanism of autophagosome closure and identifies a potential novel GABARAP E3 ligase.

Thesis title: studies on the autophagy gene WIPI4 and its interactor UBR5

Author: Ye ZHU

Acknowledgements

I would like to thank my supervisor Prof. David Rubinsztein for giving me this great opportunity to join his lab and his tremendous support during the time I am here. David always makes time to give inputs for my project, despite of his tight working schedule. He is very concerned about any difficulties I have met during research and in my life in Cambridge. His positive and cheerful attitude has also made the lab a collaborative and fun environment. I will always be grateful that I have a supervisor who believes in my potential, has stimulated my intrinsic curiosity in science, and has taught me lifelong skills that will prove helpful in a future career in the field.

Dr. Victoria Barratt has improved this thesis significantly. She is impressively detail-oriented and is very professional in scientific writing. She read through this thesis many times and changed many expressions to bring it to this quality. She helped me not only with the writing but also with many experiments including aggregate counting which requires a lot of effort. I appreciate very much her help. Otherwise there will not be this thesis.

Dr. Maria Jimenez-Sanchez and Dr. Maurizio Renna are both great mentors. They have taught me valuable techniques and spent huge amount of time to help me tackle the challenges I encountered. I will always remember that Maria spent hours in the microscopy room to help me with live imaging and designed the layout of figures in my first year report presentation. And I will not forget the recipes Maurizio wrote for me on sticky notes. Both of them are extremely professional and care a lot about my well-being. Expressing my gratitude in this paragraph is not enough at all.

Claudia and Mariella provided great suggestions in the student meetings. Claudia is very generous in sharing her magical tricks to help me improve the protocols. She is a very enthusiastic scientist and has motived me a lot. Mariella has given me many sensible and practical suggestions and always come up with ideas from new perspectives. I also want to thank Farah for helping me with the purification of recombinant proteins using ultracentrifuge.

Yoshi and Son have always been nice and willing to answer even the simplest questions I asked them. I will always remember the many long and stimulating discussions with Yoshi and the gifts from Japan. Sandra has helped me with the protocol of the *in vitro* ubiquitination assay and proofread my thesis with great patience. She is also a cake master which I knew from the cake she baked for my birthday. Her effort in making coffee everyday provide one more communication time for the lab.

It is lucky to have Gautam and Alvin as bench neighbours. Alvin is never reproachful for me swamping over on his bench and ‘borrow’ his reagents. Gautam is of great sense of humour and is extremely patient when I need a talk, no matter it is about science or latest news. Laura is very reliable when I ask for help about my writing. And I enjoy listening to her sharing latest news both inside and outside the scientific field. Cansu is of great talent at numerous things and I learned from her a lot of useful information. I also enjoy the Bap with Swati and Ryan in Hughes Hall. Ryan knows well how to enlighten people’s life, for example decorating the desk with Christmas lights and geek jokes. Coffee time with Huijung and Soyeng has made science weekends more efficient and enjoyable.

Ting is very strategic and smart, she is my first role model in Cambridge. Mariana is extremely talented and self-disciplined. I spent the first two years of my PhD with their companion and I still miss that time. Maarten is a biologist and a programmer. He taught me how to quantify vesicles in batch using Fiji programming language. I also want to thank Becca for the Indian food and cake recipes, Anne for offering scientific suggestions, Marcus for Cantonese, Silvia for the great dinner she made for us. And thanks to Luke, every Tuesday there was ‘student cake and tea’.

My PhD time in this lab is one of the most fun and rewarding time during my life. No words can express how grateful I am to the great people I knew during this experience. Also, thanks to Ge Yin, my parents, and my grandpa. I would not have made it that far without your love.

Contents

Index

Diagrams

Figures

Tables

Chapter 1 Introduction

The fact that intracellular proteins are turning over was only discovered following the usage of radioactive isotopes for labelling organic compounds in the 1940s (Rittenberg et al., 1939) and has changed the paradigm that regulation of cellular processes occurs mostly at the transcriptional and translational level. With the discovery of the lysosome (Duve 1953) and later the ubiquitin-proteasome system (Hershko 1980), protein degradation is found to be tightly regulated for the following purposes: providing the cell with amino acids and energy for the synthesis of new proteins, clearance of damaged or misfolded proteins and termination of signalling pathways that are no longer functioning at the proper level.

1.1 Lysosomal pathways

The lysosomal/vacuolar system is a discontinuous membrane system that digests both endocytosed receptor-ligand complexes and phagocytosed extracellular contents, as well as cytoplasmic proteins and organelles (autophagy). The digestive process involves maturation from early endosomes to the acidic lysosomes containing hydrolytic enzymes; or from early phagophores to autolysosomes. The two sub-routes overlap at multiple steps, such as microautophagy and amphisome formation in macroautophagy.

Autophagy refers to a series of tightly modulated processes that sequester and deliver proteins and other cellular constituents to the lysosome for degradation. It was first found to be important in protein catabolism during starvation, when autophagic degradation promotes the recycling of cellular nutrients, thereby enabling cell survival. It is now well-recognized that basal autophagy in nutrient-rich conditions is also involved in maintaining cellular homeostasis. This quality control by the degradation of damaged and dysfunctional proteins and organelles is particularly crucial in post-mitotic tissues, like neurons and muscle, where the cells are protected by autophagy from the toxic effects of dysfunctional proteins that cannot be diluted via cell division. Autophagy is required for the elimination of malfunctioning organelles and proteins. Thus, it is required for the proper functioning of cells. Dysfunction of

autophagy has been found in many diseases, including neurodegeneration diseases, cancer, and ageing (reviewed in Frake et al., 2015). There are three types of autophagy: macroautophagy, microautophagy and chaperone-mediated autophagy (CMA).

1.1.1 Macroautophagy

Macroautophagy (hereafter as autophagy) involves the formation of a bowl-shaped isolation membrane that grows and engulfs the cargo. Eventually, the rims of the bowl meet and seal. The sealed autophagosome loses all autophagy-related genes (ATGs) on the surface except for ATG8[1] family proteins. It then fuses with a lysosome to form an 'autolysosome' and degrade the substrate inside. The canonical autophagy can be broadly classified into initiation, nucleation, expansion, closure and fusion. Each step is tightly regulated to respond to various stimuli (Ravikumar 2009).

1.1.1.1 Autophagy initiation

1.1.1.1.1 ULK1/2 complex

The ULK1/2 complex is one of the most upstream elements in the machinery and acts as a signalling node for several signalling pathways that induce macroautophagy. It consists of UNC51-like kinase 1 (ULK1), or its homologue UNC51-like kinase 2 (ULK2) together with Autophagy-related 13 protein (ATG13), 200 kDa FAK Family Kinase-Interacting Protein (FIP200) and Autophagy-related 101 protein (ATG101) (Hara et al., 2008). As a serine/ threonine-specific kinase, the active ULK1 complex then phosphorylates beclin1 (BECN1) in mammalian cells, a regulatory subunit of phosphatidylinositol 3-kinase class 3 (PI3KC3, VPS34) complex, the next complex in the cascade. It also phosphorylates FIP200 and ATG13, which additively enhance the kinase activity of ULK1, including its autophosphorylation capabilities (Ganley et al., 2009). In addition, active ULK1 phosphorylates ATG14, vacuolar protein sorting 34 (VPS34), ATG101 (Hosokawa et al., 2009; Wold et al., 2016), which helps with recruitment of the VPS34 complex at the autophagosome formation site.

1: Nomenclature for yeast, worm and mammalian autophagy genes: all letters of mammalian protein symbols are in upper-case, same with their gene symbols but italic; only the first letter of yeast protein symbols is in upper-case and all the others in lower-case, same with their gene symbols but italic; all letters of worm protein symbols are in upper-case, but their gene symbols should be italic and all in lower-case. And there is a hyphen between the alphabets and the number for autophagy proteins and genes in *C. elegans*.

The interaction between ULK1 and ATG13 depends on their phosphorylation status, which is regulated by kinases like the mechanistic target of rapamycin (mTOR) and AMP-activated protein kinase (AMPK) (Ganley et al., 2009). The phosphorylation of ATG13 and ULK1 by mTOR under nutrient-rich conditions hinders the interaction between ULK1 and ATG13, thereby inactivating the complex. GABARAP loss of function decreased ATG13-pSer318 levels, suggesting an attenuation of ULK1 kinase activity (Joachim et al., 2015). GABARAP interacts with ULK1 independent of lipidation but dependent on the LIR domain.

1.1.1.1.2 Upstream signalling

mTOR

mTOR (mammalian/mechanistic target of rapamycin) is a 289 kDa serine-threonine kinase controlling growth and metabolism in response to nutrient and energy cues (reviewed in Laplante and Sabatini, 2012). It exists as the catalytic unit of two multimeric complexes, mTORC1 and mTORC2 (Jacinto et al., 2004). Both mTORC1 and mTORC2 also contain mLST8 (mammalian lethal with Sec13 protein 8, also known as GβL) and an inihibitory subunit DEPTOR (DEP domain-containing mTOR interacting protein) (Peterson et al. 2009). mTORC1 also contains RAPTOR (regulatory protein associated with mTOR), which recruits substrates and is required for the subcellular localization of mTORC1 (Saxton et al., 2017).

mTORC1 mediates inhibitory phosphorylation of ULK1, ATG13 (Hosokawa et al., 2009), transcription factor TFEB and other autophagy genes under nutrient-sufficient conditions. mTORC1 regulates cell growth and proliferation by phosphorylation of 4E-binding protein 1 (4EBP1) and ribosomal protein S6 kinase polypeptide 1 (S6K) (Guertin and Sabatini, 2007).

The mTORC1 complex reacts to signals like growth factors, genotoxic stress, energy status, oxygen availability and amino acid availability (reviewed in Laplante and Sabatini, 2012). Amino acid starvation leads to the inactivation of mTORC1, which lifts the inhibitory phosphorylation of ULK1, allowing downstream macroautophagy to proceed. Also, TFEB is no longer phosphorylated when mTORC1 is inhibited, and can translocate from cytoplasm to the nucleus, where it promotes the transcription of genes involved in macroautophagy and lysosome biogenesis.

The activity of mTORC1 is upregulated by the Leucine metabolite acetyl-coenzyme A (AcCoA) through the EP300-mediated acetylation of RAPTOR at K1097 (Son et al., 2019). mTORC1 is sensitive to rapamycin (Hara et al., 2002). Rapamycin is an anti-fungal macrolide produced by

the bacterial species *Streptomyces hygroscopicus*. Rapamycin binds to FKBP12, and this complex then binds to mTOR to narrow the catalytic cleft and partially occlude substrates from the active site (Yang et al., 2013).

mTORC2 is primarily involved in the regulation of the cytoskeleton and also regulates autophagy through the PKCα/ β-actin cascade (Renna et al., 2013). The main difference relative to the mTORC1 complex is the replacement of RAPTOR by RICTOR (rapamycin insensitive companion of mTOR), and mTORC2 is insensitive to acute rapamycin treatment.

AMPK

AMPK activates autophagy at three levels. It detects the energy levels in cells and inhibits mTORC1 complex via TSC2 and Raptor in response to decreasing ATP to AMP ratios, such as in glucose starvation (Inoki et al., 2002). In the same conditions, AMPK also directly catalyzes activating phosphorylation events on ULK1 by binding to S757, a site also subject to inhibitory phosphorylation by mTORC1 (Lee et al., 2010). ULK1 phosphorylation sites have also been identified at either S467 and S555 (Egan et al., 2011) or S317 and S777 (Kim et al., 2011). Phosphorylation at these sites upregulates the kinase activity of ULK1. Inhibition of AMPK-mediated phosphorylation of ULK1 has negative implications on bulk macroautophagy. AMPK also stimulates autophagy by phosphorylating BECN1 of the VPS34 complex (Russell et al., 2013).

mTOR independent pathways

Trehalose stimulates clearance of autophagy substrates, including mutant Huntingtin and the A30P and A53T mutants of α-synuclein, by blocking cellular glucose import through inhibition of SLC2A (also known as GLUT) transporters (Mardones & Rubinsztein et al., 2016). Another mechanism of mTOR independent autophagy regulation is via intracellular calcium (Ca^{2+}) levels. Ca^{2+} has been shown to control various stages of autophagic flux (reviewed in Bootman et al., 2018). However, there is no consensus about whether cytosolic Ca^{2+} signals trigger or inhibit autophagy. Different Ca^{2+} channels and Ca^{2+} sources have been shown to have different effects on autophagy. In addition, the JNK/Beclin/PI3KC3 complex, which promotes autophagy, is regulated by starvation but not by mTOR (Sarkar et al., 2014).

1.1.1.2 Nucleation

1.1.1.2.1 VPS34/PI-3 kinase complex

The vacuolar protein sorting-34 (Vps34) is an autophagy-specific class III phosphatidylinositol-3-kinase (PI3K), associates with BECN1 (mammalian ATG6), and subsequently recruits the sensor of membrane curvature ATG14 and phosphoinositide-3-kinase regulatory subunit 4 Vps15 (p150) (Kihara et al., 2001) and nuclear receptor binding factor 2 (NRBF2) (Lu et al., 2014) to the pre-autophagosomal structure. An active VPS34 kinase complex produces PI(3)P, which recruits WIPIs (Axe et al., 2008). ATG14 has also been reported to promote membrane tethering and fusion of autophagosomes to lysosomes by temporally and spatially controlling the fusogenic activity of the autophagic SNARE complex (Diao et al., 2015).

The Class III PI3K complex is regulated by several interactors, including the VPS34 activator autophagy and beclin 1 regulator 1 (AMBRA1, originally 'activating molecule in Beclin 1-regulated autophagy'), and BECN1 inhibitor BCL2, which also interacts with ATG12 (Liang et al., 1999; Pattingre et al., 2005; Fimia et al., 2007; Zalckvar et al., 2009; Rubinsztein et al., 2011).

Macroautophagy can be inhibited at the early stages with inhibitors of the class III PI3K complex: 3-methyladenine (3-MA) (Seglen and Gordon, 1982) and wortmannin (Powis et al., 1994), which both also target the class I PI3K (Wu et al., 2010). Several specific Class III PI3K inhibitors have been identified recently (Bago et al., 2014; Ronan et al., 2014; Pasquier et al., 2015).

1.1.1.2.2 WIPIs serve putative roles in autophagy

PROPPINs (β-propellers that bind phosphoinositides, also called WIPIs (WD repeat domain phosphoinositide-interacting)), are the only known PtdIns3P-binding proteins with conserved PI(3)P effector functions in autophagy from yeast to human (Busse et al., 2013). Subsequently, WIPIs recruit downstream regulators onto the formation site and ultimately facilitate the formation of autophagosomes. WIPIs are ubiquitously expressed (reviewed in (Proikas-Cezanne et al., 2015)).

1.1.1.2.2.1 Ancestral WIPIs

1.1.1.2.2.1.1 The evolutionary distance between mammalian and yeast WIPIs

There are four human WIPIs (WIPI1 to WIPI4) along with their splice variants, and three orthologs in the yeast (Atg18, Atg21, Hsv2). The four human WIPI members were all described independently based on their sequence homology to yeast Atg18. Phylogenetic analysis has demonstrated that human WIPI proteins are divided into two paralogous groups, one containing human WIPI1 and WIPI2 and the ancestral yeast Atg18, and the other containing human WIPI3 and WIPI4 and *C.elegans* Epg-6 (Proikas-Cezanne et al., 2004; Polson et al., 2010; Behrends et al., 2010). It is suggested that vertebrates have undergone an additional duplication in each of the two paralogous groups, suggesting that the four human WIPI proteins may have distinct roles in autophagy. Atg18 is evolutionarily closer to WIPI1/ WIPI2 than to WIPI3/WIPI4 (Krick et al., 2008). Atg21 is of similar evolutionary distance to the Atg18/WIPI1-WIPI2 group and WIPI3-WIPI4 group, so it is difficult to unambiguously identify its homologues in the PROPPIN family based on sequence similarity (Hoa Mai Nguyen et al., 2018). Hsv2 is closer to the WIPI3-WIPI4 group (Hoa Mai Nguyen et al., 2018).

1.1.1.2.2.1.2 Functions of ancestral WIPIs

I. Atg18-Atg2 complex interacts with Atg9 vesicles

Yeast Atg18 functions both in autophagy and in the vacuole targeting pathway. In the autophagy pathway, Atg18 forms a complex with Atg2 (Obara et al., 2008) and Atg18 membrane binding is dependent on both Atg2 and PI3P. Atg18 alone does not bind to PI3P-containing liposomes, although Atg18 can bind to liposomes containing $PI(3,5)P_2$. The N and C-terminals of Atg2 contribute to highly curved membrane-binding (vesicles with diameters <50 nm) independent of each other (Kotani et al., 2018). However, the Atg2 C-terminal not only binds membranes with its amphipathic helix but also is required for the specific localization on the PAS since it interacts with Atg18 which binds to PI3P. The N-terminal of Atg2 is not required for PAS localization, but functions in autophagosome expansion exerted after its localization.

Atg18 is essential for the retrieval of Atg9 from mature autophagosomes (Reggiori et al., 2004). Atg2-Atg18 complex directly interacts with Atg9 (Suzuki et al., 2007; Wang et al., 2001). The Atg2-Atg18 complex localizes to the highly curved edge of the isolation membrane during its

expansion (Suzuki et al., 2013; Graef et al., 2013). Since the Atg9 vesicles are of a diameter of 30~60 nm (Yamamoto et al., 2012), they may be easily tethered by Atg2 onto edges of expanding phagophores with the help of Atg18.

Epistasis analysis in *C. elegans* indicated that the ULK1, atg14, the LC3 conjugation system, atg-9, and atg-18 are epistatic to epg-6 (WIPI4 homolog) and atg-2 (Lu et al., 2011). Atg18 loss of function reduces autophagosome numbers, while epg-6 loss-of-function causes the accumulation of autophagosomes. Epg-6 directly interacts with atg-2 and regulates the distribution of atg-9.

II. Yeast WIPI family proteins also function in selective autophagy and microautophagy

In the vacuole targeting pathway (a selective autophagy pathway in yeast), Atg18 forms complex with the PI(3)P 5-kinase Fab1, the lipid phosphatase Fig4, Vac7, and Vac14 (Botelho et al., 2008; Jin et al., 2008). Atg18 also functions in microautophagy (Oku 2006; Guan 2001; Krick et al., 2008).

The other two Atg18 homologues in yeast are Atg21 and Hsv2 (Ygr223cp). Atg21 regulates lipidation and localization of Atg8 during uptake of Aminopeptidase I by selective autophagy (Stromhaug et al., 2004) and plays a similar role with Atg18 in the vacuole targeting pathway (Meiling-Wesse et al., 2004); it directly interacts with the coiled-coil domain of Atg16 and with Atg8. Hsv2 promotes efficient piecemeal of the nuclear (PMN) (Krick et al., 2008).

No dramatic influence on autophagy was observed when overexpressing Atg21, Atg18 or YGR223c (Krick et al., 2008).

1.1.1.2.2.2 Structural analysis of Hsv2 and WIPI3

All PROPPINs are seven-β sheet proteins (Diagram 1.1 A). Each blade consists of four anti-parallel β-strands (from i to iv). Overall, the structure resembles a ‘disk’ with ~50 Å of diameter and 25 Å of thickness (Liang et al., 2019).

Hsv2, the yeast homolog of WIPI3/4, contains two Leu/ Phe-Arg-Arg-Gly (L/FRRG) phosphoinositide-binding sites on blades 5 and 6, which are much larger than the other two PI3P binding domains, FYVE and PX domains. Mutation of either of the PI3P binding sites disrupts the lipid-binding ability of Hsv2. While both L/FRRG sites are equally important for PI3P binding, site 2 on Blade 6 seems to be more important for binding to $PI(3,5)P_2$. Recently, WIPI3 structural analysis found that WIPI3 forms a similar structure to Hsv2, although the

L/FRRG motif on Blade 6 favours PI3P, which is different from Hsv2 (Liang et al., 2019). All WIPIs binds efficiently to PI3P, PI(3,5)P_2 and PI5P, suggesting that the position of the phosphoryl group relative to the membrane matters the most, rather than the detailed positioning of the inositol hydroxyl groups. Furthermore, WIPI4 is the only PROPPIN that has only one L/RFFG site and does not bind relatively low concentrations of PI3P (Baskaran et al., 2012).

At the same time, on the interface of Hsv2 and the membrane, there are three prominent hydrophobic residues in the Blade 6 β3-β4 loop, W267A/Y272A/F273A, which are required for membrane binding. These binding sites are conserved among all PROPPINs, except for WIPI4, which only contains one of these membrane-penetrating aromatic residue (Y291) in the Blade 6 β3-β4 loop (Diagram 1.1 B). The structural analysis of Hsv2 indicates that PROPPINs are initially targeted to membranes through nonspecific electrostatic interactions and then retained at the membrane by binding to PIP (Baskaran et al., 2012).

The yeast Atg2-binding site of Hsv2 is on Blade 2, and the 3D structure suggests that the lipid-binding site and Atg2 binding site are on different facets, therefore do not disrupt each other (Baskaran et al., 2012; Krick et al., 2012). The ATG2 binding site of WIPI4 is on its Loop3 between Blade 3 and Blade 4 (Zheng et al., 2017), which is also opposed to its PI3P binding site (on Blade 6 if similar with WIPI3). WD-40 repeats often serve as platforms to assemble functional complexes through the hotspot residues of their domain surfaces (Wang et al., 2015) and are one of the most enriched functional domains in the autophagy system (Behrends et al., 2010).

A

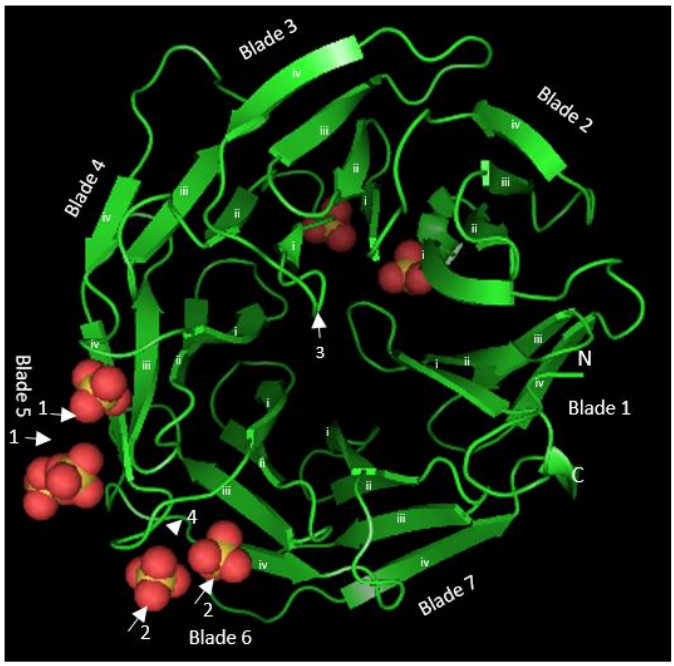

B

```
lactis Hsv2      : 253 VFEVFN-------DAENKRHV----LKDWI----------------------------NIKYFQ----------------
cerevisiae Hsv2  : 298 IFETTNTETNTPDHSRANGSSHP--LKNYIPKGLW----------------------RPKYLD----------------
cerevisiae Atg18 : 319 LGHSMSNNKLDSDDSNMEEAAADDSSLDTTSIDALSDEENPTRLAREPYVDASRKTMGRMIRYSSQKLSRRAARTLGQIFP
cerevisiae Atg21 : 377 LDD-ASNSLPGDNSSNGHWNEE-----EYILASNSNPSMGTPKEIPLS--------KPRIANYFSKKI------------
sapiens WIPI1    : 261 LEQVTNSRPEEPSTWSGYMGKMFMAATNYLP----------------------------------------------
sapiens WIPI2    : 277 LETVKEKPPEEPTTWTGYFGKVLMASTSYLP----------------------------------------------
sapiens WIPI3    : 259 AE----------DPKRNKQSS--LASASFLP----------------------KYFS----------------
sapiens WIPI4    : 266 LK----------DTRLNRRSA--LARVGKVG----------------------PMIGQYVD----------------
                                                                              Y291
```

Diagram 1.1 The structure of WIPI3 (a close homolog of WIPI4)

A. A 3D model of WIPI3-Δloop (with the deletion of two loops, Loop1: 75-80; Loop2:264-281). PDB ID: 6IYY (Liang R.B et al., 2019). WIPI3 only crystalizes well in a high sulphate environment which blocks the interactions with phosphoinsitides. Therefore, potential phosphoinsitide-binding sites should be sulphate-binding amino acids as indicated by sulphates in the figure. Only the sulphate-binding amino acids on Blade 5 and Blade 6 are confirmed to bind phosphoinsitides; the two sites on Blade 2 and Blade 4 are of unknown functions. The sites indicated by arrows and arrowheads correspond to verified positions of:
1: PI(3,5)P binding site; 2. PI3P binding site; 3. ATG2 binding site;
4. hydrophobic loop containing membrane-penetrating aromatic residue (Y291).

B. The multiple sequence alignment of Blade 6 β3-β4 hydrophobic loop of all PROPPINs in human and *Saccharomyces cerevisiae* (Baskaran et al., 2012). WIPI4 has one membrane-penetrating aromatic residue (Y291) in the hydrophobic loop on Blade 6, while other PROPPINs have at least one additional site (red and blue rectangles).

1.1.1.2.2.3 Mammalian WIPIs

A pool of WIPI1 localizes to endosomes and regulates trans-Golgi-endosomal protein trafficking in addition to controlling endosome and autophagosome dynamics (Muller et al., 2015). WIPI1 depletion stimulated the phosphorylation of MTOR itself at Ser-2448 and mTORC1 downstream target p70S6K in both melanocytes and Human MNT-1 melanoma cells, suggesting that WIPI1 suppresses the target of rapamycin complex 1 (TORC1) activity (Ho et al., 2011), although the mechanism is unknown.

There are four WIPI2 splice variants. WIPI2b binds and recruits ATG16L1 (Dooley et al., 2014) onto phagophores by interacting with PI(3)P and PI(5)P (Vicinanza et al., 2015). In HEK293A cells, silencing of WIPI2 suppresses LC3 puncta formation (Polson et al., 2010). When WIPI2 is downregulated, ATG9 accumulates at phagophores (Orsi et al., 2012). Therefore, WIPI2 may help the retrieval of ATG9 from early autophagosomes, similar to what has been reported for yeast Atg18 (Obara et al., 2008). WIPI2 has also been found to be overexpressed in kidney and pancreas cancers (Proikas-Cezanne et al., 2015).

Although WIPI1, WIPI2 and WIPI4 have all been reported to react to PI3P signals in response to starvation, and all WIPIs interact with ATG2 in mammalian cells (Bakula et al., 2017), evidence from ancestral WIPIs indicates that WIPI4 may function downstream of WIPI1/2 in the autophagy pathway. Recently, it was verified by *in vitro* experiments that WIPI4/1 facilitates ATG2A-mediated lipid transfer between PI3P containing large unilamellar vesicles. The PI3P effector WIPI4 on PI3P-containing vesicles associates with ATG2A stably, thereby facilitating ATG2A-mediated tethering and lipid transfer between PI3P-containing vesicles and PI3P-free vesicles. WIPI1 also promotes the lipid transfer by ATG2, although no direct interaction between WIPI1 and ATG2 was found *in vitro* (Maeda et al., 2019). Instead, WIPI1 induces clustering of liposomes. The function of WIPI2 and WIPI3 in lipid transfer remains to be tested.

WIPI3 and WIPI4 may also be involved in the control of autophagy upstream of PI3P production. WIPI3 associates with FIP200 and AMPK-activated TSC complex at lysosomes and regulates mTOR. WIPI4-ATG2 translocates from the AMPK-ULK1 complex to nascent autophagosomes in response to LKB1-mediated AMPK stimulation (Bakula et al., 2017).

1.1.1.3 Autophagosome elongation/expansion

Expansion of the autophagosomal membrane requires the supply and correct composition of the lipids, as well as relevant protein regulators. The known events which happen during this stage are LC3-II conjugation, transient interaction of phagophores with ATG9 vesicles and lipid transfer by ATG2.

1.1.1.3.1 LC3-II conjugation

The conjugation of ATG8s/LC3 to membranes that become autophagosomes is a defining event in autophagy, which involves two ubiquitin-like reactions.

ATG5-ATG12-ATG16L1 conjugation system

ATG7 (E1-like) activates ATG12 (ubiquitin-like molecule), and ATG10 (E2-like) attaches the C-terminal glycine of ATG12 irreversibly to an internal lysine of ATG5 (Mizushima et al., 1998). The ATG5-ATG12 conjugate then non-covalently interacts with the N-terminal of ATG16L1 and oligomerizes to form a complex of approximately 800 kDa. This complex locates to the outer membrane of the phagophore and disassociates upon maturation of autophagosomes (Suzuki et al., 2001). It is reported that ATG16L1 promotes ATG5 membrane binding by releasing the inhibition of membrane binding by ATG12 (Romanov et al., 2012). ATG16L1 regulates the localization of the ATG5–ATG12 conjugate to the cytoplasmic face of phagophore (in yeast) / isolation membranes (higher eukaryotes) and also specifies the site of ATG8/LC3 lipidation (Fujita et al., 2008).

LC3-PE conjugation system

This cascade starts with the cleavage of pro-LC3 at its C terminus by the cysteine protease Autophagy-related 4 (ATG4) to expose a free C-terminal glycine and generate cytosolic LC3-I. ATG7 activates it as an E1-like enzyme and ATG3 acts as an E2-like enzyme (Tanida et al., 2001). The ATG5-ATG12-ATG16L1 complex is thought to function as an E3-like enzyme with ATG12 binding ATG3. The C-terminal glycine of LC3 is specifically targeted to the ATG5-ATG12-ATG16L1 complex and then is covalently conjugated to phosphatidylethanolamine (PE) to form LC3-II on both inner and outer membranes (Ichimura et al., 2000). After completion of autophagosome formation, the LC3-II remains associated with the autophagosomes. After fusion, LC3-II on the cytoplasmic face is recycled back via the action of ATG4B, while the luminal LC3-II is broken down (Korolchuk et al., 2010). It is also suggested

that ATG3 is an additional conjugation target of ATG12 and ATG12-ATG3 is required for efficient basal autophagy flux, as well as late endosome function through interaction with ESCRT complex (Murrow et al., 2015). The deacetylation of LC3 promotes the cytosolic translocation of a nuclear LC3 pool, which is required for its lipidation in starvation conditions (Huang et al. 2015).

1.1.1.3.2 ATG9 trafficking

ATG9 is the only transmembrane protein of all core ATG proteins and is thought to deliver membranes to autophagosomes and autophagosome precursors (Reggiori et al., 2004; Yamamoto et al., 2012; Young et al., 2006; Karanasios et al., 2016). Autophagosome formation is inhibited after downregulation of ATG9 in yeast and mammalian systems (Zhuang et al., 2017). Previous findings have shown that the trafficking of ATG9 from the plasma membrane to the recycling endosomes via early endosomal compartments is important for the biogenesis of autophagosomes (Puri et al., 2014).

Under nutrient-sufficient conditions, ATG9A mainly traffics through the medial and TGN of the Golgi and endosomes, but during amino acid starvation, some perinuclear ATG9A derived from both the Golgi and recycling endosomes translocates onto vesicular-tubular structures which are partially positive for autophagosome markers (Orsi et al., 2012), and is similar in yeast (Mari et al., 2010). This vesicular ATG9A compartment interacts transiently with but is not incorporated into phagophores (Karanasios et al., 2016).

The ULK1/2 complex (Young et al., 2006) and SRC kinase (Zhou et al., 2017) regulate the ATG9 exit from the Golgi by phosphorylation of its interactors AP1 and AP4 (Guo et al., 2012). Sphingomyelin phosphodiesterase 1 controls ATG9A trafficking from the recycling endosome (Corcelle-Termeau et al., 2016) and its dysregulation impairs autophagosome closure. p38IP, a p38 MAPK-interacting protein (Webber et al., 2010), and Sorting nexin-18 (Søreng et al., 2018) are reported to control ATG9 trafficking from the Golgi and recycling endosomes, respectively.

Recently, additional components of ATG9A-positive membranes have been identified (Judith et al., 2019). In amino acid starvation (Earle's saline), representative proteins enriched in ATG9A-positive membranes are RAB1A, ARFIP1, ARFIP2, SH3GLB1 (BIF-1 or endophilin B), phosphatidylinositol 4 kinases (PI4KIIα and PI4KIIIβ) and TRAPPC5. In nutrient-rich media, GOLGA2, TGOLN2, and SEC22A were enriched. The levels of AP4 subunits are unchanged.

These proteins potentially modulate the composition of ATG9A-positive membranes or are transported together with ATG9 vesicles and function on autophagosomes.

RAB1B (Kakuta et al., 2017) controls trafficking between the ER and Golgi (Wang et al., 2015) and the Golgi and recycling endosomes (Marie et al., 2009). They are found to localize on ATG9A-GFP–positive vesicles. Yeast Ypt1 (RAB1 homologue), which is present on COPII vesicles and is necessary for the tethering of COPII vesicles to the Golgi during secretion, was also found on yeast Atg9 vesicles (Kakuta et al., 2012; Yamamoto et al., 2012). Ypt1 and its GEF TRAPIII localize to the PAS upon starvation (Lynch-Day et al., 2010), and TRAPIII also regulates ATG9A/Atg9 traffic (Kakuta et al., 2012; Lamb et al., 2016).

BIF-1 (Endophilin 1), ARFIP1 and ARFIP2 are all Bin/Amphiphysin/Rvs (BAR) domain-containing proteins. BIF-1 (Takahashi et al., 2011) and Dynein (Takahashi et al., 2016) are required for ATG9A-positive vesicle formation from recycling endosomes.

ARFIPs sense and generate membrane curvature (Peter et al., 2004; Frost et al., 2009). ARFIPs bind to the TGN depending on its amphipathic helix and the BAR domain (Cruz-Garcia et al., 2013). The amphipathic helix enables the specificity of ARFIPs' binding to phosphatidylinositol 4-phosphate (PI4P)–containing liposomes (Cruz-Garcia et al., 2013). Depletion of ARFIP1 does not regulate autophagy. However, depletion of ARFIP2 (also termed partner of Rac1, a Rho family GTPase (POR1)) downregulates autophagy (Judith et al., 2019).

PI4KIIα promotes autophagosome-lysosome fusion (Wang et al., 2015) and is also recruited by GABARAP, but it was still accumulated on autophagosomes in GABARAP family depleted cells (Vaites et al., 2019).

1.1.1.3.3 Lipid transfer by ATG2

Structure of ATG2 family proteins

There are two redundant ATG2 homologs in human, ATG2A and ATG2B. ATG2 proteins contain evolutionarily conserved Chorein_N (Pfam ID: PF12624), ATG_C (Pfam ID: PF09333), and ATG2_CAD (Pfam ID: PF13329) domains (Diagram 1.2A) (Chowdhury et al., 2018). Chorein_N and ATG_C are conserved with the N and C terminal of VPS13 (Pfisterer et al., 2014), a paralog of VPS13A/Chorein (Velayos-Baeza et al., 2004). The Chorein_N and ATG_C regions are also required for the localization of ATG2A to autophagosome-forming sites and

LDs (Tamura et al., 2017). The C-terminal localization region (CLR) (residues 1,723–1,829) preceding ATG_C contains an amphipathic α-helix and is also required for the localization of ATG2A to both phagophores and LDs (Velikkakath et al., 2012; Tamura et al., 2017). Mammalian ATG2 colocalizes with LC3, as well as with early autophagosomes decorated with ULK1, WIPI1 and ATG5 (Velikkakath et al., 2012).

The binding site of WIPI4 on ATG2 is located between the CAD domain and the CLR domain, but the exact site is disputable. One report suggested residues 1344, 1373, 1503 of ATG2A (Chowdhury et al., 2018). Whereas, another group suggested an evolutionarily conserved aromatic H/YF motif (1524/1525) (Zheng et al., 2017). A third study found amino acid 1358-1404 to be required for WIPI4 binding (Maeda et al., 2019).

Residue 240–920 of yeast Atg2 form repeated β-strands abundant with hydrophobic residues, where phospholipids move along (Diagram 1.2A). Residue 1,235–1,243 and 1,264–1,268 of yeast Atg2 are required for the interaction with Atg9, and the interaction with Atg9 promotes the interaction of Atg2 with Atg18 and restricts the localisation of Atg2-Atg18 complex to the extremities of the phagophore (Gómez-Sánchez et al., 2018). Another study found that aa 2-46 and 1269-1347 of Atg2 are required for its interaction with Atg18 and Atg9, while aa 10-12 are required for its localisation to the ER, suggesting that membrane localisation of Atg2 n terminal is required for its interaction with Atg9 and Atg18 (Kotani et al., 2018). Moreover, 1347-1373 is required for its localization to the PAS. The yeast ATG_C also shares similarities with the Golgi-localized protein of maize APT1, which is involved in the secretory pathway (Xu et al., 2006). S249 and S1086 of yeast Atg2 can be phosphorylated by Atg1, although the function is unknown (Papinski et al., 2014).

ATG2A/B forms a rod-shaped protein with 20 nm in length, binding the membrane with both its N-tip and CAD-tip (containing CAD and CLR domains) (Diagram 1.3A) (Chowdhury et al., 2018). The binding to the membrane is dependent on lipid packing defects, independent of the lipid type. ATG2A/Atg2 tethers small unilamellar vesicles vesicles (SUVs) of high curvature (diameter <80 nm) independent of PI3P (Chowdhury et al., 2018; Kotani et al., 2018), but cannot tether large unilamellar (LUVs) (>140 nm), possibly because its CAD-tip cannot bind stably the low curvature membrane containing fewer packing defects (Chowdhury et al., 2018). However, WIPI4-ATG2 tethers LUVs and facilitates the lipid transfer between LUVs *in vitro*, possibly by stabilizing the phagophore localization of ATG2 C-termini.

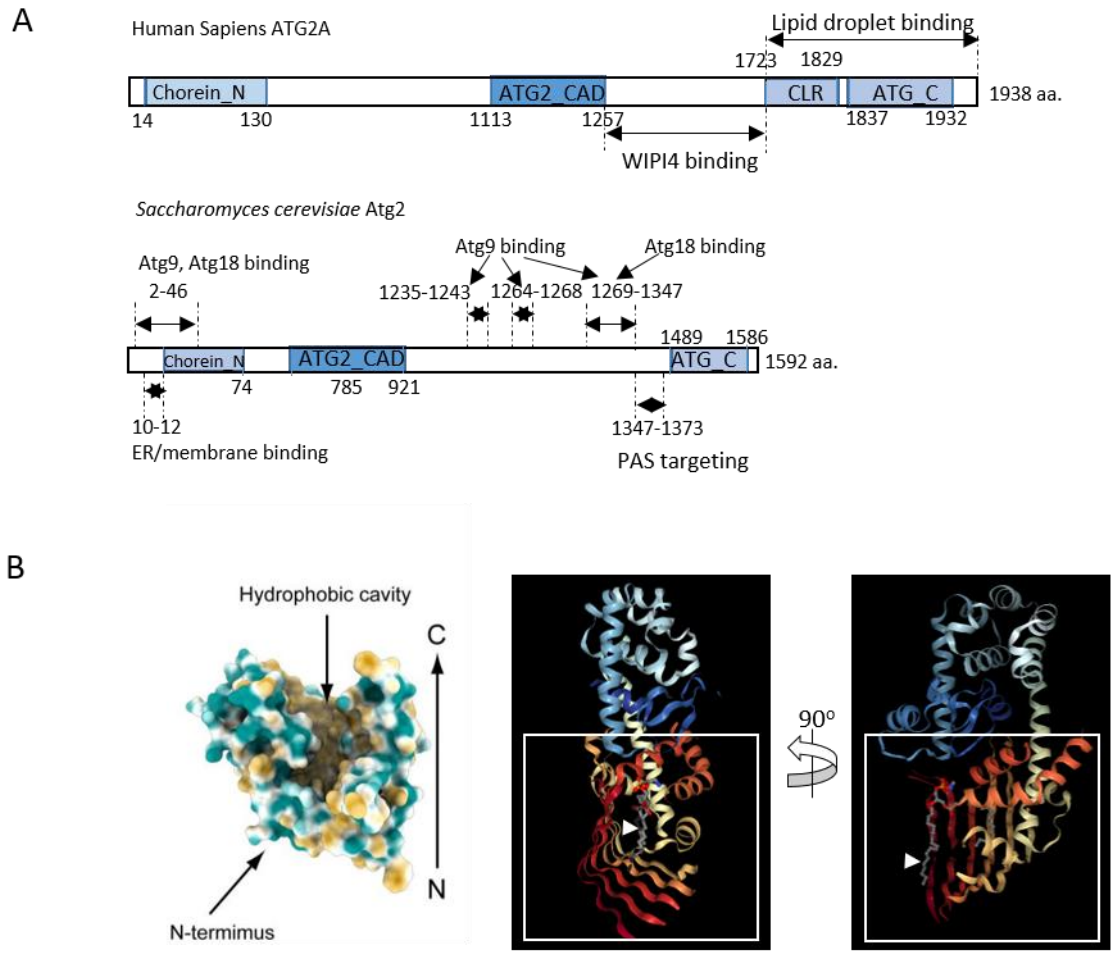

Diagram 1.2 Structures of ATG2 family proteins

A. Line represented primary structure of human ATG2A protein (top) and yeast Atg2 (bottom), with indicated conserved and functional domains.
B. Structures of ATG2A Chorein_N domain and yeast Atg2 N-terminal (1-389).
Left: surface representation of the ATG2A Chorein_N domain colored according to the hydrophobicity potential calculated in ChimeraX. Hydrophobic and hydrophilic residues are shown in khaki and turquoise, respectively. Revised from Osawa et al., 2019, authorised by the Creative Commons Attribution License.
Right: the crystal structure of PE-bound yeast Atg2 N-terminal (1-389), PDB ID: 6A9J (Osawa et al., 2019). The white square highlights the hydrophobic cavity formed by the Chorein_N domain, with an arrowhead pointing to a PE molecule (grey) located in it.

Two models of lipid transfer by ATG2 family proteins

Liquid chromatography/tandem mass spectrometry show that ATG2 family proteins solubilize lipids and that each ATG2 molecule can bind to ~20 lipid molecules. Structural analysis of ATG2A-WIPI4 complex indicates that WIPI4 flexibly associates with ATG2A in a region close to its CAD tip, inducing no significant conformational change in ATG2A (Diagram 1.3A). The binding with WIPIs may enable the CAD-tip to specifically and tightly localize to PI3P containing membranes. WIPI4-mediated tethering is required for the transfer between low curvature membrane LUVs (Chowdhury et al., 2018), suggesting that the lipid transfer requires stable tethering, which is called the 'bridge model' (Diagram 1.3B). Structural analysis of yeast Atg2 suggests that its N-tip extracts phospholipids through weakly binding the acyl chains of PE via a hydrophobic cave (Osawa et al., 2019) (Diagram 1.2B). Moreover, Atg2 lipid transfer was bidirectional and happens through concentration gradients without ATP hydrolysis, and the WIPI4 tethering does not determine the direction of transfer (Maeda et al., 2019). The N-tip of the ATG2 has been found able to localize to the ER, raising a possibility that ATG2 extracts lipids from ER to newly formed isolation membranes.

In contrast to the 'Bridge' model, an alternative 'ferry model' was presented based on the following two observations (Diagram 1.3.C). First, when anchored onto the donor membrane, aa 1-345 of ATG2A is capable to mediate lipid transfer *in vitro* without WIPI4, and this truncated form can rescue the autophagy defect in an ATG2A/B knockout cell line (Valverde et al., 2019). Second, ATG2A can bind to only one liposome and two liposomes simultaneously (Chowdhury et al., 2018). Therefore, lipid transfer is suggested to be facilitated by shuttling of the N-tip fragment (aa 1-345) of ATG2 and is not dependent on tethering of donor and acceptor membranes.

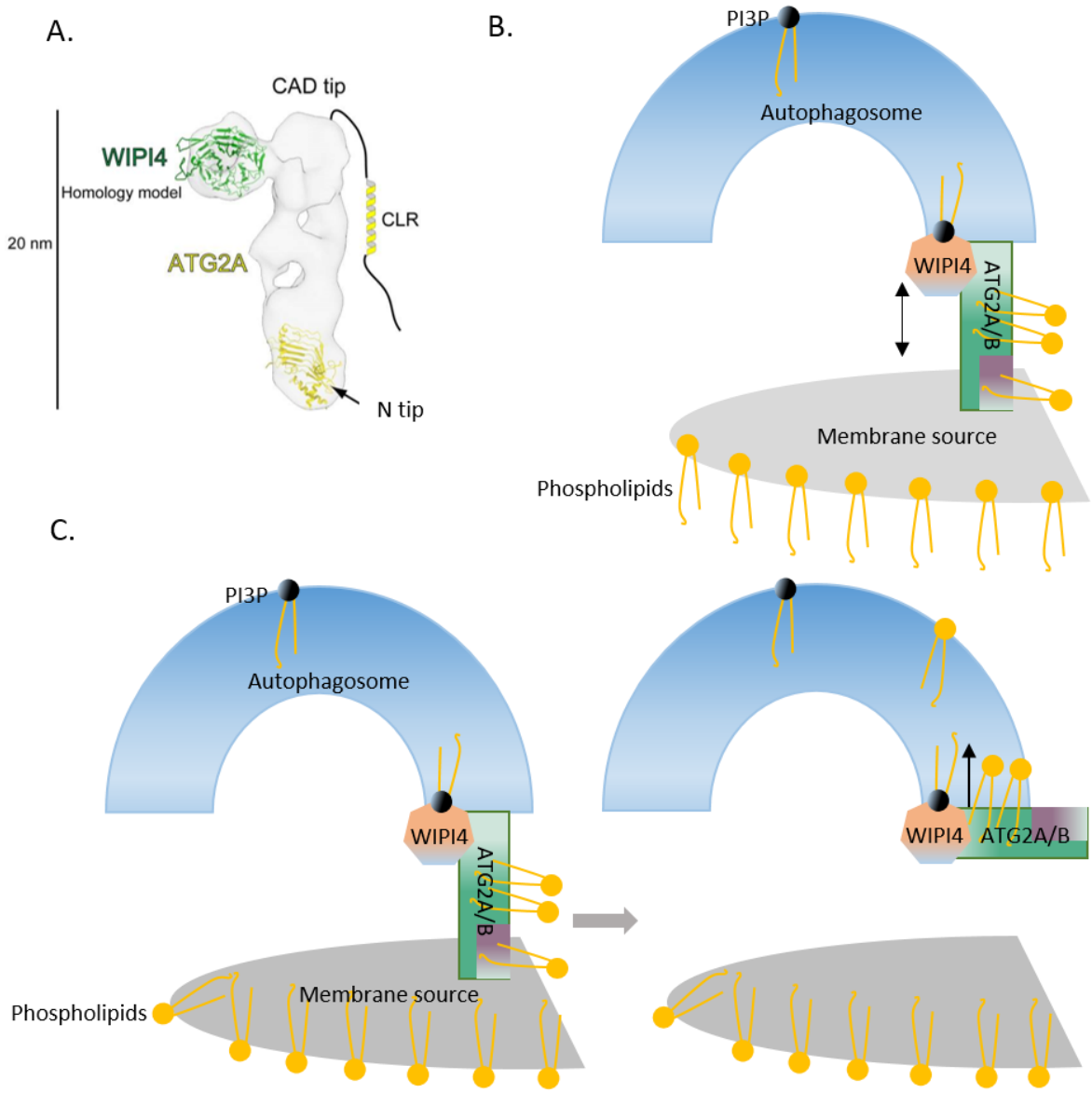

Diagram 1.3 Models of lipid transfer by ATG2

A. Negative stain reconstruction of mammalian WIPI4-ATG2A complex (EMDB ID 8899). ATG2 family proteins are rod like proteins with ~20 nm in length which can bind to membranes with both ends. WIPI4 binds to the area close to the CAD tip of ATG2 in a flexible manner. The binding with WIPI4 protein stabilizes ATG2 localisation on isolation membranes. The ribbon model representing the crystal structure of WIPI4 (actually WIPI3, PDB ID 6IYY) was manually fitted into the EM image. Revised from Osawa et al., 2019, authorised by the Creative Commons Attribution License.

B. The bridge model of ATG2 lipid transfer in autophagy. Lipids from membrane source, e.g. lipid droplets, ER, etc., are loaded onto one of the tips of ATG2, then reach the other tip by transfer through the extended hydrophobic cavity, where they are finally unloaded onto the growing autophagosomes.

C. The ferry model of ATG2 lipid transfer in autophagy. ATG2 binds the PI3P-containing membrane through the flexibly bound WIPI4, and dynamically associates with the membrane source. The extracted lipids are unloaded at the autophagosome independently of WIPI4.

1.1.1.4 Autophagosome closure

The mechanism of autophagosome closure is poorly understood, although topologically it is supposed to be a constriction of a hole followed by fission of the inner and outer membrane conjunction sites (Dimova et al., 2015), which is similar to how ESCRTs drive membrane fission at multivesicular bodies (MVBs). Given the limitations of light microscopy, the fission-dependent separation of inner and outer membranes cannot be resolved by live imaging currently. The machinery used by this process is uncertain, although clues are pointing to ESCRT complexes or ATG8 proteins.

1.1.1.4.1 ESCRT

ESCRT is a set of conserved complexes—0, I, II, and III—and many accessory proteins (e.g., the Vps4 ATPase), functioning downstream of Rab5. ESCRT was initially been found to mediate scission on multivesicular bodies (MVBs) in yeast. The cytosolic ESCRT complexes cluster ubiquitinated proteins on endosomal membranes to specific membrane domains, constrict these domains and catalyze pinching off vesicles containing these domains into the lumen of the endosome (Henne et al., 2013). It also mediates topologically similar membrane constriction and abscission in the plasma membrane (PM), abscission during cytokinesis and PM repair, exosome and microvesicle shedding and viral release from the PM (Adell et al., 2016; Christ et al., 2017).

The yeast ESCRT III subunits Snf7 and the Vps4 ATPase catalyze autophagosome closure in yeast (Yoshinori et al., 2018). The recruitment of Snf7 and Vps4 to phagophores is dependent on the Rab5 GTPase Vps21, possibly through enabling the interaction between Snf7 and Atg17/Atg11/Atg29 complex (Zhou et al., 2019). Atg17 stays on autophagosomes until after closure. Although the mammalian homolog of Snf7, CHMP4B, has not been investigated, another subunit of mammalian ESCRTIII named CHMP2A regulates the abscission of the inner and outer autophagosomal membranes together with AAA-ATPase VPS4 (Takahashi 2018). Consistently, RAB5 is dispensable for autophagosome-lysosome fusion but required for the autophagosome closure (Hegedűs et al., 2016).

The SNARE complex locates in the outside corner of two contacting membranes and reducing the angle of the corner, while ESCRTIII locates inside the membrane neck with the ATPase VPS4 tightening the CHMP2A-CHMP3 spiral to reduce the diameter of the neck (Maity et al.,

2019) (Diagram 1.4). Therefore, ESCRTIII fits the topological requirement for autophagosome closure machinery.

1.1.1.4.2 ATG8 family proteins

Atg8 family proteins are ubiquitin-like proteins, consisting of two amino-terminal α helices and a ubiquitin-like core. There is only one Atg8 protein in the yeast, but multiple homolog genes in *C.elegans* (LGG-1, LGG-2) and mammals. The *C.elegans* LGG-2 is the ortholog of mammalian microtubule-associated protein 1 light chain 3 (MAP1LC3, hereafter referred to as LC3) subfamily proteins LC3A, LC3B and LC3C, while LGG-1 is the ortholog of mammalian γ-aminobutyric acid receptor-associated protein (GABARAP) subfamily proteins (GABARAP, GABARAPL1 and Golgi-associated ATPase enhancer of 16 kDa (GATE-16)) (reviewed in Shpilka & Elazar et al., 2011). LGG-2 is required for the degradation of LGG-1 positive vesicles, suggesting that mammalian GABARAPs may function downstream of LC3 family proteins (Wu et al., 2015).

ATG8-deleted cells are defective of delivery to the lysosome and expansion, but can still complete the closure of autophagosomes by membrane fission (Nguyen et al., 2016), albeit with significantly longer time (6 hours versus < 2 hours). Nguyen and his colleagues also showed by the Proteinase K protection assay that GABARAP family and ATG8 family knockout HeLa cells only have closure defect in basal conditions, but not in BafA1 plus starvation conditions.

It was then hypothesized that fission in autophagosome closure is a subtle morphological change (Tsuboyama et al., 2016). Elliptical starvation-induced phagophores suddenly become spherical at a very late stage of maturation. In ATG3 KO MEF cells, this conversion occurred much more slowly, even reverting to fully open ‘cups’ in extreme cases. Moreover, STX17 and Lysotracker red (LTR) were used to label uncompleted/ unclosed autophagosomes. LTR labels lysosome materials and shows ring-shape when the inner membrane of autophagosome is not broken down, while STX17 labels the outer membrane of autophagosomes. With this assay, it was found that the breakdown of the inner membrane only happens after the autophagosome is completed. It was also observed that the STX17 positive-LTR ring-shaped structures were maintained for a much longer period (>30 min versus 11 min) in ATG3 knockout (KO), ATG5 KO, and ATG7 KO MEFs compared with WT and rescued ATG3 KO MEFs. Consistent with Nguyen et al., Tsuboyama’s observation also suggests that ATG8 is not absolutely required for fission. Notably, ATG3-ATG12 complex also functions at the late stage of autophagosome

formation, and ATG3 interacts with ESCRT (Murrow et al., 2015). Therefore, there is a possibility that ATG3 accelerates closure partially through the ESCRT complex.

The tethering of the phagophore edge may similarly promote autophagosome closure, raising the possibility that the mechanism of ATG8 proteins in accelerating closure is through membrane tethering. There has been numerous biophysical evidence supporting that ATG8 family proteins regulate membrane tethering (reviewed in Nakatogawa et al., 2007). Moreover, GABARAPs may form homo-oligomers (Coyle et al., 2002), raising the possibility that they may have open/close structures and bind each other on the target membrane to bridge two membranes. Although no significant conformational dynamism of one single GABARAP protein has been found (Ma et al., 2010), it was found in *C.elegans* that the closed or open conformation is isoform-specific (Wu et al., 2015). However, the role of the ATG8 proteins in tethering may also depend on the distance of the two membranes, because the ATG8 bridge is less than ~10 nm (~4 nm from each Atg8 protein) (Yu & Melia, 2017).

Moreover, there are a few studies about LC3 and GATE-16 mediating full membrane fusion *in vitro* (Weidberg et al., 2011). The mechanism is engaging lipids with their amino termini with either hydrophobic or electrostatic interactions (Weidberg et al., 2011). The required sequences identified in these *in vitro* studies are also required *in vivo*. However, most tethers cannot fuse the membranes with rare exceptions, including MFN1/2 (Eisenberg-Bord et al., 2016). Generally, tethering proteins cannot bring the opposing membranes to the distance required for fusion (a few angstroms), nor can they generate mechanical forces to overcome the energy barrier of 2 hydrated lipid bilayers opposing each other when they are that close. Consistent with the above hypothesis, no lipid mix mediated by ATG8 were observed when using stable lipid mixtures (Jotwani et al., 2012), nor when membranes are not of high curvature *in vitro* (Romanov et al., 2012). Therefore, it seems that ATG8 mediated fusion requires unstable/ highly curved membranes. However, it is unknown how unstable/ curved the edges of phagophores are *in vivo* and whether the *in vitro* reconstitution experiments lowered the energy barrier to lower than the physiological status. Thus, the *in vitro* evidence is not conclusive about whether ATG8s mediate membrane fusion directly or indirectly, and it is unknown how ATG8s accelerate autophagosome closure.

1.1.1.4.3 The other regulators of closure

WIPI4-ATG2 complex

Unclosed autophagosome-related membranes accumulated in ATG2-depleted cells (Velikkakath et al., 2012). However, another observation by EM suggests that the autophagosomes were still closed in ATG2 depleted cells (Tang et al., 2019). Moreover, proteinase K treatment can reverse the increase of liposome size facilitated by Atg2, suggesting that Atg2 cannot fuse membrane (Osawa et al., 2019). Therefore, ATG2 may indirectly affect closure through regulating the expansion, similar to ATG8. For example, ATG2 may recruit closure machinery from other organelles or vesicles through mediating lipid transfer.

TRAPPC11 is one of three components of the TRAPIII complex, which can capture vesicles by tethering or bridging two membranes (~50–100 nm) (Bröcker et al., 2010) and functions in ER-Golgi trafficking. In mammalian cells, TRAPPC11 recruits the ATG2-WIPI4 complex onto phagophores depending on ATG9 function, and its loss of function causes an autophagosome-closure defect (Stanga et al., 2019). However, the other two subunits of TRAPIII: TRAPPC12 and TRAPPC8, do not seem to have similar functions in the closure process, possibly due to having different interacting partners.

ATG9

TRAPIII also regulates ATG9 retrieval from recycling endosomes to the Golgi (Rao et al., 2016). In addition, excess sphingomyelin leads to accumulation of ATG9 in transferrin receptor-positive juxtanuclear recycling endosomes (Corcelle-Termeau et al., 2016) and impairs autophagosome degradation. EM showed that excess sphingomyelin causes accumulation of unclosed autophagosomes, and this can be rescued by the recovery of ATG9 trafficking.

WIPI4-ATG2 complex and ATG9 vesicles both function in autophagosome expansion, but it is unknown whether they regulate each other's function. Yeast Atg2-Atg18 complex has been reported to mediate the retrieval of Atg9 from the PAS to the peripheral region. And the interaction of Atg2 with Atg9 is required for Atg2 confinement to the growing phagophore extremities and subsequent association of Atg18. Atg2–Atg18 association was severely affected in the absence of Atg9 (Gómez-Sánchez et al., 2018). Mammalian ATG9 is required

for the recruitment of ATG2-WIPI4 complex onto phagophores (Stanga et al., 2019). It is unknown whether WIPI4/3 or WIPI1/2 are relevant to ATG9 trafficking in mammalian cells.

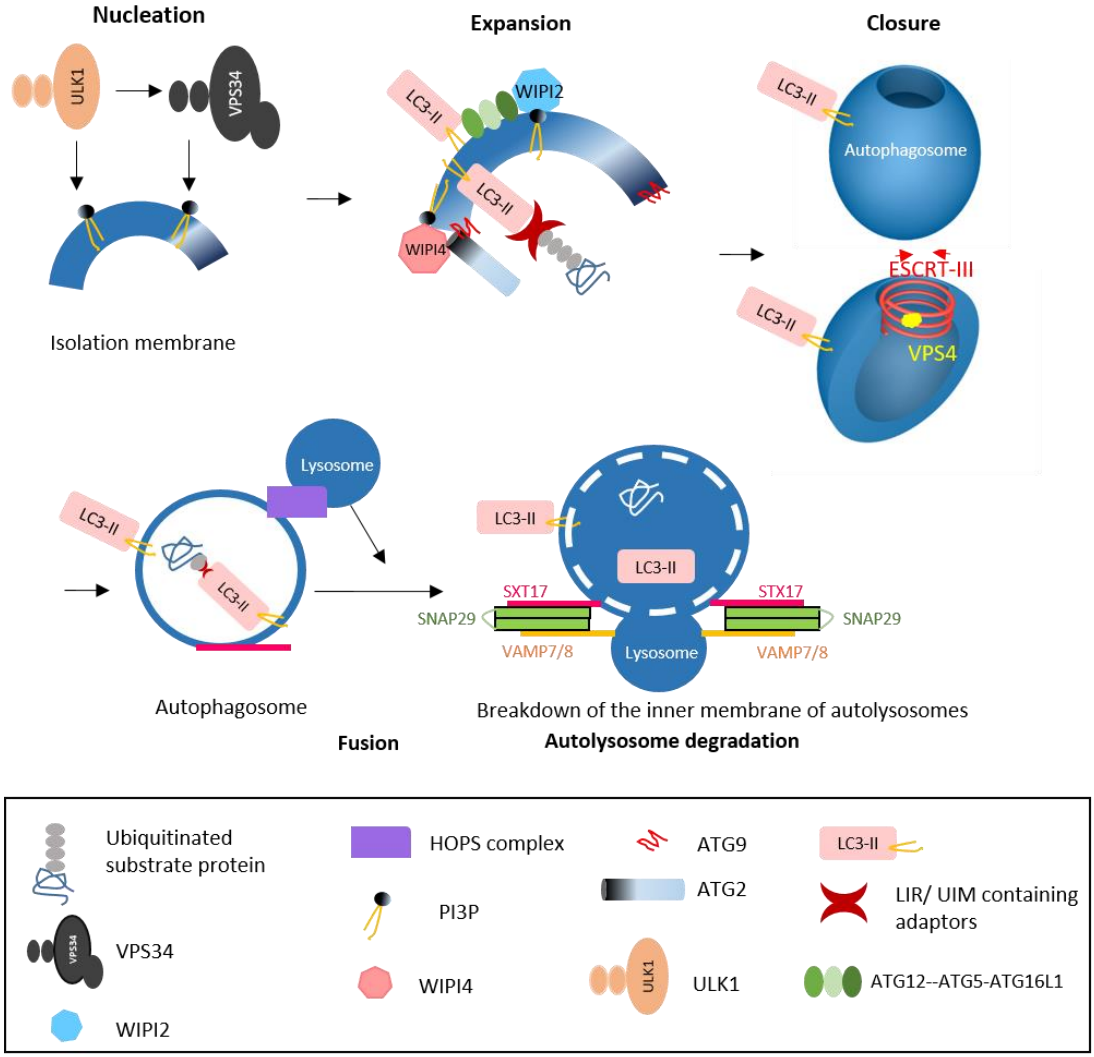

Diagram 1.4 The closure, fusion and degradation of autophagosomes

Schematic of the autophagy process highlighting function of WIPI4 in expansion and potentially in closure. Class III PI3K VPS34 produces PI3P at the phagophore, which recruits WIPI2 and the ATG12-ATG5--ATG16L1 complex to define the site for LC3-lipidation. ATG2 family proteins regulates the expansion of isolated membranes, interacting with WIPI4 and ATG9 on the edges of phagophores. Substrate selectivity is conferred by establishing a bridge between LC3-II and specific ubiquitinated cargo through their LIR/UIM and UBA domains, respectively. The mechanism of autophagosome closure is poorly understood, although topologically it is supposed to be a constriction of a hole followed by scission of the inner and outer membrane conjunction site (Knorr et al., 2015). ESCRT-III complex, a membrane fission machinery located inside the membrane (labelled by a red helix), is reported to function in closure. VPS4 (yellow) catalyzes the constriction as an ATPase for the ESCRT-III complex. Once sealed, autophagosomes fuse with lysosomes, which is mediated by the SNARE complex containing STX17, SNAP29, VMP7/8. The HOPS complex is one of the known tethering regulators, which promotes the fusion. STX17 has been observed on autophagosomes with intact inner membrane, suggesting that STX17 arrives before scission (Tsuboyama et al., 2016).

ATG4

Ultrastructural analysis of Atg4B-C74A-overexpressing cells showed that the ratio of the number of open autophagosomes versus closed autophagosomes increased by 20% compared to the empty vector transfected cells. Additionally, the size of closed autophagosomes decreased by 15% (Fujita et al., 2008). The Atg4B mutant sequesters LC3 paralogues and blocks the formation of the Atg7-LC3 intermediate (Fujita et al., 2009). However, it is unknown whether the ATG4B mutant impairs closure through defective ATG8 lipidation, and it is also unknown how defective lipidation can affect closure.

1.1.1.5 Endosomal/lysosomal fusion

Autophagosomes fuse either directly with lysosomes to form autolysosomes, or with endosomes to form amphisomes (Klionsky, 2007; Lucocq & Walker, 1997). Membrane fusion is regulated by fusion and tethering protein complexes, lipid metabolism and local cytosolic levels of calcium ions, and actin organisation (reviewed in Corona & Jackson, 2018). SNAREs and tethering factors are most representative modulators of endosomal/lysosomal fusion.

1.1.1.5.1 SNARE proteins

SNAREs are responsible for the physical fusion of the lysosome and autophagosome/amphisome membranes. The general mechanism is that the Q-SNAREs form a receptor complex on the target membrane first, awaiting R-SNARE-laden vesicles to bind to them (reviewed in Lou et al., 2016). The core SNAREs that regulate the autophagy pathway are Syntaxin 17 (STX17) or YKT6 on autophagosomes, vesicle-associated membrane protein 8 (VAMP8) on lysosomes, and Synaptosome associated protein 29 (SNAP29), which facilitate their binding (Itakura et al., 2012; Matsui et al., 2018). STX17 is a Qa-SNARE, and its localization is regulated by LAMP2 (Huber et al., 2016), LC3/GABARAP proteins (Itakura et al., 2012), and IRGM (Kumar et al., 2018). STX17 and YKT6 are collectively required for autophagosome-lysosome fusion. SNAP29 is a promiscuous, non-lipid anchored Qbc-SNARE (Diagram 1.4) that donates two coiled-coil domains to the forming SNARE bundle (Hohenstein et al., 2001). There are some other SNAREs regulating specific types of fusion events in autophagy. Autophagosomes recruit diverse SNAREs depending upon their ultimate fate (Kimura et al., 2017). SNAREs also play a role in determining the specificity of vesicles and target membranes (Sudhof et al., 2009).

1.1.1.5.2 HOPS complex

The homotypic fusion and protein sorting complex (HOPS) is an evolutionarily conserved membrane tethering complex for membranes containing the RAB7 GTPase. It tethers Rab7 positive membranes with autophagosomes through interaction with ATG8 family members. HOPS interacts with STX17 (Jiang et al., 2014) and also primes the core SNARE bundle assembly (Orr et al., 2017). PLEKHM1 promotes fusion indirectly by interacting with the HOPS complex. The switch of GTPases from RAB5 to RAB7 is also required for autophagosome-lysosome fusion (Hegedus et al., 2014).

1.1.1.5.3 GABARAP is a HOPS regulator

C18orf8/RMC1, a new subunit of the CCZ1-MON1 RAB7 guanine exchange factor (GEF) that positively regulates RAB7 recruitment to late endosomes/autophagosomes, was found to accumulate in GABARAP/L1/L2-deficient cells (Vaites et al., 2018), suggesting that GABARAP may be required for its sorting to lysosomes. The authors also found that RMC1 loss of function impairs autophagosome maturation, but did not assess whether it was a closure or fusion defect. BRUCE, which specifically interacts with GABARAP but not LC3, regulates the delivery to lysosomes through HOPS (Ebner et al., 2018). In *C. elegans,* GABARAP also directly interacts with VPS39, a subunit of HOPS complex and regulates autolysosome formation (Manil-Ségalen et al., 2014).

1.1.1.5.4 Other HOPS/ SNARE regulators

Many other fusion regulators function through interaction with the HOPS complex or SNAREs. The Atg17-ATG29 complex modulates autophagosome-lysosome fusion by interacting with a vacuolar SNARE Vam7 independently of each other (Liu et al., 2016). Atg17 also regulates autophagosome formation during stress-induced autophagy (Davies et al., 2015).

1.1.1.5.5 Lipids

Dysregulation of lipids inhibits fusion directly or indirectly through the proteins they associate with. Removal of certain Atgs (Noda et al., 2009) after closure is also required for fusion, possibly by inhibiting the recruitment of fusion factors. Depletion of Ymr1 PI3P phosphatase accumulated sealed autophagosomes with Atgs on them (Cebollero 2012).

A decrease or accumulation of lysosomal cholesterol changes the fluidity of the membrane and inhibits fusion (Fraldi 2010). The presence of PI(4)P on autophagosomes (Wang et al., 2015) and a correct balance of $PI(3,5)P_2$: PI(3)P (Hasegawa et al., 2016) are both required for delivery of autophagic content to lysosomes.

1.1.1.5.6 Microtubules and motor proteins

The positioning of lysosomes affects their membrane fusion with autophagosomes. Dynein (Ishikawa, 2012) associates with lysosomes in a dynactin-dependent manner to regulate lysosomal positioning and thereby the fusion with autophagosomes. Mature autophagosomes move along acetylated stable microtubules resistant to destabilizing nocodazole treatment, and the organisation of unacetylated microtubules does not affect the fusion. However, either nocodazole or microtubule-stabilizing paclitaxel treatment impairs the conversion of LC3-I to LC3-II (Xie et al., 2010), suggesting that microtubules are involved in some way in autophagosome formation.

1.1.1.6 Autolysosome degradation

Lysosome acidification is not required for regulation of membrane fusion but is required for the degradation of autolysosomes. The V-ATPase on lysosomes acidifies the lysosome lumen through ATP-hydrolysis and proton-pumping (Kane, 2006). The low pH stimulates the activity of lysosomal hydrolases for efficient degradation of autophagy substrates (Peri and Nusslein-Volhard, 2008). However, its proton translocation activity is not required for membrane fusion. The proton pump activity of V-ATPases can be inhibited by bafilomycin A and concanamycin A (Bowman and Bowman, 2000; Huss et al., 2002).

Cathepsin activity and maturation are used as markers of lysosome function. Cathepsin family proteins are endopeptidases. Cathepsin D is synthesized in rough ER as preprocathepsin D. After removal of the signal peptide, the 52 kDa procathepsinD is targeted to endo-lysosomes and phagosomes. Upon entering acidic compartments, the 44 amino acid N-terminal propeptide is removed and a 48 kDa single-chain intermediate forms. Further proteolytic cleavage yields the mature form composed of heavy (34 kDa) and light (14 kDa) chains, which are linked by non-covalent interactions (Benes et al., 2009).

1.1.2 Cargo selection

Autophagy can be either selective or non-selective in response to different stimuli. Almost 20 selective autophagy pathways have been described, including autophagic processes responsible for the clearance of damaged organelles like mitochondria - mitophagy, peroxisomes - pexophagy; aggregate-prone proteins - aggrephagy; and pathogens - xenophagy (reviewed in Frake et al., 2015). The specificity of selective autophagy can be mediated by autophagy adaptors and receptors which recognize cargos and bind to ATG8 family proteins (Stolz 2014).

1.1.2.1 AIM-LDS interface

Most known autophagy adaptors interact with ATG8 through their ATG8-interacting motif (AIM, or LC3-interacting region (LIR)). AIM/LIR binds to a hydrophobic patch (LDS) on ATG8.

In yeast, Atg39 regulates the degradation of the perinuclear ER/nucleus under nitrogen-deprivation conditions. Atg40, the yeast homolog of FAM134B, is a receptor for ERphagy (Mochida et al., 2015).

Nuclear receptor coactivator 4 (NCOA4) is the cargo receptor for ferritin during ferritinophagy in mammalian cells (Dowdle et al., 2014). After internalization with transferrin, iron may either be transported to specific target proteins by chaperones, enter the mitochondrial matrix through mitoferrin 1 or mitoferrin 2, or become stored in the cytosol by binding to ferritin. Iron stored within cytosolic ferritin can be released during lysosomal degradation or proteasome degradation. The delivery of iron to the mitochondria relies on the lysosomal degradation of ferritin. NCOA4 binds to ferritin and targets it to lysosomes through the autophagy pathway. Iron accumulation has been seen in some neurons that are the brain's iron reservoir, storing iron in the form of ferritin, as the blood-brain barrier limits some forms of iron from entering the brain. Iron chelators have been used to treat some other neurodegenerative diseases, including Parkinson's disease. However, excess degradation of ferritin induces ferroptosis by releasing chelated iron, which is subsequently transported back into the cytosol to induce oxidative stress (Kang et al., 2017).

Nearly half of the selective autophagy pathways identified to date are ubiquitin-driven. P62/SQSTM1, NDP52, NBR1, OPTN and TAXBP1 mediate the degradation of ubiquitinated cargos including mitochondria; they preferentially bind to linear and K63-linked chains and mono-ubiquitin compared to K48-linked chains (Wurzer et al., 2015).

1.1.2.2 UIM-UDS interface

Recently, a new class of ATG8 interactors was reported to exploit ubiquitin-interacting motif (UIM)-like sequences for binding to an alternative site on ATG8, named the ubiquitin-docking site (UDS). UIM-based ATG8 interactors play a role in clearing non-functional CDC48/p97 complexes, including some impaired in human disease.

Six proteins were found to be UIM containing adaptors. Of these, four (Epsin (EPN)-1, EPN2, EPN3, and Rabenosyn (RBSN)) interacted with both ATG8 isoforms, whereas two (Ataxin (ATXN)-3 and ATXN3L) interacted only with GABARAP (Marshall et al., 2019).

The preference of ubiquitin pathway players towards GABARAP has been reported before. Parkin-dependent mitophagy strongly relies on GABARAP dependent flux (Nguyen et al., 2016). GABARAP is more prone to proteasome degradation (Rasmussen et al., 2017). GABARAP may be more tightly regulated than LC3 due to its extra roles in vesicle trafficking. For example, GABARAP transports $GABA_A$ receptors to the plasma membrane (PM) in neurons although itself is not present on the PM, and is required for early secretory pathway (Leil et al., 2004). $GABA_A$ receptors are anionic channels that carry gamma-aminobutyric acid (GABA), which is the main inhibitory neurotransmitter in the adult central nervous system (Lester et al., 2004).

1.1.3 Autophagy and diseases

Autophagy dysfunction is implicated in neurodegeneration, metabolic diseases, cancer and infectious disease in varying roles (reviewed in Menzies, 2017 and Jiang et al., 2014).

1.1.3.1 Neurodegeneration diseases

Many genes are implicated in neurodegenerative diseases. For example, phosphatase and tensin homolog-induced putative kinase 1 (PINK1) (Valente et al., 2004) and the E3 ubiquitin ligase Parkin (Kitada et al., 1998), which are involved in mitophagy, are associated with autosomal recessive forms of Parkinson's Disease (PD). Mice with some core autophagy genes knocked out by the Nestin-Cre promoter embryonically all show early on-set neurodegeneration in the brain in neuronal precursor cells. These genes include ATG5, ATG7, FIP200, WIPI4 and ULK1/2 (reviewed in Menzies et al., 2017). Stimulation of autophagy by Beclin-1 overexpression reduces aggregates and reverted memory deficits in AD mice (Barnett and Brewer et al., 2011). Generally, autophagy is cytoprotective in neurodegenerative

diseases although amyloid β (Aβ), which forms plaques extracellularly in Alzheimer's Disease (AD), seems to be both degraded (Boland et al., 2008) as well as generated and secreted by autophagy (Yu et al., 2005; Nilsson et al., 2013).

1.1.3.1.1 BPAN

De novo mutations in WIPI4 were found to be causative for static encephalopathy in childhood with neurodegeneration in adulthood (SENDA), also known as BPAN (beta-propeller protein-associated neurodegeneration). SENDA or BPAN is an X-linked dominant subtype of neurodegeneration with iron accumulation (NBIA), a heterogeneous disorder characterized by neurological movement disorder and progressive degeneration of the nervous system (Saitsu et al., 2013). Iron deposition in the substantia nigra (SN) and globus pallidus (GP) is a diagnostic marker for BPAN but only becomes evident some years after disease onset, so the diagnosis of this disease is often quite late (Russo et al., 2018).

In lymphoblastoid cell lines derived from BPAN patients, mutations in WIPI4 result in truncated proteins that are prone-to-degradation, leading to lower amounts of protein compared to unaffected individuals. These cells showed impairment in autophagy flux and accumulation of LC3-positive autophagosome membranes that were also positive for ATG9 (Saitsu et al., 2013). These observations provide evidence that autophagy defects due to WIPI4 depletion are associated with neurodegeneration in BPAN. CNS-specific *Wdr45* knockout (*Nes-Wdr45*$^{fl/Y}$) mice generated by Zhao et al. recapitulate some phenotypes of BPAN, for example, impaired motor coordination, axon swelling and cognitive defects. Also, ubiquitin-positive protein aggregates and p62 accumulated in neurons and swollen axons of these mice, suggesting a blockage of autophagy flux. This model corroborates the link between the autophagy defect and pathogenesis of BPAN (Zhao et al., 2015). In addition to the link with BPAN, WIPI4 has been found to be overexpressed in pancreatic and kidney cancer samples (Proikas-Cezanne et al., 2004).

1.1.3.1.2 Huntington's disease and polyglutamine disorders

Huntington's disease (HD) belongs to a family of nine diseases caused by the expansion of cytosine-adenine-guanine (CAG) repeats in the coding region of genes. The CAG repeat expansions cause various effects depending on the gene context. Spinocerebellar ataxias (SCA) 1, 2, 3, 6, 7, 17 are caused by CAG repeat expansions in the Ataxin 1, 2, 3, 6, 7 and TBP genes and affect primarily the cerebellum and brainstem. Dentatorubralpallidoluysian

atrophy is related to the Atrophin 1 gene and affects the cerebellum as well as the cortex and midbrain (Nagafuchi et al., 1994; Zoghbi et al., 2000; Nagafuchi et al., 1994). Except for X-linked spinobulbar muscular atrophy, which is related to the androgen receptor (Spada et al., 1991), all are autosomal dominantly inherited.

Huntingtin (Htt) codes for a 348 kDa protein with CAG repeats in its N-termini, which translates into a homomeric polyglutamine (polyQ) stretch. HD develops when the polyQ stretch exceeds a threshold of 36 glutamines, and its length is inversely proportional with the age of onset of the disease (Narain et al., 1999). Wild-type Huntingtin protein positively regulates selective autophagy in stress conditions by binding and releasing ULK1 from mTOR and facilitating the interaction of the adaptor protein p62 with LC3 (Rui et al., 2015). However, the dominant inheritance pattern and evidence in model animals suggest that the toxicity of mutant HTT, rather than the loss of wild type HTT, is the primary cause of the disease (Bates, 2003).

Mutant HTT causes neurodegeneration by both PolyQ-HTT fibrils and intermediates/oligomers formed during the aggregation or degradation process (Sarkar et al., 2008). Although it is disputed whether polyglutamine expansion containing proteins including mutant-HTT, mutant ATXN-1, ATXN-3, impair the ubiquitin-proteasome pathway (Bence et al., 2001; Bennett et al., 2007, Bett et al. 2006), the soluble form of mutant HTT is found to be degraded by the proteasome (de Pril et al., 2010), and UBR5 has recently been identified to target it to proteasomes in iPSCs derived from Huntingtin's disease patients (Koyuncu et al., 2018). In addition, the soluble huntingtin mutant protein is also toxic and competes with protective deubiquitinating enzyme Ataxin 3 for binding with Beclin-1, thereby inhibiting autophagy. In the brain samples from HD patients, Beclin-1 levels and LC3-II levels decreased (Ashkenazi et al., 2017).

1.1.3.2 Cancer

The role of autophagy in metastatic progression is highly context-dependent. On the one hand, autophagy may decrease migration and inhibit cell cycle progression. FAK and SRC, key regulators of focal adhesion dynamics, are both regulated by autophagy (Abbi et al., 2002; Sandilands et al., 2011). On the other hand, autophagy may increase the viability of cancer cells and promote tumour progression. Deletion of ATG7 in K-ras^{G12D}-driven tumours causes shrinkage of the tumour (Xie et al., 2015). Arginine recycling facilitated by autophagy maintains tumor (Poillet-Perez et al., 2018).

1.2 Ubiquitination-proteasome system

1.2.1 Machinery

1.2.1.1 The ligase cascade

Ubiquitination is the covalent attachment of ubiquitin onto proteins to signal for proteasome degradation and other proteasome-independent processes including signalling, translocation, activation/ inactivation. The conjugation of ubiquitin is a cascade event that involves three ligases: E1, ubiquitin-activating enzyme; E2, ubiquitin-conjugating enzyme; and E3, ubiquitin ligases (Hershko et al., 1996).

E1 forms a thioester bond with the C-terminal glycine of ubiquitin in an ATP-dependent manner. The E1-ubiquitin conjugate is then transferred onto the activating cysteine of E2. The catalytic cysteine on the E3 enzyme can receive ubiquitin from the E2 and then conjugate it onto the substrate proteins (Hershko et al., 1983).

Each of the seven lysine residues on ubiquitin molecules and the N-terminal methionine residue (M1) can be linked with one or more ubiquitin molecules. The composition, including mono- or multi-Ub and the exact Ub chain, determines whether the protein is going to be degraded, and which signalling pathway the substrate protein may function in. Substrate-conjugated ubiquitin can be further modified by other post-transcriptional modifications, such as phosphorylation, and acetylation, further complicating the signalling of ubiquitination.

K48 poly-ubiquitination is the most abundant linkage type and usually signals for delivery to the proteasome for degradation (Rotin and Kumar, 2009). K11 and K27 linked ubiquitin chains also label their substrate for proteasome degradation. The K11-K48 branched-chain modulates proteasome degradation of misfolded nascent proteins and mitotic regulators (Collins et al., 2017).

K63-linked ubiquitination is the second most abundant type. Homogeneous K63 chains regulate signal transduction, endocytosis (Komander et al., 2012) and have an affinity for autophagy adaptors and receptors (Linares et al., 2013). K63 chains seeded with branched ubiquitin chains can trigger proteasomal degradation (Ohtake 2018).

Other types of lysine ubiquitination, as well as their associated function(s), are K6 (involved in DNA repair), K29 (lysosomal degradation, kinase modification) and K33 (kinase modification (Komander, 2009).

The linkages between ubiquitin molecules themselves and between ubiquitin molecules and their substrates can be hydrolyzed by deubiquitinating enzymes (DUBs) (de Poot et al., 2017), and therefore, ubiquitination is a reversible process.

1.2.1.2 The 26S proteasome

The 26S proteasome is made of the core barrel-like structure 20S proteasome and the 19S capping proteins at either end. The latter are responsible for recognising and binding of substrates (or ubiquitin receptor shuttling), deubiquitination, substrate unfolding and translocation onto the 20S core (Livneh et al., 2016). The proteasome substrates are degraded by three enzymatic mechanisms of action (trypsin-like, chymotrypsin-like and caspase-like) (Grice and Nathan, 2016).

Because of the barrel structure of the core 20S subunit, proteasome subunits need to be unfolded into peptide chains before entering. Therefore, aggregated proteins and oligomers are considered resistant to degradation by the proteasome (Verhoef et al., 2002).

1.2.2 N-end rule

1.2.2.1 Machinery and function

It has been found that the single N-terminal (Nt) residue of a protein is related to the *in vivo* half-life of the protein (Bachmair et al., 1989). In eukaryotes, substrate proteins with specific N-terminal residues are recognized by UBR-box-containing E3 ubiquitin ligases and delivered for proteasome degradation. Sometimes, additional post-transcriptional modification is required for this recognition. This destabilization of a protein by posttranslational modification of the N-terminal residues was named the ‘N-end rule’ (Sriram et al., 2011; Varshavsky, 2011), and the destabilizing N-termini residues are referred to as ‘N-degrons’.

In mammalian cells, unacetylated Nt-residues are targeted by Arg/N-degron pathway. The N-degrons of this pathway are classified into Type 1 and Type 2 (Diagram 1.5):

Type 1: positively charged, include Arg, Lys, and His.

Type 2: bulky hydrophobic, include Phe, Tyr, Trp, Leu, and Ile.

The major and strongest of them is Nt-Arg, which can also be generated by the conjugation of the amino acid L-Arg to Nt-Asp or Nt-Glu by R-transferase ATE1. Arginylation also occurs on Nt-Asn, Nt-Gln, and Nt-Cys following Nt-post-translational modifications. The residues that can be arginylated are called secondary or tertiary N-degrons. For example, regulators of G protein signaling RGS4 and RGS5, which have Nt-Cys, undergo ATE1 catalysed arginylation on its oxidized Nt-Cysteine and are then degraded by UBR1 and UBR2 (White et al., 2017; Lee et al., 2005). Hypoxia perturbs the proteolysis of RGS4 and RGS5 by inhibition of the oxidation of Nt-Cys.

The N-degrons first need to be exposed by aminopeptidase-mediated removal of the N-terminal methionine. Methionine aminopeptidase 1 and 2 in mammalian cells remove the Nt-Met efficiently when the penultimate amino acid has a side chain smaller than Valine's in both prokaryotes and eukaryotes, although there are a lot of variations regarding different species. Also, the glutamyl-aminopeptidase and leucine aminopeptidase cleave Nt-Methionine when the penultimate amino acid is lysine in *M. hyopneumoniae* (Berry et al., 2017).

In mammalian cells, UBR1, UBR2, UBR4 and UBR5 recognise Arg/N-degrons through their UBR domains (reviewed in (Kim et al., 2013)) and are named as 'N-recognins'. Only UBR5 preferentially binds type 1 N-degrons (Tasaki et al. 2009). Recently, p62 was found to bind Arg/N-degrons through its ZZ domain, but it is not an E3 ligase (Yoo et al., 2018). An N-recognin can contain several degron-recognizing sites, suggesting that an N-recognin-E3 ligase can bind not only to N-degrons but also to internal degradation signals in proteins that lack an N-degron (Varshavsky et al., 2011).

The substrate-selection of N-recognins requires multistep interactions. First, the UBR box of the E3 ligase forms transient and reversible hydrogen bonds with the free α-amino group of the N-degron. Second, the UBR box forms hydrogen bonds with the positively charged side chains in type 1 degrons and the bulky hydrophobic side chains in type 2 degrons. In a type 1 interaction, these hydrogen bonds are stabilized by a salt bridge formed between the negatively charged surface of the UBR box and a positively charged N-terminal side chain. Third, after the N-recognin binds the N-terminal residue, the side chain of the second residue may further support the interaction, whereas the side chain at position three is located away from the surface of the binding groove (Choi et al., 2010), restricting the major interactions to the first two residues.

The function of the Arg/N-Degron pathway is not limited to degradation. It can also transport a substrate that has a destabilizing Nt-residue but lacks an efficacious second-determinant lysine (Turner et al., 2000). With a similar mechanism, an Arg/N-recognin could polyubiquitylate in trans another subunit of the same complex, or, in other words, bind to one N-degron containing subunit but degrade another subunit with internal degrons (Johnson et al., 1990).

Two other N-end rule pathways, the Ac/N-degron (Hwang et al., 2010) and Pro/N-Degron (Chen et al., 2017) pathways targeting acetylated and N-terminal-Proline substrates respectively, have been identified recently.

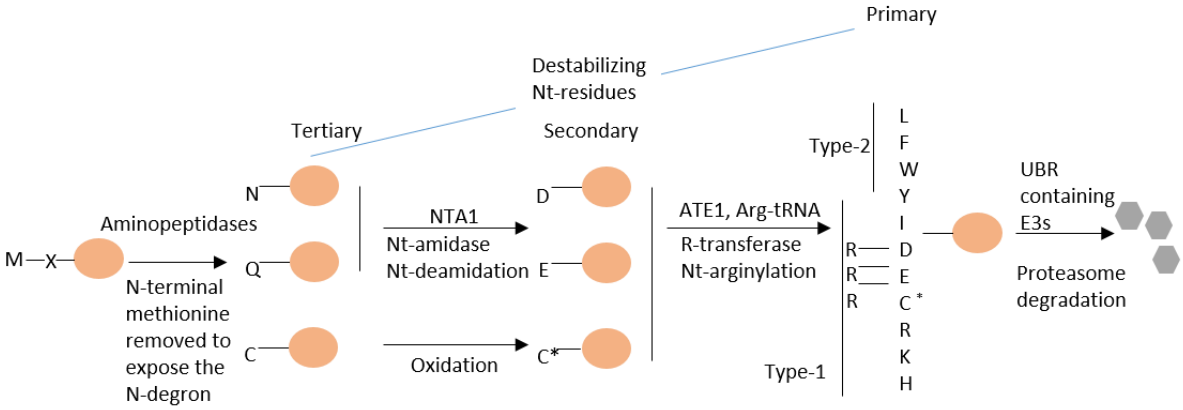

Diagram 1.5 N-degron pathways in eukaryotes

Modified from Varshavsky et al., 2019 with permission (nonexclusive License to Publish) .
Nt-residues are indicated by single-letter abbreviations. A orange oval denotes the rest of a protein substrate. Aminopeptidases remove the N-terminal methionine of the target protein to expose the N-degron. The N-terminal amidase NTA1 then deamidates tertiary destabilizing N-terminal residues Asn and Gln into secondary destabilizing N-terminal residues Asp and Glu, respectively. Subsequently, the arginyltransferase ATE1 attaches Arg to the N-terminal Asp or Glu. Eventually, UBR box containing E3 ligases recognize the type-1 or type-2 primary destabilizing N-terminal residues and target these substrates for polyubiquitylation and subsequent proteasomal degradation. N-terminal Cys oxidation-dependent degradation pathway has been found in mice and plants, but has not yet been established in yeast (Lee et al., 2005).

1.2.2.2 UBR5, a representative E3 ligase of the N-end rule pathway

1.2.2.2.1 UBR5 structure

UBR5 (309kDa) is predicted to have four domains and two nuclear localization sequences as shown in Diagram 1.6: Ubiquitin associated (UBA) domain, Ubiquitin Recognin Box (UBR), domain homologous to C-terminus of Poly-Adenylation Binding Protein (PABC, also called MLLE), and homologous to E6-AP C terminus (HECT) domain. There are also two nuclear localization sequences (NLSs) in UBR5 (reviewed in (Shearer et al., 2015)).

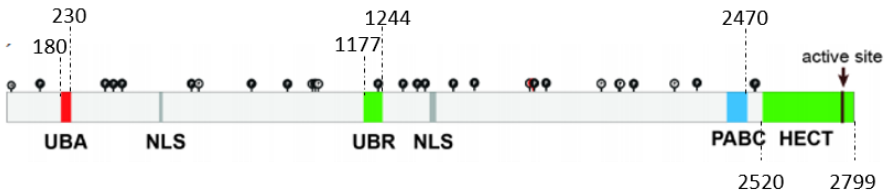

Diagram 1.6 Functional domains and known posttranslational modification sites of UBR5

Modified with permission from Shearer et al., 2015.
HECT: Homologous to E6AP carboxyl terminus domain. The catalytic cysteine in domain is indicated by the arrow.
UBA: the ubiquitin-associated protein domain.
NLS: nuclear localization sequence.
UBR: the Ubiquitin Recognin Box.
PABC/MLLE: mademoiselle domain or homologous to the C-terminal region of Poly-Adenylation Binding Protein domain.

The UBA domain binds to ubiquitin and has no strong preference for binding to polyubiquitin chains over monoubiquitin (Kozlov et al., 2007), and therefore may be involved in protein-protein interaction. The UBR domain is a zinc finger-like domain involved in recognition of type 1 N-degrons. PABC (MLLE) domain is predicted to interact with RNA and Paip1/2 (Kozlov et al., 2004; Lim et al., 2006), facilitating UBR5's function in mRNA translation. It also regulates the catalytic activity of UBR5 by binding onto the catalytic HECT domain and inhibiting its binding to substrates (Munoz-Escobar et al., 2015).

1.2.2.2.2 UBR5 function

UBR5 assembles K48/K63 branched linkages on K63-ubiquitinated TXNIP (Ohtake 2018). UBR4 and UBR5 regulate quality control for the synthesis of K11/K48 branched chains during proteotoxic stress, with UBR5 generating K48 linkage from the initially mixed conjugates (Yau et al., 2017). UBR5 binds K63-linked diubiquitin more strongly than ubiquitin monomers or K48-linked diubiquitin with its UBA domain (Ohtake 2018) and can possibly bind to working ribosomes with its RNA binding domain (Yau et al., 2017). Altogether, UBR5 seems to regulate heterotypic/branched chains in different contexts, presumably in collaboration with different E3s.

UBR5 negatively regulates double-stranded break repair of DNA by counteracting excessive spreading of ubiquitin conjugates and ubiquitin-regulated genome caretakers to undamaged chromosomes. UBR5 inhibits the K63-linked polyubiquitination of histone H2A by degrading RNF168 (Gudjonsson, 2012). Lysine-63-linked ubiquitin polymers on H2A and H2AX generate an interaction platform for chromatin-associated repair and signalling factors, including 53BP1

and the RAP80/BRCA1 complex (Bothmer et al., 2010 & 2011; Bouwman et al., 2010; Bunting et al., 2010; Coleman and Greenberg, 2011; Hu et al., 2011). In addition, UBR5 generates K48 ubiquitination of Groucho/TLE, a repressor of the Wnt enhanceosome. The ubiquitination of Groucho/TLE stabilizes β-catenin, which relieves chromatin compaction and stimulates the Wnt pathway (Flack et al., 2017).

To summarize, UBR5 has been found to regulate mRNA translation and quality control of proteins, as well as to inhibit excessive DNA repair and induce Wnt signalling.

1.2.2.2.3 Disease implications of UBR5

Neurodegenerative diseases

c.5720G>A mutation (p.Arg1907His) in the UBR5 gene was found to be associated with familial adult myoclonic epilepsy (FAME) in a Japanese FAME family (Kato et al., 2012) but no additional mutation in UBR5 was found in other pedigrees (van Rootselaar et al., 2017). FAME usually starts in the second decade of life and has been genetically associated with 4 different loci (8q24, 2p11.1-q12.2, 5p15.31-p15 and 3q26.32−3q28) (Lagorio et al., 2019). It is slowly progressive with intellectual decline and worsening of both tremor and myoclonus.

In addition, UBR5 has been found to promote the degradation of mutant HTT aggregates in iPSCs from HD patients (Koyuncu et al., 2018).

Cancer

UBR5 is involved in various areas of cancer biology, such as regulation of DNA damage (Zhang et al., 2014), metabolism (Jiang et al., 2011), transcription (Ong et al., 2014), and apoptosis (Henderson et al., 2006). Although it is unclear whether UBR5 promotes or inhibits tumour progression, presumably depend on context (Shearer et al., 2015), UBR5 amplification is the predominant genetic alteration in many types of cancers (far more prevalent than loss-of-function UBR5 mutations), and amplified UBR5 correlates with poor outcomes in breast cancer (Shearer et al., 2015).

1.3 Crosstalk between autophagy and proteasome pathways

The autophagy and the ubiquitin-proteasome system mutually regulate each other.

1.3.1 Selective autophagy degradation of ubiquitinated substrates

As discussed before, autophagy pathways degrade ubiquitination substrates through adaptors or receptors. Although most of them recognize K63 linked chains, both K48 and K63-linked ubiquitination substrates can be degraded by autophagy. For example, BAG3 delivers K48-linked ubiquitinated proteins to lysosomes through directly binding to K-48 and p62 (Rosati et al., 2011) in aggrephagy. Consistently, all ubiquitin chain types have been found enriched in the insoluble inclusions of autophagy-deficient mice (Riley et al., 2010).

1.3.2 The ubiquitin-proteasome system both induces and inhibits autophagy

Given the central role of ULK1 and PI3K–III kinase complexes in autophagy induction, the ubiquitination signals on these complexes indicate that autophagy is also regulated by the ubiquitin-proteasome system.

1.3.2.1 K63-ubiquitination induces autophagy

TRAF6 ubiquitinates ULK1 with the assistance of AMBRA1 by K63-linked chains, which promotes the self-association of ULK1 and thereby autophagy induction (Yeh et al., 2011; Nazio et al., 2013). BECLIN 1 is also a substrate of TRAF6 (Shi et al., 2010). The K63 and K117 ubiquitination on BECLIN inhibits its binding with BCL2, thereby inducing autophagy.

1.3.2.2 Degradative ubiquitination regulates autophagy termination

BECN 1 is ubiquitinated and degraded by the HECT-type E3 ligase through NEDD4 Lys-11-linked chains (Platta et al., 2012). ULK1 is degraded by NEDD4L, an E3 ligase highly homologous to NEDD4, via K27 and K29-linked polyubiquitination (Nazio et al., 2016). Another E3 ligase, CULLIN3–KHLH20, degrades ULK1, BECLIN 1, and VPS34 via K48 poly-Ub chains (Liu et al., 2016). In addition to E3 ligases, the wild-type ataxin 3 protects BECN 1 from proteasome-mediated degradation by its deubiquitination activity (Ashkenazi et al., 2017).

Altogether, the proteasome pathway may regulate the induction and termination of autophagy, either by modulating their protein levels or through activation by K63-linked ubiquitination (reviewed in Dikic et al., 2018).

1.4 Objectives

WIPI4 degradative mutations are the only causative mutations in BPAN diseases. In lymphoblastoid cell lines derived from BPAN patients, the autophagy flux was blocked (Saitsu et al., 2013), suggesting that WIPI4 depletion caused autophagy impairment is related to the BPAN pathology. However, it is unknown how WIPI4 regulates the autophagy pathway. The following work will try to understand the function of WIPI4 in the autophagy pathway and also investigate novel autophagy regulators came across within this process.

Chapter 2 Materials and Methods

2.1 Cell culture

2.1.1 Cell lines

HeLa cells, C2C12 cells and HEK293 cells were cultured in basal media: Dulbecco's Modified Eagles Medium (DMEM; Sigma D6546), supplemented with 10% Foetal Bovine Serum (FBS; Sigma F7524), 1% penicillin-streptomycin (Sigma P0781) and 1% L-glutamine (Sigma G7513). Stable cell lines (HeLa cell lines stably expressing mRFP-GFP-LC3 or GFP-Rab11 constructs were maintained with culture medium supplemented with 500 µg/mL G418 (Sigma). All lines were incubated at 37°C with 5% CO2. The HeLa GABARAP family-/- (referred to as HeLa GABARAP TRIPLE KO) cells were a gift from Prof M. Lazarou. Flp-In T-REx cell line integrated with GFP-p62 (Invitrogen, R780-07) is grown in the culture medium supplemented with 100 µg/mL hygromycin B (Calbiochem, 400051) and 7.5 µg/mL blasticidin (Invitrogen, R210-01). The expression of p62 was turned on or off by adding or removing 1 µg/mL tetracycline (Sigma, T7660) to the cells for 24 hours. Cells are tested for mycoplasma contamination every other week.

HeLa cell lines in which ATG16L1 was knocked out (referred to as HeLa ATG16L1 KO) were generated by Dr Maria Jimenez-Sanchez using double nickase Cas9. Each guide RNA results in cleavage of only one DNA strand, because only one of the two endonuclease sites of Cas9 is active using nickase Cas9. Therefore, two guide RNAs are required for a double-strand break, increasing the accuracy of the cleavage. Guide RNAs were designed to target the first exon of ATG16L1 and cloned into pSpCas9n(BB)-2A-GFP (PX461: Addgene #48410). This construct was transfected into HeLa cells, and single-cell clones were grown following fluorescence-activated cell sorting (FACS). Complete knockout of ATG16L1 was confirmed using Western blotting. HeLa cells expressing the Cas9 backbone are selected by the same way and used as a control cell line, referred to as HeLa ATG16L1+ CTRL.

2.1.2 Splitting cells

Cell lines were passaged when around 90%-100% confluent in T75 (75 cm2 area) flasks (Corning). When passaging, the media was aspirated first using a vacuum pump. Then cells were pre-washed with 3 mL phosphate buffered saline once to remove all the serum and then dissociated from the flask with 2 mL Trypsin-EDTA solution (Sigma) at 37°C for 5 minutes. The trypsin was then inactivated by mixing with 8 mL complete DMEM. Usually, the cell number was counted before seeding with countess slides (Invitrogen).

2.1.3 Drugs and reagents

Drugs and reagents used in this work are listed in Table 1.

Drug	**Action**	**Source**	**Experimental conditions**		**chapter**
			Working concentration	**Time**	
Bafilomycin A1	Lysosomal inhibitor	Enzo Sciences (BML-CML-0100)	100-400 nM	4-18 h	4,5,6
2-Iodoacetamide	Deubiquitinase inhibitor	Sigma (I1149)	10 mM	n/a	5,6
Cycloheximide	Inhibitor of translation	Sigma (C7698)	50 µg/mL	4-8 h	5,6
EBSS	Starvation media	Thermo Fisher (24010043)	n/a	45 minutes – 4 hours	4,5
Lysosensor	Label neutral (blue) and acidic (yellow) lysosomes	Yellow/Blue DND-160 (L7545)	50 nM	20 minutes	4
MG132	Proteasome inhibitor	Sigma (C2211)	10 µM	6 h	5,6
Mg2+ ATP	*In vitro* ubiquitination assay	Sigma (A2383)	2 mM	n/a	6

N-Ethylmaleimide	Deubiquitinase inhibitor	Sigma (E3876)	20 to 25 mM	n/a	5,6
Nocodazole	Microtubule depolymerization	Sigma (M1404)	5 µM	3 h	4
Phosphotase Inhibitor Cocktail 2	Protecting the phosphorylation modification	Sigma (P5726)	1%	n/a	4,5,6
Phosphotase Inhibitor Cocktail 3	Protecting the phosphorylation modification	Sigma (P0044)	1%	n/a	4,5,6
PMSF	Protease inhibitor	Sigma (78830)	1 mM	n/a	4,5,6
Protease Inhibitor cocktail tablet	Protecting proteins in cell lysates from being degraded by proteases	Roche Diagnostics (#11873580001)	1 in 2 mL ddH2O to make 25 × stock solution	n/a	4,5,6
Proteinase K	Cleavage of LC3-II to quantify the ratio of unsealed autophagosomes	Sigma (P2308)	0.5% to 2% of the total protein	5 min -30 min	4

Table 2: Drugs and reagents used in this work.

2.1.4 Transfection protocol

For siRNA, the transfection was performed using Lipofectamine 2000 transfection reagent (Life Technologies #11668019). In accordance with the manufacturer's protocol, 2.5 µl oligos were diluted in 100 µl opti-MEM (Gibco), 5 µl Lipofectamin 2000 in another 100 µl opti-MEM. Both the solutions were incubated at room temperature for 5 minutes. Then diluted Lipofectamine 2000 was added into the oligo solution drop by drop, and the mixture was incubated for 20-30 minutes. Opti-MEM was then added to the mixture (~208 µl) to make 1 mL solution. The solution was then added into one well of a 6-well plate and incubated in 37°C incubator for at least 4 hours, then changed to complete media. For two-round knockdown experiments, the transfection procedure was repeated on day 3 (48 hours later). After 72 hours or 96 hours, cells were harvested after treatment. Treatment of cells by Baf A1/ EBSS/ DMSO was carried

out 48 h after the final round of siRNA treatment. The cells were split in between if necessary. Cells were transfected at 70-80% confluency.

For DNA, the transfection was performed using TransIT 2020 (Mirus Bio #MIR5400) with a procedure similar to above. Transfection reagent (5 µl) was used for each well of a 6-well plate.

Target	Type	siRNA transfected per well of a 6-well plate (nM)	Incubation period	Chapter
WIPI4	SMARTpool	100 or (60 + 50)	72 h or 96 h	4,5,6
WIPI4	Individual siRNAs	60 + 50	96 h	4,5
ATE1	SMARTpool	50	72 h	6
ATG2A	SMARTpool	100 + 50	96 h	4
ATG2B	SMARTpool	100 + 50	96 h	4
GABARAP	SMARTpool	100 (or 37.5 when three family members are knocked down together)	72 h	5
GABARAPL1	SMARTpool		72 h	5
GABARAPL2 (GATE16)	SMARTpool		72 h	5
MIB1	SMARTpool	100	72 h	5
UBR4	SMARTpool	50	72 h	5,6
UBR5	SMARTpool	25	72 h	5,6
UBR5	Individual siRNAs	25	72 h	6

Table 3: siRNAs used in this work.

2.1.5 SiRNAs

siRNAs were ordered from Dharmacon (GE Healthcare). Details of siRNAs used in this work can be found in Table 2. siRNA in tubes was centrifuged at 5000 rpm for 5 minutes to bring the all the powder to the bottom of the tube, then dissolved in 1 × RNAase free buffer (Dharmacon) to make a 20 µM stock. The starting working concentration is 50 nM. In further experiments, the working concentration of siRNA was adjusted according to the knockdown efficiency and cell status after transfection.

2.1.6 Constructs

pMRXIP-GFP-hATG2A was a kind gift from Mizushima Lab (Velikkakath et al., 2012). RFP-LC3 was a kind gift from Yoshimori Lab (Kabeya et al., 2000), which is a rat protein. pEGFP–HTT exon-1-Q74 is a lab reagent. GFP-WIPI4, HA-ubiquitin, GFP-UBR5, GFP-UBR5-C2768A, Tag2B-UBR5 and Tag2B-UBR5-C2768A are from Addgene. pEGFP-C1 is from Clontech. pFLAG-CMV-5a is from Sigma.

nGFP-GABARAP, nGFP-GABARAPL1 and nGFP-GABARAPL2 were generated by cloning the coding sequence of relevant genes ordered from GeneScript onto the pEGFP-C1 backbone.The restriction sites used are: HindIII and BamHI (for GABARAP); EcoRI and BamH-I (GABARAPL1); EcoRI and KpnI (GABARAPL2). The plasmids were propagated in E.coli. High-efficiency DH5α competent cells (Bioline US Inc) were used for transformation according to the manufacturer's protocol. Plasmid isolation was performed using a Maxi prep isolation kit (Life technologies #K210017). The concentration was measured with a spectrophotometer (Nanodrop1000, Thermo Scientific) and TE buffer as a blank.

2.1.6.1 Site-directed mutagenesis

Point mutations were introduced into nGFP-GABARAP constructs using the Q5 Site-Directed Mutagenesis kit (NEB E0554S) according to the manufacturer's instructions. Primer sequences are found in Table 3. GABARAP mutant constructs were sequenced with universal primers. Flag-UBR5 was generated by Addgene by deleting the c-termini His tag from the Tag2B-UBR5 construct. UBR5 constructs were sequenced with both CMV-F and UBR5-2637-F (CACAGAATGTTGGTAGTTG) depending on the region of interest.

DNA construct	Mutation	Primer sequence
nGFP-K2P-Forward	K2P	CAAGCTTATGccGTTCGTGTACAAAGAAG
nGFP-K2P-Reverse		GCTCGAGATCTGAGTCCG
nGFP-G116A-Forward	G116A	AGTGTCTACGcTCTGTGAGGATC
nGFP-G116A-Reverse		TTCGTCACTGTAGGCAATG

Table 3: Primers used in site-directed mutagenesis.

2.2 Western blotting

2.2.1 Harvesting cells

Cells were harvested by Lysis buffer or Laemmli buffer.

When protein quantitation using Bradford's method is essential, for example, when samples vary in confluence or the lysates would be used for detecting aggregation clearance, lysis Buffer is necessary. Protein concentrations were assayed using the BioRAD DCTM Protein Assay kit (a modified Lowry protein assay; BioRAD 5000112) and quantified at 750 nm using a plate reader. Protein concentrations were then adjusted for each sample. Samples were loaded onto gels and the remainder frozen at -20°C.

Lysis Buffer B recipe:

10 mM Tris pH6.8, 68.5 nM NaCl, 0.5 mM EGTA, 1% Triton X100, 5% glycerol, protease inhibitor (Roche) and phosphatase inhibitors (cocktails 2 and 3 from Sigma).

If samples are of similar confluence, Laemmli buffer is advantageous because it shortens the process and reduces errors and variance.

2 × Laemmli Buffer recipe:

62.5mM Tris pH 6.8, 2% w/v SDS, 10% glycerol, 50 mM DTT, 0.01% w/v bromophenol blue. Cells were scraped with a scraper and lysates were mixed well before transferring into cold Eppendorf tubes. Samples were boiled for 5 minutes at 100°C.

Target	Host	Type	Company	Application	Chapter
Actin	rabbit	polyclonal	Sigma (A2066)	WB	3,4,5
ATE1	mouse	monoclonal	Santa Cruz (Sc271220)	WB	5
ATG2A	rabbit	polyclonal	Cell signalling (15011S)	WB/ IF	3,4
ATG16L1	rabbit	monoclonal (D6D5)	Cell Signalling (8089)	IF	3
CD63	mouse	monoclonal	Abcam (ab8219)	IF	3
CATHEPSIN D	mouse	monoclonal	BD Biosciences (610801)	WB	5

GABARAP	rabbit	polyclonal	Abgent (AP1821A)	WB/IF	4,5
GABARAPL1	rabbit	polyclonal	Abcam (ab86467)	WB/IF	4,5
GABARAPL2 (GATE16)	rabbit	polyclonal	MBL (PM038)	WB/IF	4,5
GAPDH	mouse	monoclonal, 6C5	Abcam (ab8245)	WB	5
GFP	rabbit	polyclonal	Clontech (632592)	WB, IP	3
GM130	mouse	monoclonal (clone 35)	BD Biosciences (610822)	IF	5
K48-linked ubiquitin	rabbit	polyclonal	Cell signalling (8081)	WB	4,5
K63-linked ubiquitin	rabbit	polyclonal	Cell signalling (5621)	WB	4,5
LC3B	rabbit	polyclonal	Novus Biologicals (NB100-2220)	WB	3,4
LC3B	rabbit	polyclonal	Abcam (ab192890)	WB/IF	3,4,5
MIB1	rabbit	polyclonal	Sigma (M5948)	WB	4,5
P62	mouse	monoclonal	BD Biosciences Transduction Lab (610833)	WB	5
p62	rabbit	polyclonal	MBL (PM045)	WB	5
PCM1	mouse	monoclonal	BD Biosciences (610822)	IF	4
Γ-tubulin	mouse	monoclonal	Sigma (GTU-88/ T6557)	IF	4
TGN46	rabbit	polyclonal	A kind gift from Dr Matthew Seaman	IF	6
Tubulin (α)	mouse	monoclonal (DM1A)	Sigma (T9026)	WB	5
WIPI4	rabbit	polyclonal	Proteintech (19194-1-AP)	WB/IF	3,4,5
WIPI4 (229-240)	mouse	Monoclonal	Sigma (SAB1101582)	IF	3,4,5
Ubiquitin	mouse	monoclonal	MBL (D058-3)	WB	4
UBR4	rabbit	polyclonal	Abcam (ab86738)	WB	4,5

UBR5	rabbit	polyclonal	Bethyl laboratory (A300-573A)	WB	4,5

Table 4: Primary antibodies used in this work

Secondary antibodies				
Target	Conjugation	Host	Company	Application
Rabbit IgG	IR dye 680	goat	Licor (926-32221)	WB
Rabbit IgG	IR dye 800	goat	Licor (926-32211)	WB
Rat IgG	IR dye 800	goat	Licor (926-32219)	WB
Mouse IgG	IR dye 680	goat	Licor (926-68070)	WB
Mouse IgG	IR dye 800	goat	Licor (926-32210)	WB
Mouse IgG	HRP	sheep	GE Healthcare (NA931V)	WB
Rabbit IgG	HRP	donkey	GE Healthcare (NA934V)	WB
Goat IgG	HRP	rabbit	Thermo Fisher Scientific (611620)	WB
Rabbit IgG	Alexa 488	goat	Thermo Fisher Scientific (A11008)	IF
Rabbit IgG	Alexa 647	goat	Thermo Fisher Scientific (A21428)	IF
Rabbit IgG	Alexa 555	goat	Thermo Fisher Scientific (A21245)	IF
Mouse IgG	Alexa 488	goat	Thermo Fisher Scientific (A11001)	IF
Mouse IgG	Alexa 647	goat	Thermo Fisher Scientific (A21236)	IF
Mouse IgG	Alexa 555	goat	Thermo Fisher Scientific (A21422)	IF

Table 5: Secondary antibodies used for this work.

2.2.2 Western blotting protocol

Polyacrylamide gels were prepared freshly with the percentage dependent on the size of the proteins of interest. Gels were run using Tris-glycine running buffer (25 mM Tris, 192 mM glycine, 0.05% SDS). Equal volumes of the sample were loaded in each lane and any empty lanes loaded with 1X sample buffer. Either SeeBlue Plus2 Prestained Protein Standard (ThermoFisher LC5925) or PageRuler Plus Prestained Protein Ladder (ThermoFisher 26619) were used as molecular weight markers.

Gels were transferred using the wet transfer method on to PVDF membrane (Immobilon-FL for LiCor detection, Immobilon-P for ECL detection; Merck-Millipore IPFL00010 and IPVH00010 respectively). The transfer buffer was Tris-glycine (25 mM Tris, 192 mM glycine). Activation of the PVDF membrane is performed by soaking it in pure methanol for 5-10 s. For small proteins, 20% methanol transfer buffer is recommended. Since methanol interferes with SDS-binding of large molecular weight (MW) proteins, and the protein will precipitate if transferred in a high concentration of methanol, 10% or no methanol transfer buffer was used for large MW protein, including UBR4 and UBR5. On completion of transfer, the membrane was blocked in 5% Mavel milk or 3% BSA with PBST (0.5% Tween 20) for 1 hour, shaking in room temperature. Membranes were then stained with primary and secondary antibodies diluted in block buffer with washes between and after.

For antibodies that gave strong signals, fluorophore-conjugated secondary antibodies were used, and membranes were imaged directly using LI-COR, Odyssey. For WIPI4, GABARAP-II, GABARAPL1-II, GATE16-II, UBR5, UBR4, MIB1 and ATG2A, horseradish peroxidase-linked (HRP) secondary antibody in conjunction with electrochemiluminescent detection reagents (GE Healthcare) and X-ray film are required to detect the signal.

2.2.3 Antibodies

Primary antibodies used are detailed in Table 4, and secondary antibodies in Table 5.

2.3 Confocal Microscopy

For fixed imaging, cells were cultured on coverslips, fixed with 2% paraformaldehyde in culture medium for 12-15 minutes at room temperature, or by incubation in ice-cold methanol for 5 minutes at -20°C for endogenous LC3 staining. Cells fixed with paraformaldehyde are then washed twice with PBS, followed by permeabilization with 0.2% Triton X100 in PBS for 5 minutes. Cells were blocked with 1% BSA in PBS for 30 min and incubated with primary antibodies for 1-2 hours. After two quick washes with PBS and once with 1% BSA, samples were incubated with secondary antibodies for 1 hour and washed with PBS for three times. Samples were mounted with Prolong Gold anti-fade reagent (#P36935) with DAPI and observed using Zeiss instruments (LSM710, LSM780 and LSM880). Ten to fifteen images with a mean of 4 cells per image were taken per condition per experiment. Exposure settings were unchanged throughout acquisition. Images were processed with Zen.

For live-cell imaging, cells were seeded into 3 cm MatTek glass-bottomed culture dishes (MatTek Corporation P35G-1.0-14-C). The starting confluence was 0.3×10^6 per plate. When the confluency reached 1×10^6, Herpes buffer was added to a final concentration of 20 mM to maintain the pH in media. During imaging, cells were put in a 5% CO2, 37°C incubator. Imaging was performed within 3 hours.

2.4 GFP-Htt-Q74 aggregates assay

GFP-Htt-Q74 constructs (1.5 µg) were transfected 24 hours after the final round of siRNA knockdown. Two hundred GFP-Htt-Q74 transfected cells were selected and the number of cells with aggregates were counted using fluorescence microscopy. Slides were counted blind. The experiments were performed in triplicates and repeated at least twice.

2.5 Cathepsin L activity assay

Cathepsin L activity measurement was performed with the Cathepsin L Activity Assay Kit (Fluorometric) (Abcam ab65306) according to the manual. Cathepsin L activity is determined by the release of a fluorescent moiety generated by the cleavage of a synthetic substrate by Cathepsin L. Cell samples were harvested and centrifuged (5 minutes, 13000 x g, 4°C) to remove cell debris. CL buffer was added to samples along with 200 µM Ac-FR-AFC substrate and incubated at 37°C for 2 hours before fluorescence was determined.

2.6 Protease protection

HeLa cells were suspended in homogenization buffer (10 mM HEPES-KOH, pH 7.4, 0.22 M mannitol, 0.07 M sucrose, protease inhibitors and phosphatase inhibitors of the recommended concentrations in their manuals). The homogenization was done with 10 strokes using a syringe with a 27-gauge needle. The postnuclear supernatant was recovered by centrifugation at 300 × *g* for 5 minutes. The lysate was centrifuged at 100,000 × *g* for 30 minutes. The pellets were resuspended in the 30 mM Tris-Cl pH 7.4 buffer after 2 washes. To analyze detergent solubility, each sample was incubated with 1% Triton X-100 on ice for 30 min and then centrifuged at 100,000 × *g* for 30 minutes. To examine proteinase K sensitivity, each fraction was treated with the same amount of proteinase K (the raitio of proteinase K vs total protein is

1 to 100) on ice for 20 minutes. The samples were then denatured in 4 times SDS–PAGE sample buffer, immediately boiled, and analyzed by SDS–PAGE. 10 µg of total proteins were loaded for each sample.

2.7 Immunoprecipitation

GFP-tagged proteins (GFP-WIPI4, GFP-GABARAP and GFP) were pulled down using GFP-TRAP beads (ChromoTek, #gtma-100) according to the manufacturer's protocol, but with Lysis buffer B. Cells were washed with ice-cold PBS and incubated on ice for 30 minutes in Lysis buffer B. Cells were then scraped, and the lysate centrifuged at 13000 x g for 15 minutes at 4°C and the post-nuclear supernatant kept. A protein assay was carried out, and tubes set up for each IP sample with equal amounts of protein in each and the volume adjusted to 0.5 mL with IP lysis buffer. Samples were incubated with 20 µl washed GFP-Trap Dynabeads per tube for 1 hour, at 4°C on a rotating wheel. GFP-Trap Dynabeads were washed using Lysis buffer B for three times before being resuspended in 30 µl 2x Laemmli buffer and boiled for 5 minutes to detach the protein from the beads. Samples were analysed by Western blotting. Proteins were resolved by SDS-PAGE.

2.8 Isolation of recombinant UBR5 and UBR5-C2768A Proteins

N-terminal Flag-tagged UBR5 WT and UBR5 catalytic dead mutants were purified from HEK293 cells transfected with Flag-UBR5 WT, Flag-UBR5-His, Flag-UBR5-C2768A-His plasmids 24 hours before lysis. Cells were lysed in Flag lysis buffer (20 mM Tris-HCl, pH 6.8, 137 mM NaCl, 1 mM EGTA, 1% Triton x100, 1mM DTT, 10% Glycerol, protease inhibitors cocktail, phosphatase inhibitor cocktail 2 & 3) for 15 minutes on ice and cell lysates were centrifuged at 13000 x g for 15 minutes at 4°C and the post-nuclear supernatant kept. Cell lysates were incubated with anti-FLAG-affinity beads (Sigma, #A2220) in FLAG lysis buffer in gravity columns. The beads were then washed with a series of buffers:

Wash 1: 10 mM Tris pH 7.4, 650 mM NaCl, 1 mM EDTA, 1% Triton X100, 0.5% BSA

Wash 2: 10 mM Tris pH 7.4, 650 mM NaCl, 1 mM EDTA, 1% Triton X100

Wash 3: 10 mM Tris pH 7.4, 150 mM NaCl, 1 mM EDTA, 1% Triton X100

Washes 4 and 5: 10 mM Tris pH 7.4, 650 mM NaCl, 1 mM EDTA

After washing, the proteins were eluted with 3X FLAG Peptides (#F4799, Sigma) in 10 mM Tris pH 7.4 and used for *in vitro* ubiquitination assays directly or after short storage at 4°C.

2.9 *In vitro* ubiquitination assay

There are two well-acknowledged *in vitro* ubiquitination reaction approaches. The first is to use separately purified recombinant substrate and E3 ligase proteins, supplemented with other conjugation reaction ingredients including ATP-Mg2+, recombinant ubiquitin, E1 and E2. The other method is to pull down the substrate protein together with the E3 ligase protein from cultured cells, adding supplements as listed above. Both approaches were examined, but the first gave stronger GABARAP signals with more reproducible results. The Ubiquitin Conjugation Initiation Kit (Boston Biochem, #K-995) is used for both assays with the manufacturer's protocol.

To resemble a 20 µl reaction, the following ingredients are combined in 0.5 or 1.5 mL polypropylene tubes: E3 Ligase Reaction Buffer (10X), approximately 100 µM ubiquitin, 5-10 µM His-GABARAP (in my application, 0.5-0.8 µg), 0.5 µl E2 UBCH4 (1 µM), 1 µl E1 UBA1 (100 nM), no less than 1 µM E3 ligase. If the total volume is still less than 18 µl, ddH2O may be added.

The conjugation reaction is initiated by adding 10 mM Mg^{2+}-ATP. After 30-60 minutes in a 37°C water bath, 0.5 µL EDTA (20 mM) or 1 µL DTT (100 mM) is added to terminate the reaction. The samples were then resolved by SDS-PAGE gel.

2.10 Labelling of nascent proteins by Click Chemistry

Metabolic labelling was performed using the Click-iT Metabolic Labelling kit (Life Technologies, Grand Island, NY, USA) according to the manufacturer's protocol. Cells were washed with PBS (pre-warmed) and cultured in conditioned medium (methionine-free, but all other ingredients of culture medium) for 1 hour to deplete the intracellular methionine reservoir. After that, nascent proteins begin to incorporate AHA (L-azidohomoalanine, a methionine surrogate) during a 1 hour incubation in the conditioned medium supplemented with 50 µM AHA. After labelling, the cells were lysed, and AHA-labelled proteins were conjugated to biotin. The biotinylated proteins were purified by streptavidin magnetic beads after a 2-hour incubation at

room temperature and multiple washes with 0.001% Triton PBS. AHA labelled proteins were then eluted with 2x laemmli buffer and analysed by SDS-PAGE.

2.11 Mass spectrometry analysis for WIPI4 interactors and for the poly-ubiquitination sites on GABARAP

For WIPI4 interactors, WIPI4-GFP was immunoprecipitated using GFP-Trap beads using the protocol previously described. Samples were resolved into a pre-cast 4-12% Bis-Tris polyacrylamide gel (Novex, Thermo Fisher Scientific). The lanes were excised and cut in 3 approximately equal pieces and the proteins reduced, alkylated and digested in-gel. The resulting tryptic peptides analysed by LC-MSMS using a Q Exactive coupled to an RSLCnano3000 (Thermo Scientific). Raw files were converted to mzML using MSConvert (Proteowizard) and searched against a human Uniprot database (downloaded 090614, 20,264 entries) using MASCOT 2.3.

For identification of the putative sites of ubiquitination on GABARAP, HeLa cells transfected with GABARAP-G116A-cGFP and HA-Ub, or GABARAP-K2P-G116A-cGFP and HA-Ub for 24 hours, treated in the last 6 hours with a proteasome inhibitor (MG132 10 µM). Cells were lysed in Lysis buffer B supplemented with deubiquitinase inhibitors (25 mM N-Ethylmaleimide and 10 mM 2-Iodoacetamide) and GABARAP-cGFP mutant proteins were immunoprecipitated. The samples were eluted with 2x laemmli buffer. The elutions were resolved and processed with procedures outlined above and analysed by LC-MSMS. Raw files were processed in Maxquant and PEAKs. GlyGly (K) was set as a variable modification and carbamidomethyl (C) as a fixed modification. Peptides were filtered to high confidence (0.01 FDR) using Percolator.

2.12 Sequence Alignment

Clustal Omega1 was used for multiple sequence alignment. The total or partial conservation between sequences are highlighted.

2.13 Statistics

Western blots were quantified with Image Studio Lite Ver5.2 software. Fiji-ImageJ was used to quantify membranes stained with HRP-conjugated secondary antibodies. Statistical analysis and the graphs were done with Excel and Prism 7.

Volocity software and Fiji-Image J were used for the analysis and processing of confocal images. For colocalization analysis of confocal images, Mander's Coefficient was used. A minimum of 40 cells were examined in each condition.

For simple comparisons, two-tailed Student's T-tests were used, unless there was a legitimate reason to expect the change to be in a particular direction, in which case a one-tailed test was used. $^{*}= p \leq 0.05$; $^{**}= p \leq 0.01$; $^{***}= p \leq 0.001$. A P value of 0.05 was taken as the borderline for statistical significance. Most experiments were repeated at least three times. For experiments using different conditions, the data from single representative experiments were reported to minimise effects of heterogeneity between experiments.

Chapter 3 WIPI4 regulates a late stage of autophagosome formation in basal autophagy

3.1 WIPI4 is required for the degradation of LC3-II

3.1.1 WIPI4 KD increases LC3-II in basal conditions but not in the presence of BafA1

To test whether WIPI4 is involved in autophagy, WIPI4 was knocked down in HeLa cells using small interfering RNA (siRNA), and LC3-II levels were measured. During autophagy, cytosolic LC3 is cleaved by ATG4 to form LC3-I, which is then conjugated to phosphatidylethanolamine to form LC3-II, which decorates autophagosome membranes (Kabeya et al., 2000). Therefore, LC3-II levels positively correlate with the number and volume of autophagosomes in the cells. This increase in LC3-II might be due to either increased autophagosome formation or impaired autophagosome flux. In order to differentiate between these situations, autophagosome degradation was blocked using a saturating concentration of Bafilomycin-A1 (Baf), a potent inhibitor of the lysosomal V-ATPase which impairs both autophagosome degradation and autophagosome-lysosome fusion. Thus, if there is an induction of autophagosome formation, LC3-II levels would increase in treated cells compared to the control following Baf treatment. After transfection with SMARTpool (sp) WIPI4 siRNA, the LC3-II levels increased compared to control cells transfected with control (scramble (scr) siRNA (Fig.3.1A). However, the LC3-II levels with Baf were not significantly different between control and SMARTpool knockdown, indicating that LC3-II degradation was impaired under WIPI4 depletion (Fig.3.1A). The knockdown efficiency is shown in the right panel of Fig.3.1A. WIPI4 depletion by sp siRNA also increased LC3-II levels in starvation conditions (Fig.3.1B).

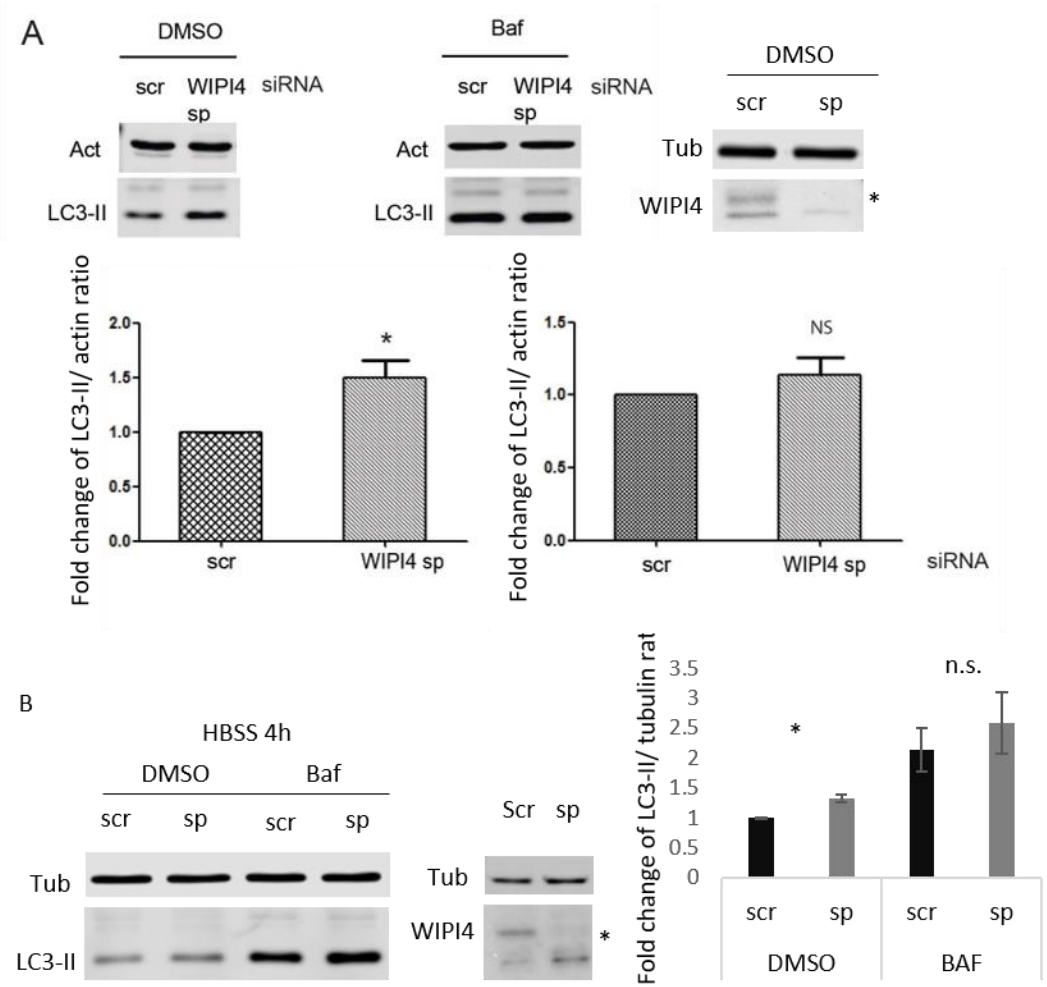

Figure 3.1 WIPI4 regulates autophagy.

A. HeLa cells transfected with two rounds of control or WIPI4 Smartpool siRNA (100 nM and 50 nM) over 5 days, were incubated with a saturating concentration (400 nM) of Bafilomycin A1 (BafA1) or DMSO during the last 4 hours and processed for LC3-II western blot. The knockdown efficiency is shown on the right. Quantification of LC3-II/actin ratio is shown in graphs below as mean ± S.E.M. * - $p<0.05$, n.s., non-significant; two-tailed one-sample t-test). This is representative data of 3 experiments.

B. HeLa cells were transfected as above, grown in Hanks balanced salt solution (HBSS) and for the final 4 hours were treated with BafA1 or DMSO. The knockdown efficiency is shown on the right. Quantification of LC3-II/actin ratio is shown in the graph as mean ± S.E.M. (*$P<0.05$, n.s., not-significant; two-tailed, unpaired t-test).

In order to exclude off-target effects, the knockdown experiments were repeated with independent deconvoluted oligos. All the oligos increased LC3-II levels in control conditions (Fig.1.2A) but did not change LC3-II levels under BafA1 treatment (Fig.3.2A). To validate the autophagy phenotype seen under WIPI4 depletion, rescue experiments were performed by overexpressing WIPI4-GFP in cells treated using WIPI4 oligo 10 siRNA. This treatment reduced LC3-II levels to the same as control cells transfected with empty-GFP, indicating that the increase of LC3-II levels in basal conditions was specifically caused by WIPI4 depletion (Fig.3.2B).

Consistent with the LC3 blots, both the size and number of endogenous LC3 vesicles increased (Fig.3.3 A&B) with WIPI4 knockdown. ATG16L1 labels autophagosome precursors that evolve into LC3 positive autophagosomes (Pavel et al., 2016). WIPI4 knockdown increased both the size and number of ATG16L1 positive vesicles (Fig.3.3 C&D). Moreover, the colocalization of ATG16L1 and LC3 increased in WIPI4 depleted cells, implying that the autophagy flux was blocked after the autophagosome recruitment of ATG16L1 and LC3 (Fig.3.4 A&B). Fig.3.4C shows the knockdown efficiency of WIPI4 siRNA in the experiment in Fig.3.3 and Fig.3.4.

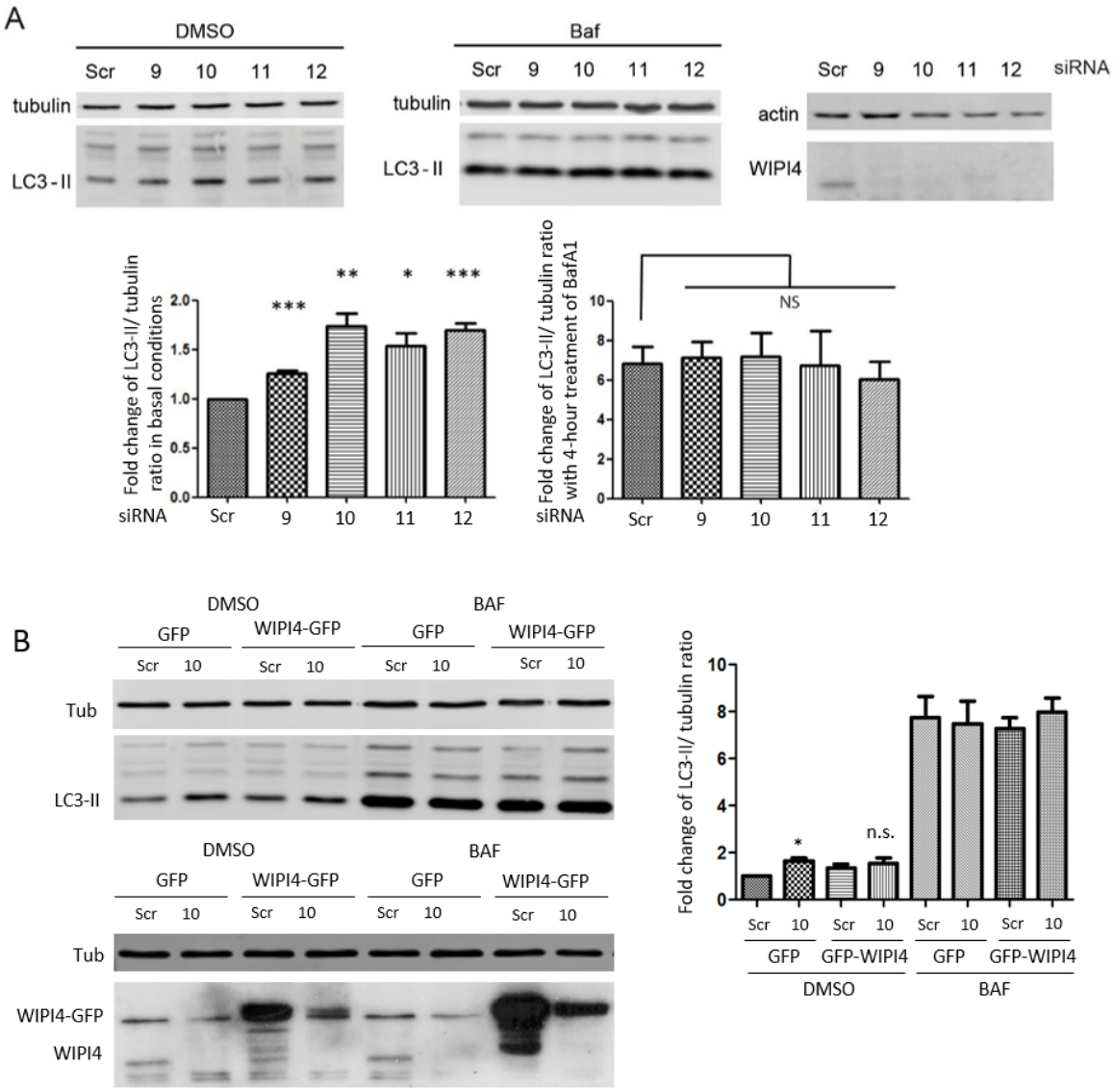

Figure 3.2 WIPI4 transient knockdown specifically targets WIPI4.

A. HeLa cells transfected with two rounds of control or WIPI4 deconvoluted siRNAs (100 nM and 50 nM) for 5 days, were incubated with 400 nM BafA1 or DMSO for the final 4 hours and processed for LC3-II western blot. The western blot panels on the right represent the effect of knockdown of deconvoluted oligos. The graphs below show the quantitative analysis of LC3-II levels relative to tubulin from the blots (*P<0.05, **P<0.01, ***P<0.001, n.s., non-significant; two-tailed unpaired student's t-test). This is representative data of 3 experiments.
B. HeLa cells were transfected with two rounds of control or WIPI4 deconvoluted siRNA Oligo 10. After 72 hours the cells were transfected with 1.0 µg GFP-WIPI4 or empty GFP vector for 24 hours and with BafA1 or DMSO for the last 4 hours before lysis. The western blot panels represent the knockdown efficiency of siRNA and the overexpression level of WIPI4-GFP. The graphs below show the quantitative analysis of LC3-II levels relative to tubulin from the blots (*P<0.05, n.s., non-significant; two-tailed one sample student's t-test). This is representative data of 3 experiments.

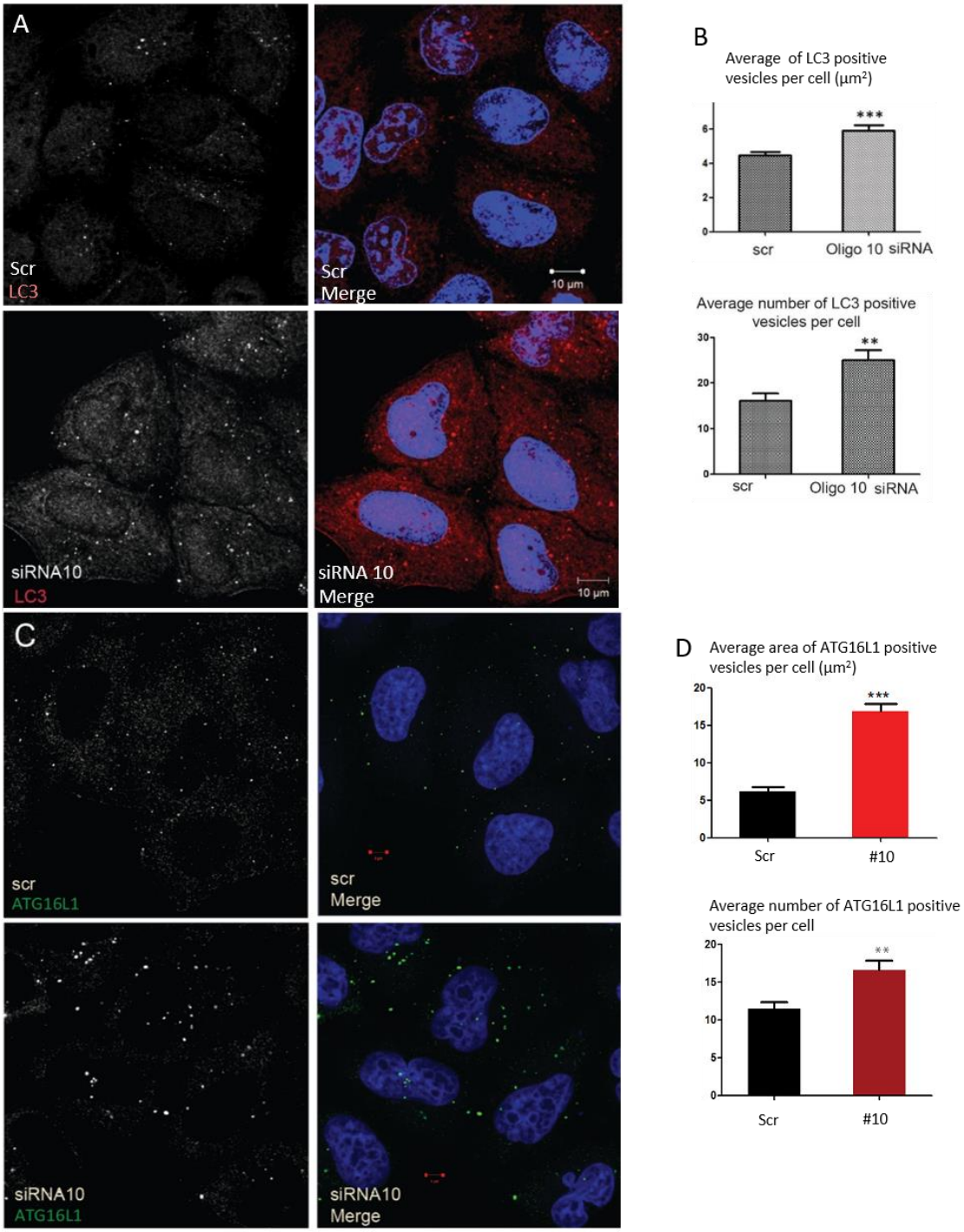

Figure 3.3 WIPI4 knockdown accumulated autophagosome markers in Hela cells

A. Effect of WIPI4 knockdown on endogenous LC3 vesicles in HeLa cells. HeLa cells were transfected with control (scr) or WIPI4 Oligo 10 siRNA 5 days before immunostaining for endogenous LC3 (visualised with Alexa 568, red). Representative images shown. Scale bar = 10µm.

B. Quantification for the size and number of LC3 vesicles of confocal images from the experiment in A. The graphs represented the mean ± SEM (n=28 for control siRNA, n=28 for WIPI4 oligo10; **P<0.01, ***P<0.001; two-tailed unpaired student's t-test throughout the figure). The size of vesicles is quantified using Image J software.

C. Endogenous ATG16L1 immunostaining in WIPI4 knockdown cells. Transfection of siRNA was performed as in A (visualized with Alexa 488, green). Representative images shown. Scale bar = 5µm.

D. Graphs representing the average size and number of ATG16L1 positive vesicles per cell ± SEM (n=15 for scramble control, n=28 for WIPI4 oligo10).

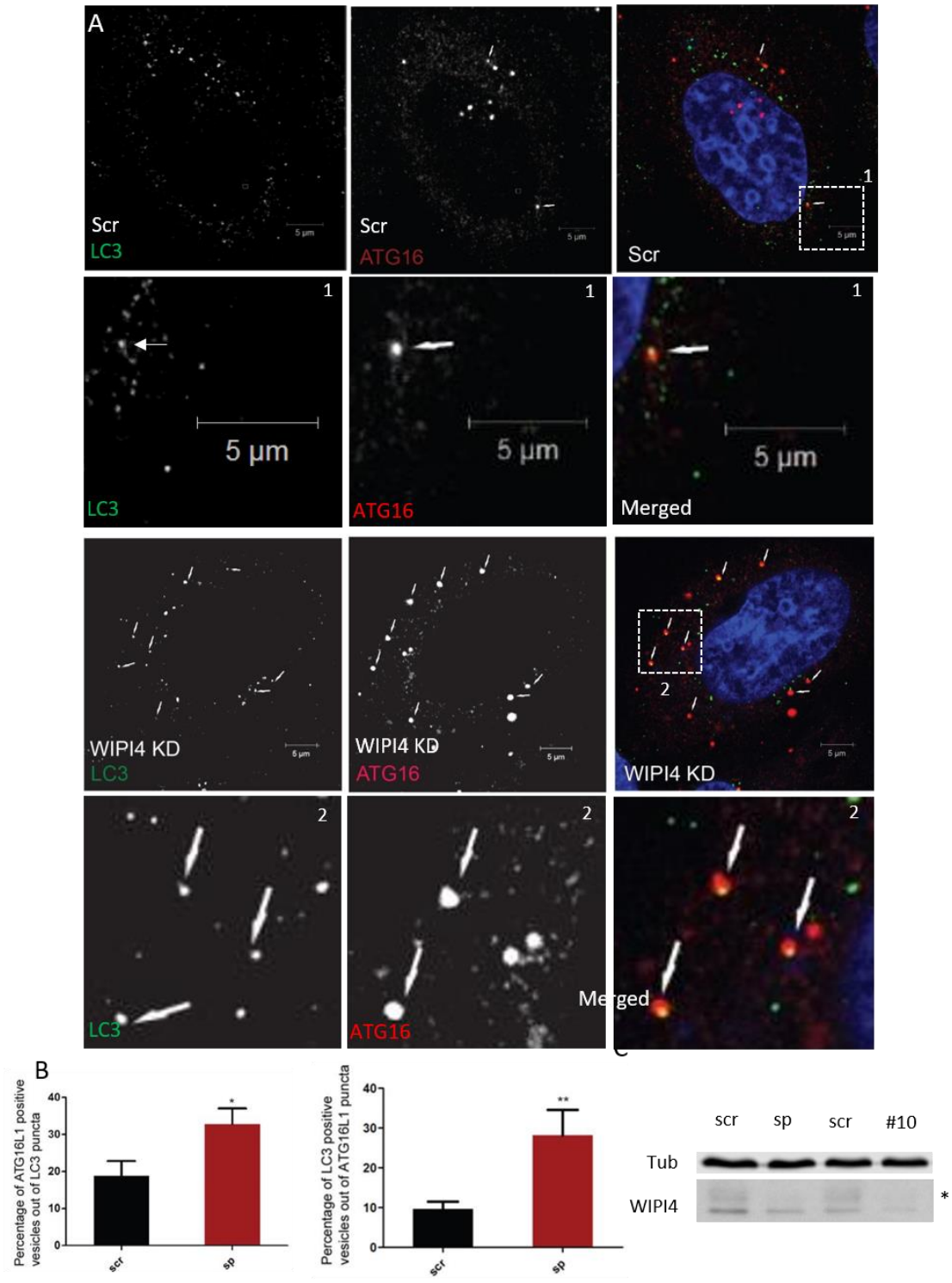

Figure 3.4 WIPI4 knockdown increased the colocalisation of ATG16L1 and LC3 in HeLa cells

A. Effect of WIPI4 knockdown on the colocalization of endogenous ATG16L1 and LC3 vesicles in HeLa cells. Cells were transfected with control (Scr) or WIPI4 SMARTpool siRNA 5 days before immunostaining. Representative images of immunostaining for endogenous LC3 (visualised with Alexa 488, green) and ATG16L1 (Alexa 568, red) are shown. Scale bar = 5 µm.
B. Quantification of confocal images for Mander's colocalization between ATG16L1 and LC3 vesicles in control (Scr) cells or cells transfected with WIPI4 SMARTpool/ Oligo 10 siRNA.
C. The western blot panels show the effeciency of WIPI4 knockdown.

3.1.2 Knockdown of WIPI4 blocked phagophore-autolysosome transition

In order to confirm which stage of the autophagic pathway was impaired, HeLa cells stably expressing tandem fluorescent-tagged LC3 (Sarkar et al., 2009) were used to quantify autophagosomes (including precursors) and autolysosomes with and without WIPI4 knockdown. Tandem fluorescent-tagged LC3 (mRFP-GFP-LC3) is an assay which can be used to monitor autophagic flux. In newly formed autophagosomes at physiological pH, both mRFP and GFP are stable, whereas the autolysosomes have only mRFP signal due to quenching of the GFP in the acidic lysosomal environment (Kimura et al., 2007).

HeLa cells stably expressing mRFP-GFP-LC3 were transfected with deconvoluted WIPI4 siRNA Oligos 10 and 12 and analysed by live cell imaging. Interestingly, knockdown of WIPI4 with both oligos led to an increase in the number of GFP vesicles but a decrease of RFP-only vesicles in full media (Fig.3.5 A&B). BafA1 treatment was used as a positive control to verify the reliability of this experiment. As shown in Fig.3.5B, the number of GFP vesicles greatly increased in BafA1 treated cells (Fig.3.5B). Fig.3.5C shows the knockdown efficiency of WIPI4 by both oligos. This observation indicated that WIPI4 knockdown increases LC3-II levels by reducing its degradation.

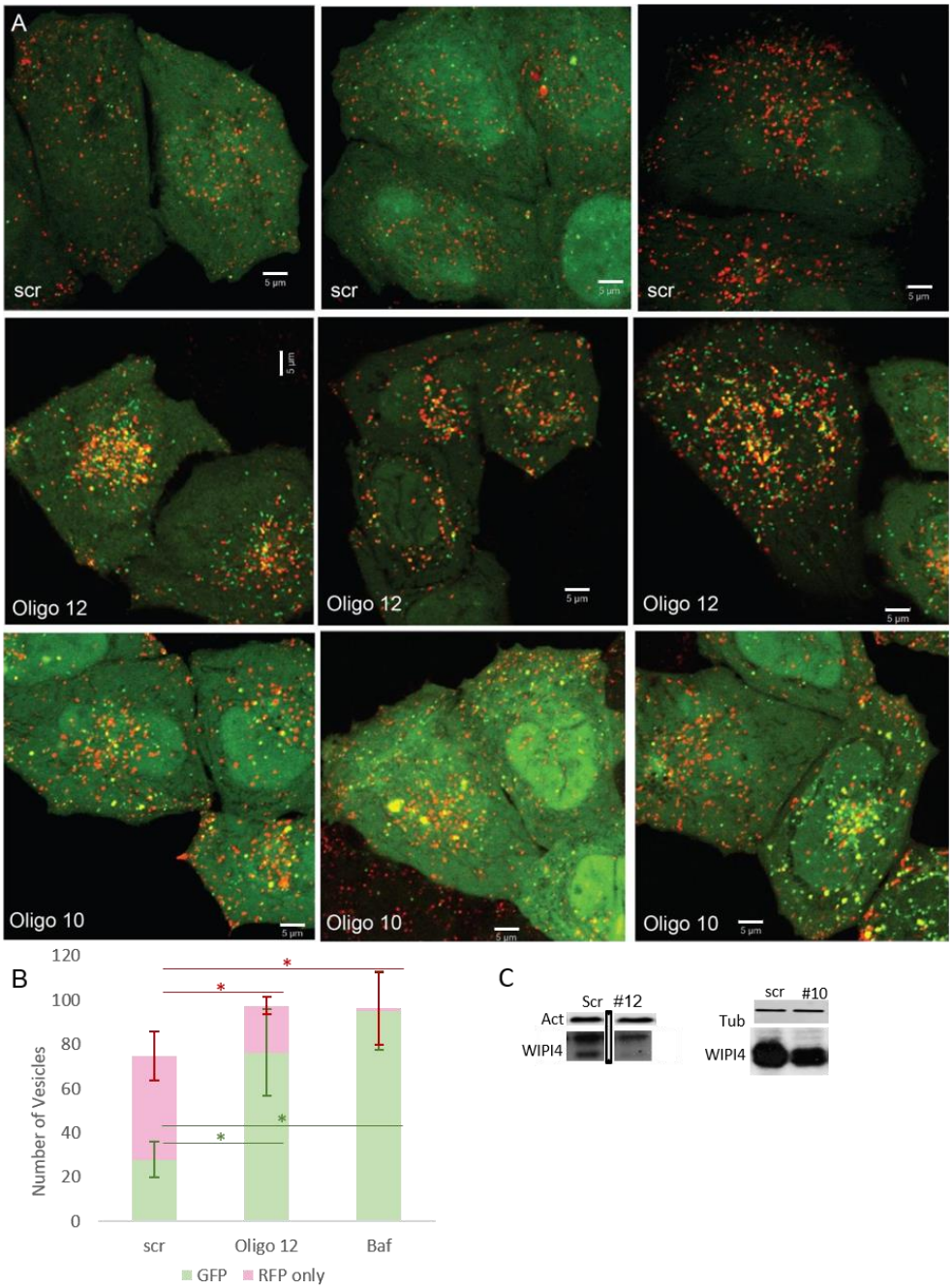

Figure 3.5 WIPI4 transient knockdown blocks autophagosome-autolysosome transition in basal conditions

A. HeLa cells stably expressing the mRFP-GFP-LC3 reporter which were treated with control or WIPI4 (Oligo 12, Oligo 10) siRNAs. Cells were imaged live after 5 days. These are representative data of three repeated experiments. Scale bars throughout the panels are 5 µm.

B. Quantification of confocal images (control and WIPI4 Oligo 12 siRNA) for the number of GFP positive dots (autophagosomes) and RFP only dots (autolysosomes) (A). Graphs represent the mean ± SEM (n>80 for control, n=100 for WIPI4 oligo10; *P<0.05; one-tailed unpaired student's t-test). Bafilomycin A1 was used to generate a positive control of impaired autophagy flux. The two western blot panels demonstrate the knockdown efficiency of WIPI4 in the above experiments. Tubulin and actin were used as loading controls.

C. Western blots showing the protein levels of WIPI4 in control (Scr), Oligo10 and Oligo 12 treated samples.

3.1.3 WIPI4 knockdown impairs the removal of autophagy substrates

If WIPI4 depletion blocks autophagic flux, it should also slow down the clearance of autophagy substrates. Therefore, aggregate-prone proteins (GFP-Htt-Q74 and GFP-p62) were used to monitor clearance. As an autophagy substrate, the proportion of cells with GFP-Htt-Q74 aggregates increases linearly with its expression levels (Narain et al., 1999) and correlates inversely with autophagy activity (Ravikumar et al., 2002). Consequently, the clearance efficiency of GFP-Htt-Q74 can be measured by the percentage of cells with aggregates. The proportion of cells with GFP-Htt-Q74 aggregates increased in WIPI4 knockdown cells compared to control cells (Fig.3.6A).

p62/SQSTM1 (hereafter p62) is an autophagy cargo protein which physically links autophagy substrates to LC3/GABARAP family members located on the autophagosome membranes. p62 localised at the inner surface of phagophores will be encapsulated in autophagosomes and be degraded together with other luminal contents (Korolchuk et al., 2010). Thus, p62 can also be classified as an autophagy substrate, and its levels inversely correlate to the autophagy activity. GFP-p62 Flp-In T-REx cell line is an inducible autophagy flux reporter system (Larsen et al., 2010). The expression of p62 can be turned on or off by adding or removing the inducer (tetracycline). Following expression, the inducer is removed, and the autophagic flux can be determined as the rate of decay of GFP-p62. GFP-p62 clearance was significantly retarded 24 hours after turning-off the induced expression in WIPI4 siRNA treated cells compared to control (Fig.3.6C). The knockdown efficiency of WIPI4 is shown in Fig.3.6 B&D. Altogether, WIPI4 depletion compromised the clearance of autophagy substrates, indicating that WIPI4 is a positive regulator of autophagy function.

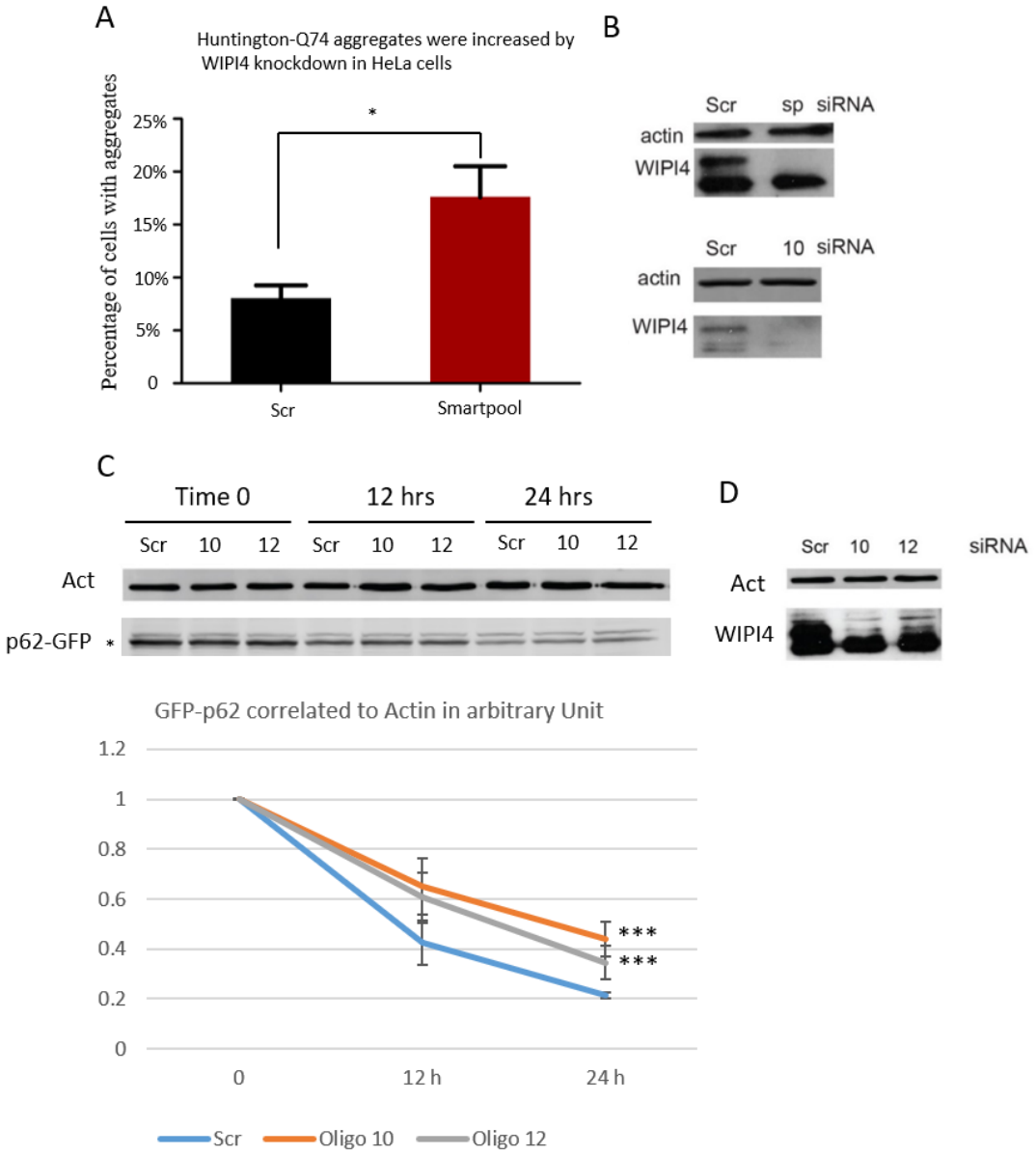

Figure 3.6 WIPI4 is a positive regulator of autophagy function

A. HeLa cells were transfected with control or WIPI4 SMARTpool siRNA 48 hours prior to a second transfection with GFP-Htt-Q74. After 36 hours, aggregates were counted. WIPI4 knockdown cells (17.3%) had two-fold more aggregates compared to control cells (7.9%), p=0.03, two-tailed unpaired t-test.

B. Western blots showing WIPI4 knockdown efficiency in cells treated with siRNA Oligo 10.

C. WIPI4 knockdown blocked p62-GFP clearance. GFP-p62 Flp-In T-REx 293 cells were transfected with either control, WIPI4 Oligo 10 or WIPI4 Oligo 12 siRNAs for 72 hours, after which the GFP-p62 expression was induced for 24 hours. p62-GFP levels were significantly higher compared to control cells following removal of the inducer (scr vs 10, p=0.009; scr vs 12, p=0.006, *** p<0.01). The same trend was observed at 12 hours (Scr vs 10, p=0.274; scr vs 12, p=0.302) but was not significant.

D. Both oligo 10 and Oligo 12 siRNA knocked down WIPI4 in GFP-p62 Flp-In T-Rex 293 cell line.

3.1.4 WIPI4 knockdown slows down the degradation of nascent LC3-II proteins

To clarify whether LC3-II accumulation was caused by the increase in its formation or a defect of its degradation, Click-iT assay was performed to measure the formation and degradation rate of LC3-II. Cells treated with control and WIPI4 siRNA were incubated with conditioned media, and newly synthesized protein was labelled during the incubation with L-azidohomoalanine (AHA). The labelled protein, including LC3-II, was biotinylated and purified by streptavidin beads. The levels of AHA-LC3-II synthesized during one hour were not significantly changed by WIPI4 depletion (Fig.3.7 A&C). However, after three hours, the AHA-LC3-II levels began to decrease much slower in WIPI4-depleted cells compared to control cells (Fig.3.7 A&D). The AHA-LC3-II levels increased for the first three hours following incubation with AHA. This is likely to be due to a pool of AHA in the cells which has not been exhausted and protein synthesis continuing.

In summary, the depletion of WIPI4 downregulates autophagy functions. The LC3-II western blots demonstrate that autophagosomes accumulate in WIPI4 depleted cells. Htt-Q74-GFP aggregation assay and GFP-p62 clearance experiment show that WIPI4 is a positive regulator of autophagy. The experiment with the mRFP-GFP-LC3 stable cell line and Click-iT assay confirmed that the loss of WIPI4 function accumulates LC3-II by impairing its degradation. Defects in any of the three following processes can cause the impaired degradation of LC3:

i. LC3-II degradation in lysosomes, or lysosome degradative function
ii. The trafficking of LC3 positive autophagosomes to lysosomes, namely autophagosome-lysosome fusion
iii. Autophagosome formation delay between LC3 conjugation and autophagosome closure

The three processes above were assessed separately to understand which of them is /are responsible for the WIPI4 knockdown phenotype.

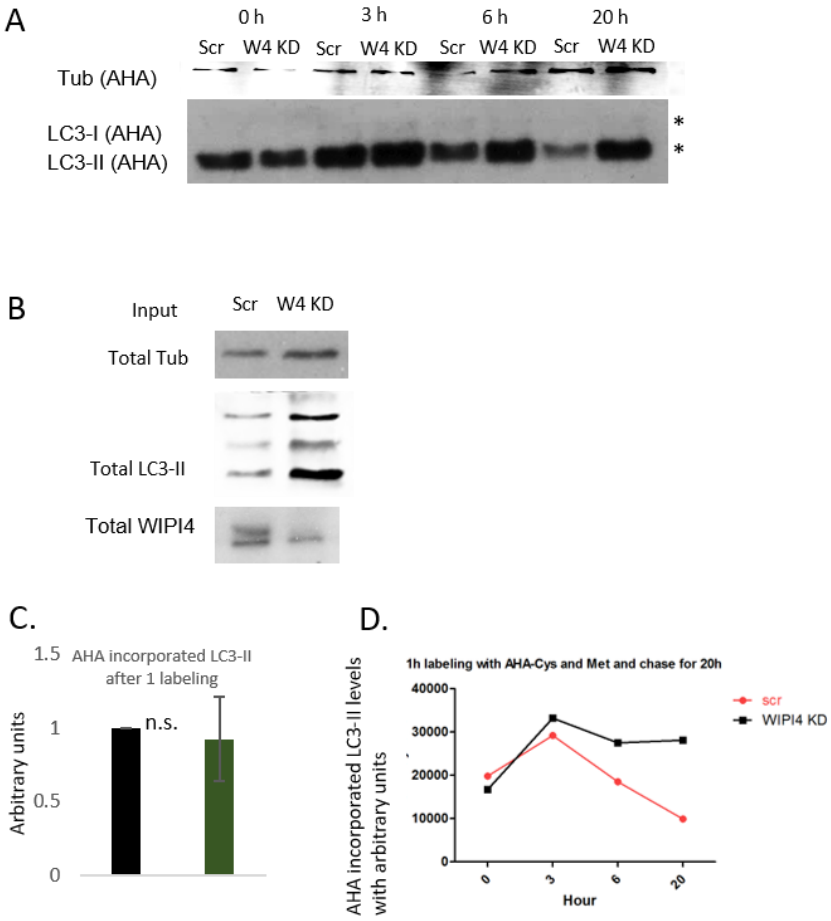

Figure 3.7 WIPI4 loss of function does not impair nascent LC3-II formation

A. Representative blots showing the levels of L-AHA labelled LC3 and tubulin (L-azidohomoalanine (L-AHA), C10102, Thermo Fisher Scientific). Formation and degradation of L-AHA labelled LC3-II was assessed in HeLa cells 72 hours after transfection of control or WIPI4 SMARTpool siRNA. 1-hour L-AHA labelling was performed as described in Best et al., in 2009, except with an extension of chase time to 20 hours in adaptation to monitor degradation. For samples of Time zero (0), cells were washed with PBS after 1-hour labelling with L-AHA, followed by western blot analysis. The L-AHA labelled proteins were then biotinylated and purified from the total lysates by streptavidin beads and assessed by western blot.
B. Western blots showing the knockdown efficiency of WIPI4 with L-AHA labelled total lysates.
C. Quantification of the nascent L-AHA-LC3-II levels synthesized in 1 hour (Time 0).
D. Quantification of the levels of proteins in both Time 0 and chase samples in A.

3.2 WIPI4 knockdown impairs a late stage of autophagosome formation

3.2.1 Lysosome activity was not impaired by WIPI4 knockdown

If WIPI4 knockdown blocks autophagy through disrupting lysosomal structures, the activity of the lysosomes may be reduced. The lysosome activity was monitored by three markers: Cathepsin L activity, Cathepsin D maturation by western blot, and pH.

First, the activity of Cathepsin L as a marker of lysosome function was measured. Cathepsins are soluble lysosomal aspartic endopeptidases. Less active Cathepsins indicate the decrease of the degradative capability of lysosomes. Conversely, the Cathepsin L activity increased in basal media by WIPI4 knockdown (Fig.3.8).

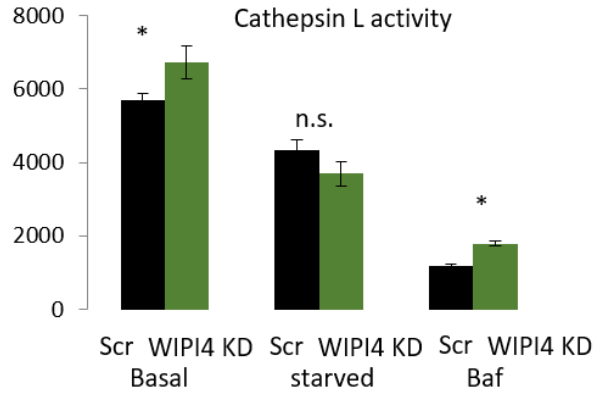

Figure 3.8 WIPI4 knockdown did not decrease Cathepsin L activity in basal

HeLa cells were transfected with control or WIPI4 SMARTpool siRNA and grown in full media/ EBSS media for 72 hours. 4 hour BafA1 treated cells were used as negative control. 1-5 x 10^6 cells were lysed with 50 µL of chilled CL Buffer for 10 minutes. 2 µL 10 mM Ac-FR-AFC substrate was added to each sample and incubated for 1 hour. Fluorescence intensity was measured with Ex/Em = 400/505 nm, and was expressed in arbitrary units (n=3; *P<0.05; two-tailed unpaired t-test).

Second, a decrease of mature Cathepsin D and increase of procathepsin D and intermediates indicate decreased lysosome function and defective endo-lysosome trafficking (Benes et al., 2009). On the contrary, Cathepsin D maturation was not decreased by WIPI4 knockdown (Fig.3.9). Instead, the procathepsin D and intermediate levels increased similarly with mature Cathepsin D.

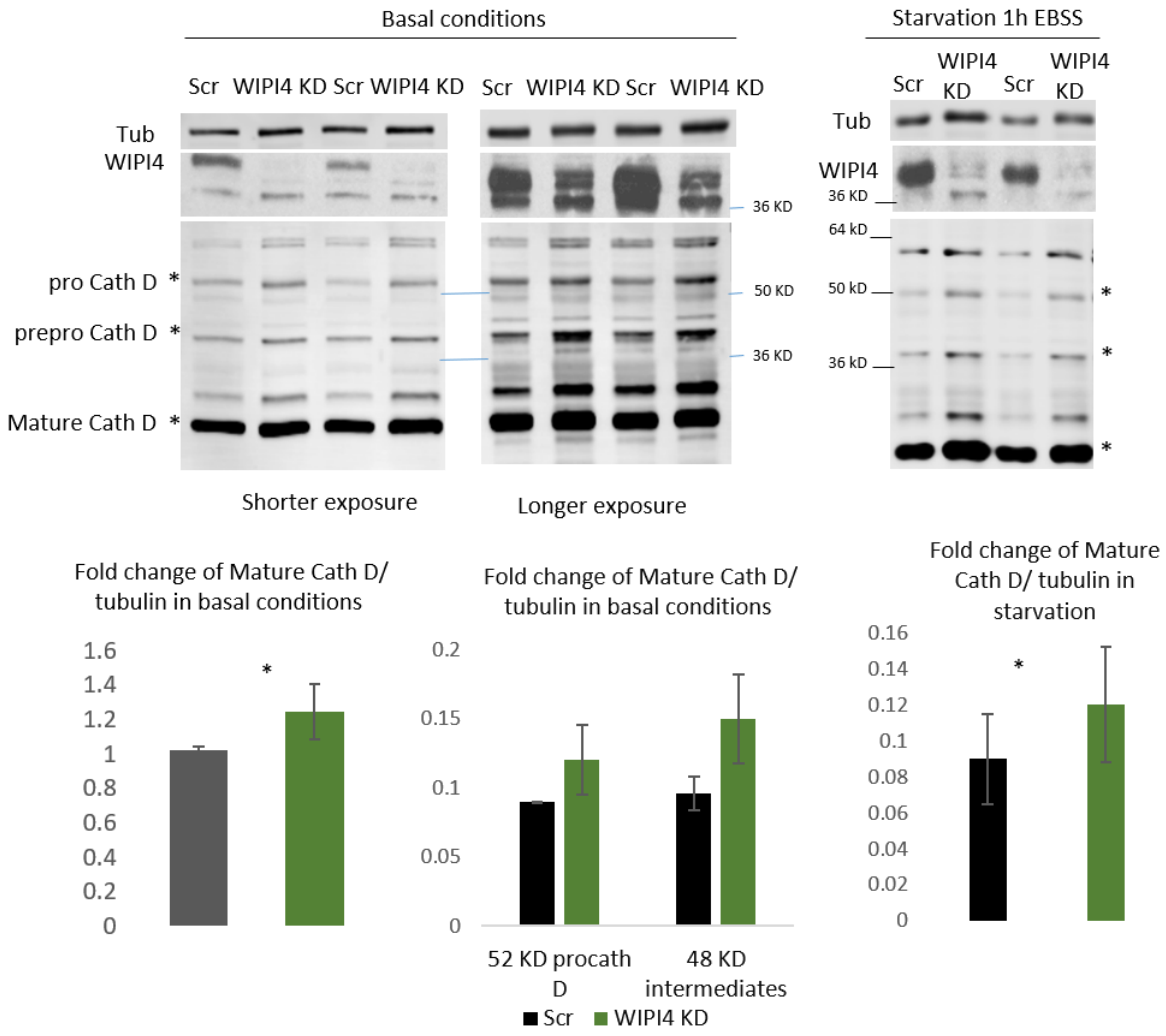

Figure 3.9 WIPI4 knockdown did not decrease the protein levels of mature Cathepsin D

Western blot showing Cathepsin D (CTSD) maturation in WIPI4 knockdown HeLa cells in basal and starvation conditions. Graphs below showing the quantification of mature and precursor CTSD as mean ± s.d. (n=3; *P<0.05; two-tailed unpaired t-test).

Third, since an acidified environment is required for the activation of digestive enzymes in the lysosomes, acidification of lysosomes with and without WIPI4 siRNA treatment was measured with LysoSensor. Consistently, WIPI4 depletion slightly increased the ratio of acidified lysosomes versus neutral lysosomes in both basal and starved conditions (Fig.3.10). BafA1 treatment decreased the ratio of acidified to neutral lysosomes and was used as a negative control. The mechanism of WIPI4 upregulating lysosome function is beyond the scope of this chapter. Cells of Fig.3.9& 3.10 are from the same siRNA transfection experiment and the knockdown efficiency of WIPI4 proteins shown in Fig.3.9.

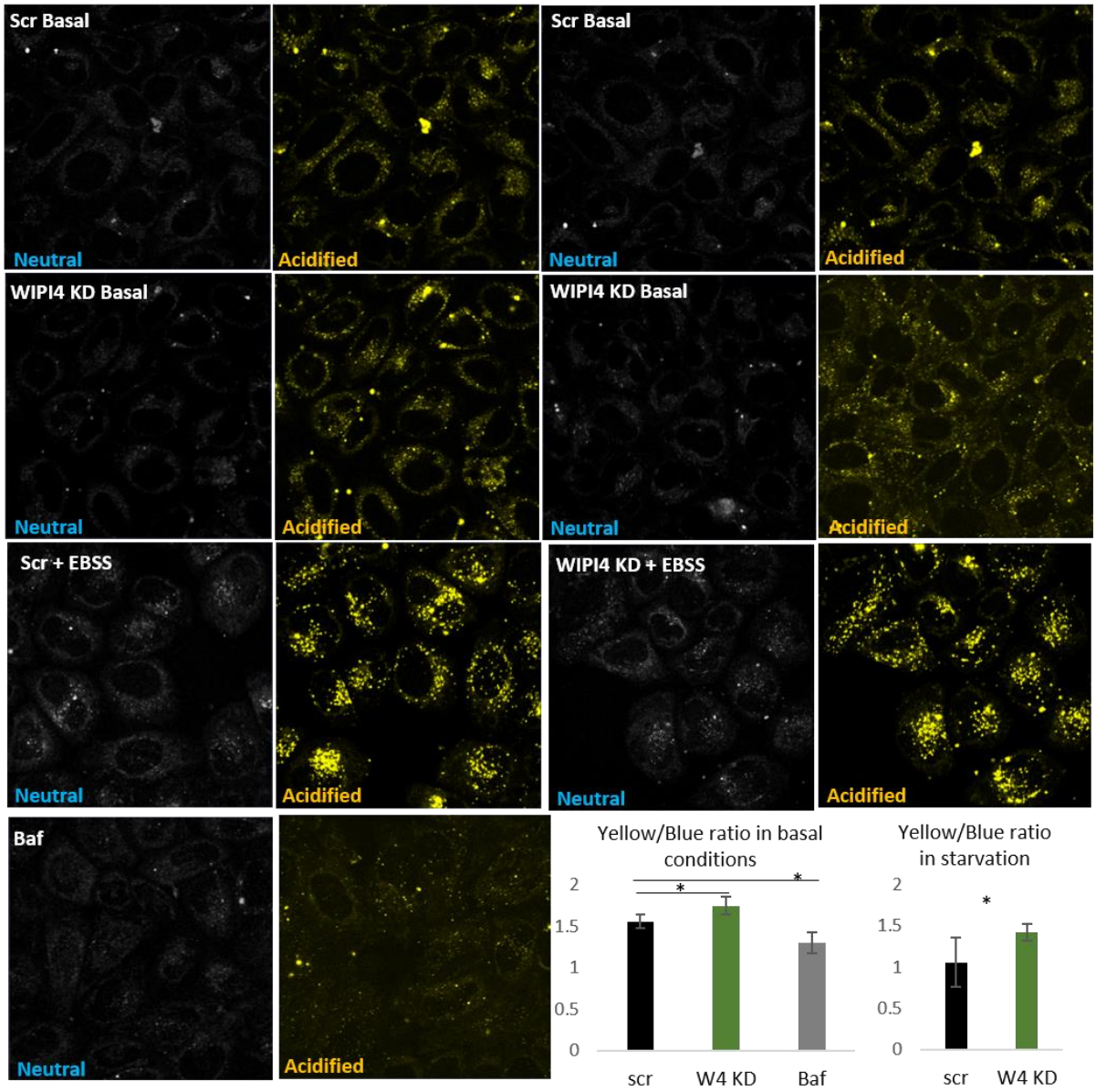

Figure 3.10 Lysosome acidification was increased by WIPI4 KD in basal and starvation conditions

Lysosomal pH in WIPI4-depleted cells. The Lysosensor Yellow Blue intensity was measured in both yellow and blue channels. Intensities ratio is a qualitative measure of lysosomal pH. Bafilomycin A1 (Baf A1) was used as a positive control (400 nM, 4 hours) for increased lysosomal pH. More than 50 cells were analysed per experiment, for each condition. The experiment was performed at least 3 times with similar results. (*P<0.05; two-tailed unpaired t-test).

Taken together, WIPI4 depletion does not decrease the levels of functional lysosome enzymes.

3.2.2 WIPI4 knockdown does not block autophagosome-lysosome fusion

The above observations indicated that WIPI4 regulates autophagy by promoting autophagosome-maturation or the trafficking of autophagosome to lysosomes (fusion). First, to understand whether there is a defect in fusion, the colocalization of LC3 and lysosome markers were analysed. If WIPI4 knockdown impairs the traffic of autophagosomes to the lysosomes, the colocalization of LC3 (autophagosome marker) and LAMP1/CD63 (lysosome/late endosome markers) should be decreased. The increased size/number or clustering of lysosomes may artefactually increase the colocalization. Nocodazole is a microtubule-depolymerizing drug, which dissociates lysosomes from the non-fused autophagosomes in their close proximity (Kuhn et al., 2006).

As shown in Fig.3.11, WIPI4 knockdown increased the colocalization of endogenous LC3 and CD63 under basal conditions. However, there was no significant increase when cells were exposed to Nocodazole (Fig.3.12). Therefore, the traffic of autophagosomes to lysosomes was not affected. The knockdown efficiency of WIPI4 proteins of Fig.3.10 & 3.11 is shown in Fig.3.10 because the cells are from the same siRNA transfection experiment.

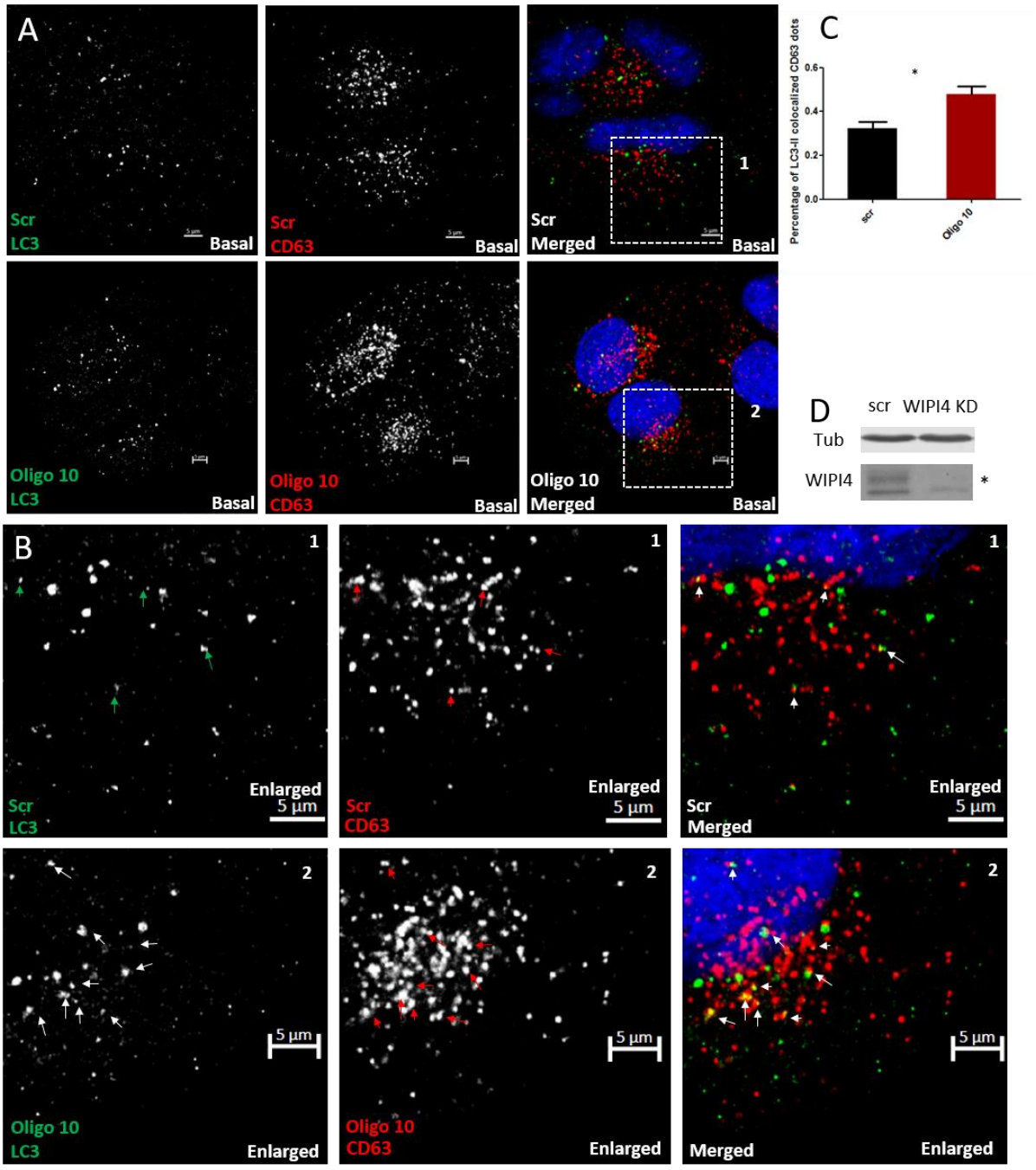

Figure 3.11 WIPI4 knockdown increased the colocalization of LC3 and CD63 in basal conditions

A. Representative images of LC3 (anti-mouse Alexa 488) and CD63 (anti-rabbit Alexa 568) colocalization in HeLa cells with and without depletion of WIPI4 in basal conditions.
B. Enlarged images showing increased LC3 and CD63 vesicles in images in A.
C. Quantification of colocalization (Mander's coefficient). More than 50 cells were counted per condition. Bars—means±s.e.m. (*P<0.05, two-tailed t-test). Similar results were achieved in at least two independent experiments.
D. Western blots showing the knockdown efficiency of WIPI4.

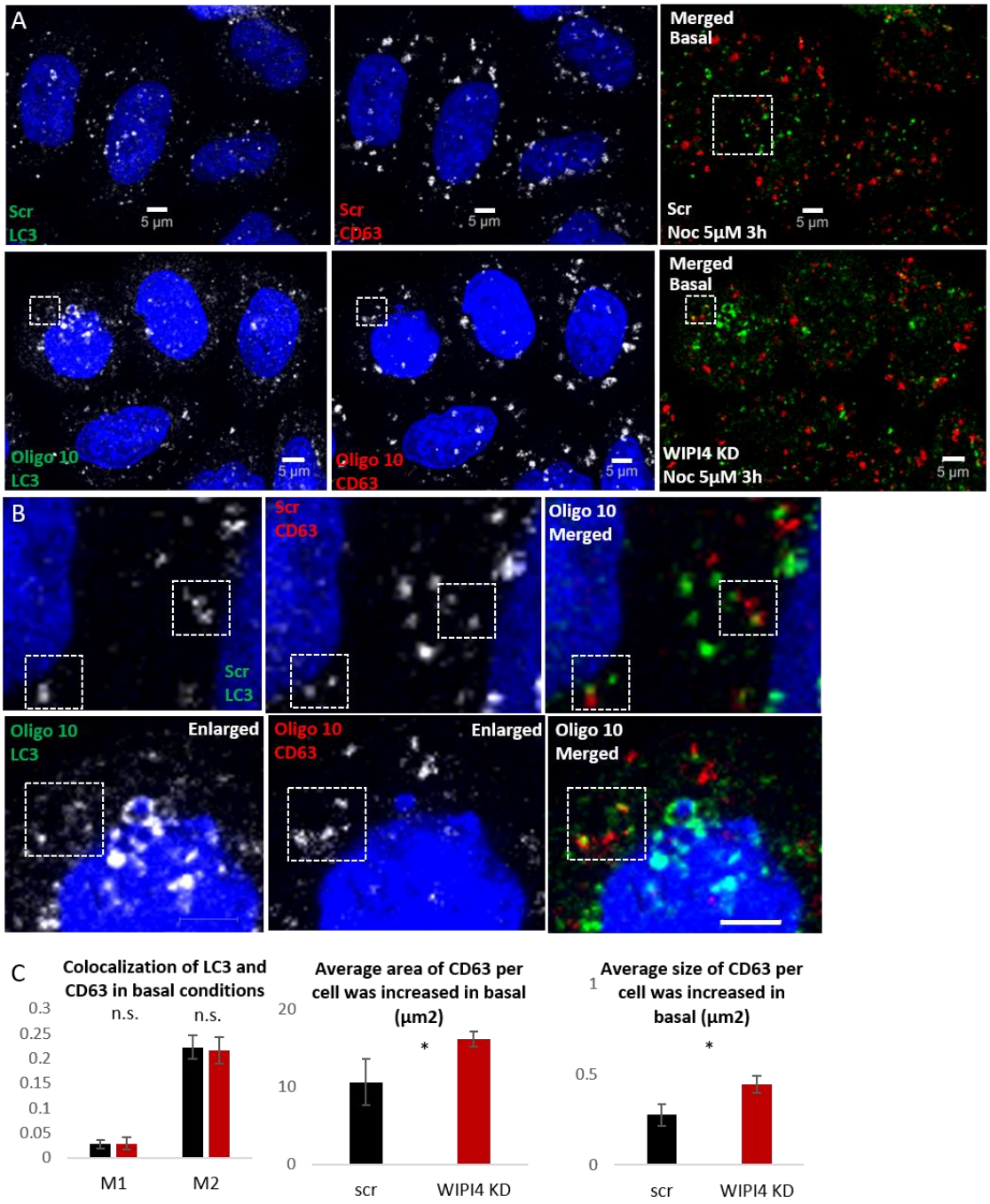

Figure 3.12 WIPI4 knockdown does not change the colocalization of LC3 and CD63 in basal with Nocodazole treatment

A. LC3 (anti-mouse Alexa 488) and CD63 (anti-rabbit Alexa 568) colocalization in HeLa cells. Cells depleted for WIPI4 were co-immunostained for CD63 and LC3. The cells were then exposed to nocodazole treatment 5 µM, 3 hours.

B. Enlarged images showing increased LC3 and CD63 vesicles in images in A. Scale bars throughout the panel are 5 µm.

C. Quantification of colocalization by Mander's coefficient and the average area and size of CD63 positive vesicles. More than 50 cells per were counted for each condition. Bars represent the mean ± SEM (***P<0.001, *P<0.05, n.s. – not significant; two-tailed t-test). Similar results were achieved in at least another independent experiment.

3.2.3 WIPI4 regulates a late stage of autophagosomes formation, which is later than ATG2 regulated expansion but no later than the closure

The final stage to investigate is after LC3-II conjugation and no later than autophagosome closure. Proteinase K cleaves LC3-II from exposed autophagosome membranes (Velikkakath et al., 2012). Therefore, sealed autophagosomes would have a lower ratio of cleavable versus uncleavable LC3-II proteins compared to unsealed autophagosomes. As shown in Fig.3.13, ATG2A/B knockdown resulted in less LC3-II after proteinase K treatment, suggesting an increased ratio of cleavable and uncleavable LC3-II, which means either a bigger proportion of unsealed autophagosomes or smaller autophagosomes. In comparison, WIPI4 knockdown only slightly sensitised LC3-II levels to proteinase K treatment in basal conditions.

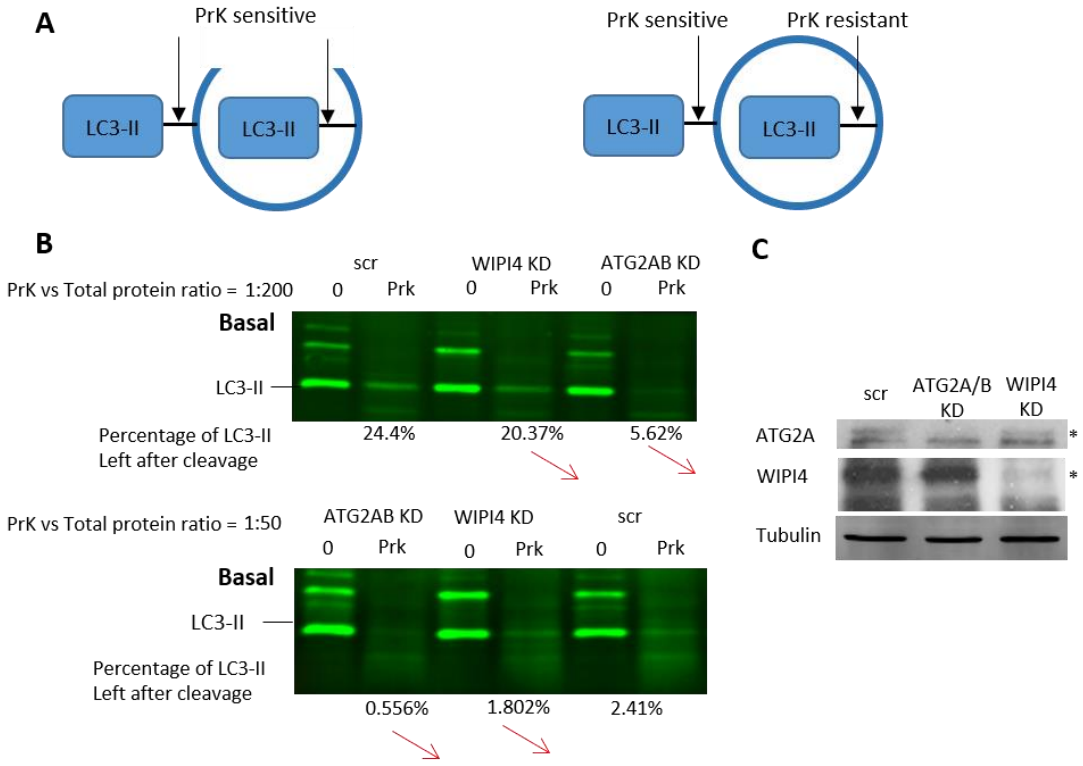

Figure 3.13 Cleavable LC3-II was slightly different in cells with and without WIPI4 depletion

A. Schematic drawing showing the different sensitivity of sealed and unsealed autophagomes to the proteinase K treatment.
B. HeLa cells transfected with control (Scr), WIPI4 and ATG2A/B siRNAs were homogenized and the postnuclear supernatant (PNS) was subject to ultracentrifugation. The high-speed pellet (HSP) fraction was treated with proteinase K as indicated in the manufacturer's protocol (the ratio is the concentration of proteinase K relative to the concentration of total proteins in the sample). The reactions were then boiled in SDS loading buffer and analyzed by western blot using anti-LC3 and anti-tubulin antibodies.
C. Representative blots showing the knockdown efficiency of WIPI4 and ATG2A proteins.

This observation suggests that WIPI4 and ATG2A/B regulate the ratio of cleavable LC3-II versus uncleavable LC3-II differently, which reminded me of the fact that ATG2 loss of function reduces the size of autophagosomes (Tang et al., 2019) while WIPI4 loss of function increases the size of autophagosomes (Fig.3.3). Altogether, the above information indicates that WIPI4 functions in expansion but later than ATG2, and WIPI4 also functions no later than closure because the autophagosome size is still adjustable/ autophagosomes are not yet completed when WIPI4 functions. The specificity of ATG2A and ATG2B siRNAs has been verified previously in the lab and data is not shown here.

Next, it was examined whether there was a defect after LC3-II conjugation and before the closure. Rab11 tubules form a platform for autophagosome formation (Puri et al., 2018). LC3-II positive membrane buds off from Rab11 positive recycling endosomes to form autophagosomes. If WIPI4 is required for the scission of LC3-II positive structures from recycling endosomes, the colocalization of Rab11 and LC3 should increase when WIPI4 is depleted. However, Fig.3.14 shows that the colocalization of Rab11-GFP and LC3 was not changed in both basal and starved conditions. Based on the above results, WIPI4 regulates the closure of autophagosomes, which may happen after the scission of LC3-II structures from recycling endosomes.

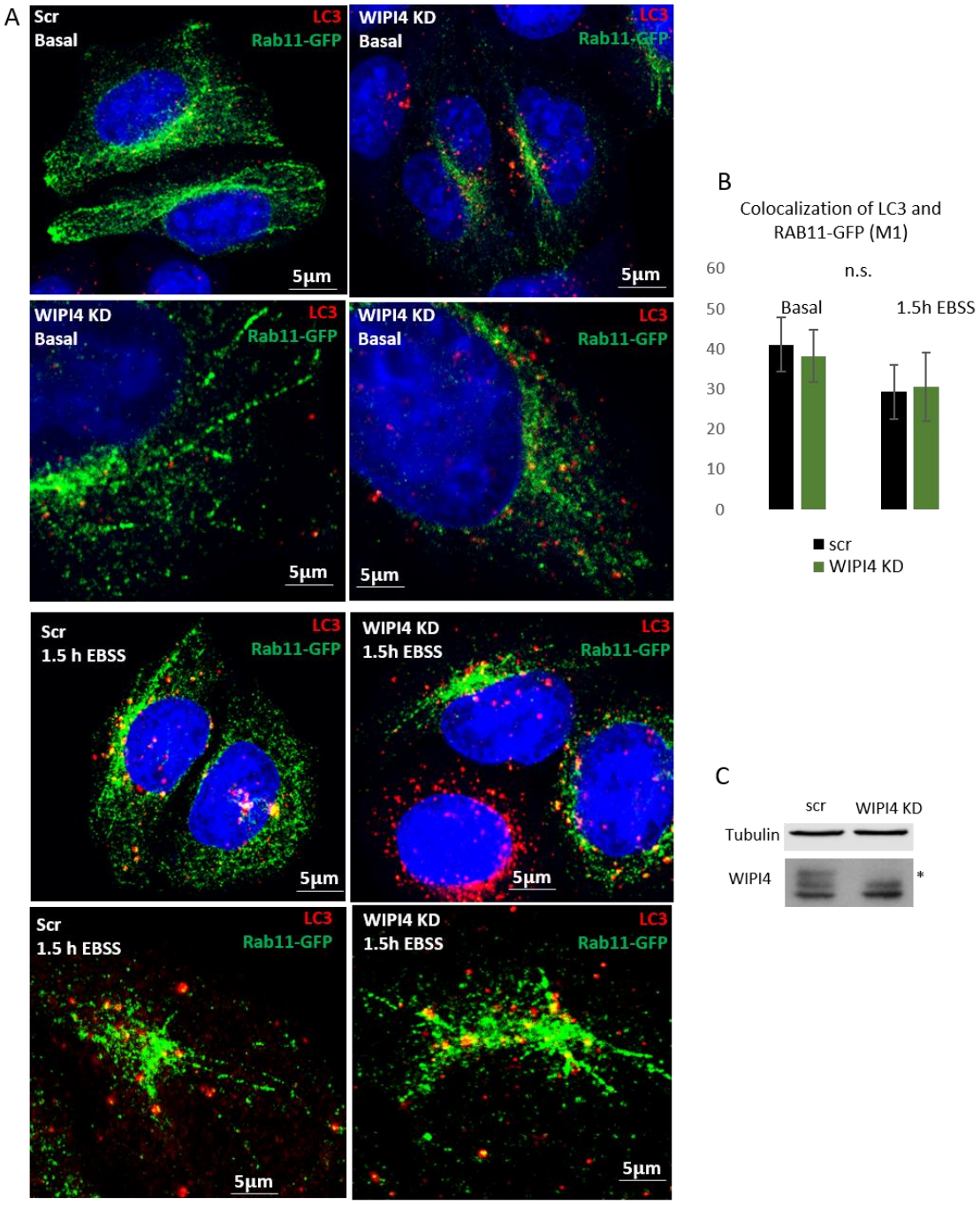

Fig.3.14 LC3-II was not accumulated on Rab11-GFP tubules by WIPI4 knockdown

A. Colocalization of Rab11-GFP and LC3 (anti-mouse Alexa 568) in HeLa cells. RAB11-GFP stable cell line depleted for WIPI4 were incubated in the culture media or EBSS for 1.5 hours prior to immunostaining for LC3. Scale bars throughout the panel are 5 μm.

B. Quantification of colocalization by Mander's (M1 represents the LC3 localization in the lysosomal compartment) coefficients. More than 40 cells were counted in each condition. Bars represent the mean ± SEM (n.s., not significant, two-tailed unpaired t-test). The experiment was repeated with similar results.

C. The knockdown efficiency of WIPI4.

3.3 WIPI4 interacts with ATG2 but is not required for the recruitment of ATG2 onto autophagosomes

WIPI4 and ATG2 may function in the same stage of the autophagy pathway (Lu et al., 2011). Also, Mizushima et al., 2012 claimed that ATG2 has a function in autophagosome closure. Therefore, it was hypothesized that WIPI4 and ATG2 might interact with each other and cooperate to regulate autophagosome closure in HeLa cells.

3.3.1 WIPI4 colocalizes and interacts with ATG2

To examine whether and how WIPI4 and ATG2 function together, the interaction and colocalization of WIPI4 with ATG2 in HeLa cells was examined. Endogenous WIPI4 locates both in the cytosol and on puncta in fed conditions (Fig.3.15A). More WIPI4 is recruited onto vesicles after 1-2 hours starvation (Fig.3.15A), whereas WIPI4-GFP is mostly cytosolic in fed conditions. WIPI4-GFP vesicles dramatically increase after 1-2 hours of starvation (Fig.3.15B). To obtain a quantifiable number of ATG2 and WIPI4 vesicles, the immunofluorescence was performed in starvation conditions. ATG2 and WIPI4 colocalised after starvation, 30% of WIPI4 vesicles were positive for ATG2 (Fig.3.15B), and 23% of ATG2 vesicles were WIPI4-positive (Fig.3.15B). The absolute number of WIPI4-GFP vesicles in starvation was approximately 85 per cell, comparable with the number of autophagosomes (Fig.3.15C). Moreover, it was confirmed that WIPI4 interacts with ATG2 in HeLa cells (Chapter 4, Fig.4.6). These data indicate that WIPI4 and ATG2 function together or serially.

3.3.2 WIPI4 loss of function was rescued by ATG2-GFP in basal conditions

To further confirm whether WIPI4 and ATG2-GFP function in the same process, ATG2-GFP rescue experiment was performed by quantifying LC3 dots immunofluorescence.

In conjunction with western blots, with the same treatments were examined. Fig3.16A shows that the number and area of LC3-II vesicles were increased by WIPI4 knockdown, and the increase was rescued by WIPI4-GFP overexpression (Fig.3.16B). LC3 vesicles in WIPI4 depleted cells transfected with GFP constructs were bigger compared to that rescued by WIPI4-GFP as shown in Fig.3.16C. As shown in Fig.3.16D, the WIPI4 siRNA transfected cell with ATG2-GFP vesicles (labelled by the white rectangle) contains much less LC3 vesicles than the one without ATG2-GFP (labelled by the blue rectangle) vesicles. The LC3 vesicles

in WIPI4 knockdown cells expressing ATG2-GFP were also less than in the WIPI4 siRNA and GFP transfected cells. The knockdown efficiency of WIPI4 and overexpression of WIPI4-GFP is shown in Fig.3.16F. To summarize, WIPI4 may function together with ATG2, and WIPI4 loss of function can be partially masked by overexpression of ATG2 in basal conditions. However, more experiments would be required to conclusively demonstrate this.

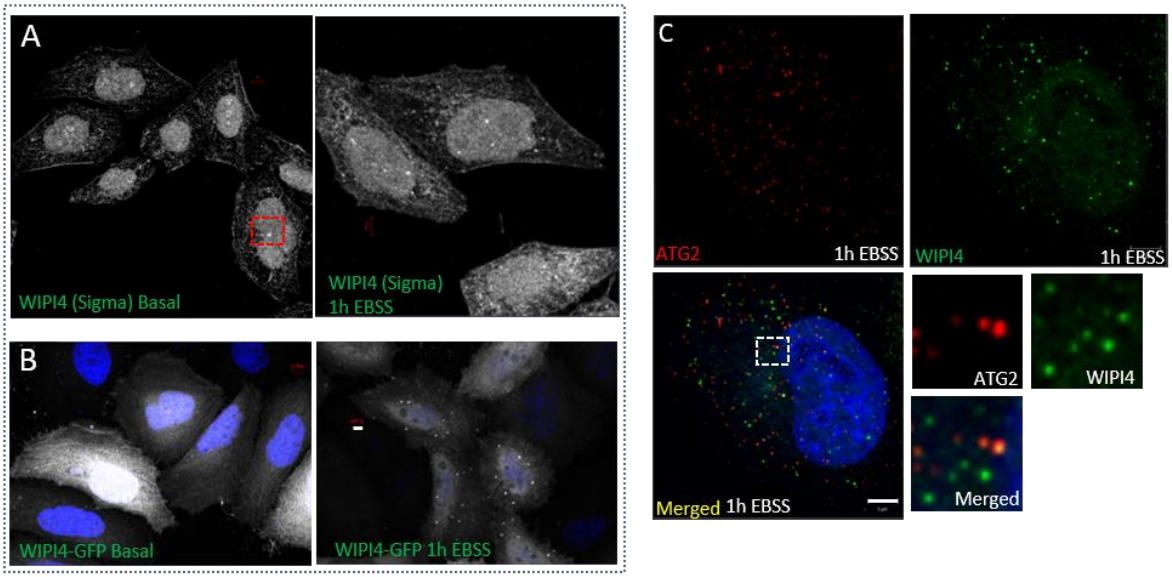

Figure 3.15 WIPI4 colocalizes with ATG2

A. The subcellular location of endogenous WIPI4 in wild-type HeLa cells grown in culture media and 1 hour in EBSS was assessed by WIPI4 antibody (Sigma) immunostaining. Scale bar = 5μm for all panels.

B. Subcellular location of WIPI4-GFP in wild-type HeLa cells grown in culture media and 1 hour in EBSS. HeLa cells were stained for DAPI (blue).

C. Endogenous ATG2 and WIPI4 immunostaining in HeLa cells. The endogenous WIPI4 localized on vesicles and these cells had ATG2 positive vesicles. Before fixation, cells were starved in EBSS for 4 hours and immunostained for endogenous ATG2 (Alexa 568) and WIPI4 (Alexa 488). Images were taken from 10-15 fields with 3-4 cells per field for each condition. The arrows show WIPI4 and ATG2 double positive vesicles.

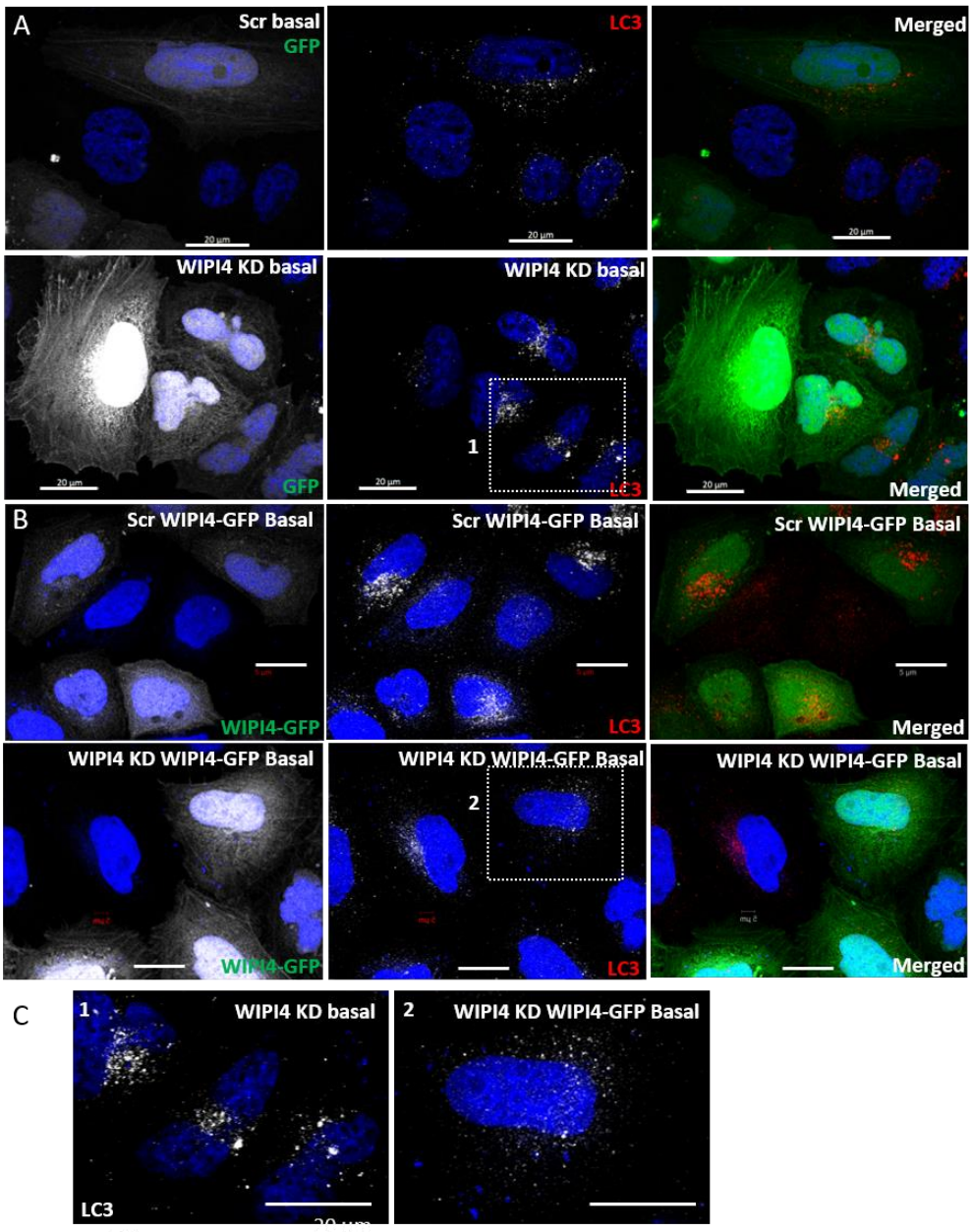

Figure 3.16 ATG2-GFP rescues WIPI4 knockdown caused increase of LC3-II vesicles under basal conditions

HeLa cells were transfected with two rounds of control or WIPI4 SMARTpool siRNAs. After the second transfection (72 hours), the cells were transfected with 1.5 µg GFP, or WIPI4-GFP or ATG2-GFP DNA constructs. Cells were incubated in growth media for another 24 hours until fixation and immunostaining for LC3 (anti-mouse Alexa 594).

A. HeLa cells transfected with GFP constructs. Scale bar: 20 µm
B. HeLa cells transfected with WIPI4-GFP constructs. Scale bar: 20 µm (white).
C. Enlarged images showing the LC3 puncta in HeLa cells transfected with GFP or WIPI4-GFP constructs after WIPI4 smartpool siRNA treatment.

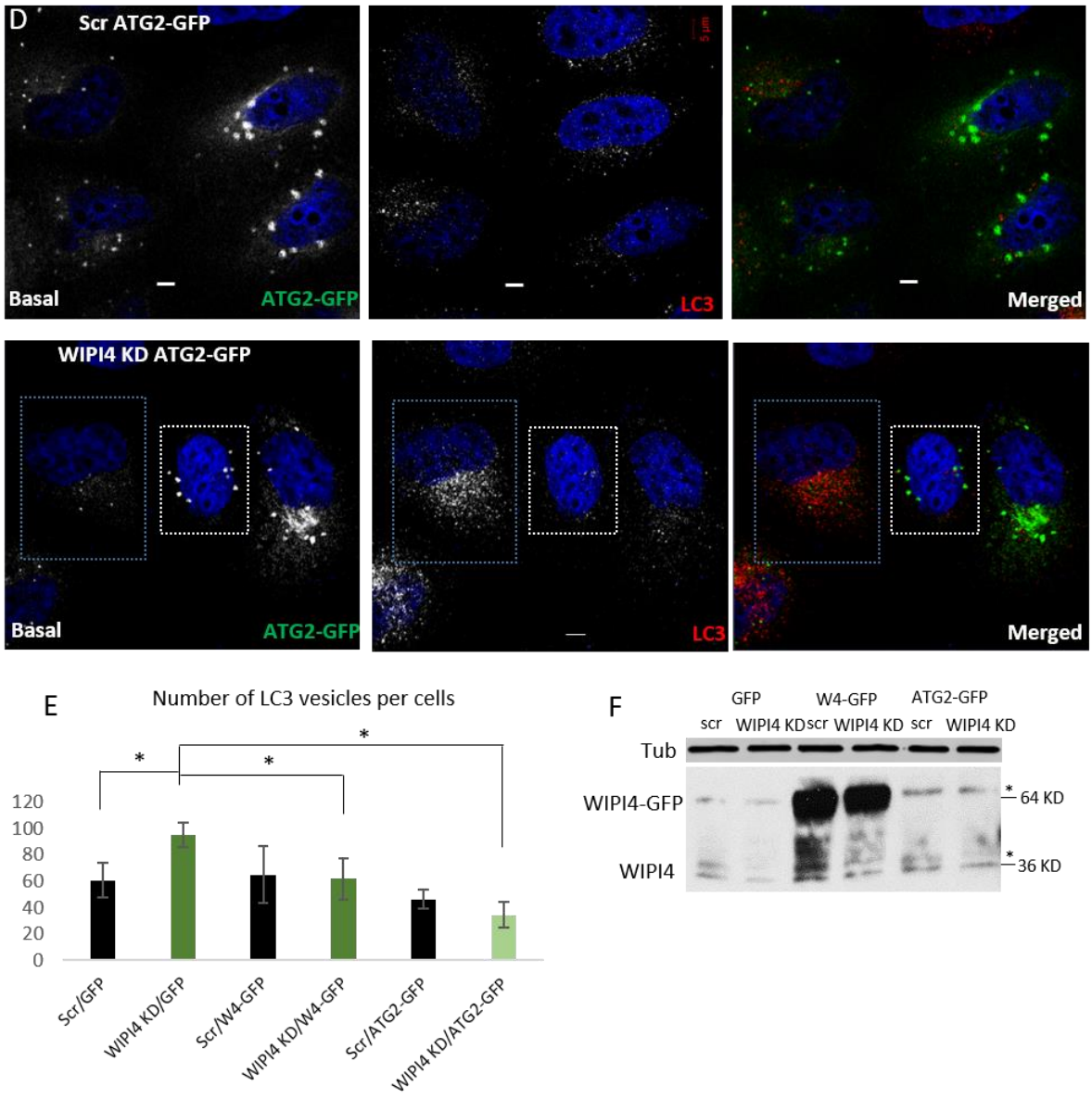

Figure 3.16 ATG2-GFP rescues WIPI4 knockdown by the number of LC3-II vesicles under basal conditions

D. HeLa cells transfected with ATG2-GFP constructs in combination with 100 nM Scrambled or ATG2A/B smartpool siRNA. Scale bars: 5 µm
E. The quantification of the number of LC3 vesicles in each condition. Mean ± SEM (*P<0.05, n.s. – not significant; two-tailed unpaired t-test). This experiment was repeated with similar results.
F. Knockdown efficiency of WIPI4 and overexpression levels of WIPI4-GFP.

3.3.3 WIPI4 depletion did not change the localization of ATG2-GFP on autophagosomes

The structure analysis of WIPI4 homolog Hsv2 indicates that it has all its membrane binding sites on the same side. Therefore WIPI4 may not tether membranes by itself. Instead, it may regulate autophagosome closure together with its interactors. The possible mechanisms are:

1) Recruiting ATG2 onto autophagosomes and facilitate the tethering of isolation membrane ends/autophagosomes and lysosomes.
2) Instead of recruiting ATG2 onto membrane structures, WIPI4 may function with ATG2 interdependently.
3) WIPI4 may be required for the recruitment or activity of other closure regulators.

First, it was examined if WIPI4 recruits ATG2 onto autophagosomes. In yeast, there is contradictory evidence about the sequential recruitment of Atg2 and Atg18. Takatori et al. 2012, claimed that Atg18 is required for the recruitment of Atg2 onto the PAS (phagophore assembling site). However, Gómez-Sánchez et al. suggest that the Atg2 association to Atg9 induces a conformational change that together in the presence of PtsIns3P on autophagosomal membranes, promotes the specific recruitment of Atg18. To understand how WIPI4 assists ATG2 function in tethering large vesicles, experiments were performed to identify if WIPI4 regulates the localization of ATG2 onto autophagosomes and lysosomes.

If WIPI4 recruits ATG2 onto autophagosomes, WIPI4 knockdown should decrease the colocalization of ATG2-GFP and LC3. Fig.3.17 shows that the colocalization of ATG2-GFP with LC3 was not changed by WIPI4 knockdown in basal conditions. In parallel, the colocalization of ATG2-GFP and LC3 was not changed by WIPI4 knockdown in starvation conditions (Fig.3.18). Therefore, WIPI4 is not upstream of ATG2 in the autophagosome closure process. Instead, WIPI4 and ATG2 may regulate autophagosome closure interdependently.

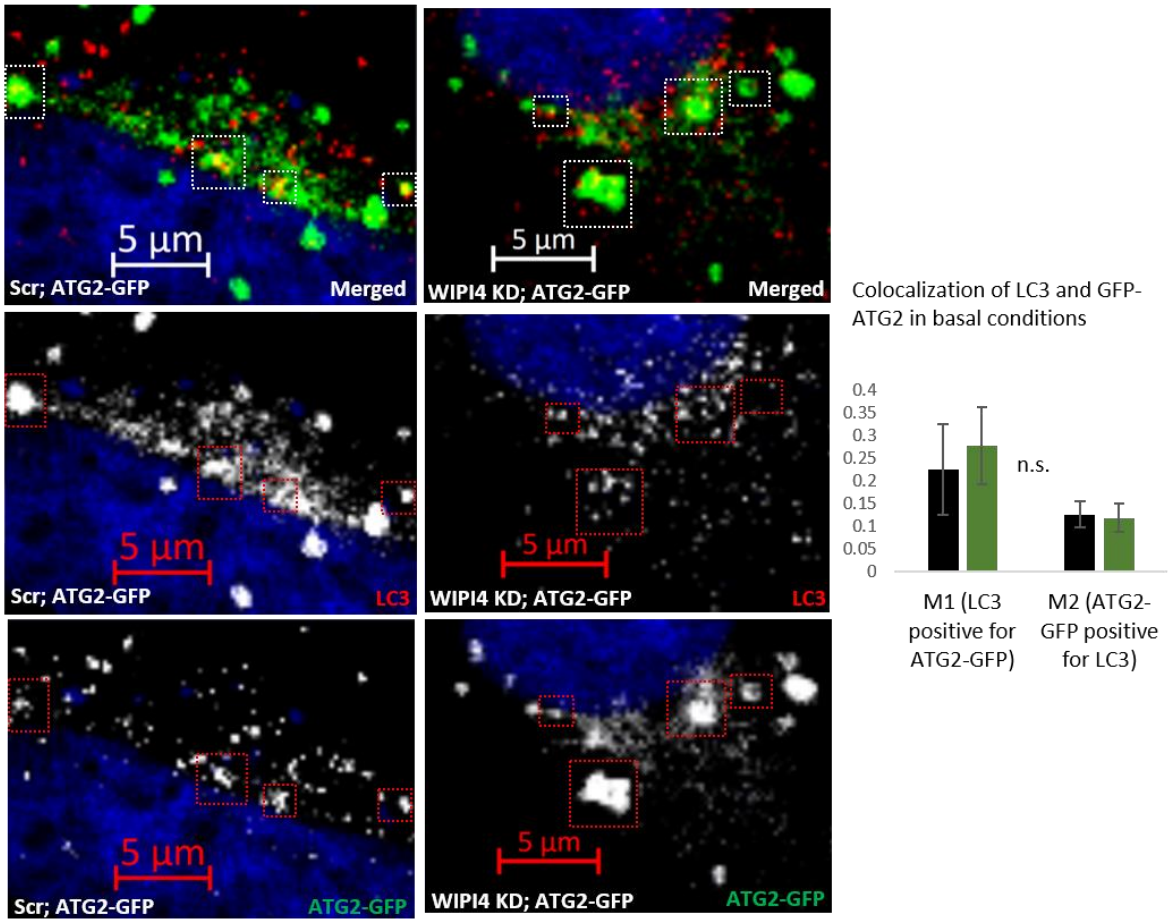

Figure 3.17. WIPI4 is not required for the autophagosome localisation of GFP-ATG2A in basal conditions

HeLa cells were transfected with two rounds of control or WIPI4 SMARTpool siRNAs. After the second transfection (72 hours), the cells were transfected with 1.0 µg GFP-ATG2A and cultured in growth media. Cells were immunostained for LC3 (anti-mouse Alexa 594) after 24 hours. Scale Bars: 5 µm.The colocalization of GFP-ATG2A with LC3 was measured by Mander's coefficient M1 which represents the percentage of LC3 vesicles positive for ATG2-GFP and M2 which represents the percentage of ATG2-GFP positive for LC3. (n.s., non-significant; two-tailed unpaired student's t-test).

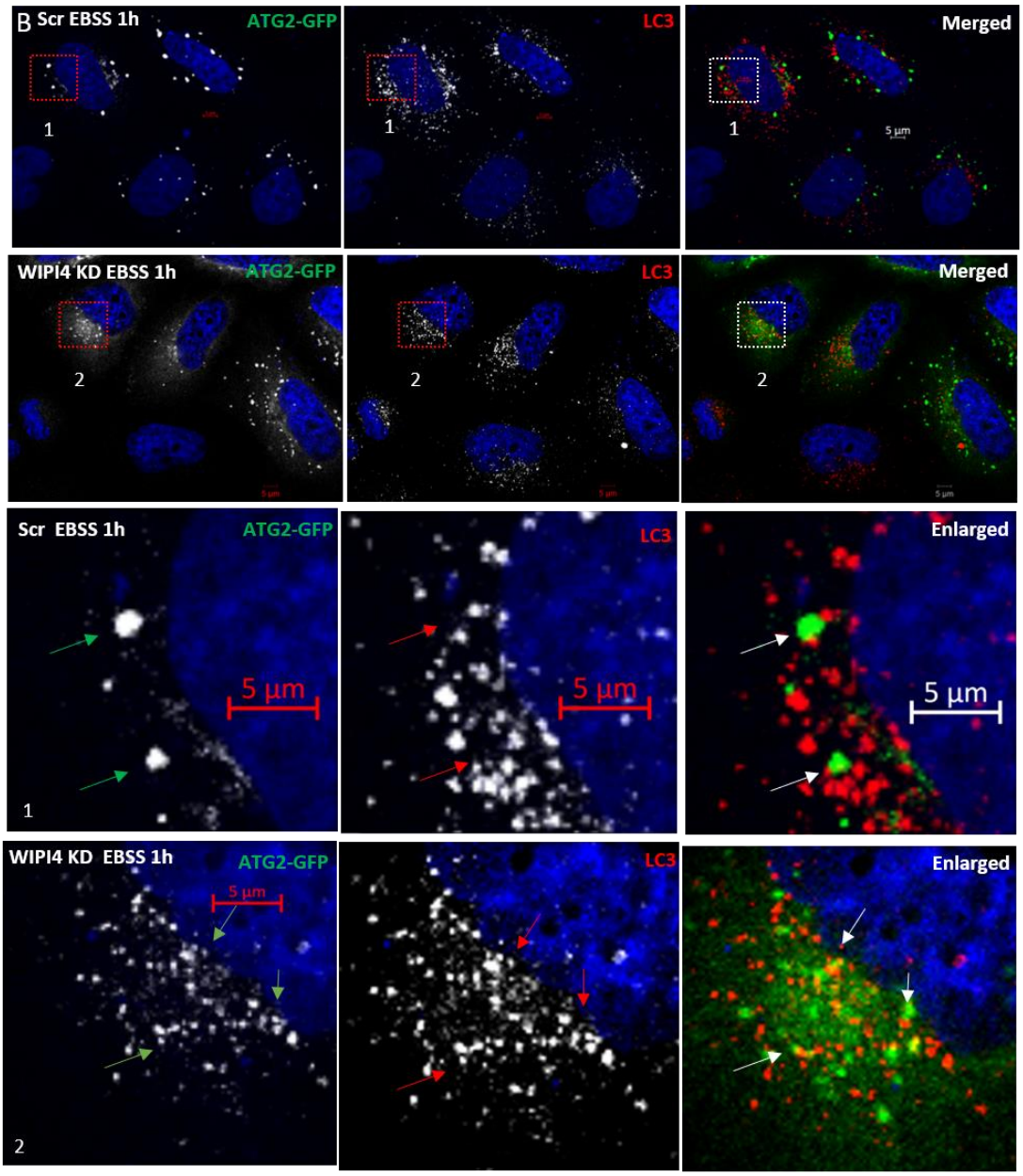

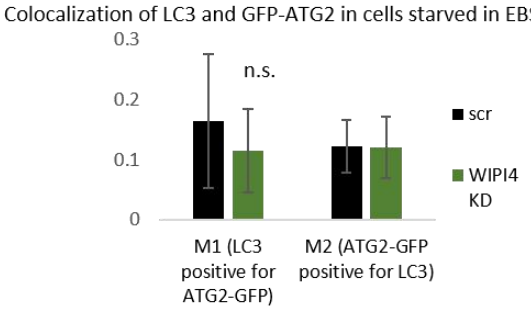

Figure 3.18 WIPI4 is not required for autohagosome localisation of GFP-ATG2A in starvation
Experiments were done similarly with that in Figure 3.17 but cells were incubated in EBSS for 1h prior to fixation.

3.4 Summary of results

The experiments in this chapter showed that WIPI4 knockdown increased LC3-II by protein levels in basal conditions, but did not change that in the presence of BafA1; GFP-RFP-LC3 reporter assay indicated that the number of autolysosomes decreased. Moreover, the clearance of autophagy substrates, both Huntingtin-Q74 and p62-GFP, was slowed down in WIPI4 knockdown conditions, implying that the autophagy function is impaired. However, since the LC3-II was accumulated as shown by both western blots as well as the number and size of LC3-II positive vesicles, WIPI4 loss of function may block the autophagy flux at a step after LC3 conjugation. Therefore, all the steps after LC3 conjugation were assessed. It was found that WIPI4 loss of function did not stop the autophagosomes leaving the recycling endosomes, or their fusion with lysosomes, or the lysosome degradative ability. The left possibilities are the late expansion or the closure of phagophores. In addition, loss of function of WIPI4 and ATG2 affects lysosome acidification differently (Fig.3.10 & 3.19), suggesting that WIPI4 may also have other functions independent of ATG2.

Next, the potential mechanisms of WIPI4 regulating the late stage of autophagosome formation were explored. WIPI4 is not required for the recruitment of ATG2, its interactor, onto autophagosomes.

Altogether, the experiments above defined the stage of the autophagy pathway where WIPI4 functions and found that WIPI4 regulates the late stage of autophagosome formation in basal conditions together with ATG2.

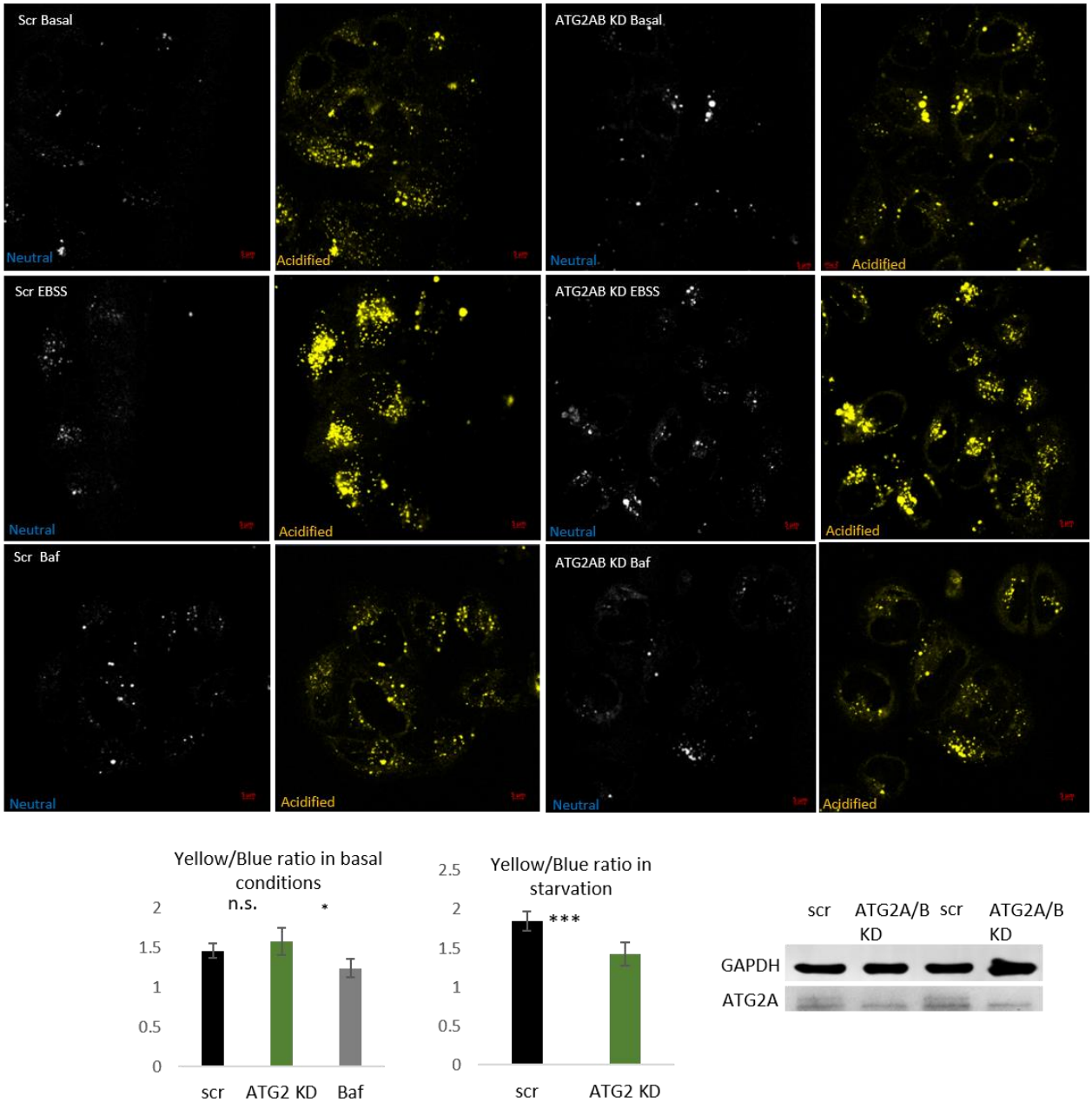

Figure 3.19 Lysosome acidification was decreased by ATG2AB knockdown in starvation conditions

Lysosomal pH in ATG2A/B-depleted cells in both basal and starved conditions. The Lysosensor Yellow/ Blue intensity was measured in both yellow and blue channels. Intensity ratio is a qualitative measure of lysosomal pH. Bafilomycin A1 (Baf A1) was used as a positive control (400 nM, 4 hours) for increased lysosomal pH. More than 50 cells were analysed per experiment, for each condition. Experiments were performed at least 3 times with similar results. (*P<0.05; ***P<0.05; n.s., not significant; two-tailed unpaired t-test). The blots show the knockdown efficiency of ATG2A.

Chapter 4 The mechanism of WIPI4 function in autophagy

The previous chapter illustrates that WIPI4 regulates the late stage of autophagosome formation in basal conditions. However, the closure defect was minor compared to that caused by ATG2A/B knockdown, suggesting that WIPI4 may have additional functions independent of ATG2. Thus, this chapter will explore further the function of WIPI4 in closure and other autophagy processes if there are.

4.1 WIPI4 regulates GABARAP levels

First, the colocalization of WIPI4 with autophagosome markers was explored to understand whether WIPI4 localizes on autophagosomes. To gain clear WIPI4 staining, multiple antibodies and cell lines were tested. C2C12 cells give much better WIPI4 staining than in HeLa cells. Fig.4.1 demonstrates that WIPI4 colocalizes with ATG8 in both HeLa (Fig.4.1A) and C2C12 cells (Fig.4.1B), but to a more significant extent with GABARAP. In starved HeLa cells, less than 10% of mRFP-LC3 vesicles colocalize with WIPI4-GFP vesicles (Fig.4.1C). Instead, many of them are adjacent to each other. As shown by live imaging (Fig.4.1D), mRFP-LC3 vesicles were observed to travel around WIPI4-GFP vesicles (observed in two separate experiments).

GABARAP recruits autophagosome-lysosome tethering regulators (Manil-Ségalen et al., 2017) (Albanesi et al., 2015), and ATG8 lipidation may accelerate autophagosome closure (Tsuboyama et al., 2016), suggesting that GABARAP may function in either or both closure and fusion steps, in other words, together or downstream of WIPI4 in the maturation of autophagosomes. To investigate this, GABARAP levels in cells depleted of WIPI4 were first examined.

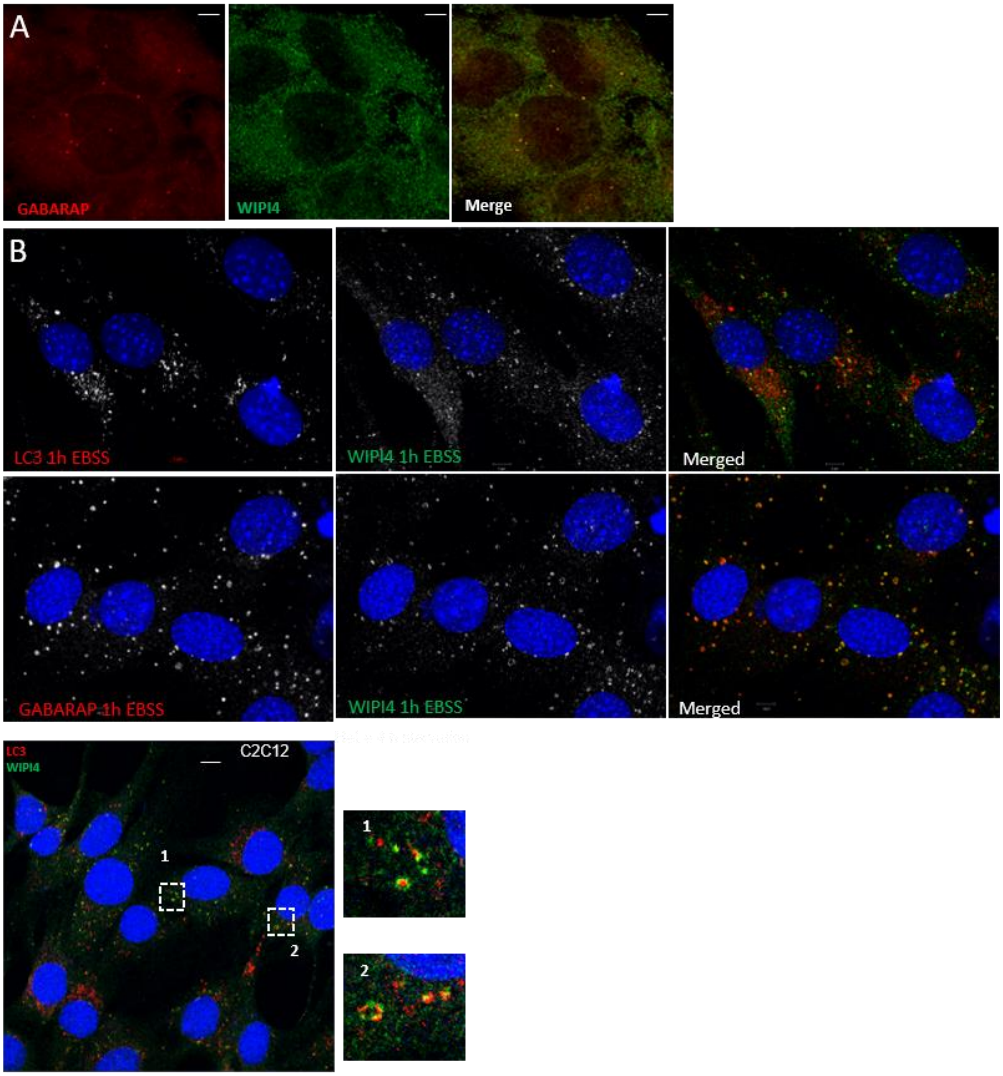

Figure 4.1. WIPI4 colocalizes with mammalian ATG8 family proteins

A. Representative images showing the colocalization of GABARAP (anti-rabbit Alexa 594) and WIPI4 (anti-mouse Alexa 488) in HeLa cells. Before fixation, cells were incubated in EBSS for 4 hours. Bars: 5 μm.

B. Representative images showing the colocalization of LC3 (anti-rabbit Alexa 594) with WIPI4 (anti-mouse Alexa 488) and GABARAP (anti-rabbit Alexa 594) with WIPI4 (anti-mouse Alexa 488) in C2C12 cells starved for 4 hours in EBSS. The three panels below are enlarged images showing the colocalization of endogenous LC3 and WIPI4.

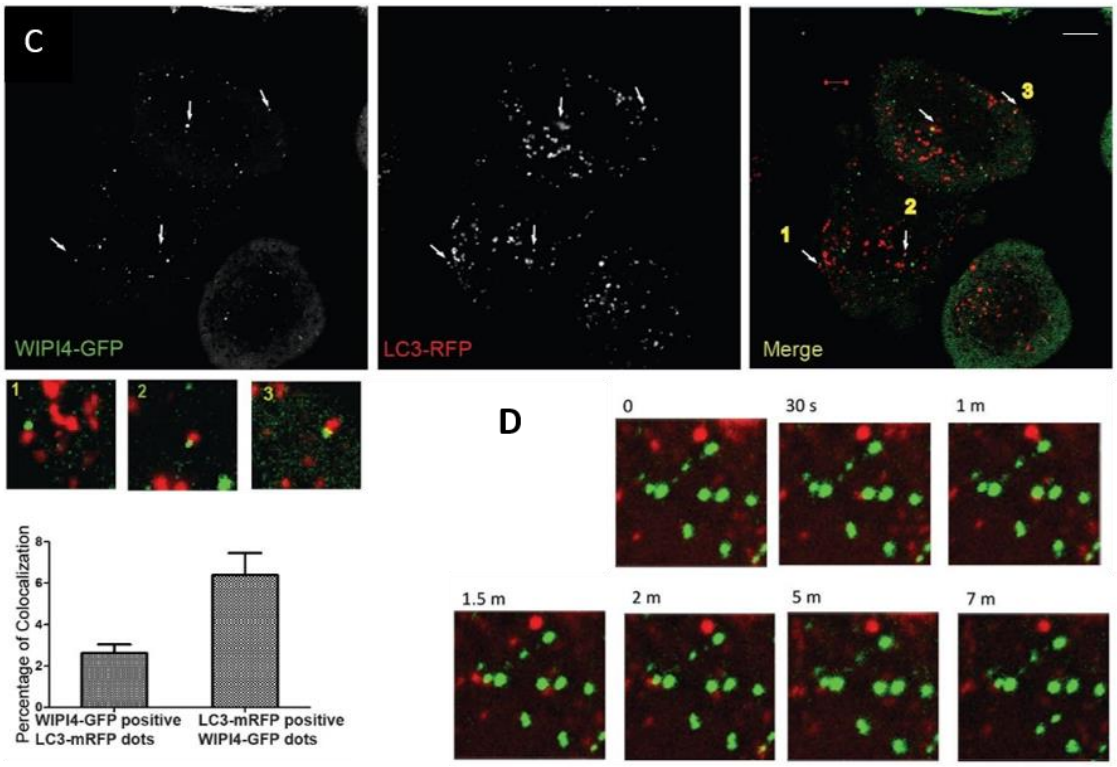

Figure 4.1. WIPI4 colocalizes with mammalian ATG8 family proteins

C. Representative WIPI4-GFP and mRFP-LC3 immunostaining in HeLa cells. HeLa cells were transfected with WIPI4-GFP and mRFP-LC3 24 hours prior to incubation in EBSS (3 hours) and visualized by live cell imaging. Some WIPI4-GFP positive vesicles were observed near mRFP-LC3 positive vesicles (enlarged areas showed below). Quantification of WIPI4-GFP positive mRFP-LC3 vesicles in C. The graph represented the mean ± SEM (n=20) of a representative experiment of three biological replicates.

D. Images from a movie taken in C showing WIPI4-GFP vesicles interact with RFP-LC3 vesicles. Before imaging, cells were incubated in EBSS for 4 hours. Images were captured every 30 seconds for 7 minutes.

4.1.1 WIPI4 knockdown decreases GABARAP-I levels

As shown in Figure 4.2A, GABARAP-I but not GABARAP-II levels were decreased by WIPI4 knockdown in HeLa cells. In contrast, LC3-I levels were not changed, and LC3-II levels were increased in both basal and starvation conditions (Fig.4.2B). The knockdown efficiency of WIPI4 is shown in Figure 4.2C. Similarly, GABARAPL1-I levels were decreased, but GABARAPL1-II levels were not significantly altered (Figure 4.3).

This indicates that WIPI4 regulates the abundance of GABARAP. To understand whether this regulation is required for WIPI4 function in autophagy, it was first assessed whether GABARAP knockdown phenocopies WIPI4 knockdown regarding LC3 levels and if WIPI4 knockdown still blocks autophagic flux in GABARAP depleted conditions.

4.1.2 GABARAP is required for WIPI4 function

4.1.2.1 GABARAP knockdown blocks autophagy flux

Similar to WIPI4 knockdown, the knockdown of GABARAP alone and three GABARAP family proteins together increased LC3-II levels in the absence of BafA1 but did not change LC3-II levels in the presence of BafA1 (Figure 4.4 A&B). GABARAP-GFP overexpression also decreased the percentage of cells containing Htt-Q74 aggregates (Figure 4.4C). This suggests that GABARAP functions in late stages of autophagosome formation, downstream of LC3 conjugation, similar to WIPI4.

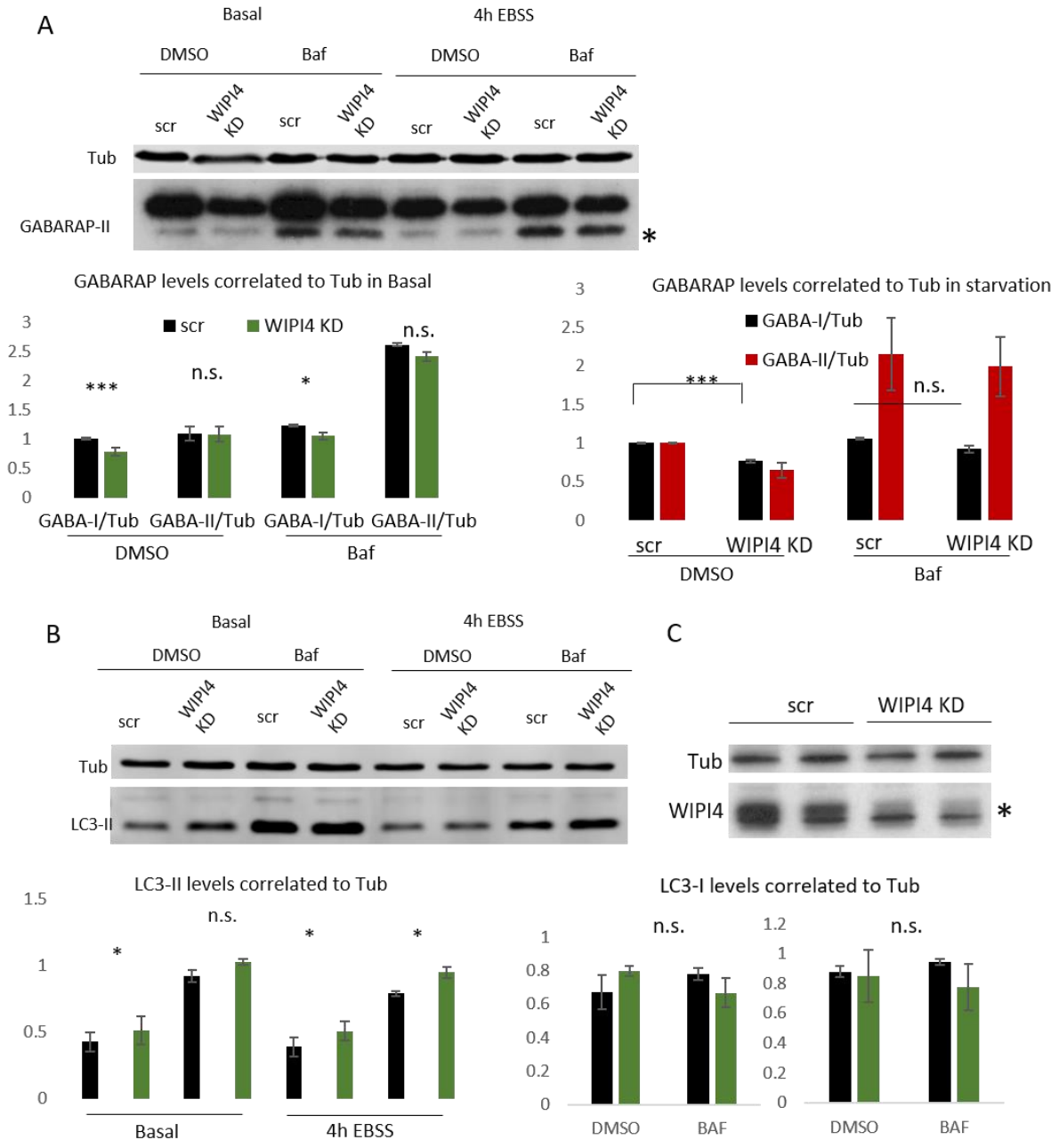

Figure 4.2. WIPI4 knockdown decreases GABARAP-I levels

A. Effects of WIPI4 knockdown on GABARAP levels with tubulin as the internal control. HeLa cells transfected with two rounds of control or WIPI4 SMARTpool siRNA (60 nM) for 5 days were incubated with 400 nM BafA1 or DMSO in culture media or EBSS for the final 4 hours before analysis by western blots. The graphs below show the quantitative analysis of GABARAP-I/II levels relative to tubulin from the blots (*P<0.05, n.s., non-significant; two-tailed unpaired student's t-test). This is representative data of 3 experiments.

B. Effects of WIPI4 knockdown on LC3 levels in the samples in A.

C. Western blots showing the knockdown efficiency of WIPI4 proteins of the samples in A & B.

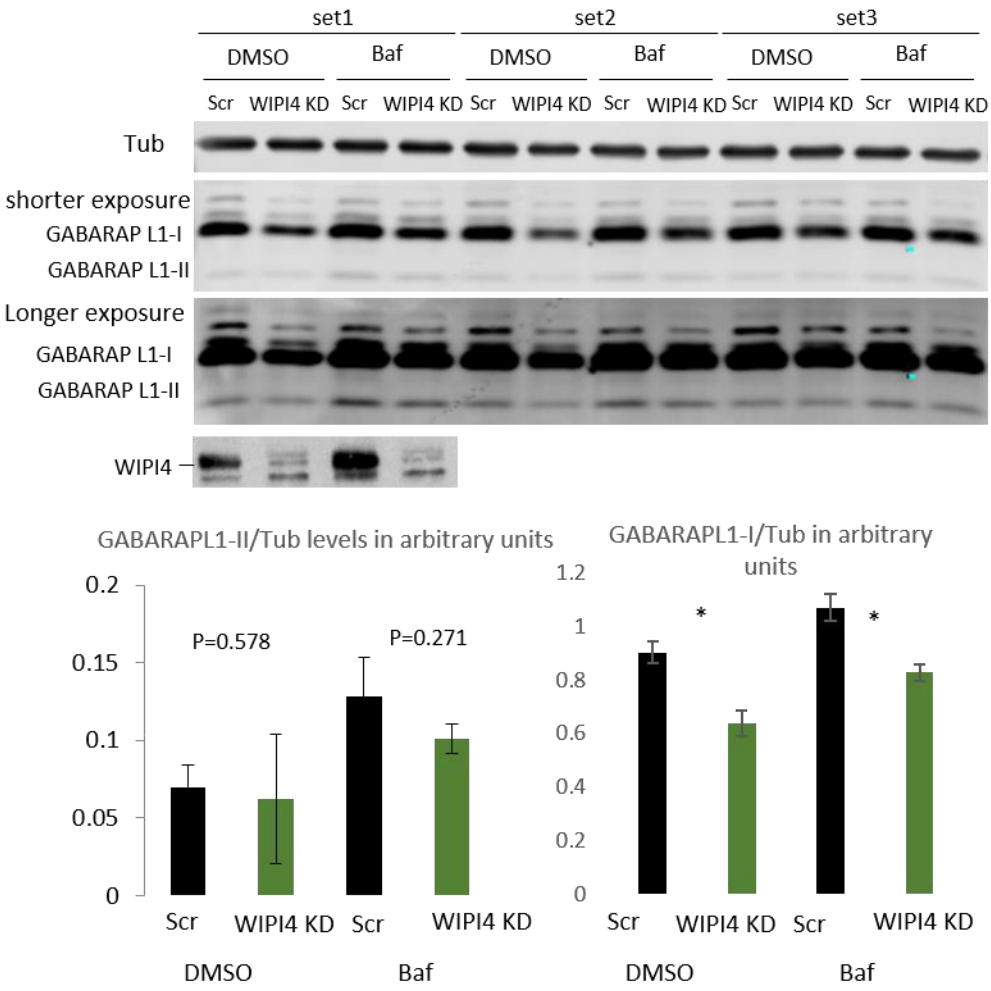

Figure 4.3 WIPI4 KD decreased GABARAPL1-I levels

HeLa cells were transfected with two rounds of control or WIPI4 SMARTpool siRNA (60 nM) for 5 days, were incubated with 400 nM BafA1 or DMSO in culture media. The graphs below show the quantitative analysis of GABARAPL1-I/II and WIPI4 levels relative to tubulin from the blots (*P<0.05, n.s., non-significant; two-tailed unpaired student's t-test).

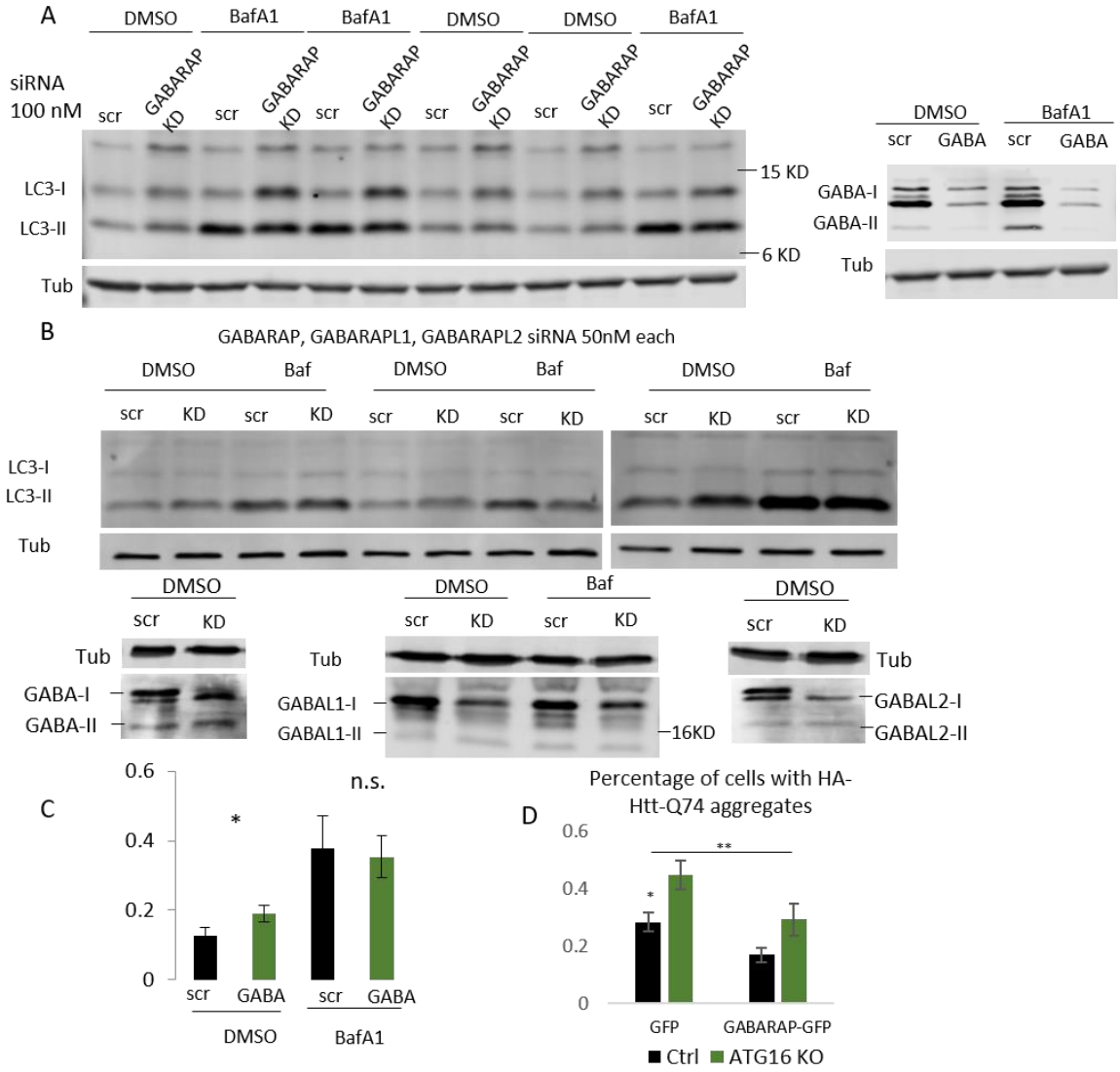

Figure 4.4. GABARAP loss of function inhibits the autophagy flux

A. Effects of GABARAP knockdown on LC3-II levels with tubulin as the internal control. HeLa cells were transfected with control or GABARAP SMARTpool siRNA (100nM) for 72 hours and incubated with 400 nM BafA1 or DMSO in culture media. The small western blot panel shows the knockdown efficiency of GABARAP.

B. HeLa cells were transfected with control (Scr 150 nM) and GABARAP/GABARAPL1/GABARAPL2 siRNA (50 nM SMARTpool for each) for 72 hours, then incubated with 400 nM BafA1 or DMSO in culture media. The blots below represent the knockdown efficiency of each GABARAP family proteins with tubulin as the internal control.

C. The graph represents the quantitative analysis of LC3-I/II levels relative to tubulin from the blots in A (*P<0.05, n.s., non-significant; two-tailed unpaired student's t-test). This is representative data of 3 experiments.

D. Quantification of EGFP-HTT (Q74) aggregation in GABARAP family protein-depleted wild-type and ATG16L1 knockout HeLa cells. Cells were seeded on coverslips in triplicates, transfected with siRNAs targeting control or all GABARAP proteins, followed by 1 µg of EGFP-HTT(Q74) overexpression. More than 300 cells on each slide were counted. Bars—means of percentages of cells with aggregates ± s.d. (n=3; **P<0.01; *P<0.05; two-tailed unpaired t-test). Similar results were observed in repeated experiments.

4.1.2.2 WIPI4 knockdown does not increase LC3-II levels in GABARAP triple knockout HeLa cells.

Figure 4.5 shows that there is no accumulation of LC3-II in GABARAP triple knockout HeLa cells transfected with WIPI4 siRNA compared to scrambled siRNA, suggesting that WIPI4 functions at the same level or upstream of GABARAP.

The above results confirm the previous hypothesis that WIPI4 functions together or upstream of GABARAP in the autophagy pathway.

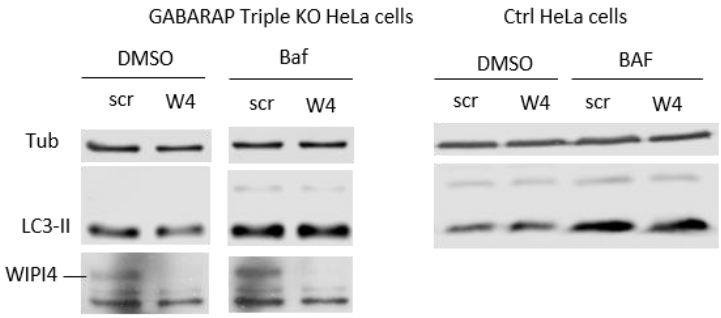

Figure 4.5. WIPI4 function in autophagy is GABARAP dependent

Representative blots showing the effect of WIPI4 knockdown on LC3-II levels in GABARAP triple KO and CTRL HeLa cells. Cells were transfected with 60 nM siRNA for 72 hours, then were incubated in culture media containing 400 nM BafA1 or DMSO before harvesting.

4.1.3 WIPI4 indirectly regulates the subcellular localization of GABARAP

The next question is how WIPI4 regulates GABARAP and whether this regulation is required for closure. Based on the fact that total GABARAP protein levels were reduced by WIPI4 loss of function, the autophagy-active GABARAP pool may be regulated by WIPI4:

i. through regulating GABARAP lipidation;
ii. through direct interaction with it;
iii. through indirectly regulating GABARAP subcellular trafficking independent of lipidation.

It is known that GABARAP and LC3 are lipidated through the same machinery (Zens et al., 2014), while GABARAP and LC3 are differently regulated by WIPI4 as shown in Figure 4.2, suggesting that WIPI4 may not regulate GABARAP through the lipidation machinery.

Figure 4.6 suggests that WIPI4 does not interact with GABARAP. ATG2 was blotted as a positive control for the co-IP experiment. Thus, if WIPI4 regulates the localization of GABARAP, it might be through regulating its trafficking indirectly.

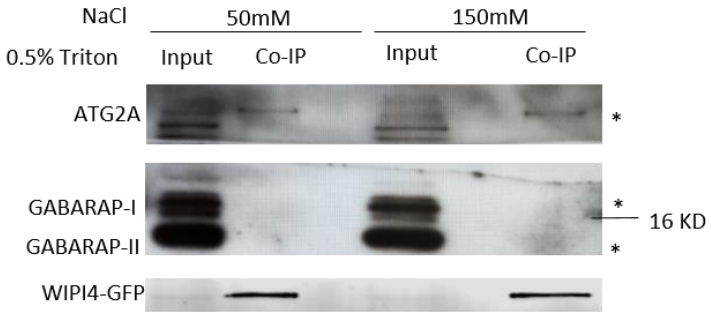

Figure 4.6. WIPI4 does not interact with GABARAP

Transiently overexpressed WIPI4-GFP in HeLa cells were immunoprecipitated by GFP-Trap beads. The elutions in laemmli buffer were resolved by western blotting and probed for GABARAP and ATG2. IP buffer with different concentrations of NaCl was used to stabilize the potential interaction between WIPI4-GFP and GABARAP.

4.1.4 WIPI4 does not decrease the autophagosome localization of GABARAP-II.

If WIPI4 recruits GABARAP onto autophagosomes, WIPI4 knockdown may decrease the number of GABARAP positive vesicles. However, the blockage of autophagy flux accumulates and increases the absolute number of autophagosomes, as shown in ATG2AB knockdown (Figure 4.7). The accumulation of autophagy markers caused by the blockage of autophagy flux may impair the observation of recruitment defects.

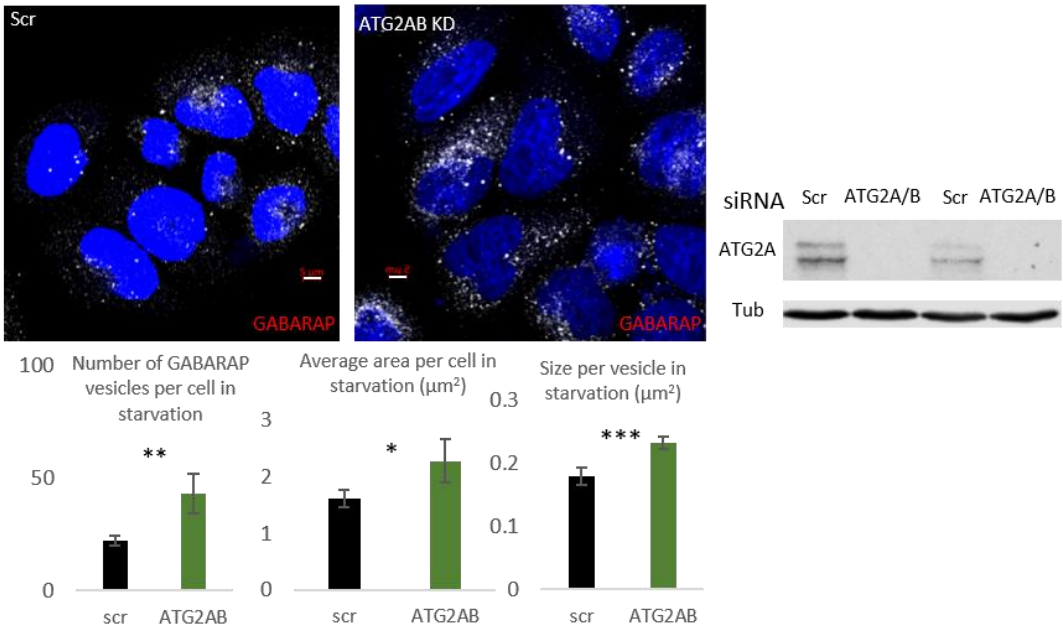

Figure 4.7 ATG2A/B knockdown blocks autophagy flux and accumulated GABARAP vesicles

HeLa cells transfected with control or ATG2A/B siRNA were labelled for GABARAP (Alexa 594 rabbit). The number and area of GABARAP vesicles /cell are shown in the graphs below. Data are means ± SEM; more than 40 cells were counted in each condition. This experiment was repeated twice. Scale Bar: 5 µm. ***p<0.001, **p<0.01,*p<0.05, unpaired two-tailed t-test.

To determine if there was a recruitment defect, LC3 and ATG16 were used as internal positive controls, since vesicles positive for LC3 and ATG16 accumulate when WIPI4 is knocked down. If there is reduced recruitment of GABARAP onto autophagosomes, there should be a decrease in the percentage of GABARAP-positive LC3 and ATG16 vesicles out of all LC3 and ATG16 vesicles. However, WIPI4 knockdown did not change the colocalization of GABARAP with LC3 or ATG16 (Figure 4.8).

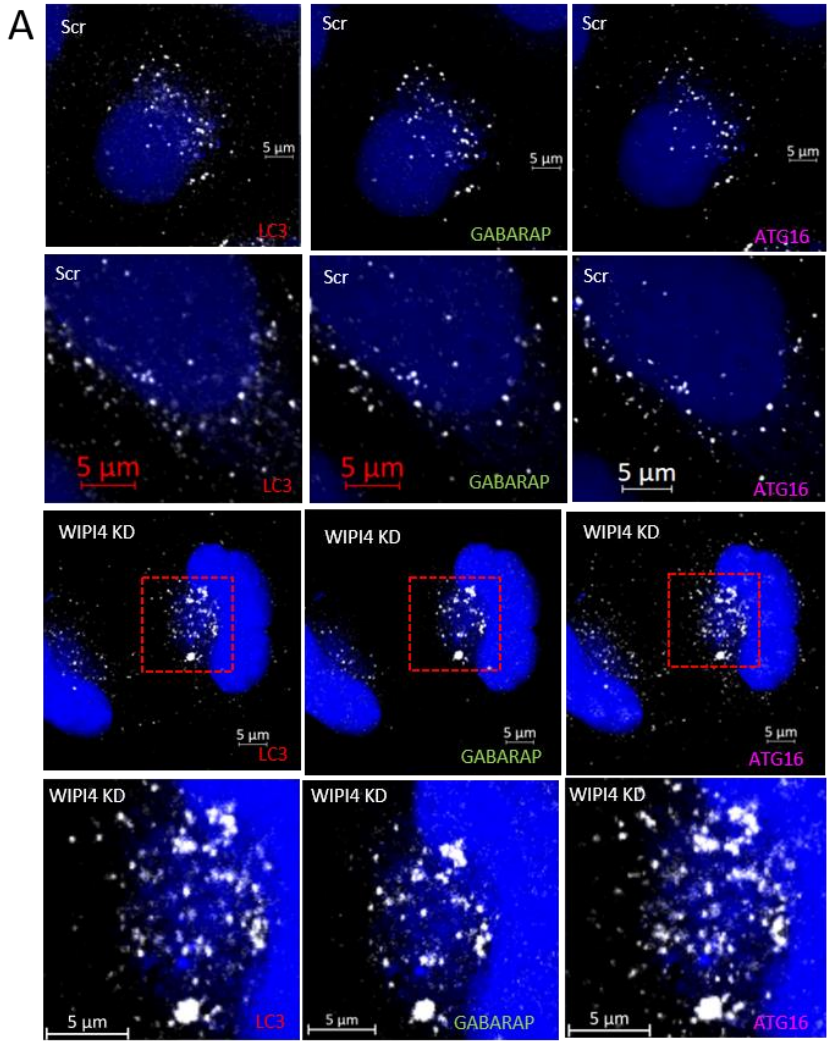

Figure 4.8. GABARAP is normally recruited onto autophagsomes in WIPI4 knockdown cells

HeLa cells were transfected with WIPI4 siRNA for 72 hours. In order to get clear GABARAP staining, cells were incubated in EBSS during the last hour before fixation.

A. Single channel images showing the increase of LC3, GABARAP, ATG16 positive vesicles in WIPI4 depleted cells. Scale bar: 5 µm.

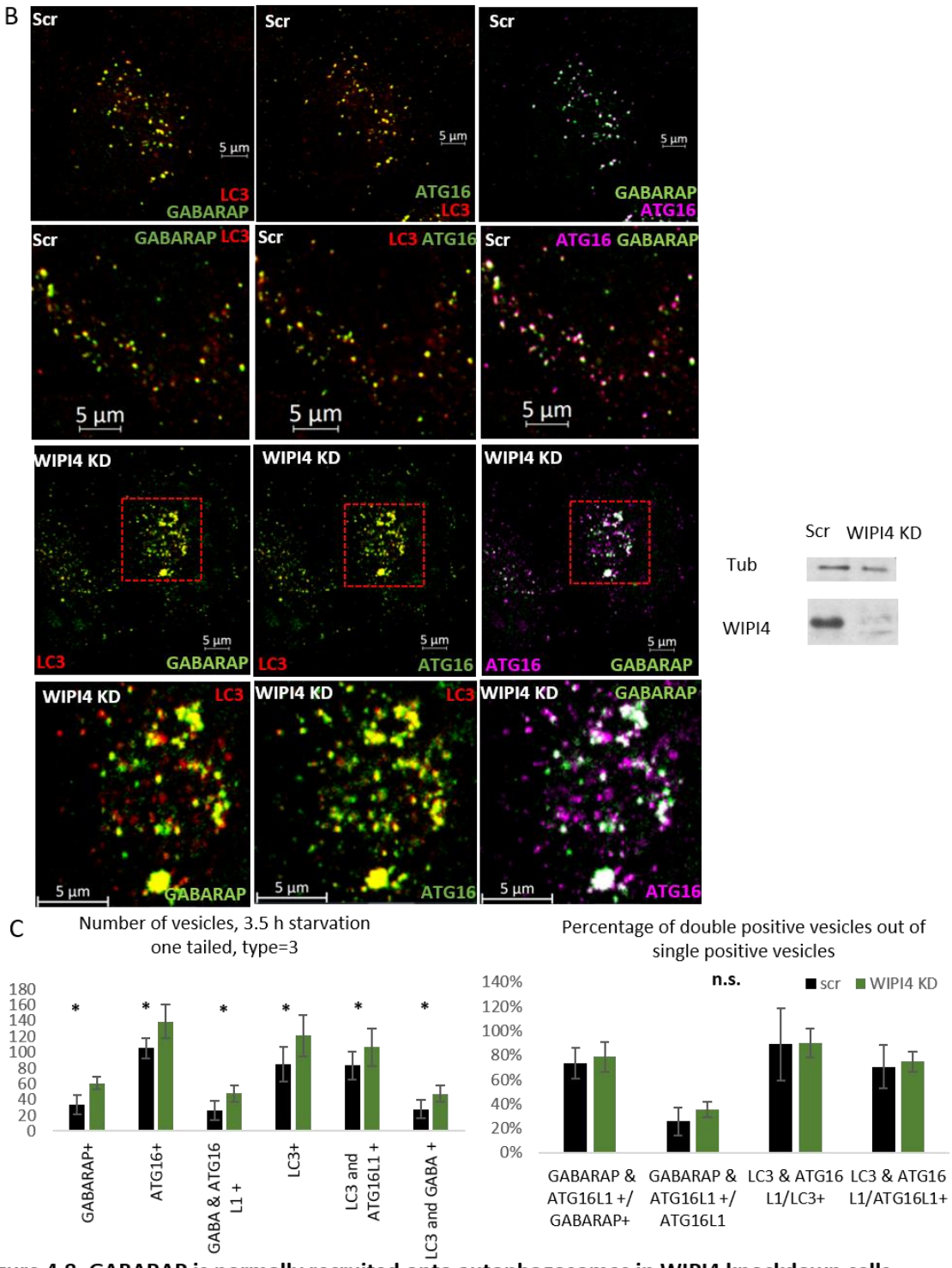

Figure 4.8. GABARAP is normally recruited onto autophagosomes in WIPI4 knockdown cells

B. Representative images showing that the colocalization of GABARAP with LC3 and GABARAP with ATG16 both increased in WIPI4 depleted cells. Scale bar: 5 µm.

C. Quantification of the number of LC3, GABARAP and ATG16 vesicles and the number of double positive vesicles. Means ± SEM, more than 40 cells were counted. ,*p<0.05, unpaired one-tailed *t-test*.

D. Measurement of the overlap of GABARAP-ATG16L1 double positive vesicles and total ATG16L1 vesicles, and the overlap of ABARAP-ATG16L1 double positive vesicles and total GABARAP vesicles, which indicate the relative enrichment of GABARAP compared to ATG16L1, a marker of early-stage autophagosomes. n.s., not significant, unpaired one-tailed *t-test*. The knockdown efficiency of WIPI4 is shown next to the graph by western blots.

4.1.5 WIPI4 regulates the trafficking of GABARAP

Even with the ATG16 and LC3 internal control, it is not enough to exclude the possibility that the block of autophagy flux accumulates GABARAP on autophagosomes. Therefore, the other membrane compartments on GABARAP trafficking route was examined to understand whether the active GABARAP pool is reduced.

Joachim reported in 2015 and 2017 that there is an active GABARAP-I reservoir on the centrosome satellites which can translocate onto autophagosomes during starvation. When the centrosome satellites are abnormally disassembled by PCM1 knockdown, centrosomal MIB1 can assess and degrade GABARAP; other centrosomal GABARAP accumulates on GM130 positive structures and becomes inactive (Diagram 4.1).

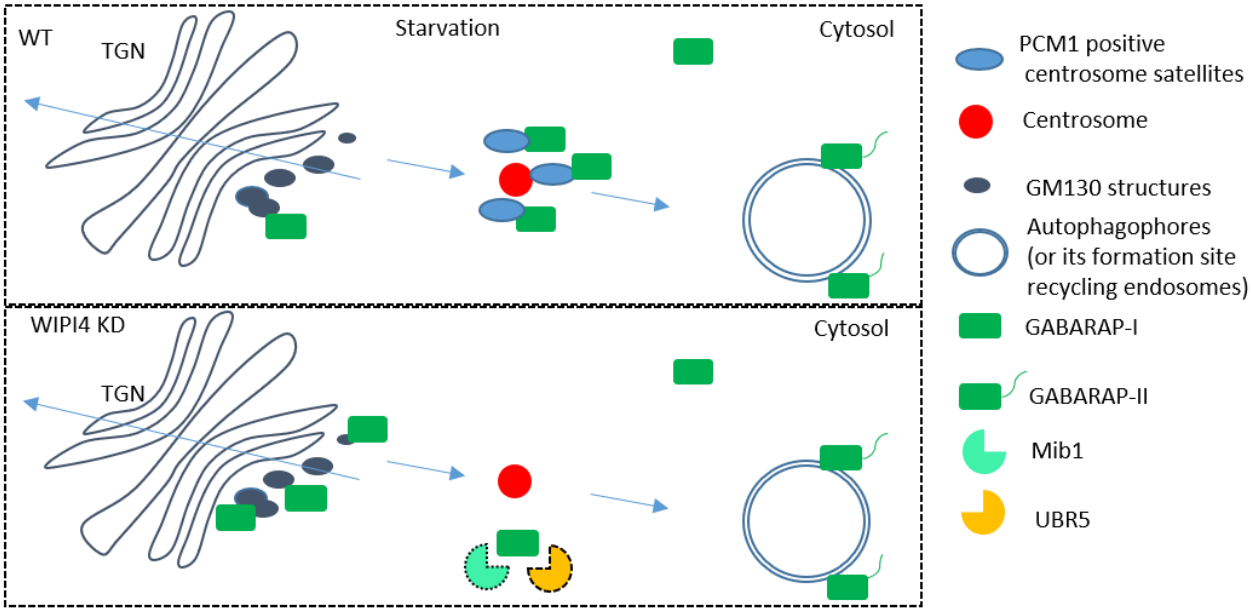

Diagram 4.1. The partial map of GABARAP trafficking: active GABARAP pool (on centrosome satellites) and inactive GABARAP pool (on GM130-positive structures)

As reported, GABARAP promotes the secretory transport from TGN but is not present on plasma membrane (reviewed in Mele & Duarte et al., 2019). Joachim et al. reported in 2015 and 2016 that there are at least two GABARAP pools: GABARAP on centrosome satellites and together with GM130. The former can be recruited onto autophagosomes in starvation conditions; the latter cannot.

Thus, centrosome satellite structures and the colocalization of GABARAPL1 with GM130 were examined. GABARAPL1 was similarly decreased in WIPI4 knockdown conditions, as shown in Figure 4.2. WIPI4 knockdown reduced the centrosome satellite marker PCM1 in both basal and starved conditions (Figure 4.9) and increased the GABARAPL1 colocalization with GM130 in basal conditions only (Figure 4.10). To summarise, WIPI4 knockdown reduces the active GABARAP pool.

Next, I tried whether rescuing the active GABARAP pool can rescue the block of autophagy flux.

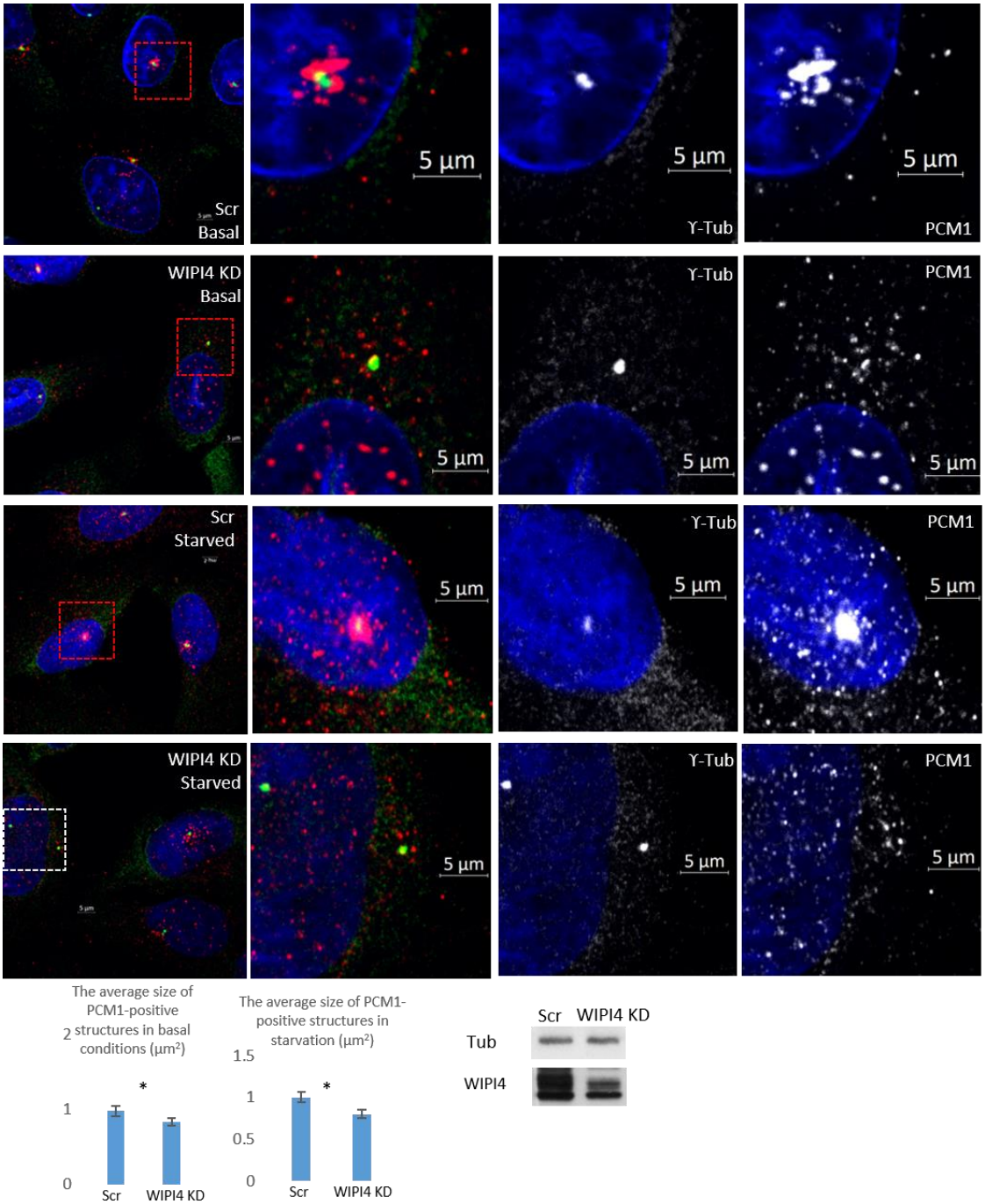

Figure 4.9. Centrosome satellites were disassembled by WIPI4 knockdown
Effect of WIPI4 knockdown on the centrosome satellite structure. HeLa cells were transfected with WIPI4 siRNA for 72 hours and incubated in culture medium or EBSS during the last 2 hours before fixation. Cells were stained for centrosome marker γ-tubulin (Alexa 488: mouse) and centrosome satellite marker PCM1 (Alexa 594: rabbit). The graphs below show the quantification of the average size of centrosome satellites, which is considered to be the total PCM1 signal in the cell. The knockdown efficiency of WIPI4 is shown by the western blots on the right

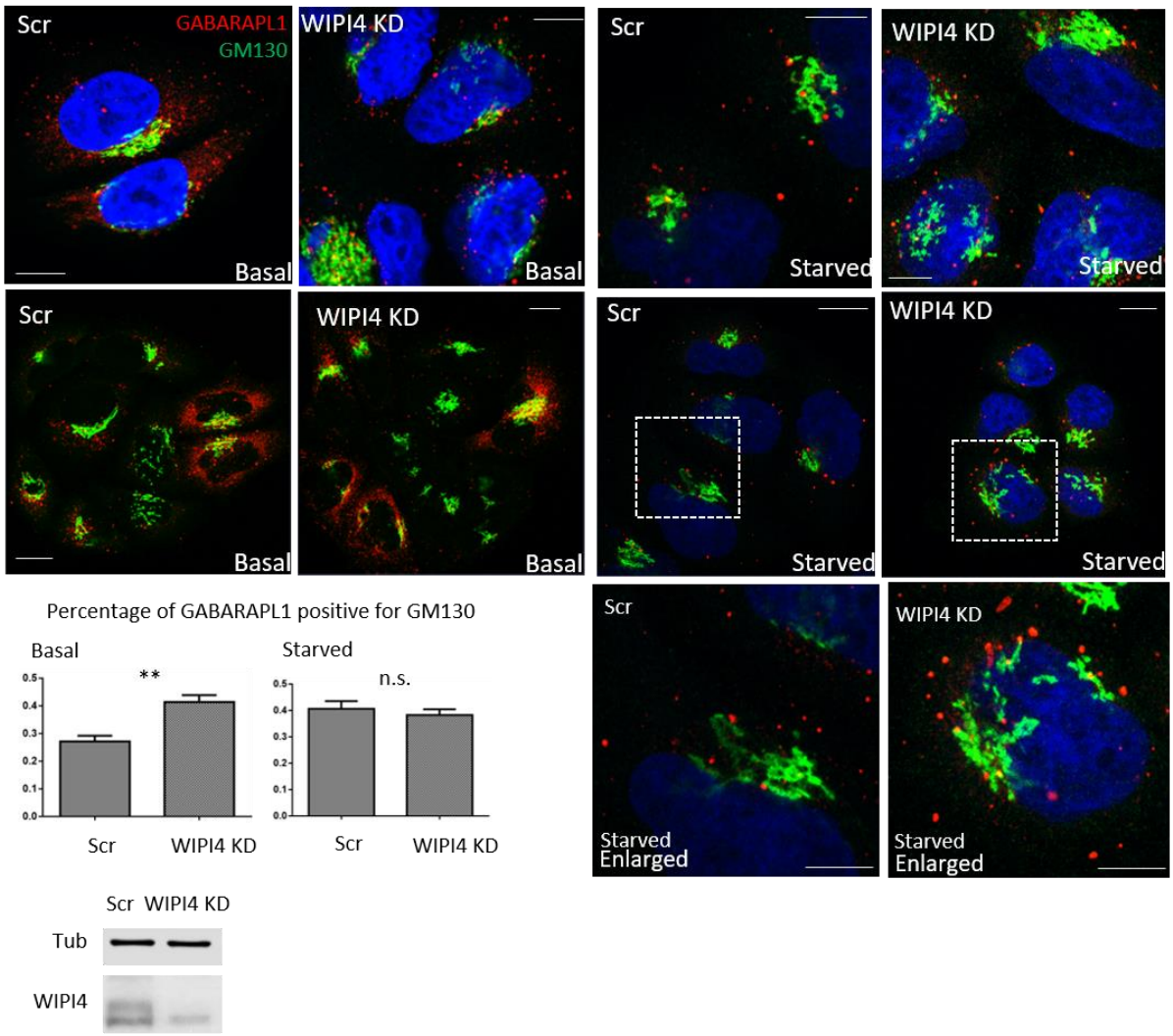

Figure 4.10. WIPI4 knockdown increased the colocalization of GABARAPL1 and GM130 in basal conditions.

Effect of WIPI4 knockdown on the inactive GABARAP (L1) pool labelled by GM130. HeLa cells were transfected with WIPI4 siRNA for 72 hours and incubated in culture medium or EBSS during the last 2 hours before fixation. Cells were stained for cis-Golgi marker GM130 (Alexa 488: mouse) and GABARAPL1 (Alexa 594: rabbit). The graphs show the percentage of GM130-positive GABARAPL1 out of all GABARAPL1. Means ± SEM, **p<0.01; *p<0.05, unpaired two-tailed t-test. Scale bar: 10 µm. The western blot panels show the protein levels of WIPI4 in control (scr) and WIPI4 knockdown samples.

4.2 WIPI4 knockdown destabilized GABARAP through the proteasome pathway

The decrease of GABARAP-I levels could be caused by either the decrease of transcription / translation or an increase in degradation. Cycloheximide treatment experiments suggest that GABARAP degradation was increased by WIPI4 knockdown (Figure 11).

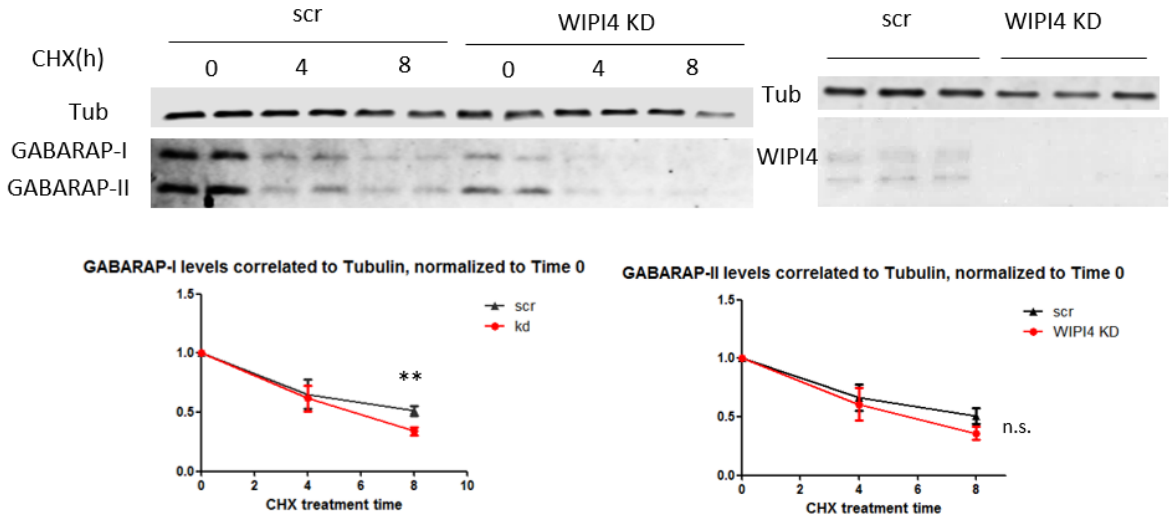

Figure 4.11. WIPI4 knockdown increased the degradation of endogenous GABARAP

A. Control or WIPI4 knockdown HeLa cells were subjected to cycloheximide (CHX) treatment for the indicated number of hours prior to immunoblotting. The panels on the right show the knockdown efficiency of WIPI4 siRNAs.
B. Quantification of A. Mean ± SEM; n = 3; unpaired Student's t-test; **p < 0.01.

4.2.1 GABARAP degradation regulated by WIPI4 is proteasome-dependent.

GABARAP is degraded by both the proteasome and autophagy pathways. To understand which pathway is utilised by WIPI4 to regulate GABARAP degradation, the proteasome pathway was blocked by MG132. Interestingly, MG132 treatment blocked the increase of GABARAP degradation (Figure 12), suggesting that WIPI4 regulates GABARAP levels through the proteasome pathway.

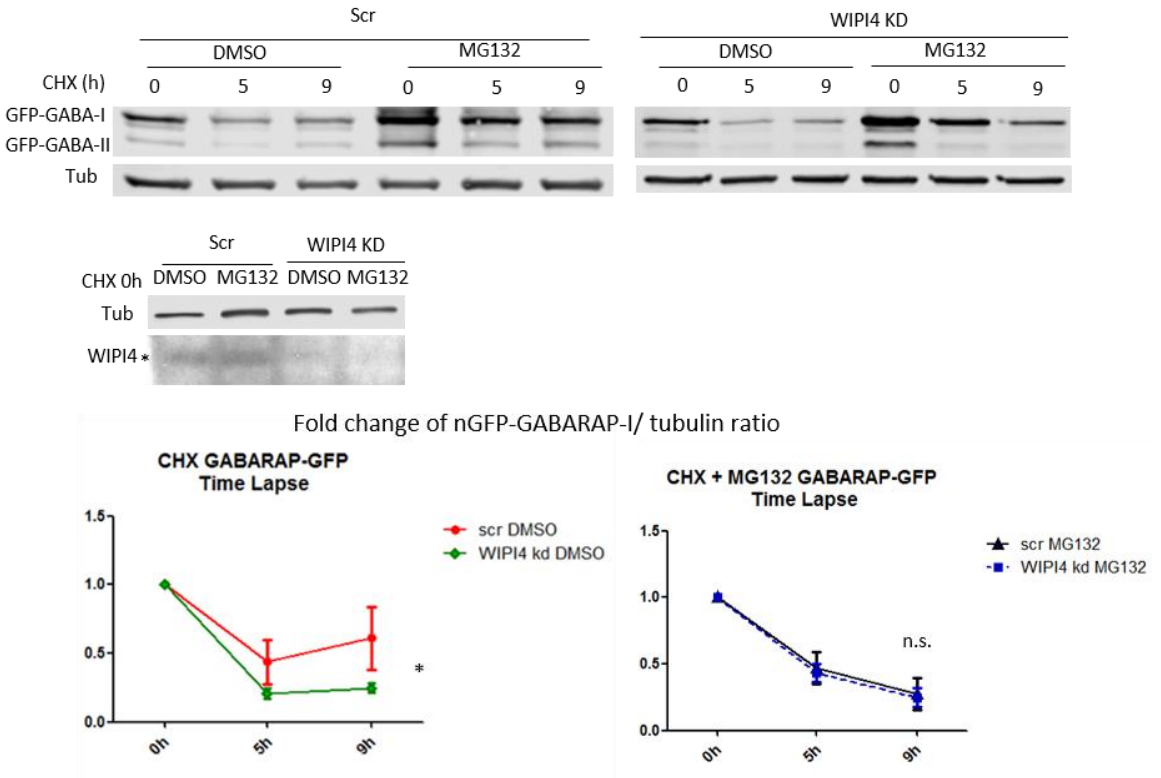

Figure 4.12. The increased degradation of GFP-GABARAP caused by WIPI4 knockdown is proteasome dependent

Control or WIPI4 knockdown HeLa cells were subjected to cycloheximide (CHX) treatment in combination with DMSO or MG132 for the indicated hours. MG132 was only used for the last 5 hours before the harvesting of each sample. The western blots below show the knockdown efficiency of WIPI4. The graphs show the quantification of A. Mean ± SEM; n = 3; unpaired Student's t-test; *p<0.05, n.s., not significant.

4.2.2 WIPI4 knockdown increased the proteasome degradation of GABARAP

WIPI4 knockdown may alter the exposure of GABARAP to specific E3 ligases / DUBs or inhibit the proteasome pathway in general. However, WIPI4 knockdown did not significantly increase the total levels of ubiquitinated proteins (Figure 4.13). In addition, there is an accumulation of ubiquitinated proteins in WIPI4 siRNA, and cycloheximide-treated samples, suggesting that the degradation of ubiquitinated proteins was slowed down, possibly by dysfunction of autophagy. Moreover, WIPI4 knockdown increased the K48, K63, and total ubiquitination of GFP-GABARAP (Figure 4.14). Therefore, WIPI4 may regulate the exposure of GABARAP to specific E3 ligases / DUBs.

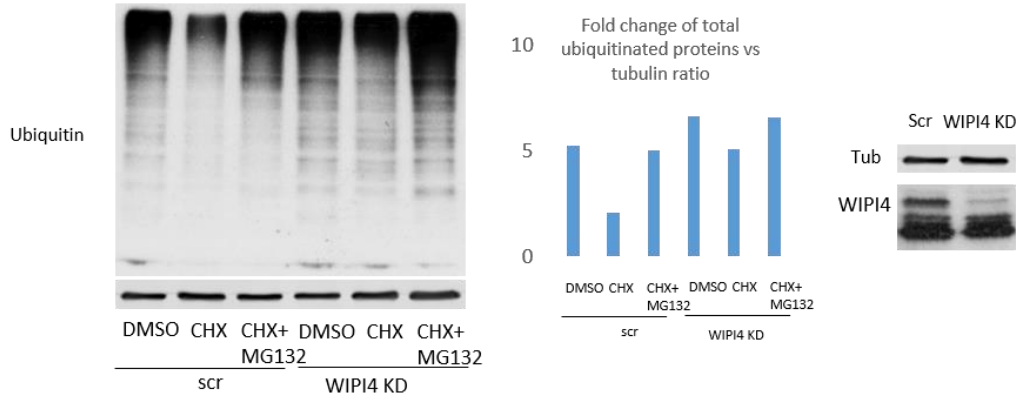

Figure 4.13. WIPI4 knockdown did not block proteasome function in general

The blots on the left are representative blots showing the effect of WIPI4 knockdown on the total levels of ubiquitinated proteins, with cycloheximide treatment showing the effect on degradation of ubiquitinated proteins. The membrane was stained by the anti-ubiquitin antibody. Cycloheximide and MG132 double treated samples were used as a control to show the levels of ubiquitinated proteins respond to different treatments. The graph shows the quantification of the blots on the left. The blot panels on the right show the knockdown efficiency of WIPI4 in this experiment.

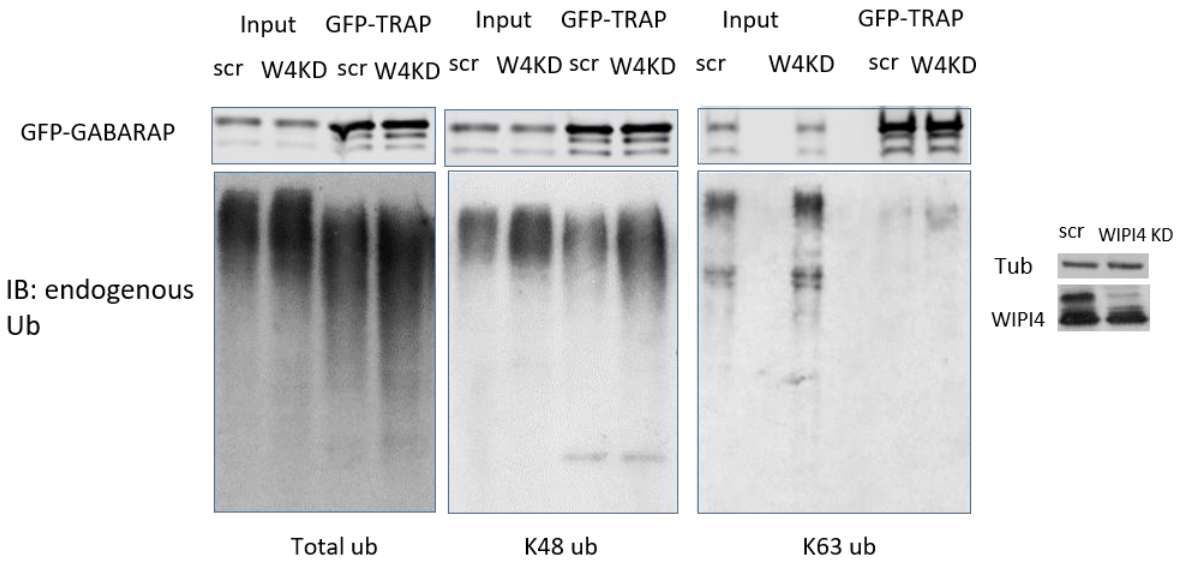

Figure 4.14. WIPI4 knockdown increased the ubiquitination of GABARAP

Representative blots showing the effect of WIPI4 knockdown on GABARAP ubiquitination modification. HeLa cells transfected with GABARAP-GFP were lysed and subjected to immunoprecipitation using GFP-Trap beads. The inputs and GFP-GABARAP elutions were resolved by western blot and probed for total ubiquitin, K48-linked ubiquitin and K63-linked ubiquitin. The western blots on the right show the knockdown efficiency of WIPI4 in this experiment.

4.3 WIPI4 regulates GABARAP levels through UBR5

A screen was done to identify E3 ligases targeting GABARAP and regulated by WIPI4 at the same time. There are several E3 ligases and DUBs identified by the WIPI4-GFP mass spectrometry analysis (see Chapter 3), and WIPI4-GFP was immunoprecipitated to confirm their interaction. UBR5 was found to interact with WIPI4 and GABARAP (data in Chapter 3).

4.3.1 UBR5 interacts more with GABARAP when WIPI4 is depleted

To test whether the interaction of UBR5 and GABARAP is regulated by WIPI4, GABARAP-GFP was immunoprecipitated from transiently transfected HeLa cells and blotted for UBR5. As shown in Figure 4.15, WIPI4 knockdown increased UBR5 and GABARAP interaction.

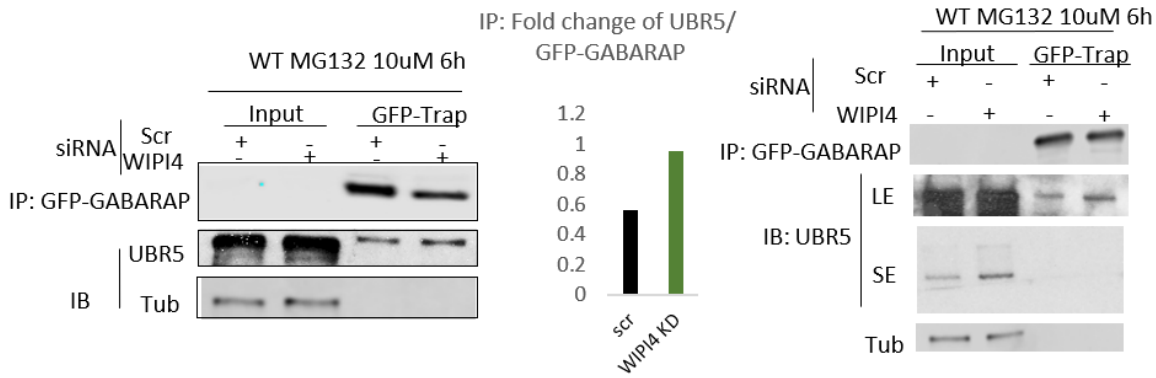

Figure 4.15. WIPI4 knockdown increased the interaction of GABARAP and UBR5

Two representative blots showing the effect of WIPI4 depletion on UBR5-GABARAP interaction. Control or WIPI4 knockdown HeLa cells were transfected with GFP-GABARAP and treated with MG132 during the last 6 hours before harvesting. The lysates were then immunoprecipitated for GFP-GABARAP and blotted for UBR5. The graph shows the UBR5 levels relative to GFP-GABARAP in the IP samples.

4.3.2 UBR5 knockdown rescued the decreased levels of GABARAP caused by WIPI4 knockdown

To understand whether WIPI4 regulates autophagy through the UBR5-GABARAP interaction, the rescue of WIPI4 knockdown was explored by knocking down UBR5. MIB1, a published E3 ligase of GABARAP (Joachim et al., 2017), was knocked down as a positive control. Both MIB1 and UBR5 knockdown rescued the decrease of GABARAP-I levels in WIPI4 knockdown cells (Figure 4.16 A-C). Knockdown of UBR4, an E3 ligase from the same family of UBR5, failed to rescue GABARAP levels. This may be relevant to the fact that UBR4 loss of function also increases WIPI4 levels while UBR5 loss of function does not regulate WIPI4 levels (Figure 4.16D).

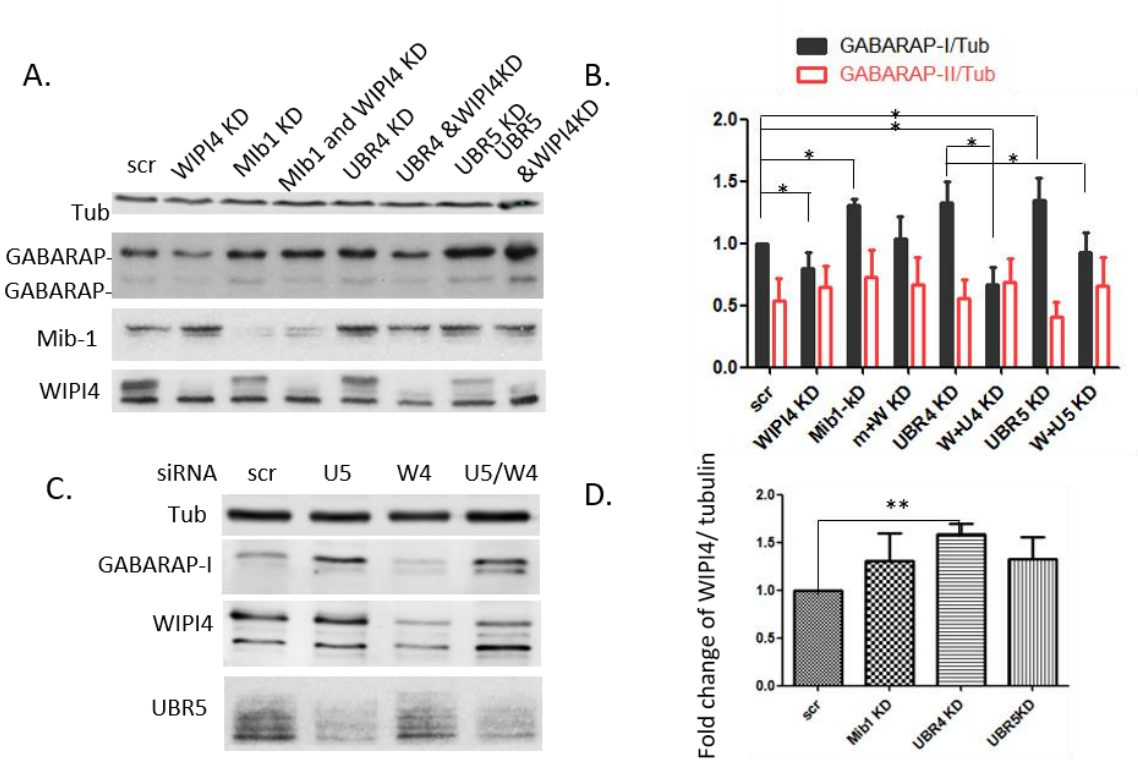

Figure 4.16. UBR5 knockdown rescued GABARAP-I decrease caused by WIPI4 depletion

HeLa cells were transfected with siRNAs as indicated. For the double knockdown, WIPI4 siRNA was transfected first and the other siRNAs (Mib1, UBR4 and UBR5) were transfected 48 hours after the first transfection. The graph on the right shows the quantification of the experiment on the left. Means ± SEM, *p<0.05, unpaired two-tailed t-test.

A. Representative blots showing the GABARAP, MIB1 and WIPI4 levels with the indicated treatment, with tubulin as the internal control.
B. Quantification of the western blots. Means ± SEM, *p<0.05, unpaired two-tailed t-test.
C. Representative blots showing the GABARAP and WIPI4 levels of the samples with the indicated treatment, with tubulin as the internal control.
D. Quantification of WIPI4 levels relative to tubulin in the rescue experiment. The levels of WIPI4 were not altered by UBR5 or MIB2 knockdown, but was increased by UBR4 knockdown. Means ± SEM, **p<0.05, unpaired two-tailed t-test.

4.4 Exploration of other autophagosome closure/ maturation regulators potentially recruited by WIPI4 onto autophagosomes

Mass spectrometry analysis was performed to identify other proteins potentially regulated by WIPI4. Data will be shown in the next chapter.

4.5 Summary of Results

In this chapter, it is confirmed that GABARAP (L1) functions downstream of WIPI4 and upstream of autolysosome degradation. Because:

i. WIPI4 depletion does not accumulate LC3-II in GABARAP-family knockout cells.
ii. Depletion of GABARAP family proteins accumulated LC3-II.
iii. GABARAP (L1) trafficking is disrupted by WIPI4 depletion.
iv. GABARAP-I and GABRAPL1-I protein levels are decreased by WIPI4 loss of function.

Moreover, it was confirmed that the WIPI4 regulates GABARAP protein levels through regulating its interaction with an E3 ligase, UBR5. Knockdown of UBR5 and another known E3 ligase targeting GABARAP, MIB1, both rescued the decrease of GABARAP levels caused by WIPI4 loss of function. More work is required to understand whether GABARAP regulates autophagosome closure or other biological processes downstream of WIPI4.

Chapter 5 UBR5 regulates autophagy pathway by modulating GABARAP stability

WIPI4 knockdown decreased GABARAP-I but not GABARAP-II levels due to increased degradation of the total GABARAP pool through the proteasome pathway. Therefore, WIPI4 loss of function may change the activity or the levels of at least one of the following: E3 ligases degrading GABARAP, deubiquitylating (DUB) enzymes protecting GABARAP, or general proteasome pathway components. Since WIPI4 loss of function did not increase the levels of ubiquitinated proteins, it may regulate the exposure of GABARAP to specific E3 ligases or DUBs.

To be able to investigate the components of the ubiquitination pathway affected by WIPI4 knockdown, E3 ligases and DUBs identified as potential interactors of WIPI4-GFP by Mass Spectrometry analysis were screened.

5.1 Analysis of Mass Spectrometry hits

The hits that are at least twice (1.5 times if the peptide count is above 100) more abundant in WIPI4-GFP samples than in the GFP samples are considered to be potential interactors of WIPI4. ATG2 was identified (data not shown), validating that WIPI4 and ATG2 interact with each other and that the experiments were technically reliable.

To understand proteins of which pathways are relatively enriched by WIPI4-GFP compared to the human genome, the 206 potential interactors were first clustered by http://www.pantherdb.org/. Proteins of catalytic activities including DNA polymerases, deubiquitinases, ATPase regulators, chaperone clients and ubiquitin (-like) protein interactors were enriched by 32.13, 16.18, 10.62, 7.59 and 5.57 fold each when compared to the human genome. In order to identify potential WIPI4 interactors from the UPS pathway, the 206 hits were categorized according to the biological processes they function in by https://david.ncifcrf.gov/home.jsp and https://string-db.org/. As shown in Figure 1A, Proteasome subunits were found with high abundance in WIPI4-GFP overexpressed samples. Two E3 ligases，UBR4 (20:0), UBR5 (18:0), and one DUB，USP9x (5:0), which are most

enriched by WIPI4-GFP according to the peptide count, were examined first. Additionally, MIB1 was considered since it has been reported as a GABARAP E3 ligase (Joachim et al., 2017). Figure 1B showed other membrane-binding proteins identified and will be discussed in the discussion later.

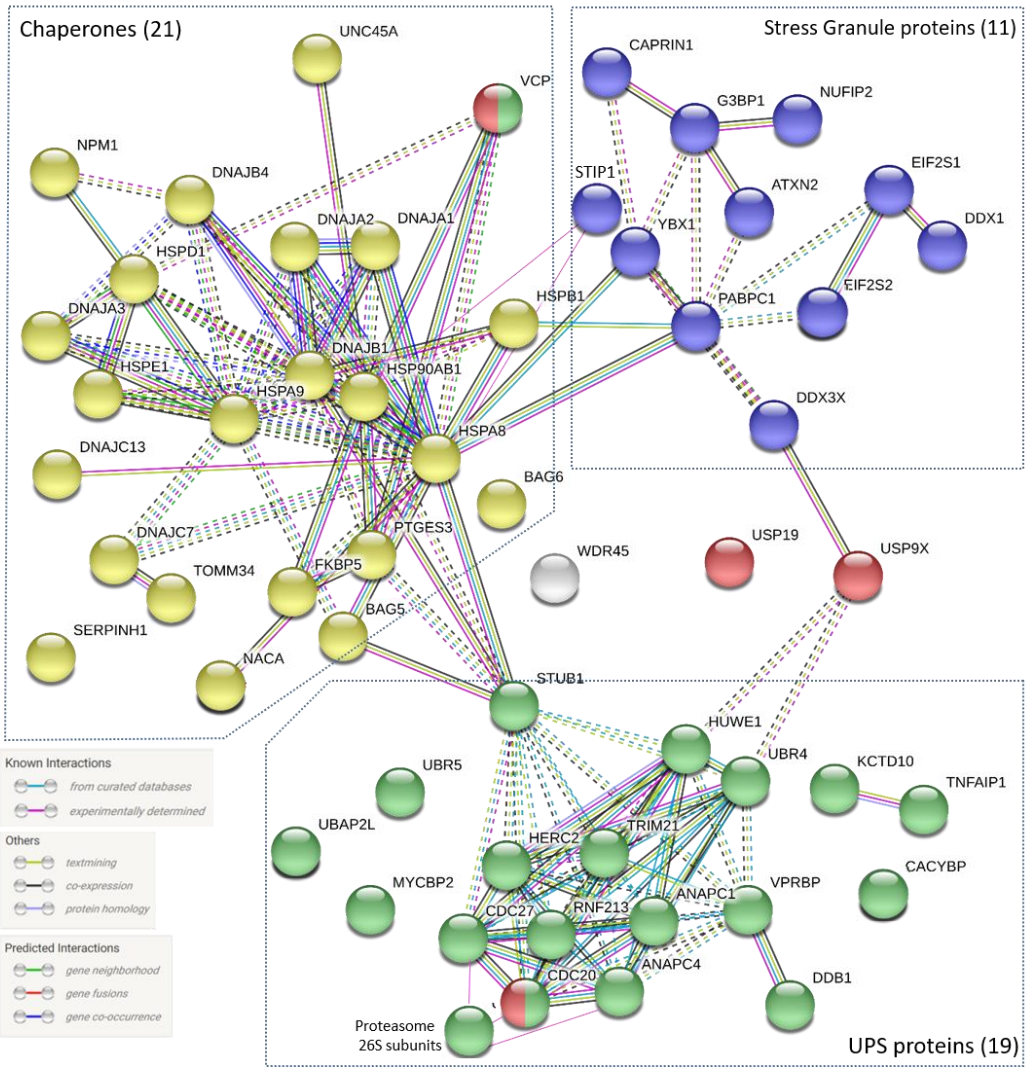

Figure 5.1. WIPI4-GFP proteomics analysis

Hits of Mass spec experiments were analysed by https://string-db.org/. Minimum required interaction score = 0.7. The most enriched function groups are shown.

A. UPS proteins, chaperones and stress granule proteins are enriched. Nodes represent proteins. Splice isoforms or post-translational modifications are collapsed, i.e. each node represents all the proteins produced by a single, protein-coding gene locus. Green: UPS pathway components, including E3 ligases and adaptors that binding E3 ligases; Red: deubiquitinases; Yellow: chaperones; Violet: stress granule proteins. Edges indicate two proteins share certain functions, not necessarily that they are physically binding each other. CDC20, CDC27, and ANAPC4 are not from WIPI4 Mass spec data, however,STRING predicted that they would be in the interaction network because they are interactors of ANAPC1 (Kramer, 2000).

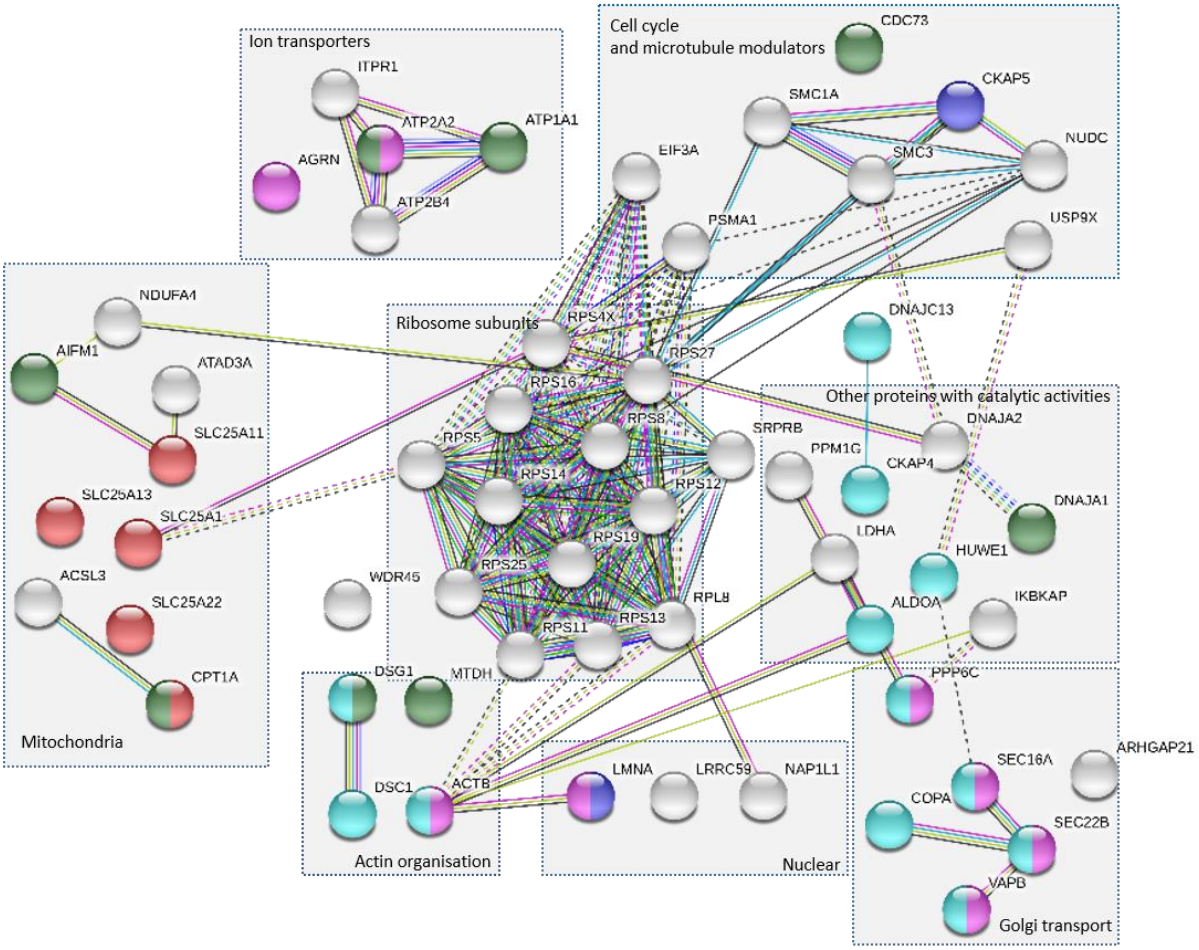

Figure 5.1. WIPI4-GFP proteomics analysis

B. 70 membrane proteins were found, which locate on multiple membrane structures including mitochondria, the Golgi compartment or in association with cytoskeletons. 21 proteins have catalytic activities. The colours of the nodes represent the biological processes that the proteins are involved in according to predictions made by STRING. Red: mitochondrial transport; Magenta: membrane organisation; Green: response to lipid; Turquoise: vesicle-mediated transport.

5.2 UBR5 interacts with GABARAP

To identify the potential regulators of GABARAP which interact with WIPI4, WIPI4-GFP and GABARAP-GFP were pulled down separately as bait proteins for immunoprecipitation. As shown in Figure 2A, MIB1 and UBR4 did not co-precipitate with WIPI4-GFP (Figure 5.2A), although MIB1 was pulled down with GABARAP-GFP. UBR5 and USP9x interacted with both WIPI4-GFP and GABARAP-GFP (Figure 5.2 A&B). A trace amount of USP9x was immunoprecipitated with GFP protein in the control sample suggesting that USP9x binds to

WIPI4-GFP and GABARAP-GFP partially through the GFP tag rather than specifically with WIPI4 and GABARAP. Hence, I focused on UBR5 because it not only interacts with GABARAP but also interacts with WIPI4.

Interestingly, UBR5 immunoprecipitated much less with GFP-LC3 compared to that with GFP-GABARAP (Figure 5.3A). Moreover, UBR5 interacts with GABARAP in both wildtype and autophagy-null cells (ATG16 knockout cells) in both basal and starved conditions (Figure 5.3B). Experiments in ATG16-null cells which confirmed the GABARAP-UBR5 interaction suggests that this interaction is with GABARAP that is not conjugated to lipid (GABARAP-I) since lipidation does not occur in these cells (Bento et al., 2016).

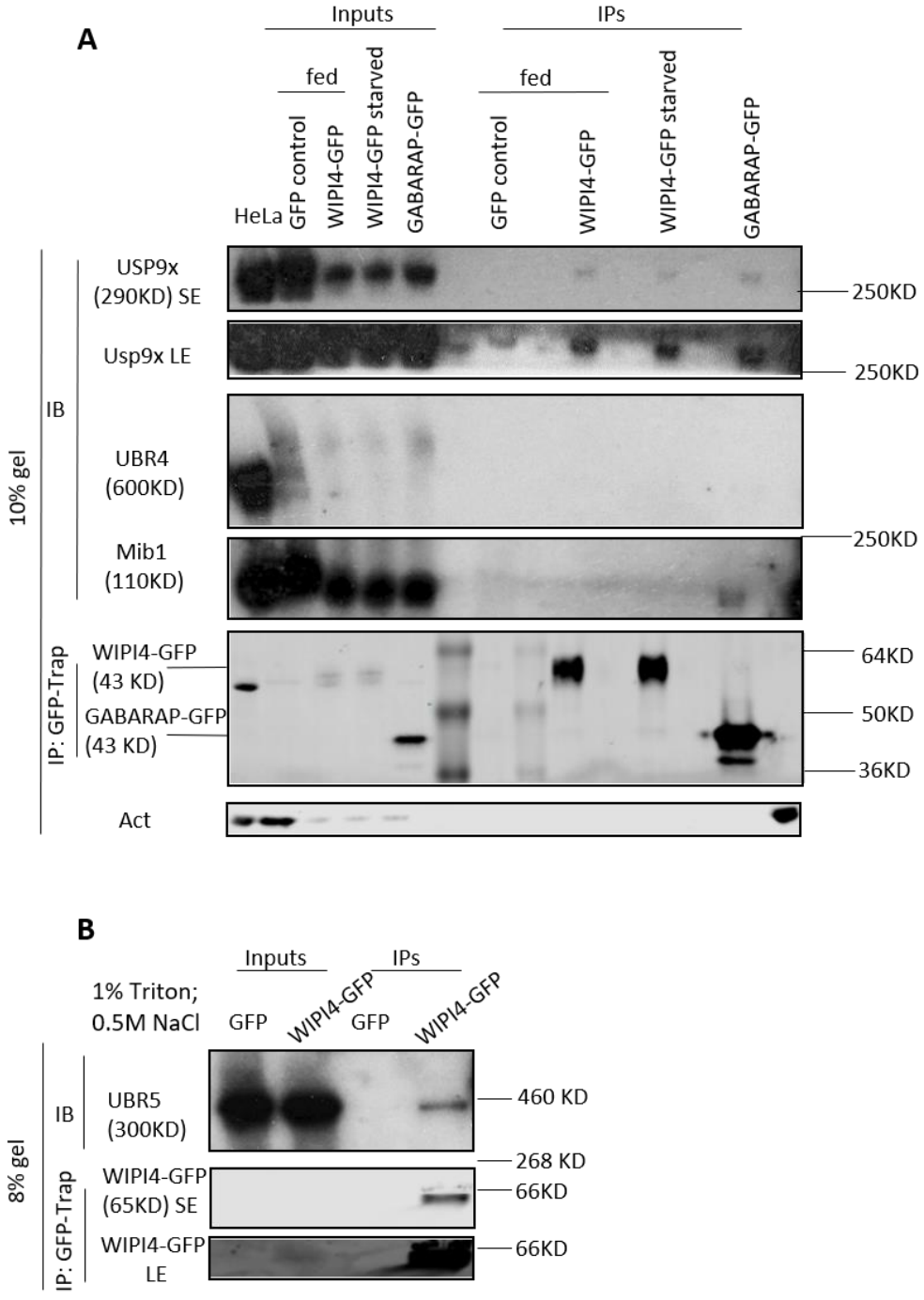

Figure 5.2. UBR5 interacts with GFP-GABARAP but less with GFP-LC3

A. HeLa cells were transiently transfected with GFP-WIPI4 or GFP-GABARAP for 24 hours, with or without EBSS for 4 hours prior to lysis with lysis buffer B. Immunoprecipitation was done with GFP-Trap system and analysed by western blot. Representative images shown. pCMV-GFPC1 construct was used as the negative control.

B. HeLa cells were transiently transfected with GFP-WIPI4 and immunoprecipitation was performed with GFP-Trap Dynabeads with IP lysis buffer containing1% Triton. pCMV-GFPC1 construct was used as the negative control.

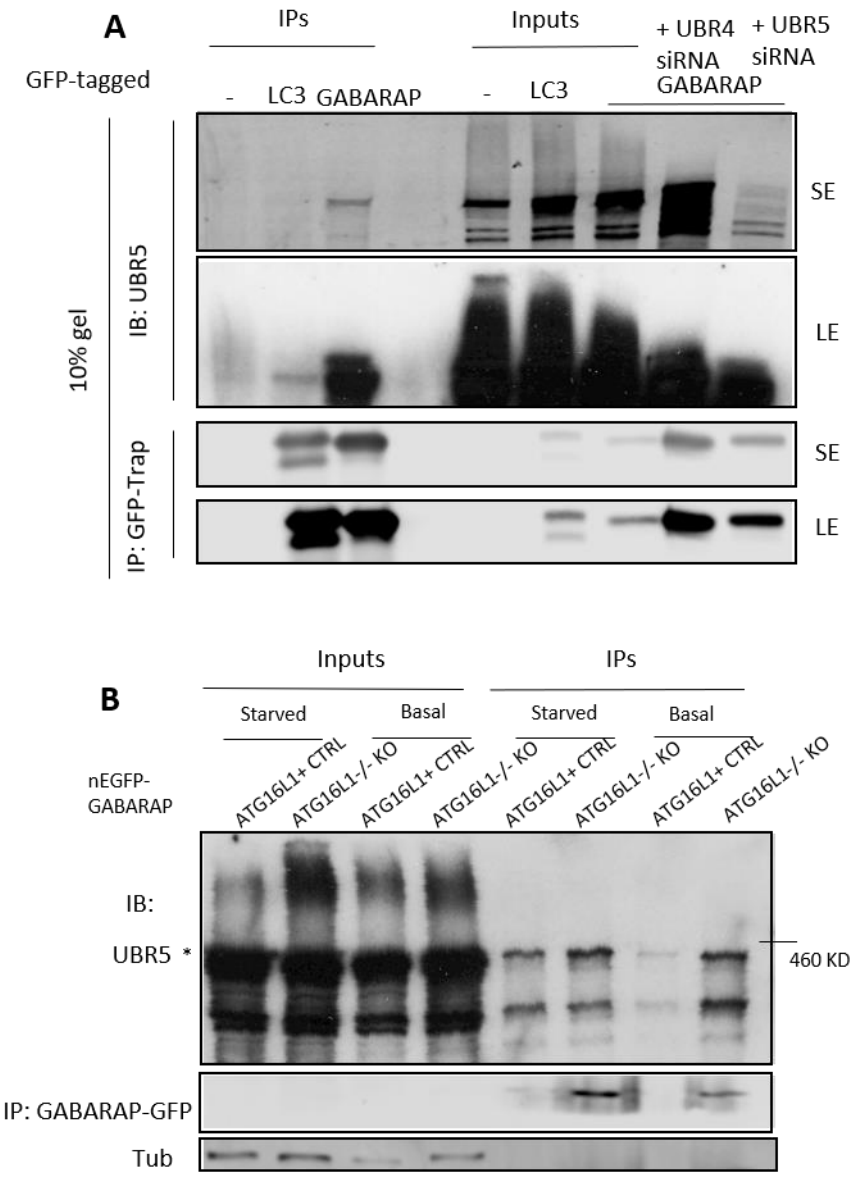

Figure 5.3. UBR5 interacts with GFP-GABARAP but less with GFP-LC3

A. Experiment was performed as in a, with UBR5 and UBR4 knockdown to show the position of UBR5 band on the gel. Representative image shown.

B. ATG16L1-/- KO HeLa cells and the wildtype control cells were transiently transfected with nGFP-GABARAP for 24 hours, with or without incubation in EBSS for 4 hours prior to lysis with lysis buffer B. Immunoprecipitation was done with GFP-Trap system and analysed by western blot. Representative images shown.

5.3 UBR5 negatively regulates GABARAP-I levels

The immunoprecipitation experiment results suggest that UBR5 interacts with GABARAP, which is consistent with the hypothesis that UBR5 is an E3 ligase of GABARAP. To corroborate this hypothesis, UBR5 should negatively regulate GABARAP protein levels post-transcriptionally and should ubiquitinate GABARAP *in vivo* and *in vitro*.

5.3.1 UBR5 siRNA treatment increased GABARAP-I levels

UBR4 is from the same E3 ligase family as UBR5 and may have similar activity to UBR5. However, UBR4 was not shown to interact with GABARAP, but its molecular weight of 600 kDa may have affected the efficiency of the co-IP experiment. Therefore, the effect on GABARAP levels of UBR4 and UBR5 knockdown was assessed separately. Figure 5.4A shows that both UBR4 and UBR5 siRNA knockdown in HeLa cells significantly increased endogenous GABARAP-I levels under basal conditions. UBR4 knockdown also increased GABARAP-II levels. However, there was only a slight, but not significant increase of GABARAP-II levels in UBR5 siRNA treated cells. WIPI4 knockdown decreased GABARAP-I as discussed in Chapter 4. The knockdown efficiency of UBR4, WIPI4 and UBR5 is shown below. If UBR5 downregulates GABARAP-I levels directly rather than through autophagy, it should perform the same function in autophagy-null cells. UBR5 knockdown increased GABARAP-I levels in both wild type and ATG16 KO HeLa cells in both fed and starvation conditions (Figure 5.4B). The bands above GABARAP-I bands may be GABARAP with other modifications.

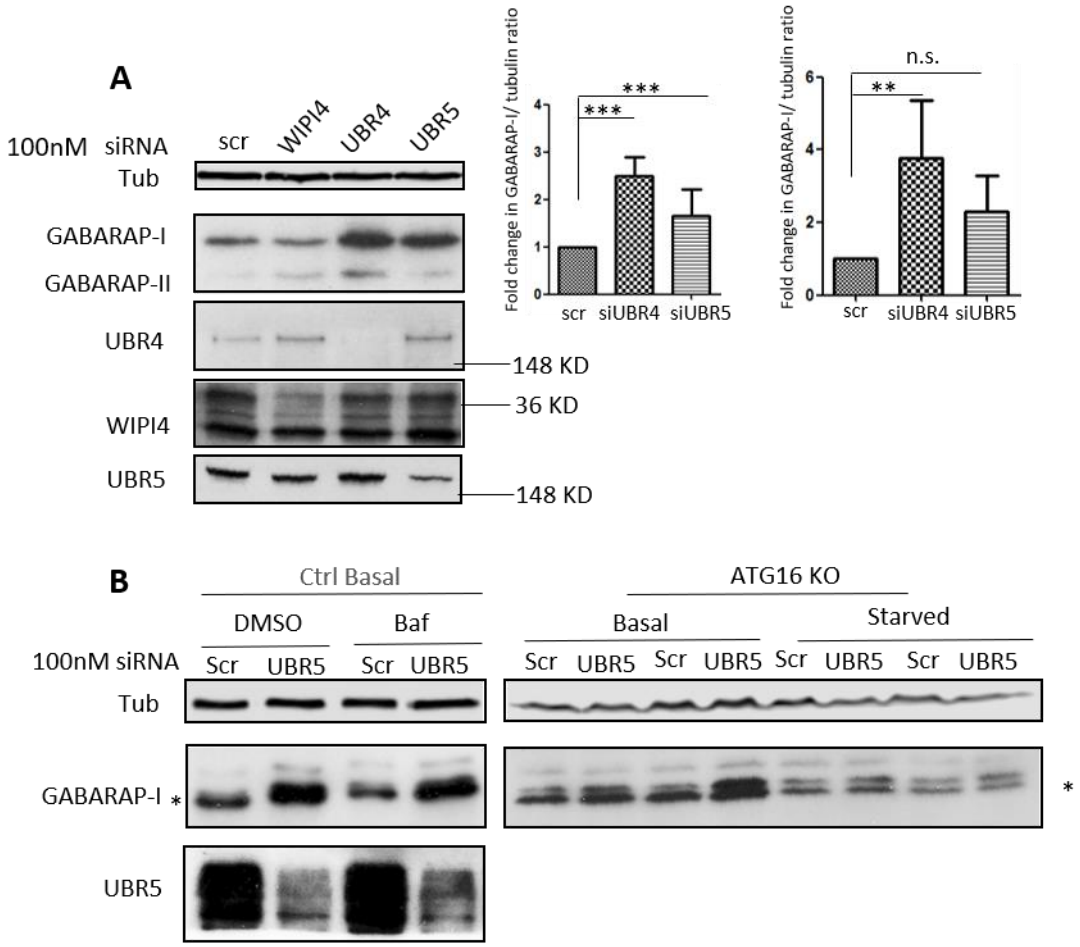

Figure 5.4. UBR5 negatively regulates GABARAP-I levels independent of autophagy

A. Representative western blots showing the GABARAP-I and GABRAP-II levels with tubulin as a loading control in scrambled (100 nM), WIPI4 (70 nM Oligo 12 + 30 nM scrambled), UBR4 (100 nM SMARTpool) or UBR5 (100 nM SMARTpool) siRNA double transfected HeLa cells. The western blot panels below represent the effect of knockdown with the above oligos. Quantification of western blots for GABARAP-I/II. **denotes $p<0.01$, *** $p<0.005$, and n.s. denotes non-significant with two-tailed unpaired t-test, n=4.

B. Representative western blots showing the GABARAP-I and UBR5 levels with tubulin as a loading control. Autophagy null and CRISPR control cells transfected with two rounds of control or UBR5 SMARTpool siRNA, treated with BafA1/DMSO, incubated in EBSS for 4 hours as indicated and analysed by western blot.

5.3.2 UBR5 loss of function inhibits GABARAP degradation

Since UBR5 has been reported to play a role in the transcription regulation (Flack et al., 2017), there was a question about whether UBR5 transcriptionally inhibits the expression of GABARAP or destabilises the GABARAP protein. HeLa cells were treated with cycloheximide in combination with the control and UBR5 siRNAs. UBR5 knockdown slowed down the degradation of both endogenous GABARAP-I (Figure 5.5A) and overexpressed nEGFP-GABARAP-I (Figure 5.5B) during 5-hour treatment. UBR4 siRNA treated samples showed a similar trend. Two other members of GABARAP family, GATE-16 and GABARAPL1, were similarly protected from degradation by UBR5 and UBR4 knockdown (Figure 5.5A). Although UBR5 interacts with WIPI4, it does not regulate the protein levels of WIPI4 (Figure 3.16.C&D, Chapter 3).

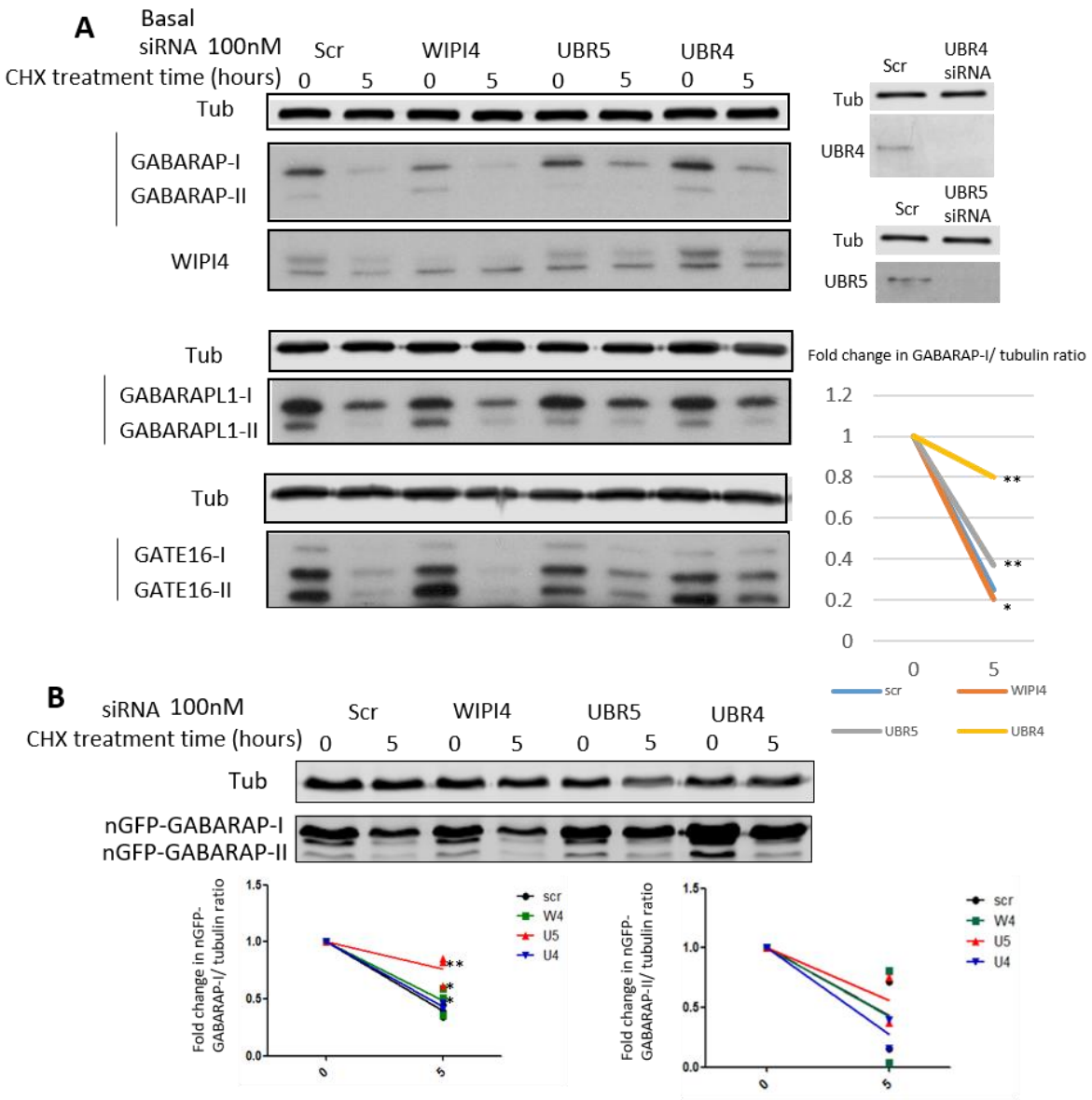

Figure 5.5. UBR5 promotes GABARAP-I degradation

A. Representative western blots showing the levels of GABARAP subfamily proteins with tubulin as a loading control. HeLa cells transfected as in Figure 3.a were treated with 50 µg/mL cycloheximide before analysis by western blot. The efficiency of knockdown is represented in the graphs. Quantification of western blots for GABARAP-I: *denotes $p<0.05$, ** $p<0.01$, and n.s. denotes non-significant with two-tailed unpaired t-test, n=3.

B. HeLa cells from the same experiment in a. were transfected with 1.0 µg GFP-GABARAP 72 hours post siRNA transfection. Cells were treated with 50 µg/mL cycloheximide for the indicated time before analysis by western blot. The graphs below show the quantitative analysis of nGFP-GABARAP-I/II levels relative to tubulin from the blots (** $p<0.01$, *$P<0.05$, n.s., not significant; two-tailed unpaired t-test, n=3).

To check whether the increase of GABARAP-I levels was specifically caused by UBR5 knockdown or off-target effects of UBR5 SMARTpool siRNA, HeLa cells were treated with UBR5 deconvoluted siRNAs, and GABARAP protein levels were analysed by western blots. Figure 5.6 demonstrates that knockdown by every deconvoluted oligo significantly increased the levels of GABARAP-I in basal conditions. Furthermore, every oligo knocked down UBR5 efficiently to a similar degree, suggesting that the increase of GABARAP-I levels was specifically caused by UBR5 knockdown.

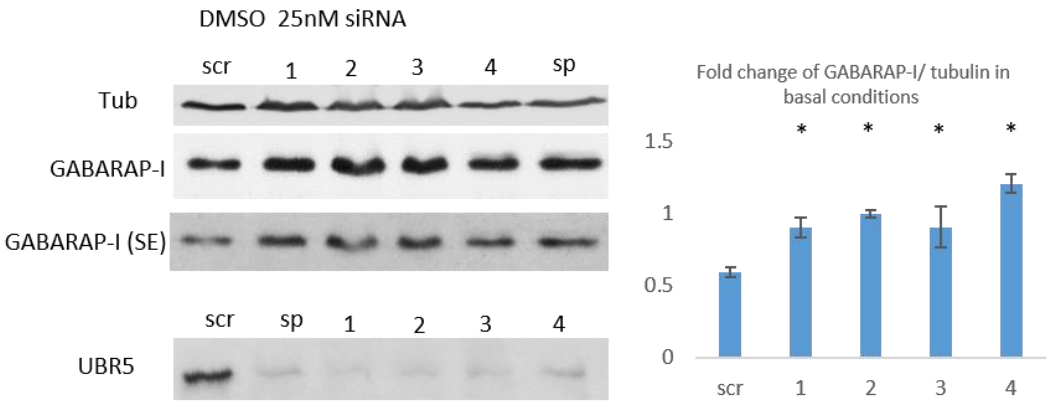

Figure 5.6 GABARAP-I levels were increased by treatment of all UBR5 deconvoluted oligos in basal conditions

HeLa cells were transfected with scrambled or separate deconvoluted oligonucleotides 1-4 and lysed after 72 hours. GABARAP and UBR5 levels were assessed by western blot and quantified relative to tubulin. ** $p<0.01$, two-tailed unpaired t-test, n=3.

5.3.3 Transient transfection of wild type UBR5 decreased GABARAP-I levels compared to the UBR5 catalytically dead construct

If UBR5 is an E3 ligase for GABARAP, its overexpression should decrease GABARAP protein levels. Wildtype UBR5 and the catalytic dead mutant of UBR5 (2768 cysteine mutated to alanine, hereafter as UBR5-C2768A) constructs were transfected into HEK293 cells separately. As shown in Figure 5.7A, GABARAP-I levels in cells expressing Flag-UBR5-His were lower than that in Flag-UBR5-C3768A-His samples. To summarize, wildtype UBR5 protein decreased GABARA-I protein levels compared to the catalytic dead UBR5 mutant. Consistently, GFP-UBR5 overexpression decreased GABARAP-I levels in HEK293 cells compared to GFP-UBR5-C2768A (Figure 5.7B). Taken together, UBR5 overexpression decreases GABARAP-I levels.

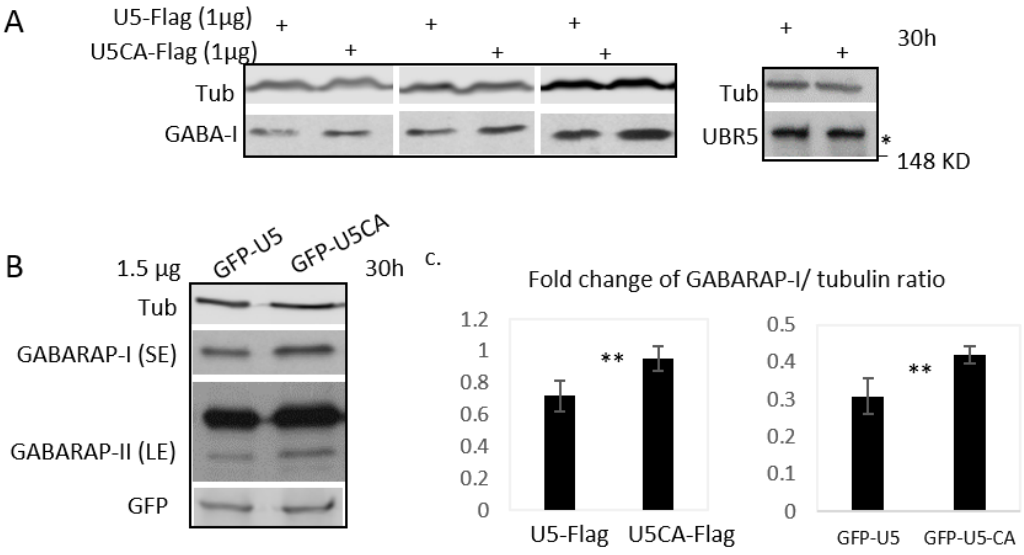

Figure 5.7 Transient overexpression of wild type UBR5 decreased GABARAP-I levels.

A. Representative western blots showing the GABARAP-I levels with tubulin as a loading control in HeLa cells transfected with 1µg Flag-UBR5-His or Flag-UBR5-C2768A-His constructs. The transfection efficiency was assessed by UBR5 staining.
B. Representative western blots showing the GABARAP-I levels with tubulin as a loading control in HEK293T cells transfected with 1.5 µg GFP-UBR5 or GFP-UBR5-C2768A constructs. The transfection efficiency was assessed by GFP staining.
C. Protein levels of GABARAP quantified relative to tubulin in arbitrary units. ** $p<0.01$, two-tailed unpaired t-test, n=3.

5.4 UBR5 directly ubiquitinates GABARAP

5.4.1 UBR5 loss of function decreased ubiquitination levels of GABARAP *in vivo*

If UBR5 degrades GABARAP through the proteasome pathway, GABARAP should be less ubiquitinated in cells depleted of UBR5. To verify this, HeLa cells were transfected with nGFP-GABARAP in combination with K63-linked HA-Ubiquitin or K48-linked HA-Ubiquitin constructs. Recombinant nGFP-GABARAP was immunoprecipitated with GFP-Trap Dynabeads, and the HA-ubiquitin conjugated onto them was analysed by western blots. As demonstrated in Figure 5.8, immunoprecipitated nGFP-GABARAP was less conjugated with both K63 and K48 ubiquitin chains in UBR5 siRNA-treated HeLa cells. UBR5 loss of function also reduces greatly the K48 and K63 in the inputs, which is consistent with previous literature that UBR5 is involved in ubiquitination of many proteins and peptides and is one of the most important K48 ubiquitin conjugators (Yau et al., 2017).

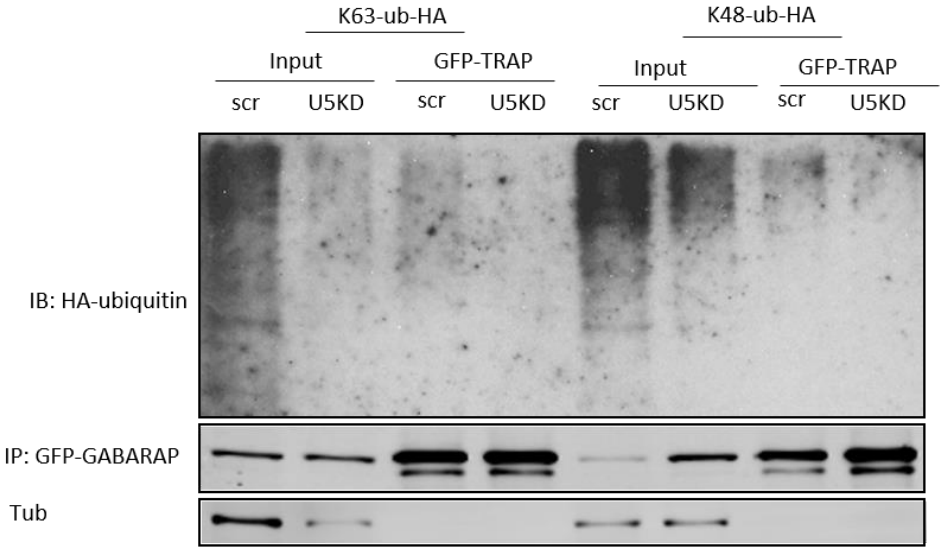

Figure 5.8. UBR5 Knockdown decreased the ubiquitination levels of GABARAP

Representative western blot showing the K63-linked HA-Ubiquitin and K48-linked HA-Ubiquitin modification levels of nGFP-GABARAP. HeLa cells transfected with 25 nM scrambled or UBR5 SMARTpool siRNA. After 72 hours the cells were co-transfected with HA ubiquitin (HA-tagged Ubiquitin) and nGFP-GABARAP and incubated for the last 6 hours with the proteasome inhibitor MG132 (10 μM). The lysates were subjected to immunoprecipitation with GFP-Trap Dynabeads. The immunocomplexes were eluted by boiling with loading buffer for 5 minutes and assessed by western blot. The membrane was immunoblotted with anti-K63-linked Ubiquitin and anti-K48-linked Ubiquitin antibodies.

5.4.2 UBR5 ubiquitinates GABARAP *in vitro*

In vitro ubiquitination assays were performed to examine whether UBR5 directly ubiquitinates GABARAP. Flag-UBR5 and Flag-UBR5-C2768A were purified separately from HEK293 cells transiently transfected with UBR5 constructs. Cells transiently transfected with CMV-Flag constructs were processed by the same protocol, and the elution was used as a negative control. His-GABARAP protein was used as the substrate.

According to Figure 5.9A, GABARAP staining showed several bands of high molecular weight in the sample of wild type UBR5, while in the Flag control sample the staining is much less, suggesting that Flag-UBR5 increased the molecular weight of proteins which contained GABARAP, possibly GABARAP conjugated with ubiquitin molecules, as confirmed by the K48 staining of the same samples re-run on another gel (Figure 5.9A).

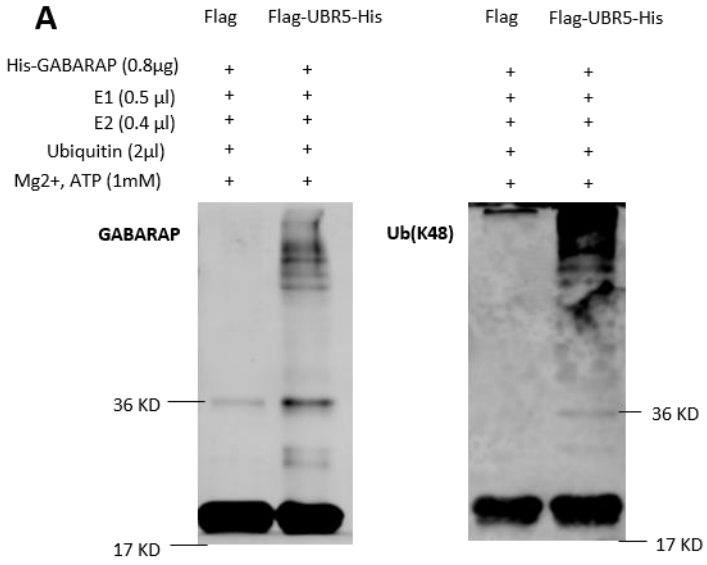

Figure 5.9. UBR5-His poly-ubiquitinates GABARAP *in vitro*

A. Flag-UBR5-His transiently expressed in HEK293T cells were lysed after 24 hours, immunoprecipitated with anti-Flag affinity beads, and eluted with 3XFlag peptides. pCMV-Flag construct was used to generate the control elution. The elutions were incubated with recombinant His-GABARAP and other proteins required for ubiquitin conjugation reaction for 1 hour at 37°C. Ubiquitinated GABARAP levels were assessed by running the reactions twice and assessing with anti-GABARAP and anti-K48-linked ubiquitin antibodies separately, since both antibodies were rabbit-derived.

Figure 5.8B shows multiple ubiquitinated GABARAP (GABARAP-(Ub)n) signals in only two reaction products with wild type Flag-UBR5 (Lanes 6 & 7). The quantity correlates to the amount of E1 added, indicating that the signal is produced by a ubiquitination reaction and the E1 concentration is not over saturated. The levels of UBR5 proteins in the elutes used in these experiments are shown in Figure 5.9C.

Similarly, Figure 5.9D demonstrates that the GABARAP signal is stronger at high molecular weight sections of the membrane in the Flag-UBR5 reaction product (Lane 2) than the UBR5-C2768A mutant reaction products (Lanes 3 and 4), although there is much less wild type UBR5 protein than UBR5-C2768A protein. Therefore, the enzymatic activity of UBR5 is required for the reaction. Also, the GABARAP signal overlaps partially with K48 ubiquitin signal, indicating that this staining is probably ubiquitinated GABARAP. Although the GABARAP staining may be both from His-GABARAP and endogenous GABARAP pulled down together with UBR5, there is no GABARAP-(Ub)n signal in the no E1 control (Lane 1). This implies that the GABARAP-(Ub)n signal is produced by the *in vitro* ubiquitination reaction. Taken together, UBR5 ubiquitinates GABARAP *in vitro*.

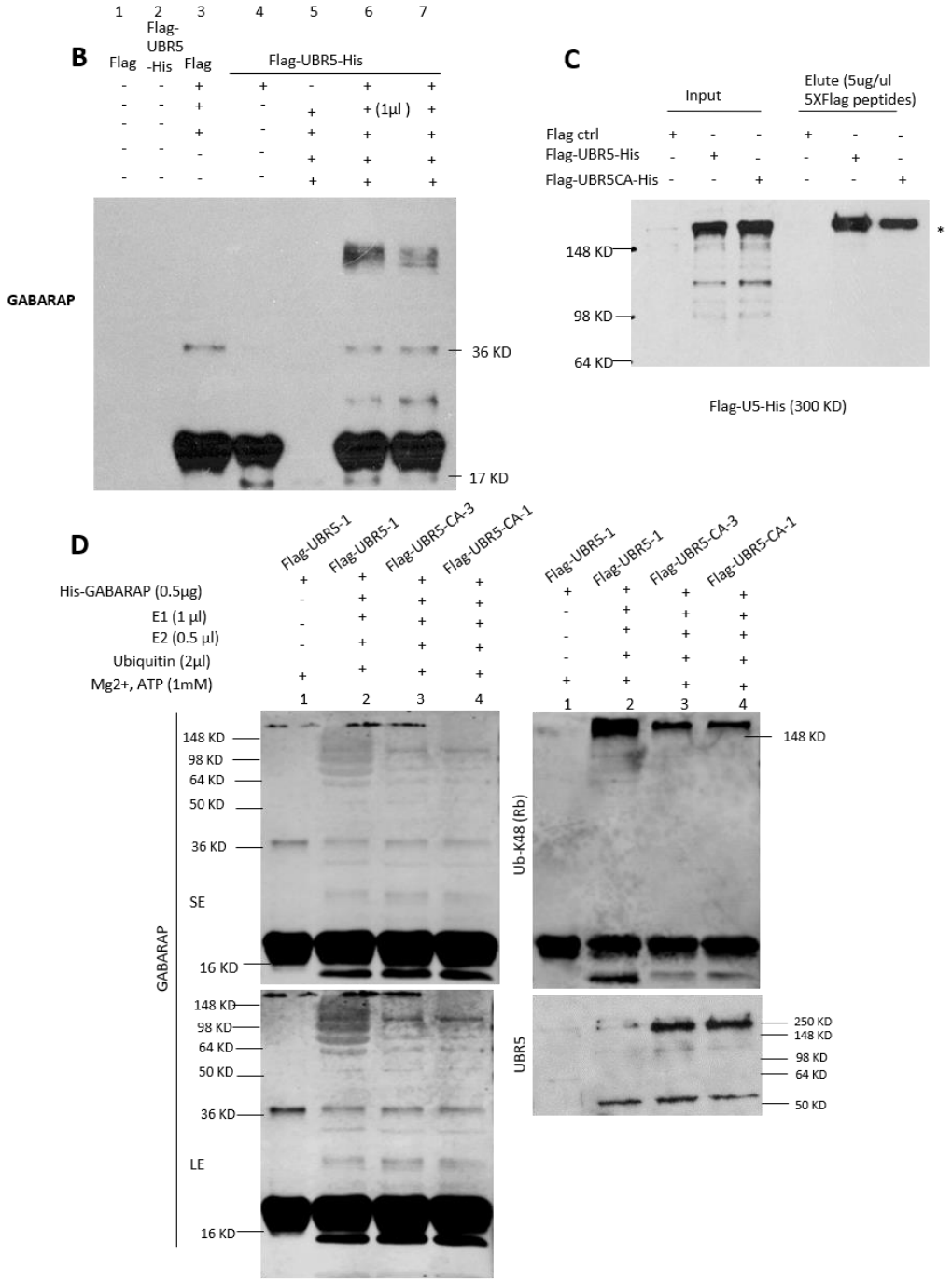

Figure 5.9 UBR5-His poly-ubiquitinates GABARAP *in vitro*

B. *In vitro* ubiquitination assays were performed as in a, with further negative controls of different combinations of reaction ingredients as indicated. Reactions were analysed for ubiquitination using anti-GABARAP antibodies.

C. Representative western blots assessing UBR5 protein levels in the elutions used in a and b.

D. *In vitro* ubiquitination reactions were performed as in a and b but with Flag-UBR5 or Flag-UBR5-C2768A proteins. Ubiquitinated GABARAP levels were assessed using anti-GABARAP and anti-K48-linked ubiquitin antibodies after stripping of the membrane. The membrane was stripped again and incubated with anti-UBR5 antibody to analyse the protein levels of Flag-UBR5 and Flag-UBR5-C2768A in the reactions.

5.5 Identification of the lysine's modified by UBR5

5.5.1 The N-degron mutated and lipidation insensitive GABARAP mutant (K2P-G116A-GABARAP-cGFP) is less ubiquitinated than the lipidation insensitive GABARAP mutant (G116A-GABARAP-cGFP)

UBR5 is a UBR-box family E3 ligase, which recognizes destabilizing N-terminal residues (N-degrons) by the UBR-box. This recognition may be required or helpful for their interaction. If UBR5 ubiquitinates GABARAP following the N-end rule mechanism, the second lysine on GABARAP should be an N-degron. To test whether the second-lysine is involved in the ubiquitination of GABARAP, an N-degron mutated and lipidation insensitive GABARAP-cGFP construct (GABARAP-k2P-G116A-cGFP) was made and transiently expressed in HeLa cells to examine its interaction with UBR5. Lipidation insensitive GABARAP-G116A-cGFP was made as a control (Figure 5.10). The GFP tag was added onto the c-terminal because it was unknown whether an N-terminal GFP tag would block the interaction of UBR-box and the N-degron. To avoid the c-cGFP tag from being cleaved off by ATG4, the glycine which would be recognized by ATG4 was mutated to alanine.

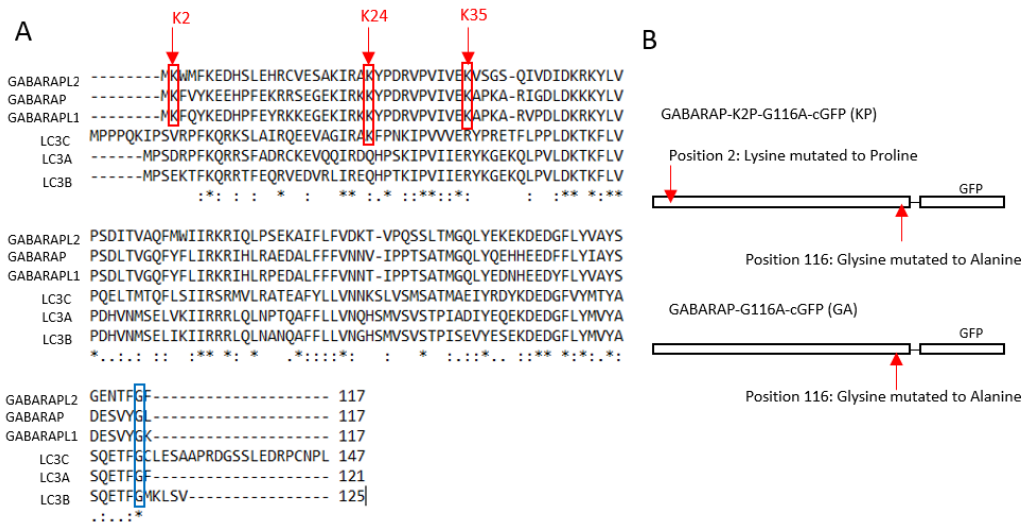

Figure 5.10 Strategy for mutagenesis of GABARAP

A. Sequence alignment of human ATG8-family orthologs using Clustal. Red arrows indicate residues further analyzed in this study. The shared glycine recognised by ATG4 for cleavage is boxed. An asterisk (*) indicates positions which have a single, fully conserved residue. A colon (:) indicates conservation between groups of strongly similar properties equivalent to scoring > 0.5 in the Gonnet PAM 250 matrix. A period (.) indicates conservation between groups of weakly similar properties equivalent to scoring =< 0.5 and > 0 in the Gonnet PAM 250 matrix.

B. Diagram showing the amino acids mutated in GABARAP-K2P-G116A-cGFP (KP) and GABARAP-G116A (GA) mutants.

Consistent with the hypothesis that GABARAP is an N-end-rule pathway substrate, immunoprecipitated K2P-G116A-GABARAP-cGFP was less K48-ubiquitinated than G116A-GABARAP-cGFP in GABARAP-subfamily triple knockout HeLa cells, both with endogenous ubiquitin and overexpressed HA-ubiquitin (Figure 5.11). Thus, the N-degron of GABARAP promotes the K48 poly-ubiquitin modification on G116A-GABARAP-cGFP *in vivo*.

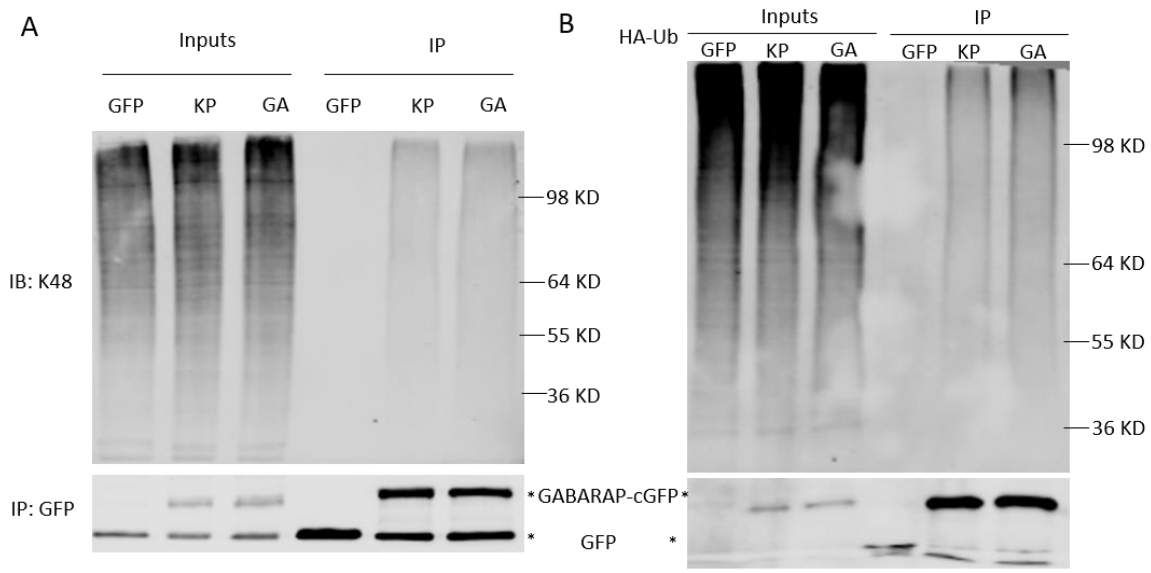

Figure 5.11. N-degron mutation decreases K48-linked ubiquitination of G116A mutated GABARAP

HeLa cells were transfected as indicated for 24 hours and incubated for the last 6 hours with culture media containing the proteasome inhibitor MG132 (10 µM). Cells were lysed in the presence of protease inhibitors, DUB inhibitors and phosphatase inhibitors. KP and GA mutated GABARAP-cGFP were immunoprecipitated with GFP-affinity Dynabeads for ubiquitination analysis.

A. Representative blots showing endogenous K48-linked ubiquitin modification.
B. Representative blots showing K48-linked ubiquitin modification with both endogenous and HA-Ubiquitin.

5.5.2 ATE1 loss of function increased GABARAP levels

Based on the principle of N-end rule, GABARAP has primary N-degrons, rather than a penultimate amino acid that can be processed to be secondary/ tertiary N-degrons. To understand whether this applies to the recognition of UBR5 of GABARAP, I tested whether ATE1 function affects GABARAP stability. As ATE1 is required for the generation of secondary N-degrons, its loss of function should not change GABARAP protein stability. Surprisingly, ATE1 siRNA treatment in HeLa cells increased GABARAP-I and GABARAP-II levels (Figure 5.12A). However, LC3 levels were similarly increased by ATE1 knockdown (Figure 5.12B) although LC3 does not have an N-degron. Therefore, with the assumption that ATE1 siRNA has no off-target effects, ATE1 regulates LC3 and GABARAP levels indirectly, rather than directly regulating the stability of GABARAP proteins through the N-end rule pathway. Conclusively, this experiment cannot reveal whether UBR5 recognises GABARAP through primary degrons or secondary/ tertiary N-degrons, but rather raised another scientific question of how ATE1 regulates autophagy.

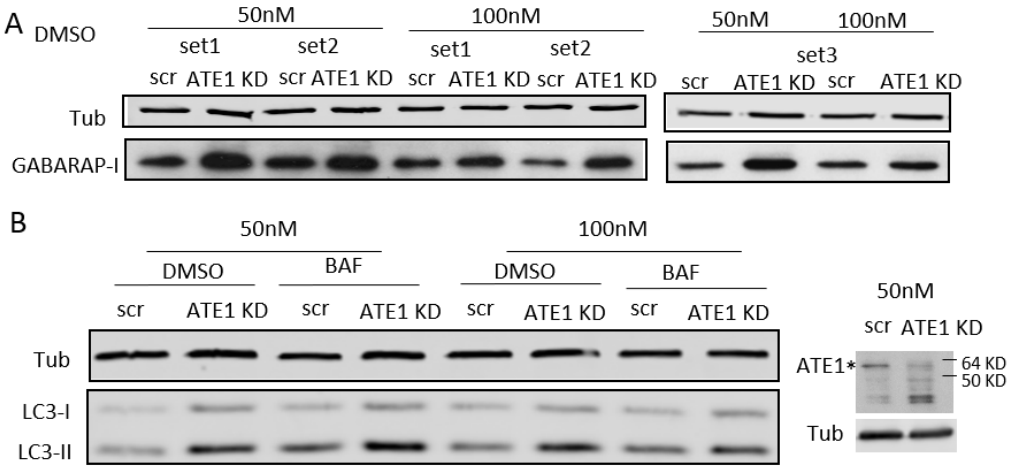

Figure 5.12 ATE1 KD protects GABARAP-I and LC3-I/II

A. Representative western blot showing GABARAP levels relative to the internal control tubulin in HeLa cells transfected with ATE1 SMARTpool siRNA at indicated concentrations for 72 hours.
B. Representative western blot showing LC3-I/II levels relative to the internal control tubulin for samples shown in a. Cells were treated with or without 400 nM BafA1 for 4 hours as indicated before lysis. The protein levels of ATE1 relative to tubulin in the 50 nM siRNA transfected samples are shown in the panels on the right.

5.5.3 Mass Spectrometry analysis results indicated that K35 and K24 of G116A-GABARAP-cGFP but not the K2P-G116A-GABARAP-cGFP are subjected to ubiquitination.

Two groups of post-transcription-modification Mass Spec analyses were done to identify poly-ubiquitination sites specific for UBR5:

Group 1: K2P-G116A-GABARAP-cGFP (KP) and G116A-GABARAP-cGFP (GA)

If UBR5 follows the N-end rule when it ubiquitinates GABARAP, KP mutant should be less ubiquitinated on certain lysines compared to GA control.

Group 2: G116A-GABARAP-cGFP, control or UBR5 siRNA

If UBR5-GABARAP ubiquitination does follow the N-end rule, the G116A-GABARAP-cGFP in control siRNA treated samples should be more ubiquitinated on certain lysines compared to that in the UBR5 siRNA treated group.

Experiments were performed in HeLa ATG8 Hexa knockout cells (HeLa cell line knocked out of all ATG8 family proteins by CRISPR-Cas9, a kind gift from Michael Lazarou) because the ubiquitination would be focused on the overexpressed GABARAP protein when the endogenous ATG8 proteins are absent. GFP-trap immunoprecipitation products were submitted for Mass Spectrometry analysis. The results of the Group 1 analysis suggest that K35 and K24 were ubiquitinated only in G116A-GABARAP-cGFP, not in K2P-G116A-GABARAP-cGFP. In comparison, K6 was only ubiquitinated in K2P-G116A-GABARAP-cGFP, not in G116A-GABARAP-cGFP. K35 modification is of higher confidence than that of K24 and K6 (Figure 5.13).

Since the results of Group 1 suggested that the N-degron changed the ubiquitination status of GABARAP, the analysis of Group 2 samples was cancelled.

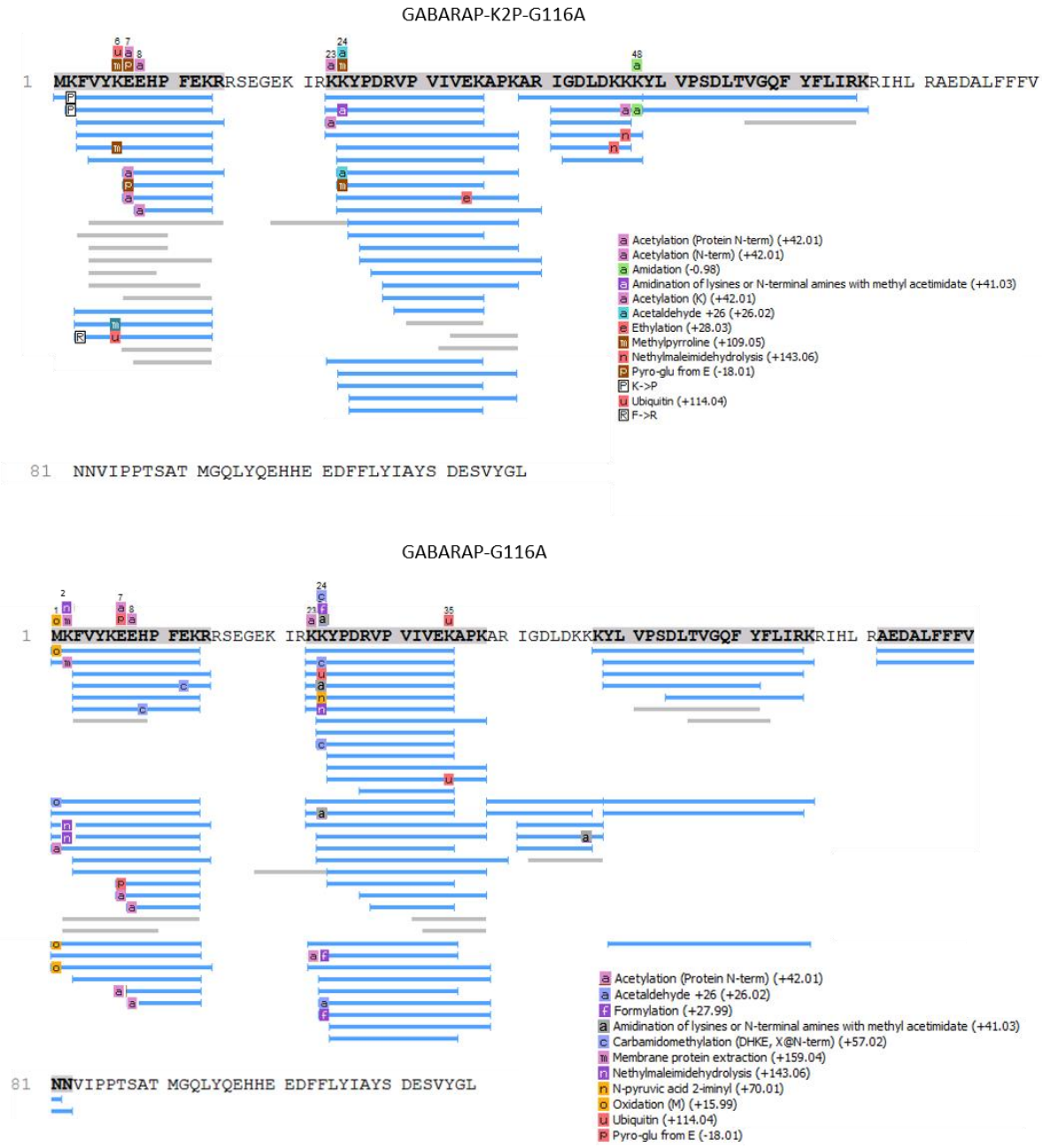

Figure 5.13 GABARAP-G116A-cGFP and GABARAP-K2P-G116A-cGFP are differently ubiquitinated

HeLa cells were transfected with GABARAP-KP-GA-cGFP or GABARAP-GA-cGFP constructs. Following 24 hours overexpression, the cells were treated with 10 µmol/L MG132 for 6 hours to accumulate the ubiquitinated GABARAP-cGFP mutants. Cells were lysed in the presence of protease inhibitors, DUB inhibitors and phosphatase inhibitors. KP and GA mutated GABARAP-cGFP were immunoprecipitated with GFP-affinity Dynabeads and eluted by boiling in LDS buffer for 5 minutes. The elutions were assessed by Mass Spectrometry and the proteomic data was analysed using the software package MaxQuant to identify post-transcription modifications. Diagram of peptides identified shown with the modifications. GABARAP-G116A-cGFP is ubiquitinated on K35 and K24 while GABARAP-K2P-G116A-cGFP is ubiquitinated on K6.

5.6 Summary of results

UBR5, an N-recognin, interacts with both WIPI4 and GABARAP as verified by immunoprecipitation. It negatively regulates the protein level of GABARAP family proteins by promoting their degradation. *In vitro* ubiquitination assays confirmed that UBR5 ubiquitinates GABARAP with K48-linked ubiquitin chain, and UBR5 loss of function *in vivo* reduced both K48/K63-linked ubiquitination of NGFP-GABARAP proteins. Moreover, mutation of the lysine at Position 2 to proline reduced the K48-linked ubiquitination of GABARAP-GA-cGFP protein, suggesting that the N-degron of GABARAP may improve the ubiquitination of GABARAP. Further, Mass spec analysis identified two potential ubiquitination sites that are only modified on N-degron-present GABARAP protein, implying that they are potential internal degrons recognized by UBR5. Further experiments are required for the confirmation of these ubiquitination sites. For example, mutations at K35 and K24 may be used to test whether their mutation prevented ubiquitination of GABARAP and extended its half-life.

Chapter 6 Discussion

This thesis explored the function of WIPI4 in autophagy and found that WIPI4 regulates autophagosome closure as well as the stability and trafficking of GABARAP, another autophagy protein downstream of it. Given that ATG8 proteins were the only known machinery triggering the autophagosome closure while working on this project, this thesis further explored the possibility of it regulating the autophagosome closure downstream of WIPI4. This discussion will first summarize the current understanding and suggest future research directions about WIPI4 function in autophagy based on findings in this thesis and the very recent literature.

The second section will cover the open questions about how UBR5 regulates GABARAP. UBR5 is a novel N-recognin E3 ligase for GABARAP, which is subject to the regulation of WIPI4. Consistent with this function, the N-degron of GABARAP promotes its ubiquitination.

6.1 The function of WIPI4

6.1.1 ATG2-dependent functions

Given that the overexpression of WIPI4-GFP and ATG2-GFP separately increased LC3-II levels in control cells (Chapter 3, Figure 3.16 B&D), and that HEK293 cells lacking endogenous ATG2A/B also accumulated LC3-II (Tamura et al., 2017), WIPI4 and ATG2 appear to function synergistically in both overexpression and loss-of-function conditions. Moreover, ATG2 loss of function reduced WIPI4 levels but not vice versa (Figure 6.1). This suggests that ATG2 is the major component of the WIPI4-ATG2 complex. *In vitro* analysis showed that one of the functions of WIPI4 is to form a complex with ATG2 and that this interaction stabilized the interaction of ATG2 with PI3P containing vesicles.

The N-terminal fragment of ATG2, which has no tethering domains, still rescues the autophagy defect of the ATG2 KO cell line (Osawa et al., 2019), suggesting that the lipid transfer function of ATG2 is responsible for its main function in autophagy.

6.1.1.1 Promoting ATG2 function in the late stage of autophagosome formation

The lipid transfer function of WIPI4-ATG2 complex may facilitate the recruitment of certain lipids and proteins which drives maturation of autophagosomes. To be specific, the ATG2-WIPI4 complex may maintain or change the lipid composition of phagophores by non-vesicular transport. This may lead to:

i. Stability or change of physical properties of membranes, e.g. curvature/ fluidity.
ii. Stability or change of downstream lipid effectors, which may be closure/maturation modulators.

Identification of the modulators potentially recruited will help shed light on the mechanism of WIPI4-ATG2 in autophagosome closure. An analysis of proteins/lipids on vesicles that accumulate in cells depleted of WIPI4, as well as proteins enriched on autophagosomes in WT but not WIPI4 loss of function conditions, may help identify the closure regulators recruited by WIPI4-ATG2 complex.

Lipid transfer proteins are usually first defined by highly controlled in vitro experiments. Evidence of the same reactions in cells is required to support the functional relevance. However, the in vivo techniques for studying lipid transport pathways are currently limited. For example, deletion of certain lipid transfer proteins may induce cellular adaptations, in particular by hypertrophy of parallel pathways. In such a circular environment, blocking any of the steps leads to hypertrophy of other routes. Therefore, although it is uncontroversial that ATG2 and WIPI4 mediate net lipid traffic, it might be much harder to determine whether the rates of in vivo lipid traffic are affected by ATG2 and WIPI4 levels. *In vivo* function analysis in this thesis helped understand the exact biological process and provided implications about other potential interactors in that process

6.1.1.2 Inhibition/ adjusting the lipid transfer function of ATG2

However, if the function of WIPI4 is simply to assist ATG2's lipid transfer function in expanding the phagophores, WIPI4 loss of function should cause similar defect with ATG2 loss of function. In contrast, multiple evidence suggests that WIPI4 may also inhibit/ adjust the lipid transfer function of ATG2:

i. WIPI4 loss-of-function increased the size of autophagosomes in HeLa cells; while ATG2 loss of function reduced the size of autophagosomes dramatically in U2OS cells. The smaller autophagosomes can still mature into autolysosomes (Tang et al., 2019).
ii. WIPI4 loss-of-function only slightly increased the ratio of proteinase K sensitive LC3-II out of the total LC3-II, while ATG2 loss of function greatly increased the ratio. This suggests that the proteinase K assay, although designed to test the closure defect, may mainly reflect the expansion defect and changes of autophagosome size rather than the closure defect, as ATG2 has been proved to be a regulator of expansion, rather than closure.
iii. HeLa cells still respond to BafA1 treatment when WIPI4 is depleted (Chapter 3, Figure 3.1&3.2), while ATG2-depleted HEK293 cells cannot (Valverde et al., 2019; Tang et al., 2019). This suggests that WIPI4 functions later than ATG2 in a late stage of phagophore expansion, and it is not clear whether there is closure defect.

The difference of the proportion of proteinase K cleavable LC3-II out of total LC3-II in WIPI4 and ATG2 depleted cells may be caused by the increase of the size of autophagosomes. Because the total surface area of bigger autophagosomes is less compared to that of the smaller autophagosomes formed by the same amount of materials.

In addition, the observations in Chapter 3 suggests that WIPI4 is not required for the autophagosome localization of ATG2. WIPI4 may stabilize the tethering of PI3P containing membranes by ATG2 C-termini only after ATG2 binds to phagophores, but may not be the only protein able to recruit ATG2 onto autophagosomes. ATG9, for example, regulates the PAS localization of ATG2.

Therefore, the main function of WIPI4 may be to ‘tell’ ATG2 when to stop expansion and proceed to closure; without WIPI4, ATG2 may exist overlong on autophagosomes and inject more lipid of wrong types to generate bigger but less functional autophagosomes with the wrong composition of lipid, or impair ATG proteins like ATG9 to exit in time from autophagosomes.

6.1.1.3 Expansion defects may indirectly impair closure

While working on this project, the other cases reported to impair autophagosome, in addition to WIPI4-ATG2 complex, are all indirect and not specific to the closure step. The first one is the ATG4B mutant, which increases the ratio of unsealed autophagosomes and the number of all autophagosomes through sequestering unlipidated LC3 (Fujita et al., 2009). The second is depletion of the ATG8 lipidation system (Tsuboyama et al., 2016), which increases the time for autophagosomes to breakdown. The third is an excess of sphingolipids, which accumulates ATG9 at non-autophagy compartments (Corcelle-Termeau et al., 2016). However, Corcelle-Termeau and his colleagues observed unsealed autophagosomes by EM but did not confirm with proteinase K protection experiment or quantification of EM images. All of the proteins mentioned have known roles in phagophore expansion and are not specific to closure, similar to the yeast Atg2-Atg18 complex. The former two (ATG4B and ATG8 lipidation system) both impact the ATG8 family proteins. However, ATG8 family proteins accelerate the closure but are not required for that, and the mechanism whereby they accelerate the closure is unknown, with biophysical evidence pointing to either tethering or fusion. It is unknown whether tethering of the edges of the membranes also promotes the closure, and the *in vitro* evidence showing ATG8 proteins regulate membrane fusion need further analysis. Therefore, ATG8 proteins may accelerate the closure of phagophores directly or indirectly, but was the only known machinery while working on this project.

6.1.1.3.1 Whether GABARAP is a closure regulator downstream of WIPI4

Reports that ATG8 proteins are not required for but accelerate the closure (Tsuboyama et al., 2016), and GABARAP family and ATG8 family knockout cell lines have only closure defect in basal conditions but not in starvation plus BafA1 conditions (Nguyen et al., 2016) by proteinase K assay, suggest that GABARAP may play a supportive role in closure but is not required. This thesis tested GABARAP because WIPI4 depletion also causes a relatively minor defect in closure and ATG8 proteins were the only known potential closure machinery at that moment.

However, GABARAP still colocalizes with autophagosome marker ATG16, and LC3 in WIPI4 depleted cells. Although this might be an artefact of impairment of GABARAP dissociation from the membrane caused by the block of autophagy flux, it suggests that the presence of GABARAP on the membrane is not enough to promote closure. Preliminary experiments rescuing GABARAP protein levels with MIB1 or UBR5 knockdown cannot rescue the

accumulation of LC3-II in WIPI4 depleted cells (data not shown). Therefore, WIPI4 depletion may also disrupt other processes in addition to decrease GABARAP levels.

The fragmented TGN structures in WIPI4 knockdown conditions (Fig.6.2) suggest that WIPI4 may regulate not only GABARAP trafficking but also vesicular trafficking in general. Future work will first examine whether mis-trafficking of GABARAP or defects of general vesicular trafficking accounts for the defect.

GABARAP is reported to recruit a series of autophagosome-lysosome tethering regulators onto autophagosomes: PI4K2A/PI4KIIα need to be recruited from the TGN onto autophagosomes by GABARAP; BRUCE and PLEKHM1 both promote the tethering of autophagosomes with lysosomes by interacting with GABARAP. The RAB7 effector RMC1 also accumulates in GABARAP family protein depleted cells (Vaites et al., 2019). There is no report about GABARAP recruiting closure regulators. However, Rab5 is reported recently to regulate autophagosome closure by facilitating the interaction of ESCRTIII complex subunit Snf7 with Atg17 (yeast FIP200) in yeast (Zhou 2019). Interestingly, FIP200 is a subunit of ULK1 complex, and all subunits in that complex (ULK1, FIP200 and ATG13) preferentially bind GABARAP subfamily members (Joachim 2015). FIP200 also binds WIPI3 (Bakula et al., 2017). Further research may explore whether GABARAP regulates the trafficking of closure regulators, e.g. ESCRT complex components, Rab5 effectors, and so on. If not, the mis-trafficking of GABARAP may be a side-effect of the blockage of autophagy flux. The work will be redirected onto whether WIPI4-ATG2 regulates the trafficking of closure regulators independent of GABARAP.

6.1.1.3.2 ESCRT complex may be recruited by expansion regulators

WIPI4 may indirectly regulate closure by regulating the ESCRT-III complex and its regulators during the late expansion. No ESCRT-III or Rab5 related proteins were identified by the WIPI4 Mass Spec, suggesting that either there are unknown ESCRT-III regulators or WIPI4 regulates ESCRT-III/Rab5 complexes indirectly.

Additionally, according to the Mass Spec results (Chapter 5) and as confirmed by Bakula in 2017, WIPI4 interacts with the nuclear migration protein (NUDC), an Hsp90 co-chaperone that stabilizes actin organisation modulator Cofilin 1 (Zhang 2016). Also, it was observed that WIPI4 loss of function disrupted centrosome satellites (Chapter 4). Interestingly, microtubule is required for the constriction function of ESCRT-III in membrane fission (Kharkwal et al., 2014).

Therefore, it is possible that WIPI4 also facilitates the constriction function of the ESCRT-III complex through regulating microtubule organisation.

6.1.2 ATG2-independent functions

The regulation of lysosomes by WIPI4 seems to be independent of ATG2. WIPI4 loss of function increased the lysosome pH in basal and starvation conditions (Chapter 3, Figure 3.10), while ATG2A/B depletion did not increase the pH of lysosomes (Chapter 3, Figure 3.19). Consistent with the observation in mammalian cells, Atg2 is not involved in lysosome fragmentation in yeast (Navin et al., 2017), while Atg18, one of the yeast homologs of WIPIs, has been reported to trigger the scission of lysosome-like vacuoles through inserting an amphipathic α-helix into the membrane and self-oligomerization (Gopaldass et al. 2017). This regulation of Atg18 on vacuole fragmentation is dependent on PI(3,5)P2, not PI3P, suggesting that this is an autophagy-independent function. WIPI4 loss of function caused ER stress independent on the ERphagy pathway (Wan et al., 2019). As shown in Figure 6.2, the Trans Golgi marker TGN46 was greatly dispersed by WIPI4 knockdown, these structures are either fragmented Golgi structures (reviewed in Machamer et al., 2015), or vesicles failed to dock on autophagosomes because of WIPI4 loss of function. Therefore, WIPI4 may regulate ER-Golgi trafficking.

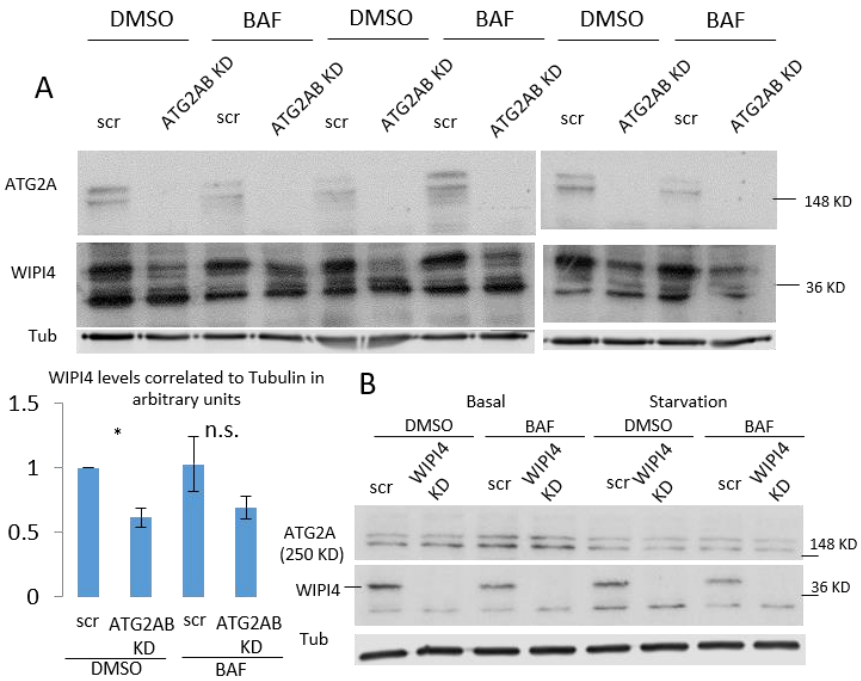

Figure 6.1. ATG2 depletion decreases WIPI4 levels but not vice versa

A. Effects of ATG2A/B knockdown on WIPI4 levels with tubulin as the internal control. HeLa cells were transfected with control or ATG2A/B SMARTpool siRNA (100 nM each) for 72 hours and incubated with 400 nM BafA1 or DMSO in culture media during the last 4 hours before harvesting. The graph shows the quantification of WIPI4 levels relative to tubulin from the blots (*P<0.05, n.s., non-significant; two-tailed unpaired student's t-test). This is representative data of 3 experiments.

B. Effects of WIPI4 knockdown on ATG2A levels with tubulin as the internal control. HeLa cells were transfected with control or WIPI4 SMARTpool siRNA (60 nM) for 72 hours and incubated with 400 nM BafA1 or DMSO in culture media for 4 hours prior to harvesting.

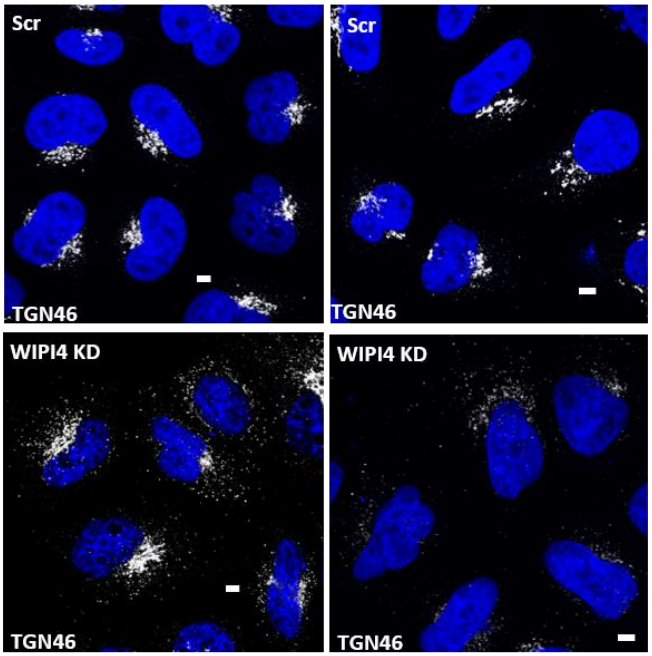

Figure 6.2. WIPI4 loss of function causes a redistribution of TGN46 positive structures

Representative images showing that the TGN46 (Alexa 594 anti-rabbit) positive structures change from ribbon-like pattern to a more scattered pattern. Scale Bars: 5 µm.

6.1.3 Identification of the WIPI4 function in autophagy helps to understand the BPAN pathology

Iron accumulation in the basal ganglia represents a common hallmark between the different classes of NBIA (Arber et al., 2016). The fibroblasts from BPAN patients are of higher levels of ferrous iron transporter without the iron response element ((−)IRE/DMT1) and decreased levels of transferrin receptor (TfR) than in healthy controls, which suggests intracellular ferrous iron overload and an increased risk of iron accumulation (Ingrassia et al., 2017). The dysregulation of iron metabolism was corroborated by another study that BPAN patients' fibroblasts and neurons are of decreased ferritin levels and higher iron levels (Seibler et al., 2018). The aberration of (-)IRE/DMT1 and TfR levels in BPAN patients was further induced by starvation (Ingrassia et al., 2017), indicating that WIPI4 may balance intracellular ferrous iron levels by degrading (-)IRE/DMT1 through autophagy. Moreover, WIPI4 loss of function induced multiple pathological alterations and higher oxidative stress in fibroblasts and neurons of BPAN patients, as shown by decreased mitochondrial membrane potential, reduced production of ATP, reduced LAMP1 and LAMP2, and elevated levels of superoxide dismutase 2 (SOD2) (Seibler et al., 2018).

It is still unknown which peculiarity is upstream: the defect in iron metabolism or autophagy. One fact manifesting the role of iron metabolism pathway in BPAN pathology is that all BPAN patients are found with strong iron deposition in the substantia nigra (SN) and globus pallidus (GP), while only a subset of Parkinson's disease patients are found with iron deposition. Interestingly, BPAN patients are subject to the degeneration of a bigger brain region, including important dopamine receiving cells, bigger than those affected in PD. PD is caused by degeneration of cells in the substantia nigra and a subsequent reduction of dopamine in the brain, and the administration of the l-isomer of 3,4-dihydroxyphenylalanine (l-DOPA), a dopamine precursor (Triarhou et al., 2002), is an effective treatment of PD. In contrast, BPAN patients do not respond to similar administration. Lately, ferritinophagy provides a novel link between iron homeostasis dysfunction and autophagy impairment. Iron deposition leads to defective autophagy, as well as increased α-synuclein levels and ROS, in both primary dopaminergic neurons and SH-SY5Y cells (Wan et al., 2017).

However, the role of WIPI4 in iron metabolism is not required for developing mobility and cognitive impairments. CNS-specific Wdr45 knockout (Nes-Wdr45fl/Y) mice recapitulate impaired motor coordination, axon swelling and cognitive defects of BPAN patients, but not

iron accumulation, suggesting that the role of WIPI4 in iron trafficking in human is absent in mice (Zhao et al. 2015).

Altogether, WIPI4's function in autophagy seems more important for understanding BPAN pathology. This thesis helps shed light on the pathology of BPAN by narrowing down the function of WIPI4 in basal and starvation-induced autophagy to late expansion and closure.

6.2 UBR5 is a potential E3 ligase of GABARAP

The mutation of the lysine at Position 2 of GABARAP sequence protected GABARAP from degradation, suggesting that GABARAP may be an N-end rule substrate. Since UBR5 interacts with and negatively regulates GABARAP levels, UBR5 is very likely an E3 ligase that specifically ubiquitinates GABARAP, which has been verified preliminarily by *in vitro* ubiquitination assays.

Although GABARAP has been found to interact with several E3 ligases to regulate macroautophagy or mitophagy (Behrends et al., 2015; Ambivero et al. 2014; Poetsch et al., 2018), there has been only one E3 ligase, MIB1, reported degrading GABARAP. There have been no previous publications suggesting that UBR5 functions in autophagy. In addition, since GABARAP is required for autophagy, UBR5 might play dual roles in both proteasome and autophagic pathways. Therefore, it will be of both novelty and importance to elucidate the function that UBR5 and GABARAP play together.

Future work is to identify poly-ubiquitination sites on GABARAP that are recognized by UBR5. Mass spec analyses indicate that K35 and K24 are not ubiquitinated when the N-degron of GABARAP is mutated, suggesting that they may be modified by the N-end rule pathway E3 ligases. To assess this possibility, ubiquitination levels of K35R mutated GABARAP, K24R mutated GABARAP, and K35R-K24R double mutated GABARAP proteins will be evaluated by immunoprecipitation. The mutant(s) with lower ubiquitination levels may be possible ubiquitination sites of UBR5. Interestingly, K35 is only conserved among GABARAP subfamily proteins but cannot be found in LC3 subfamily proteins; K24 is only conserved among GABARAP subfamily proteins and LC3C (GATE16); K6 is conserved among all proteins in the mammalian ATG8 family. This suggests that when the N-terminal of GABARAP is mutated to the same as the N-terminal of LC3, the preferred position for ubiquitin modification of GABARAP is changed to a lysine shared by LC3 and GABARAP.

In addition to the ubiquitination sites, there are several other questions worth considering.

6.2.1 The possible interacting site of UBR5 and GABARAP

Preliminary data shows that the mutation of the N-degron of GABARAP does not decrease its interaction with UBR5 (data not shown) but decreased its ubiquitination levels, suggesting that the N-degron of GABARAP is not required its interaction with UBR5. Instead, there are other mechanisms facilitating UBR5-GABARAP interaction. Other possible mechanisms facilitating the interaction between UBR5 and GABARAP include:

i. Hydrophobic pockets on GABARAP with potential LIR domain on UBR5,
ii. UIM docking sites found on GABARAP with potential ubiquitin-interacting motif (UIM)-like sequences on UBR5 (Vierstra et al., 2019).

In addition, as shown in Chapter 5 (Figure 5.2C), more UBR5 is immunoprecipitated by GFP-GABARAP compared to GFP-LC3. However, further experiments are required to understand whether UBR5 preferentially binds GABARAP, or simply because the proportion of cytosolic GABARAP-I (possibly more approachable for UBR5) to membrane-bound GABARAP-II is much higher than that of LC3 in HeLa cells. Co-IP of UBR5 with GFP tagged GABARAP, and LC3 proteins in autophagy-null cells (ATG16 knockout HeLa) may help evaluate the above hypotheses. If there is still more UBR5 pulled down by GABARAP compared to LC3, UBR5 may interact more stably with GABARAP. These experiments will help understand the interaction mechanism of UBR5 with GABARAP.

6.2.2 ATE1, another component of the N-end rule pathway, regulates autophagy

Both GABARAP and LC3 levels were increased by ATE1 knockdown, although according to N-end rule, neither should be processed by ATE-1 for degradation. If ATE1 siRNA did not cause off-target effect, this suggests one of the two possibilities:

i. ATE1 indirectly affects their levels by regulating the stability of their positive regulators;
ii. The degradation intermediates exposed to the internal degrons are recognized by the N-end rule pathway, which indirectly hastens the depletion of full-length GABARAP and LC3.

The latter possibility is consistent with the previous understanding that the N-end rule pathway is important for the degradation of peptides and protein fragments. For example, C-terminal fragments of PINK1 are degraded by the N-end rule pathway (Youle et al., 2013). However, this does not contradict the hypothesis that UBR5 degrades full-length GABARAP protein. There has been research showing that full length proteins are UBR5 substrates, including the DNA damage response protein RNF168 (Gudjonsson et al., 2012), ATMIN (Zhang et al., 2014), transcription factors pregnane X receptor (Ong et al., 2014), translational machinery CDK9 (Cojocaru et al., 2011), PAIP2 (Yoshida et al., 2006), the KATNA1 subunit of the cell cycle-related protein KATANIN (Maddika et al., 2009) and the rate-limiting enzyme in gluconeogenesis PEPCK (Jiang et al., 2011).

6.2.3 UBR5 is associated with familial adult myoclonic epilepsy 1 (FAME1)

c.5720G>A mutation (p.Arg1907His) in the *UBR5* gene was found to be associated with familial adult myoclonic epilepsy 1, which is linked to 8q24. FAME is a heterogeneous disorder, and distinct phenotypic traits might reflect different genetic mutations, although in most cases Purkinje cell changes were observed (Rootselaar AF et al., 2007). Cen et al. considered the presence of TTTTA and TTTCA expansion repeats to be the founder effect linked to the FAME1 locus. Different from their opinion, Ende et al. think the candidate genes are involved in Purkinje cell outgrowth or encoding for ion channels or neurotransmitters. For example, a gain of function mutation in the *ADRA2B* (adrenoceptor alpha 2B) gene found in Italian patients could potentially reduce gamma-aminobutyric acid (GABA) neurotransmission (Fusco et al., 2014). A reduction in cortical GABA neurotransmission is associated with cortical myoclonus in rats (Ganos et al., 2014). Treatment with anti-epileptic drugs (AEDs) increasing GABA neurotransmitter levels can relieve the symptoms (White et al., 2007). In addition, UBR5 has been identified to interact with $GABA_A$ ρ receptor (Wang et al., 2013) by another group with Mass spec. The results in this thesis, together with the above studies, presenting one possibility that UBR5 mutation increases the risk of a subtype of FAME through changing the stability of $GABA_A$ receptors or interactors of $GABA_A$ receptors. More evidence is required to confirm or turn down the relevance of UBR5 with GABA transmission and FAME.

Chapter 7 References

1. Abbi S, Ueda H, Zheng CH, Cooper LA, Zhao JH, Christopher R, et al. Regulation of focal adhesion kinase by a novel protein inhibitor FIP200. Molecular Biology of the Cell. 2002;13(9):3178-91.

2. Adell MAY, Migliano SM, Teis D. ESCRT-III and Vps4: a dynamic multipurpose tool for membrane budding and scission. Febs J. 2016;283(18):3288-302.

3. Albanesi J, Wang HZ, Sun HQ, Levine B, Yin H. GABARAP-mediated targeting of PI4K2A/PI4KII to autophagosomes regulates PtdIns4P-dependent autophagosome-lysosome fusion. Autophagy. 2015;11(11):2127-9.

4. Ambivero CT, Cilenti L, Main S, Zervos AS. Mulan E3 ubiquitin ligase interacts with multiple E2 conjugating enzymes and participates in mitophagy by recruiting GABARAP. Cell Signal. 2014;26(12):2921-9.

5. Aristarkhov A, Eytan E, Moghe A, Admon A, Hershko A, Ruderman JV. E2-C, a cyclin-selective ubiquitin carrier protein required for the destruction of mitotic cyclins. Proc Natl Acad Sci U S A. 1996;93(9):4294-9.

6. Ashkenazi A, Bento CF, Ricketts T, Vicinanza M, Siddiqi F, Pavel M, et al. Polyglutamine tracts regulate beclin 1-dependent autophagy. Nature. 2017;545(7652):108-+.

7. Axe EL, Walker SA, Manifava M, Chandra P, Roderick HL, Habermann A, et al. Autophagosome formation from membrane compartments enriched in phosphatidylinositol 3-phosphate and dynamically connected to the endoplasmic reticulum. J Cell Biol. 2008;182(4):685-701.

8. Bachmair A, Varshavsky A. The degradation signal in a short-lived protein. Cell. 1989;56(6):1019-32.

9. Bago R, Malik N, Munson MJ, Prescott AR, Davies P, Sommer E, et al. Characterization of VPS34-IN1, a selective inhibitor of Vps34, reveals that the phosphatidylinositol 3-phosphate-binding SGK3 protein kinase is a downstream target of class III phosphoinositide 3-kinase. Biochem J. 2014;463(3):413-27.

10. Bakula D, Muller AJ, Zuleger T, Takacs Z, Franz-Wachtel M, Thost AK, et al. WIPI3 and WIPI4 beta-propellers are scaffolds for LKB1-AMPK-TSC signalling circuits in the control of autophagy. Nat Commun. 2017;8:15637.

11. Barnett A, Brewer GJ. Autophagy in aging and Alzheimer's disease: pathologic or protective? J Alzheimers Dis. 2011;25(3):385-94.

12. Baskaran S, Ragusa MJ, Boura E, Hurley JH. Two-site recognition of phosphatidylinositol 3-phosphate by PROPPINs in autophagy. Mol Cell. 2012;47(3):339-48.

13. Bates G. Huntingtin aggregation and toxicity in Huntington's disease. Lancet. 2003;361(9369):1642-4.

14. Behrends C, Sowa ME, Gygi SP, Harper JW. Network organization of the human autophagy system. Nature. 2010;466(7302):68-76.

15. Benes P, Vetvicka V, Fusek M. Cathepsin D--many functions of one aspartic protease. Crit Rev Oncol Hematol. 2008;68(1):12-28.

16. Bennett EJ, Shaler TA, Woodman B, Ryu KY, Zaitseva TS, Becker CH, et al. Global changes to the ubiquitin

system in Huntington's disease. Nature. 2007;448(7154):704-8.

17. Bento CF, Ashkenazi A, Jimenez-Sanchez M, Rubinsztein DC. The Parkinson's disease-associated genes ATP13A2 and SYT11 regulate autophagy via a common pathway. Nat Commun. 2016;7:11803.

18. Berry IJ, Jarocki VM, Tacchi JL, Raymond BBA, Widjaja M, Padula MP, et al. N-terminomics identifies widespread endoproteolysis and novel methionine excision in a genome-reduced bacterial pathogen. Sci Rep. 2017;7(1):11063.

19. Bett JS, Goellner GM, Woodman B, Pratt G, Rechsteiner M, Bates GP. Proteasome impairment does not contribute to pathogenesis in R6/2 Huntington's disease mice: exclusion of proteasome activator REGgamma as a therapeutic target. Hum Mol Genet. 2006;15(1):33-44.

20. Boland B, Kumar A, Lee S, Platt FM, Wegiel J, Yu WH, et al. Autophagy induction and autophagosome clearance in neurons: relationship to autophagic pathology in Alzheimer's disease. J Neurosci. 2008;28(27):6926-37.

21. Bonissone S, Gupta N, Romine M, Bradshaw RA, Pevzner PA. N-terminal protein processing: a comparative proteogenomic analysis. Mol Cell Proteomics. 2013;12(1):14-28.

22. Botelho RJ, Efe JA, Teis D, Emr SD. Assembly of a Fab1 phosphoinositide kinase signaling complex requires the Fig4 phosphoinositide phosphatase. Mol Biol Cell. 2008;19(10):4273-86.

23. Bothmer A, Robbiani DF, Di Virgilio M, Bunting SF, Klein IA, Feldhahn N, et al. Regulation of DNA end joining, resection, and immunoglobulin class switch recombination by 53BP1. Mol Cell. 2011;42(3):319-29.

24. Bothmer A, Robbiani DF, Feldhahn N, Gazumyan A, Nussenzweig A, Nussenzweig MC. 53BP1 regulates DNA resection and the choice between classical and alternative end joining during class switch recombination. J Exp Med. 2010;207(4):855-65.

25. Bouwman P, Aly A, Escandell JM, Pieterse M, Bartkova J, van der Gulden H, et al. 53BP1 loss rescues BRCA1 deficiency and is associated with triple-negative and BRCA-mutated breast cancers. Nature Structural & Molecular Biology. 2010;17(6):688-U56.

26. Bowman EJ, Bowman BJ. Cellular role of the V-ATPase in Neurospora crassa: analysis of mutants resistant to concanamycin or lacking the catalytic subunit A. J Exp Biol. 2000;203(Pt 1):97-106.

27. Brocker C, Engelbrecht-Vandre S, Ungermann C. Multisubunit Tethering Complexes and Their Role in Membrane Fusion. Curr Biol. 2010;20(21):R943-R52.

28. Bunting SF, Callen E, Wong N, Chen HT, Polato F, Gunn A, et al. 53BP1 Inhibits Homologous Recombination in Brca1-Deficient Cells by Blocking Resection of DNA Breaks. Cell. 2010;141(2):243-54.

29. Busse RA, Scacioc A, Hernandez JM, Krick R, Stephan M, Janshoff A, et al. Qualitative and quantitative characterization of protein-phosphoinositide interactions with liposome-based methods. Autophagy. 2013;9(5):770-7.

30. Cebollero E, van der Vaart A, Zhao M, Rieter E, Klionsky DJ, Helms JB, et al. Phosphatidylinositol-3-phosphate clearance plays a key role in autophagosome completion. Curr Biol. 2012;22(17):1545-53.

31. Chen SJ, Wu X, Wadas B, Oh JH, Varshavsky A. An N-end rule pathway that recognizes proline and destroys gluconeogenic enzymes. Science. 2017;355(6323).

32. Chi C, Leonard A, Knight WE, Beussman KM, Zhao Y, Cao Y, et al. LAMP-2B regulates human cardiomyocyte function by mediating autophagosome-lysosome fusion. Proc Natl Acad Sci U S A. 2019;116(2):556-65.

33. Choi WS, Jeong BC, Joo YJ, Lee MR, Kim J, Eck MJ, et al. Structural basis for the recognition of N-end rule substrates by the UBR box of ubiquitin ligases. Nat Struct Mol Biol. 2010;17(10):1175-81.

34. Chowdhury S, Otomo C, Leitner A, Ohashi K, Aebersold R, Lander GC, et al. Insights into autophagosome biogenesis from structural and biochemical analyses of the ATG2A-WIPI4 complex. Proc Natl Acad Sci U S A. 2018;115(42):E9792-E801.

35. Christ L, Raiborg C, Wenzel EM, Campsteijn C, Stenmark H. Cellular Functions and Molecular Mechanisms of the ESCRT Membrane-Scission Machinery. Trends Biochem Sci. 2017;42(1):42-56.

36. Ciechanover A, Heller H, Elias S, Haas AL, Hershko A. ATP-dependent conjugation of reticulocyte proteins with the polypeptide required for protein degradation. Proc Natl Acad Sci U S A. 1980;77(3):1365-8.

37. Coleman KA, Greenberg RA. The BRCA1-RAP80 Complex Regulates DNA Repair Mechanism Utilization by Restricting End Resection. Journal of Biological Chemistry. 2011;286(15):13669-80.

38. Collins GA, Goldberg AL. The Logic of the 26S Proteasome. Cell. 2017;169(5):792-806.

39. Corcelle-Termeau E, Vindelov SD, Hamalisto S, Mograbi B, Keldsbo A, Brasen JH, et al. Excess sphingomyelin disturbs ATG9A trafficking and autophagosome closure. Autophagy. 2016;12(5):833-49.

40. Corona AK, Jackson WT. Finding the Middle Ground for Autophagic Fusion Requirements. Trends Cell Biol. 2018;28(11):869-81.

41. Coyle JE, Qamar S, Rajashankar KR, Nikolov DB. Structure of GABARAP in two conformations: Implications for GABA(A) receptor localization and tubulin binding. Neuron. 2002;33(1):63-74.

42. Cruz-Garcia D, Ortega-Bellido M, Scarpa M, Villeneuve J, Jovic M, Porzner M, et al. Recruitment of arfaptins to the trans-Golgi network by PI(4)P and their involvement in cargo export. Embo Journal. 2013;32(12):1717-29.

43. Davies CW, Stjepanovic G, Hurley JH. How the Atg1 complex assembles to initiate autophagy. Autophagy. 2015;11(1):185-6.

44. Davies JE, Rubinsztein DC. Over-expression of BCL2 rescues muscle weakness in a mouse model of oculopharyngeal muscular dystrophy. Hum Mol Genet. 2011;20(6):1154-63.

45. de Duve C. The lysosome turns fifty. Nat Cell Biol. 2005;7(9):847-9.

46. De Fusco M, Vago R, Striano P, Di Bonaventura C, Zara F, Mei D, et al. The alpha(2B)-Adrenergic Receptor Is Mutant in Cortical Myoclonus and Epilepsy. Ann Neurol. 2014;75(1):77-87.

47. de Poot SAH, Tian G, Finley D. Meddling with Fate: The Proteasomal Deubiquitinating Enzymes. J Mol Biol. 2017;429(22):3525-45.

48. de Pril R, Hobo B, van Tijn P, Roos RA, van Leeuwen FW, Fischer DF. Modest proteasomal inhibition by aberrant ubiquitin exacerbates aggregate formation in a Huntington disease mouse model. Mol Cell Neurosci. 2010;43(3):281-6.

49. Diao J, Liu R, Rong Y, Zhao M, Zhang J, Lai Y, et al. ATG14 promotes membrane tethering and fusion of autophagosomes to endolysosomes. Nature. 2015;520(7548):563-6.

50. Dooley HC, Razi M, Polson HE, Girardin SE, Wilson MI, Tooze SA. WIPI2 links LC3 conjugation with PI3P, autophagosome formation, and pathogen clearance by recruiting Atg12-5-16L1. Mol Cell. 2014;55(2):238-52.

51. Dowdle WE, Nyfeler B, Nagel J, Elling RA, Liu S, Triantafellow E, et al. Selective VPS34 inhibitor blocks autophagy and uncovers a role for NCOA4 in ferritin degradation and iron homeostasis in vivo. Nat Cell Biol. 2014;16(11):1069-79.

52. Ebner P, Poetsch I, Deszcz L, Hoffmann T, Zuber J, Ikeda F. The IAP family member BRUCE regulates autophagosome-lysosome fusion. Nat Commun. 2018;9(1):599.

53. Egan D, Kim J, Shaw RJ, Guan KL. The autophagy initiating kinase ULK1 is regulated via opposing phosphorylation by AMPK and mTOR. Autophagy. 2011;7(6):643-4.

54. Eisenberg-Bord M, Shai N, Schuldiner M, Bohnert M. A Tether is a Tether is a Tether: Tethering at Membrane Contact Sites. Developmental Cell. 2016;39(4):395-409.

55. Fimia GM, Stoykova A, Romagnoli A, Giunta L, Di Bartolomeo S, Nardacci R, et al. Ambra1 regulates autophagy and development of the nervous system. Nature. 2007;447(7148):1121-5.

56. Fitzgerald JB, Johnson BW, Baum J, Adams S, Iadevaia S, Tang J, et al. MM-141, an IGF-IR- and ErbB3-directed bispecific antibody, overcomes network adaptations that limit activity of IGF-IR inhibitors. Mol Cancer Ther. 2014;13(2):410-25.

57. Flack JE, Mieszczanek J, Novcic N, Bienz M. Wnt-Dependent Inactivation of the Groucho/TLE Co-repressor by the HECT E3 Ubiquitin Ligase Hyd/UBR5. Molecular Cell. 2017;67(2):181-+.

58. Frake RA, Ricketts T, Menzies FM, Rubinsztein DC. Autophagy and neurodegeneration. J Clin Invest. 2015;125(1):65-74.

59. Fraldi A, Annunziata F, Lombardi A, Kaiser HJ, Medina DL, Spampanato C, et al. Lysosomal fusion and SNARE function are impaired by cholesterol accumulation in lysosomal storage disorders. EMBO J. 2010;29(21):3607-20.

60. Frost A, Unger VM, De Camilli P. The BAR Domain Superfamily: Membrane-Molding Macromolecules. Cell. 2009;137(2):191-6.

61. Fujita N, Hayashi-Nishino M, Fukumoto H, Omori H, Yamamoto A, Noda T, et al. An Atg4B mutant hampers the lipidation of LC3 paralogues and causes defects in autophagosome closure. Mol Biol Cell. 2008;19(11):4651-9.

62. Fujita N, Itoh T, Omori H, Fukuda M, Noda T, Yoshimori T. The Atg16L complex specifies the site of LC3 lipidation for membrane biogenesis in autophagy. Mol Biol Cell. 2008;19(5):2092-100.

63. Fujita N, Noda T, Yoshimori T. Atg4B(C74A) hampers autophagosome closure: a useful protein for inhibiting autophagy. Autophagy. 2009;5(1):88-9.

64. Ganley IG, Lam du H, Wang J, Ding X, Chen S, Jiang X. ULK1.ATG13.FIP200 complex mediates mTOR signaling and is essential for autophagy. J Biol Chem. 2009;284(18):12297-305.

65. Ganos C, Kassavetis P, Erro R, Edwards MJ, Rothwell J, Bhatia KP. The role of the cerebellum in the pathogenesis of cortical myoclonus. Mov Disord. 2014;29(4):437-43.

66. Genau HM, Huber J, Baschieri F, Akutsu M, Dotsch V, Farhan H, et al. CUL3-KBTBD6/KBTBD7 ubiquitin ligase cooperates with GABARAP proteins to spatially restrict TIAM1-RAC1 signaling. Mol Cell. 2015;57(6):995-1010.

67. Gopaldass N, Fauvet B, Lashuel H, Roux A, Mayer A. Membrane scission driven by the PROPPIN Atg18. EMBO J. 2017;36(22):3274-91.

68. Graef M, Friedman JR, Graham C, Babu M, Nunnari J. ER exit sites are physical and functional core autophagosome biogenesis components. Mol Biol Cell. 2013;24(18):2918-31.

69. Grice GL, Nathan JA. The recognition of ubiquitinated proteins by the proteasome. Cell Mol Life Sci. 2016;73(18):3497-506.

70. Grumati P, Dikic I. Ubiquitin signaling and autophagy. Journal of Biological Chemistry. 2018;293(15):5404-13.

71. Guan J, Stromhaug PE, George MD, Habibzadegah-Tari P, Bevan A, Dunn WA, Jr., et al. Cvt18/Gsa12 is required for cytoplasm-to-vacuole transport, pexophagy, and autophagy in Saccharomyces cerevisiae and Pichia pastoris. Mol Biol Cell. 2001;12(12):3821-38.

72. Gudjonsson T, Altmeyer M, Savic V, Toledo L, Dinant C, Grofte M, et al. TRIP12 and UBR5 suppress spreading of chromatin ubiquitylation at damaged chromosomes. Cell. 2012;150(4):697-709.

73. Guertin DA, Sabatini DM. Defining the role of mTOR in cancer. Cancer Cell. 2007;12(1):9-22.

74. Guo YJ, Chang CM, Huang R, Liu B, Bao L, Liu W. AP1 is essential for generation of autophagosomes from the trans-Golgi network. Journal of Cell Science. 2012;125(7):1706-15.

75. Hara K, Maruki Y, Long X, Yoshino K, Oshiro N, Hidayat S, et al. Raptor, a binding partner of target of rapamycin (TOR), mediates TOR action. Cell. 2002;110(2):177-89.

76. Hara T, Takamura A, Kishi C, Iemura S, Natsume T, Guan JL, et al. FIP200, a ULK-interacting protein, is required for autophagosome formation in mammalian cells. J Cell Biol. 2008;181(3):497-510.

77. Hasegawa J, Iwamoto R, Otomo T, Nezu A, Hamasaki M, Yoshimori T. Autophagosome-lysosome fusion in neurons requires INPP5E, a protein associated with Joubert syndrome. EMBO J. 2016;35(17):1853-67.

78. He W, Wang Q, Srinivasan B, Xu J, Padilla MT, Li Z, et al. A JNK-mediated autophagy pathway that triggers c-IAP degradation and necroptosis for anticancer chemotherapy. Oncogene. 2014;33(23):3004-13.

79. Hegedus K, Takats S, Boda A, Jipa A, Nagy P, Varga K, et al. The Ccz1-Mon1-Rab7 module and Rab5

control distinct steps of autophagy. Molecular Biology of the Cell. 2016;27(20):3132-42.

80. Henderson MJ, Munoz MA, Saunders DN, Clancy JL, Russell AJ, Williams B, et al. EDD mediates DNA damage-induced activation of CHK2. J Biol Chem. 2006;281(52):39990-40000.

81. Henne WM, Stenmark H, Emr SD. Molecular Mechanisms of the Membrane Sculpting ESCRT Pathway. Csh Perspect Biol. 2013;5(9).

82. Hershko A. Lessons from the discovery of the ubiquitin system. Trends Biochem Sci. 1996;21(11):445-9.

83. Ho H, Kapadia R, Al-Tahan S, Ahmad S, Ganesan AK. WIPI1 coordinates melanogenic gene transcription and melanosome formation via TORC1 inhibition. J Biol Chem. 2011;286(14):12509-23.

84. Hohenstein AC, Roche PA. SNAP-29 is a promiscuous syntaxin-binding SNARE. Biochem Biophys Res Commun. 2001;285(2):167-71.

85. Hosokawa N, Hara T, Kaizuka T, Kishi C, Takamura A, Miura Y, et al. Nutrient-dependent mTORC1 association with the ULK1-Atg13-FIP200 complex required for autophagy. Mol Biol Cell. 2009;20(7):1981-91.

86. Hosokawa N, Sasaki T, Iemura S, Natsume T, Hara T, Mizushima N. Atg101, a novel mammalian autophagy protein interacting with Atg13. Autophagy. 2009;5(7):973-9.

87. Hu YD, Scully R, Sobhian B, Xie AY, Shestakova E, Livingston DM. RAP80-directed tuning of BRCA1 homologous recombination function at ionizing radiation-induced nuclear foci. Gene Dev. 2011;25(7):685-700.

88. Huang R, Xu Y, Wan W, Shou X, Qian J, You Z, et al. Deacetylation of nuclear LC3 drives autophagy initiation under starvation. Mol Cell. 2015;57(3):456-66.

89. Hubert V, Peschel A, Langer B, Groger M, Rees A, Kain R. LAMP-2 is required for incorporating syntaxin-17 into autophagosomes and for their fusion with lysosomes. Biol Open. 2016;5(10):1516-29.

90. Huss M, Ingenhorst G, Konig S, Gassel M, Drose S, Zeeck A, et al. Concanamycin A, the specific inhibitor of V-ATPases, binds to the V(o) subunit c. J Biol Chem. 2002;277(43):40544-8.

91. Hwang CS, Shemorry A, Varshavsky A. N-Terminal Acetylation of Cellular Proteins Creates Specific Degradation Signals. Science. 2010;327(5968):973-7.

92. Ichimura Y, Kirisako T, Takao T, Satomi Y, Shimonishi Y, Ishihara N, et al. A ubiquitin-like system mediates protein lipidation. Nature. 2000;408(6811):488-92.

93. Ikeda F. The anti-apoptotic ubiquitin conjugating enzyme BIRC6/BRUCE regulates autophagosome-lysosome fusion. Autophagy. 2018;14(7):1283-4.

94. Ingrassia R, Memo M, Garavaglia B. Ferrous Iron Up-regulation in Fibroblasts of Patients with Beta Propeller Protein-Associated Neurodegeneration (BPAN). Front Genet. 2017;8:18.

95. Inoki K. mTOR signaling in autophagy regulation in the kidney. Semin Nephrol. 2014;34(1):2-8.

96. Itakura E, Kishi-Itakura C, Koyama-Honda I, Mizushima N. Structures containing Atg9A and the ULK1 complex independently target depolarized mitochondria at initial stages of Parkin-mediated mitophagy. J Cell Sci. 2012;125(Pt 6):1488-99.

97. Itakura E, Kishi-Itakura C, Mizushima N. The hairpin-type tail-anchored SNARE syntaxin 17 targets to autophagosomes for fusion with endosomes/lysosomes. Cell. 2012;151(6):1256-69.

98. Jacinto E, Loewith R, Schmidt A, Lin S, Ruegg MA, Hall A, et al. Mammalian TOR complex 2 controls the actin cytoskeleton and is rapamycin insensitive. Nat Cell Biol. 2004;6(11):1122-8.

99. Jiang P, Mizushima N. Autophagy and human diseases. Cell Res. 2014;24(1):69-79.

100. Jiang P, Nishimura T, Sakamaki Y, Itakura E, Hatta T, Natsume T, et al. The HOPS complex mediates autophagosome-lysosome fusion through interaction with syntaxin 17. Mol Biol Cell. 2014;25(8):1327-37.

101. Jiang W, Wang S, Xiao M, Lin Y, Zhou L, Lei Q, et al. Acetylation regulates gluconeogenesis by promoting PEPCK1 degradation via recruiting the UBR5 ubiquitin ligase. Mol Cell. 2011;43(1):33-44.

102. Jin N, Chow CY, Liu L, Zolov SN, Bronson R, Davisson M, et al. VAC14 nucleates a protein complex essential for the acute interconversion of PI3P and PI(3,5)P(2) in yeast and mouse. EMBO J. 2008;27(24):3221-34.

103. Joachim J, Jefferies HB, Razi M, Frith D, Snijders AP, Chakravarty P, et al. Activation of ULK Kinase and Autophagy by GABARAP Trafficking from the Centrosome Is Regulated by WAC and GM130. Mol Cell. 2015;60(6):899-913.

104. Joachim J, Tooze SA. Control of GABARAP-mediated autophagy by the Golgi complex, centrosome and centriolar satellites. Biol Cell. 2018;110(1):1-5.

105. Johnson ES, Gonda DK, Varshavsky A. cis-trans recognition and subunit-specific degradation of short-lived proteins. Nature. 1990;346(6281):287-91.

106. Jotwani A, Richerson DN, Motta I, Julca-Zevallos O, Melia TJ. Approaches to the study of Atg8-mediated membrane dynamics in vitro. Methods Cell Biol. 2012;108:93-116.

107. Judith D, Jefferies HBJ, Boeing S, Frith D, Snijders AP, Tooze SA. ATG9A shapes the forming autophagosome through Arfaptin 2 and phosphatidylinositol 4-kinase IIIbeta. J Cell Biol. 2019;218(5):1634-52.

108. Kabeya Y, Mizushima N, Ueno T, Yamamoto A, Kirisako T, Noda T, et al. LC3, a mammalian homologue of yeast Apg8p, is localized in autophagosome membranes after processing. EMBO J. 2000;19(21):5720-8.

109. Kakuta S, Yamaguchi J, Suzuki C, Sasaki M, Kazuno S, Uchiyama Y. Small GTPase Rab1B is associated with ATG9A vesicles and regulates autophagosome formation. FASEB J. 2017;31(9):3757-73.

110. Kakuta S, Yamamoto H, Negishi L, Kondo-Kakuta C, Hayashi N, Ohsumi Y. Atg9 vesicles recruit vesicle-tethering proteins Trs85 and Ypt1 to the autophagosome formation site. J Biol Chem. 2012;287(53):44261-9.

111. Karanasios E, Walker SA, Okkenhaug H, Manifava M, Hummel E, Zimmermann H, et al. Autophagy initiation by ULK complex assembly on ER tubulovesicular regions marked by ATG9 vesicles. Nat Commun. 2016;7:12420.

112. Kato T, Tamiya G, Koyama S, Nakamura T, Makino S, Arawaka S, et al. UBR5 Gene Mutation Is Associated with Familial Adult Myoclonic Epilepsy in a Japanese Family. ISRN Neurol. 2012;2012:508308.

113. Kawashima I, Ohsawa M, Fukushige T, Nagayama Y, Niida Y, Kotani M, et al. Cytochemical analysis of storage materials in cultured skin fibroblasts from patients with I-cell disease. Clin Chim Acta. 2007;378(1-2):142-6.

114. Kharkwal H, Smith CG, Wilson DW. Blocking ESCRT-mediated envelopment inhibits microtubule-dependent trafficking of alphaherpesviruses in vitro. J Virol. 2014;88(24):14467-78.

115. Kihara A, Noda T, Ishihara N, Ohsumi Y. Two distinct Vps34 phosphatidylinositol 3-kinase complexes function in autophagy and carboxypeptidase Y sorting in Saccharomyces cerevisiae. J Cell Biol. 2001;152(3):519-30.

116. Kim J, Kundu M, Viollet B, Guan KL. AMPK and mTOR regulate autophagy through direct phosphorylation of Ulk1. Nat Cell Biol. 2011;13(2):132-41.

117. Kim ST, Tasaki T, Zakrzewska A, Yoo YD, Sa Sung K, Kim SH, et al. The N-end rule proteolytic system in autophagy. Autophagy. 2013;9(7):1100-3.

118. Kimura S, Noda T, Yoshimori T. Dissection of the autophagosome maturation process by a novel reporter protein, tandem fluorescent-tagged LC3. Autophagy. 2007;3(5):452-60.

119. Kimura T, Jia J, Kumar S, Choi SW, Gu Y, Mudd M, et al. Dedicated SNAREs and specialized TRIM cargo receptors mediate secretory autophagy. EMBO J. 2017;36(1):42-60.

120. Kitada T, Asakawa S, Hattori N, Matsumine H, Yamamura Y, Minoshima S, et al. Mutations in the parkin gene cause autosomal recessive juvenile parkinsonism. Nature. 1998;392(6676):605-8.

121. Knorr RL, Lipowsky R, Dimova R. Autophagosome closure requires membrane scission. Autophagy. 2015;11(11):2134-7.

122. Komander D, Rape M. The ubiquitin code. Annu Rev Biochem. 2012;81:203-29.

123. Korolchuk VI, Menzies FM, Rubinsztein DC. Mechanisms of cross-talk between the ubiquitin-proteasome and autophagy-lysosome systems. FEBS Lett. 2010;584(7):1393-8.

124. Kotani T, Kirisako H, Koizumi M, Ohsumi Y, Nakatogawa H. The Atg2-Atg18 complex tethers pre-autophagosomal membranes to the endoplasmic reticulum for autophagosome formation. Proc Natl Acad Sci U S A. 2018;115(41):10363-8.

125. Koyuncu S, Saez I, Lee HJ, Gutierrez-Garcia R, Pokrzywa W, Fatima A, et al. The ubiquitin ligase UBR5 suppresses proteostasis collapse in pluripotent stem cells from Huntington's disease patients. Nat Commun. 2018;9(1):2886.

126. Kozlov G, De Crescenzo G, Lim NS, Siddiqui N, Fantus D, Kahvejian A, et al. Structural basis of ligand recognition by PABC, a highly specific peptide-binding domain found in poly(A)-binding protein and a HECT ubiquitin ligase. EMBO J. 2004;23(2):272-81.

127. Kozlov G, Nguyen L, Lin T, De Crescenzo G, Park M, Gehring K. Structural basis of ubiquitin recognition by the ubiquitin-associated (UBA) domain of the ubiquitin ligase EDD. J Biol Chem. 2007;282(49):35787-95.

128. Kramer ER, Scheuringer N, Podtelejnikov AV, Mann M, Peters JM. Mitotic regulation of the APC activator proteins CDC20 and CDH1. Mol Biol Cell. 2000;11(5):1555-69.

129. Krick R, Henke S, Tolstrup J, Thumm M. Dissecting the localization and function of Atg18, Atg21 and Ygr223c. Autophagy. 2008;4(7):896-910.

130. Kuhn M. The microtubule depolymerizing drugs nocodazole and colchicine inhibit the uptake of Listeria monocytogenes by P388D1 macrophages. FEMS Microbiol Lett. 1998;160(1):87-90.

131. Kumar S, Jain A, Farzam F, Jia J, Gu Y, Choi SW, et al. Mechanism of Stx17 recruitment to autophagosomes via IRGM and mammalian Atg8 proteins. J Cell Biol. 2018;217(3):997-1013.

132. La Spada AR, Wilson EM, Lubahn DB, Harding AE, Fischbeck KH. Androgen receptor gene mutations in X-linked spinal and bulbar muscular atrophy. Nature. 1991;352(6330):77-9.

133. Lagorio I, Zara F, Striano S, Striano P. Familial adult myoclonic epilepsy: A new expansion repeats disorder. Seizure. 2019;67:73-7.

134. Lagorio I, Zara F, Striano S, Striano P. Familial adult myoclonic epilepsy: A new expansion repeats disorder. Seizure-Eur J Epilep. 2019;67:73-7.

135. Lamb CA, Nuhlen S, Judith D, Frith D, Snijders AP, Behrends C, et al. TBC1D14 regulates autophagy via the TRAPP complex and ATG9 traffic. EMBO J. 2016;35(3):281-301.

136. Laplante M, Sabatini DM. mTOR signaling in growth control and disease. Cell. 2012;149(2):274-93.

137. Larsen KB, Lamark T, Overvatn A, Harneshaug I, Johansen T, Bjorkoy G. A reporter cell system to monitor autophagy based on p62/SQSTM1. Autophagy. 2010;6(6):784-93.

138. Lee MJ, Tasaki T, Moroi K, An JY, Kimura S, Davydov IV, et al. RGS4 and RGS5 are in vivo substrates of the N-end rule pathway. Proc Natl Acad Sci U S A. 2005;102(42):15030-5.

139. Lee YK, Lee WS, Kim GS, Park OJ. Anthocyanins are novel AMPKalpha1 stimulators that suppress tumor growth by inhibiting mTOR phosphorylation. Oncol Rep. 2010;24(6):1471-7.

140. Leil TA, Chen ZW, Chang CSS, Olsen RW. GABA(A) receptor-associated protein traffics GABA(A) receptors to the plasma membrane in neurons. J Neurosci. 2004;24(50):11429-38.

141. Lester HA, Dibas MI, Dahan DS, Leite JF, Dougherty DA. Cys-loop receptors: new twists and turns. Trends Neurosci. 2004;27(6):329-36.

142. Liang R, Ren J, Zhang Y, Feng W. Structural Conservation of the Two Phosphoinositide-Binding Sites in WIPI Proteins. J Mol Biol. 2019;431(7):1494-505.

143. Liang XH, Jackson S, Seaman M, Brown K, Kempkes B, Hibshoosh H, et al. Induction of autophagy and inhibition of tumorigenesis by beclin 1. Nature. 1999;402(6762):672-6.

144. Liao YD, Jeng JC, Wang CF, Wang SC, Chang ST. Removal of N-terminal methionine from recombinant proteins by engineered E. coli methionine aminopeptidase. Protein Sci. 2004;13(7):1802-10.

145. Lim NS, Kozlov G, Chang TC, Groover O, Siddiqui N, Volpon L, et al. Comparative peptide binding studies of the PABC domains from the ubiquitin-protein isopeptide ligase HYD and poly(A)-binding protein. Implications for HYD function. J Biol Chem. 2006;281(20):14376-82.

146. Lin X, Antalffy B, Kang D, Orr HT, Zoghbi HY. Polyglutamine expansion down-regulates specific neuronal genes before pathologic changes in SCA1. Nat Neurosci. 2000;3(2):157-63.

147. Linares JF, Duran A, Yajima T, Pasparakis M, Moscat J, Diaz-Meco MT. K63 Polyubiquitination and Activation of mTOR by the p62-TRAF6 Complex in Nutrient-Activated Cells. Molecular Cell. 2013;51(3):283-96.

148. Liu CC, Lin YC, Chen YH, Chen CM, Pang LY, Chen HA, et al. Cul3-KLHL20 Ubiquitin Ligase Governs the Turnover of ULK1 and VPS34 Complexes to Control Autophagy Termination. Molecular Cell. 2016;61(1):84-97.

149. Liu X, Mao K, Yu AYH, Omairi-Nasser A, Austin J, 2nd, Glick BS, et al. The Atg17-Atg31-Atg29 Complex Coordinates with Atg11 to Recruit the Vam7 SNARE and Mediate Autophagosome-Vacuole Fusion. Curr Biol. 2016;26(2):150-60.

150. Livneh I, Cohen-Kaplan V, Cohen-Rosenzweig C, Avni N, Ciechanover A. The life cycle of the 26S proteasome: from birth, through regulation and function, and onto its death. Cell Res. 2016;26(8):869-85.

151. Lou X, Shin YK. SNARE zippering. Biosci Rep. 2016;36(3).

152. Lu J, He L, Behrends C, Araki M, Araki K, Jun Wang Q, et al. NRBF2 regulates autophagy and prevents liver injury by modulating Atg14L-linked phosphatidylinositol-3 kinase III activity. Nat Commun. 2014;5:3920.

153. Lu Q, Yang P, Huang X, Hu W, Guo B, Wu F, et al. The WD40 repeat PtdIns(3)P-binding protein EPG-6 regulates progression of omegasomes to autophagosomes. Dev Cell. 2011;21(2):343-57.

154. Lucocq J, Walker D. Evidence for fusion between multilamellar endosomes and autophagosomes in HeLa cells. Eur J Cell Biol. 1997;72(4):307-13.

155. Lynch-Day MA, Bhandari D, Menon S, Huang J, Cai H, Bartholomew CR, et al. Trs85 directs a Ypt1 GEF, TRAPPIII, to the phagophore to promote autophagy. Proc Natl Acad Sci U S A. 2010;107(17):7811-6.

156. Ma PX, Mohrluder J, Schwarten M, Stoldt M, Singh SK, Hartmann R, et al. Preparation of a Functional GABARAP-Lipid Conjugate in Nanodiscs and its Investigation by Solution NMR Spectroscopy. Chembiochem. 2010;11(14):1967-70.

157. Machamer CE. The Golgi complex in stress and death. Front Neurosci. 2015;9:421.

158. Maity S, Caillat C, Miguet N, Sulbaran G, Effantin G, Schoehn G, et al. VPS4 triggers constriction and cleavage of ESCRT-III helical filaments. Sci Adv. 2019;5(4):eaau7198.

159. Manil-Segalen M, Lefebvre C, Jenzer C, Trichet M, Boulogne C, Satiat-Jeunemaitre B, et al. The C. elegans LC3 acts downstream of GABARAP to degrade autophagosomes by interacting with the HOPS subunit VPS39. Dev Cell. 2014;28(1):43-55.

160. Mari M, Griffith J, Rieter E, Krishnappa L, Klionsky DJ, Reggiori F. An Atg9-containing compartment that functions in the early steps of autophagosome biogenesis. J Cell Biol. 2010;190(6):1005-22.

161. Marie M, Dale HA, Sannerud R, Saraste J. The function of the intermediate compartment in pre-Golgi trafficking involves its stable connection with the centrosome. Mol Biol Cell. 2009;20(20):4458-70.

162. Marshall RS, Hua Z, Mali S, McLoughlin F, Vierstra RD. ATG8-Binding UIM Proteins Define a New Class of Autophagy Adaptors and Receptors. Cell. 2019;177(3):766-81 e24.

163. Matsui T, Jiang P, Nakano S, Sakamaki Y, Yamamoto H, Mizushima N. Autophagosomal YKT6 is required for fusion with lysosomes independently of syntaxin 17. J Cell Biol. 2018;217(8):2633-45.

164. McCullough J, Clippinger AK, Talledge N, Skowyra ML, Saunders MG, Naismith TV, et al. Structure and membrane remodeling activity of ESCRT-III helical polymers. Science. 2015;350(6267):1548-51.

165. Meiling-Wesse K, Barth H, Voss C, Eskelinen EL, Epple UD, Thumm M. Atg21 is required for effective recruitment of Atg8 to the preautophagosomal structure during the Cvt pathway. J Biol Chem. 2004;279(36):37741-50.

166. Menzies FM, Fleming A, Caricasole A, Bento CF, Andrews SP, Ashkenazi A, et al. Autophagy and Neurodegeneration: Pathogenic Mechanisms and Therapeutic Opportunities. Neuron. 2017;93(5):1015-34.

167. Mizushima N, Klionsky DJ. Protein turnover via autophagy: implications for metabolism. Annu Rev Nutr. 2007;27:19-40.

168. Mizushima N, Noda T, Yoshimori T, Tanaka Y, Ishii T, George MD, et al. A protein conjugation system essential for autophagy. Nature. 1998;395(6700):395-8.

169. Mochida K, Oikawa Y, Kimura Y, Kirisako H, Hirano H, Ohsumi Y, et al. Receptor-mediated selective autophagy degrades the endoplasmic reticulum and the nucleus. Nature. 2015;522(7556):359-62.

170. Mollereau B, Walter L. Is WDR45 the missing link for ER stress-induced autophagy in beta-propeller associated neurodegeneration? Autophagy. 2019;15(12):2163-4.

171. Muller AJ, Proikas-Cezanne T. Function of human WIPI proteins in autophagosomal rejuvenation of endomembranes? FEBS Lett. 2015;589(14):1546-51.

172. Munoz-Escobar J, Matta-Camacho E, Kozlov G, Gehring K. The MLLE domain of the ubiquitin ligase UBR5 binds to its catalytic domain to regulate substrate binding. J Biol Chem. 2015;290(37):22841-50.

173. Murrow L, Debnath J. ATG12-ATG3 connects basal autophagy and late endosome function. Autophagy. 2015;11(6):961-2.

174. Murrow L, Malhotra R, Debnath J. ATG12-ATG3 interacts with Alix to promote basal autophagic flux and late endosome function. Nat Cell Biol. 2015;17(3):300-10.

175. Nagafuchi S, Yanagisawa H, Ohsaki E, Shirayama T, Tadokoro K, Inoue T, et al. Structure and expression of the gene responsible for the triplet repeat disorder, dentatorubral and pallidoluysian atrophy (DRPLA). Nat Genet. 1994;8(2):177-82.

176. Nagafuchi S, Yanagisawa H, Sato K, Shirayama T, Ohsaki E, Bundo M, et al. Dentatorubral and pallidoluysian atrophy expansion of an unstable CAG trinucleotide on chromosome 12p. Nat Genet. 1994;6(1):14-8.

177. Nakatogawa H, Ichimura Y, Ohsumi Y. Atg8, a ubiquitin-like protein required for autophagosome formation, mediates membrane tethering and hemifusion. Cell. 2007;130(1):165-78.

178. Namba Y, Sogawa C, Okusha Y, Kawai H, Itagaki M, Ono K, et al. Depletion of Lipid Efflux Pump ABCG1 Triggers the Intracellular Accumulation of Extracellular Vesicles and Reduces Aggregation and Tumorigenesis of Metastatic Cancer Cells. Front Oncol. 2018;8:376.

179. Narain Y, Wyttenbach A, Rankin J, Furlong RA, Rubinsztein DC. A molecular investigation of true dominance in Huntington's disease. J Med Genet. 1999;36(10):739-46.

180. Nazio F, Carinci M, Valacca C, Bielli P, Strappazzon F, Antonioli M, et al. Fine-tuning of ULK1 mRNA and protein levels is required for autophagy oscillation. Journal of Cell Biology. 2016;215(6):841-56.

181. Nazio F, Strappazzon F, Antonioli M, Bielli P, Cianfanelli V, Bordi M, et al. mTOR inhibits autophagy by controlling ULK1 ubiquitylation, self-association and function through AMBRA1 and TRAF6. Nature Cell Biology. 2013;15(4):406-+.

182. Nguyen HM, Liu S, Daher W, Tan F, Besteiro S. Characterisation of two Toxoplasma PROPPINs homologous to Atg18/WIPI suggests they have evolved distinct specialised functions. PLoS One. 2018;13(4):e0195921.

183. Nguyen TN, Padman BS, Usher J, Oorschot V, Ramm G, Lazarou M. Atg8 family LC3/GABARAP proteins are crucial for autophagosome-lysosome fusion but not autophagosome formation during PINK1/Parkin mitophagy and starvation. J Cell Biol. 2016;215(6):857-74.

184. Nilsson P, Loganathan K, Sekiguchi M, Matsuba Y, Hui K, Tsubuki S, et al. Abeta secretion and plaque formation depend on autophagy. Cell Rep. 2013;5(1):61-9.

185. Noda T, Fujita N, Yoshimori T. The late stages of autophagy: how does the end begin? Cell Death Differ. 2009;16(7):984-90.

186. Obara K, Sekito T, Niimi K, Ohsumi Y. The Atg18-Atg2 complex is recruited to autophagic membranes via phosphatidylinositol 3-phosphate and exerts an essential function. J Biol Chem. 2008;283(35):23972-80.

187. Ohtake F, Tsuchiya H, Saeki Y, Tanaka K. K63 ubiquitylation triggers proteasomal degradation by seeding branched ubiquitin chains. Proc Natl Acad Sci U S A. 2018;115(7):E1401-E8.

188. Oku M, Nishimura T, Hattori T, Ano Y, Yamashita S, Sakai Y. Role of Vac8 in formation of the vacuolar sequestering membrane during micropexophagy. Autophagy. 2006;2(4):272-9.

189. Ong SS, Goktug AN, Elias A, Wu J, Saunders D, Chen T. Stability of the human pregnane X receptor is regulated by E3 ligase UBR5 and serine/threonine kinase DYRK2. Biochem J. 2014;459(1):193-203.

190. Orr A, Song H, Rusin SF, Kettenbach AN, Wickner W. HOPS catalyzes the interdependent assembly of each vacuolar SNARE into a SNARE complex. Mol Biol Cell. 2017;28(7):975-83.

191. Orsi A, Razi M, Dooley HC, Robinson D, Weston AE, Collinson LM, et al. Dynamic and transient interactions of Atg9 with autophagosomes, but not membrane integration, are required for autophagy. Mol Biol Cell. 2012;23(10):1860-73.

192. Osawa T, Kotani T, Kawaoka T, Hirata E, Suzuki K, Nakatogawa H, et al. Atg2 mediates direct lipid transfer between membranes for autophagosome formation. Nat Struct Mol Biol. 2019;26(4):281-8.

193. Osawa T, Noda NN. Atg2: A novel phospholipid transfer protein that mediates de novo autophagosome biogenesis. Protein Science. 2019;28(6):1005-12.

194. Otomo T, Chowdhury S, Lander GC. The rod-shaped ATG2A-WIPI4 complex tethers membranes in vitro. Contact (Thousand Oaks). 2018;1.

195. Pacheco V, Ma PX, Thielmann Y, Hartmann R, Weiergraber OH, Mohrluder J, et al. Assessment of GABARAP self-association by its diffusion properties. J Biomol Nmr. 2010;48(1):49-58.

196. Papinski D, Schuschnig M, Reiter W, Wilhelm L, Barnes CA, Maiolica A, et al. Early steps in autophagy depend on direct phosphorylation of Atg9 by the Atg1 kinase. Mol Cell. 2014;53(3):471-83.

197. Pasquier B. Autophagy inhibitors. Cell Mol Life Sci. 2016;73(5):985-1001.

198. Pattingre S, Tassa A, Qu X, Garuti R, Liang XH, Mizushima N, et al. Bcl-2 antiapoptotic proteins inhibit Beclin 1-dependent autophagy. Cell. 2005;122(6):927-39.

199. Peter BJ, Kent HM, Mills IG, Vallis Y, Butler PJG, Evans PR, et al. BAR domains as sensors of membrane curvature: The amphiphysin BAR structure. Science. 2004;303(5657):495-9.

200. Pfisterer SG, Bakula D, Cezanne A, Robenek H, Proikas-Cezanne T. WIPI beta-propellers at the crossroads of autophagosome and lipid droplet dynamics. Biochem Soc T. 2014;42:1414-7.

201. Platta HW, Abrahamsen H, Thoresen SB, Stenmark H. Nedd4-dependent lysine-11-linked polyubiquitination of the tumour suppressor Beclin 1. Biochemical Journal. 2012;441:399-406.

202. Poillet-Perez L, Xie XQ, Zhan L, Yang Y, Sharp DW, Hu ZS, et al. Autophagy maintains tumour growth through circulating arginine. Nature. 2018;563(7732):569-+.

203. Polson HE, de Lartigue J, Rigden DJ, Reedijk M, Urbe S, Clague MJ, et al. Mammalian Atg18 (WIPI2) localizes to omegasome-anchored phagophores and positively regulates LC3 lipidation. Autophagy. 2010;6(4):506-22.

204. Powis G, Bonjouklian R, Berggren MM, Gallegos A, Abraham R, Ashendel C, et al. Wortmannin, a potent and selective inhibitor of phosphatidylinositol-3-kinase. Cancer Res. 1994;54(9):2419-23.

205. Proikas-Cezanne T, Takacs Z, Donnes P, Kohlbacher O. WIPI proteins: essential PtdIns3P effectors at the nascent autophagosome. J Cell Sci. 2015;128(2):207-17.

206. Proikas-Cezanne T, Waddell S, Gaugel A, Frickey T, Lupas A, Nordheim A. WIPI-1alpha (WIPI49), a member of the novel 7-bladed WIPI protein family, is aberrantly expressed in human cancer and is linked to starvation-induced autophagy. Oncogene. 2004;23(58):9314-25.

207. Puri C, Renna M, Bento CF, Moreau K, Rubinsztein DC. ATG16L1 meets ATG9 in recycling endosomes: additional roles for the plasma membrane and endocytosis in autophagosome biogenesis. Autophagy. 2014;10(1):182-4.

208. Rao Y, Perna MG, Hofmann B, Beier V, Wollert T. The Atg1-kinase complex tethers Atg9-vesicles to initiate autophagy. Nat Commun. 2016;7:10338.

209. Ravikumar B, Duden R, Rubinsztein DC. Aggregate-prone proteins with polyglutamine and polyalanine expansions are degraded by autophagy. Hum Mol Genet. 2002;11(9):1107-17.

210. Ravikumar B, Futter M, Jahreiss L, Korolchuk VI, Lichtenberg M, Luo S, et al. Mammalian macroautophagy

at a glance. J Cell Sci. 2009;122(Pt 11):1707-11.

211. Reggiori F, Tucker KA, Stromhaug PE, Klionsky DJ. The Atg1-Atg13 complex regulates Atg9 and Atg23 retrieval transport from the pre-autophagosomal structure. Dev Cell. 2004;6(1):79-90.

212. Riley BE, Kaiser SE, Shaler TA, Ng ACY, Hara T, Hipp MS, et al. Ubiquitin accumulation in autophagy-deficient mice is dependent on the Nrf2-mediated stress response pathway: a potential role for protein aggregation in autophagic substrate selection. Journal of Cell Biology. 2010;191(3):537-52.

213. Romanov J, Walczak M, Ibiricu I, Schuchner S, Ogris E, Kraft C, et al. Mechanism and functions of membrane binding by the Atg5-Atg12/Atg16 complex during autophagosome formation. EMBO J. 2012;31(22):4304-17.

214. Ronan B, Flamand O, Vescovi L, Dureuil C, Durand L, Fassy F, et al. A highly potent and selective Vps34 inhibitor alters vesicle trafficking and autophagy. Nat Chem Biol. 2014;10(12):1013-9.

215. Rosati A, Graziano V, De Laurenzi V, Pascale M, Turco MC. BAG3: a multifaceted protein that regulates major cell pathways. Cell Death Dis. 2011;2.

216. Rotin D, Kumar S. Physiological functions of the HECT family of ubiquitin ligases. Nat Rev Mol Cell Biol. 2009;10(6):398-409.

217. Rui YN, Xu Z, Patel B, Chen Z, Chen D, Tito A, et al. Huntingtin functions as a scaffold for selective macroautophagy. Nat Cell Biol. 2015;17(3):262-75.

218. Russell RC, Tian Y, Yuan H, Park HW, Chang YY, Kim J, et al. ULK1 induces autophagy by phosphorylating Beclin-1 and activating VPS34 lipid kinase. Nat Cell Biol. 2013;15(7):741-50.

219. Russo C, Ardissone A, Freri E, Gasperini S, Moscatelli M, Zorzi G, et al. Substantia Nigra Swelling and Dentate Nucleus T2 Hyperintensity May Be Early Magnetic Resonance Imaging Signs of beta-Propeller Protein-Associated Neurodegeneration. Mov Disord Clin Pract. 2019;6(1):51-6.

220. Saitsu H, Nishimura T, Muramatsu K, Kodera H, Kumada S, Sugai K, et al. De novo mutations in the autophagy gene WDR45 cause static encephalopathy of childhood with neurodegeneration in adulthood. Nat Genet. 2013;45(4):445-9, 9e1.

221. Sandilands E, Serrels B, McEwan DG, Morton JP, Macagno JP, McLeod K, et al. Autophagic targeting of Src promotes cancer cell survival following reduced FAK signalling. Nat Cell Biol. 2011;14(1):51-60.

222. Sarkar S, Krishna G, Imarisio S, Saiki S, O'Kane CJ, Rubinsztein DC. A rational mechanism for combination treatment of Huntington's disease using lithium and rapamycin. Hum Mol Genet. 2008;17(2):170-8.

223. Saxton RA, Sabatini DM. mTOR Signaling in Growth, Metabolism, and Disease. Cell. 2017;169(2):361-71.

224. Schwarzmann G, Breiden B, Sandhoff K. Membrane-spanning lipids for an uncompromised monitoring of membrane fusion and intermembrane lipid transfer. J Lipid Res. 2015;56(10):1861-79.

225. Seglen PO, Gordon PB. 3-Methyladenine: specific inhibitor of autophagic/lysosomal protein degradation in isolated rat hepatocytes. Proc Natl Acad Sci U S A. 1982;79(6):1889-92.

226. Shearer RF, Iconomou M, Watts CK, Saunders DN. Functional Roles of the E3 Ubiquitin Ligase UBR5 in Cancer. Mol Cancer Res. 2015;13(12):1523-32.

227. Shi CS, Kehrl JH. Traf6 and A20 differentially regulate TLR4-induced autophagy by affecting the ubiquitination of Beclin 1. Autophagy. 2010;6(7):986-7.

228. Shpilka T, Weidberg H, Pietrokovski S, Elazar Z. Atg8: an autophagy-related ubiquitin-like protein family. Genome Biol. 2011;12(7):226.

229. Skytte Rasmussen M, Mouilleron S, Kumar Shrestha B, Wirth M, Lee R, Bowitz Larsen K, et al. ATG4B contains a C-terminal LIR motif important for binding and efficient cleavage of mammalian orthologs of yeast Atg8. Autophagy. 2017;13(5):834-53.

230. Son SM, Park SJ, Lee H, Siddiqi F, Lee JE, Menzies FM, et al. Leucine Signals to mTORC1 via Its Metabolite Acetyl-Coenzyme A. Cell Metab. 2019;29(1):192-201 e7.

231. Soreng K, Munson MJ, Lamb CA, Bjorndal GT, Pankiv S, Carlsson SR, et al. SNX18 regulates ATG9A

trafficking from recycling endosomes by recruiting Dynamin-2. EMBO Rep. 2018;19(4).

232. Sriram SM, Kim BY, Kwon YT. The N-end rule pathway: emerging functions and molecular principles of substrate recognition. Nat Rev Mol Cell Biol. 2011;12(11):735-47.

233. Stanga D, Zhao Q, Milev MP, Saint-Dic D, Jimenez-Mallebrera C, Sacher M. TRAPPC11 functions in autophagy by recruiting ATG2B-WIPI4/WDR45 to preautophagosomal membranes. Traffic. 2019;20(5):325-45.

234. Stolz A, Ernst A, Dikic I. Cargo recognition and trafficking in selective autophagy. Nat Cell Biol. 2014;16(6):495-501.

235. Stromhaug PE, Reggiori F, Guan J, Wang CW, Klionsky DJ. Atg21 is a phosphoinositide binding protein required for efficient lipidation and localization of Atg8 during uptake of aminopeptidase I by selective autophagy. Mol Biol Cell. 2004;15(8):3553-66.

236. Sudhof TC, Rothman JE. Membrane fusion: grappling with SNARE and SM proteins. Science. 2009;323(5913):474-7.

237. Suzuki K, Akioka M, Kondo-Kakuta C, Yamamoto H, Ohsumi Y. Fine mapping of autophagy-related proteins during autophagosome formation in Saccharomyces cerevisiae. J Cell Sci. 2013;126(Pt 11):2534-44.

238. Suzuki K, Kirisako T, Kamada Y, Mizushima N, Noda T, Ohsumi Y. The pre-autophagosomal structure organized by concerted functions of APG genes is essential for autophagosome formation. EMBO J. 2001;20(21):5971-81.

239. Suzuki K, Kubota Y, Sekito T, Ohsumi Y. Hierarchy of Atg proteins in pre-autophagosomal structure organization. Genes Cells. 2007;12(2):209-18.

240. Takahashi Y, He HY, Tang ZY, Hattori T, Liu Y, Young MM, et al. An autophagy assay reveals the ESCRT-III component CHMP2A as a regulator of phagophore closure. Nature Communications. 2018;9.

241. Takahashi Y, Meyerkord CL, Hori T, Runkle K, Fox TE, Kester M, et al. Bif-1 regulates Atg9 trafficking by mediating the fission of Golgi membranes during autophagy. Autophagy. 2011;7(1):61-73.

242. Takahashi Y, Tsotakos N, Liu Y, Young MM, Serfass J, Tang Z, et al. The Bif-1-Dynamin 2 membrane fission machinery regulates Atg9-containing vesicle generation at the Rab11-positive reservoirs. Oncotarget. 2016;7(15):20855-68.

243. Tamura N, Nishimura T, Sakamaki Y, Koyama-Honda I, Yamamoto H, Mizushima N. Differential requirement for ATG2A domains for localization to autophagic membranes and lipid droplets. FEBS Lett. 2017;591(23):3819-30.

244. Tang ZY, Takahashi Y, He HY, Hattori T, Chen C, Liang XW, et al. TOM40 Targets Atg2 to Mitochondria-Associated ER Membranes for Phagophore Expansion. Cell Reports. 2019;28(7):1744-+.

245. Tanida I, Tanida-Miyake E, Ueno T, Kominami E. The human homolog of Saccharomyces cerevisiae Apg7p is a Protein-activating enzyme for multiple substrates including human Apg12p, GATE-16, GABARAP, and MAP-LC3. J Biol Chem. 2001;276(3):1701-6.

246. Tasaki T, Zakrzewska A, Dudgeon DD, Jiang Y, Lazo JS, Kwon YT. The substrate recognition domains of the N-end rule pathway. J Biol Chem. 2009;284(3):1884-95.

247. Triarhou LC. Introduction. Dopamine and Parkinson's disease. Adv Exp Med Biol. 2002;517:1-14.

248. Tsuboyama K, Koyama-Honda I, Sakamaki Y, Koike M, Morishita H, Mizushima N. The ATG conjugation systems are important for degradation of the inner autophagosomal membrane. Science. 2016;354(6315):1036-41.

249. Turner GC, Varshavsky A. Detecting and measuring cotranslational protein degradation in vivo. Science. 2000;289(5487):2117-20.

250. Vaites LP, Paulo JA, Huttlin EL, Harper JW. Systematic Analysis of Human Cells Lacking ATG8 Proteins Uncovers Roles for GABARAPs and the CCZ1/MON1 Regulator C18orf8/RMC1 in Macroautophagic and Selective Autophagic Flux. Mol Cell Biol. 2018;38(1).

251. Valente EM, Abou-Sleiman PM, Caputo V, Muqit MM, Harvey K, Gispert S, et al. Hereditary early-onset Parkinson's disease caused by mutations in PINK1. Science. 2004;304(5674):1158-60.

252. Valverde DP, Yu S, Boggavarapu V, Kumar N, Lees JA, Walz T, et al. ATG2 transports lipids to promote autophagosome biogenesis. J Cell Biol. 2019.

253. van den Ende T, Sharifi S, van der Salm SMA, van Rootselaar AF. Familial Cortical Myoclonic Tremor and Epilepsy, an Enigmatic Disorder: From Phenotypes to Pathophysiology and Genetics. A Systematic Review. Tremor Other Hyperk. 2018;8.

254. van Rootselaar AF, van der Salm SM, Bour LJ, Edwards MJ, Brown P, Aronica E, et al. Decreased cortical inhibition and yet cerebellar pathology in 'familial cortical myoclonic tremor with epilepsy'. Mov Disord. 2007;22(16):2378-85.

255. Varshavsky A. The N-end rule pathway and regulation by proteolysis. Protein Sci. 2011;20(8):1298-345.

256. Varshavsky A. N-degron and C-degron pathways of protein degradation. Proc Natl Acad Sci U S A. 2019;116(2):358-66.

257. Velayos-Baeza A, Vettori A, Copley RR, Dobson-Stone C, Monaco AP. Analysis of the human VPS13 gene family. Genomics. 2004;84(3):536-49.

258. Velikkakath AKG, Nishimura T, Oita E, Ishihara N, Mizushima N. Mammalian Atg2 proteins are essential for autophagosome formation and important for regulation of size and distribution of lipid droplets. Molecular Biology of the Cell. 2012;23(5):896-909.

259. Verhoef LG, Lindsten K, Masucci MG, Dantuma NP. Aggregate formation inhibits proteasomal degradation of polyglutamine proteins. Hum Mol Genet. 2002;11(22):2689-700.

260. Vicinanza M, Korolchuk VI, Ashkenazi A, Puri C, Menzies FM, Clarke JH, et al. PI(5)P regulates autophagosome biogenesis. Mol Cell. 2015;57(2):219-34.

261. Villani A, Benjaminsen J, Moritz C, Henke K, Hartmann J, Norlin N, et al. Clearance by Microglia Depends on Packaging of Phagosomes into a Unique Cellular Compartment. Dev Cell. 2019;49(1):77-88 e7.

262. Waelsch H, Rittenberg D. The Metabolism of Glutathione. Science. 1939;90(2340):423-4.

263. Wan H, Wang Q, Chen X, Zeng Q, Shao Y, Fang H, et al. WDR45 contributes to neurodegeneration through regulation of ER homeostasis and neuronal death. Autophagy. 2019:1-17.

264. Wang CW, Kim J, Huang WP, Abeliovich H, Stromhaug PE, Dunn WA, Jr., et al. Apg2 is a novel protein required for the cytoplasm to vacuole targeting, autophagy, and pexophagy pathways. J Biol Chem. 2001;276(32):30442-51.

265. Wang H, Sun HQ, Zhu X, Zhang L, Albanesi J, Levine B, et al. GABARAPs regulate PI4P-dependent autophagosome:lysosome fusion. Proc Natl Acad Sci U S A. 2015;112(22):7015-20.

266. Wang J, Davis S, Menon S, Zhang J, Ding J, Cervantes S, et al. Ypt1/Rab1 regulates Hrr25/CK1delta kinase activity in ER-Golgi traffic and macroautophagy. J Cell Biol. 2015;210(2):273-85.

267. Wang Y, Hu XJ, Zou XD, Wu XH, Ye ZQ, Wu YD. WDSPdb: a database for WD40-repeat proteins. Nucleic Acids Res. 2015;43(Database issue):D339-44.

268. Wang YJ, Han DY, Tabib T, Yates JR, 3rd, Mu TW. Identification of GABA(C) receptor protein homeostasis network components from three tandem mass spectrometry proteomics approaches. J Proteome Res. 2013;12(12):5570-86.

269. Webber JL, Tooze SA. Coordinated regulation of autophagy by p38alpha MAPK through mAtg9 and p38IP. EMBO J. 2010;29(1):27-40.

270. Weidberg H, Shpilka T, Shvets E, Abada A, Shimron F, Elazar Z. LC3 and GATE-16 N termini mediate membrane fusion processes required for autophagosome biogenesis. Dev Cell. 2011;20(4):444-54.

271. White HS, Smith MD, Wilcox KS. Mechanisms of action of antiepileptic drugs. Int Rev Neurobiol. 2007;81:85-110.

272. White MD, Klecker M, Hopkinson RJ, Weits DA, Mueller C, Naumann C, et al. Plant cysteine oxidases are dioxygenases that directly enable arginyl transferase-catalysed arginylation of N-end rule targets. Nat Commun. 2017;8:14690.

273. Wickner W. Membrane Fusion: Five Lipids, Four SNAREs, Three Chaperones, Two Nucleotides, and a Rab, All Dancing in a Ring on Yeast Vacuoles. Annu Rev Cell Dev Bi. 2010;26:115-36.

274. Wingfield PT. N-Terminal Methionine Processing. Curr Protoc Protein Sci. 2017;88:6 14 1-6 3.

275. Wold MS, Lim J, Lachance V, Deng Z, Yue Z. ULK1-mediated phosphorylation of ATG14 promotes autophagy and is impaired in Huntington's disease models. Mol Neurodegener. 2016;11(1):76.

276. Wu F, Watanabe Y, Guo XY, Qi X, Wang P, Zhao HY, et al. Structural Basis of the Differential Function of the Two C. elegans Atg8 Homologs, LGG-1 and LGG-2, in Autophagy. Mol Cell. 2015;60(6):914-29.

277. Wu YT, Tan HL, Shui G, Bauvy C, Huang Q, Wenk MR, et al. Dual role of 3-methyladenine in modulation of autophagy via different temporal patterns of inhibition on class I and III phosphoinositide 3-kinase. J Biol Chem. 2010;285(14):10850-61.

278. Wurzer B, Zaffagnini G, Fracchiolla D, Turco E, Abert C, Romanov J, et al. Oligomerization of p62 allows for selection of ubiquitinated cargo and isolation membrane during selective autophagy. Elife. 2015;4:e08941.

279. Xie R, Nguyen S, McKeehan WL, Liu L. Acetylated microtubules are required for fusion of autophagosomes with lysosomes. BMC Cell Biol. 2010;11:89.

280. Xie X, Koh JY, Price S, White E, Mehnert JM. Atg7 Overcomes Senescence and Promotes Growth of BrafV600E-Driven Melanoma. Cancer Discov. 2015;5(4):410-23.

281. Xu ZN, Dooner HK. The maize aberrant pollen transmission 1 gene is a SABRE/KIP homolog required for pollen tube growth. Genetics. 2006;172(2):1251-61.

282. Yamamoto H, Kakuta S, Watanabe TM, Kitamura A, Sekito T, Kondo-Kakuta C, et al. Atg9 vesicles are an important membrane source during early steps of autophagosome formation. J Cell Biol. 2012;198(2):219-33.

283. Yamashita S, Oku M, Wasada Y, Ano Y, Sakai Y. PI4P-signaling pathway for the synthesis of a nascent membrane structure in selective autophagy. J Cell Biol. 2006;173(5):709-17.

284. Yau RG, Doerner K, Castellanos ER, Haakonsen DL, Werner A, Wang N, et al. Assembly and Function of Heterotypic Ubiquitin Chains in Cell-Cycle and Protein Quality Control. Cell. 2017;171(4):918-33 e20.

285. Yeh YY, Shah KH, Herman PK. An Atg13 Protein-mediated Self-association of the Atg1 Protein Kinase Is Important for the Induction of Autophagy. Journal of Biological Chemistry. 2011;286(33):28931-9.

286. Yoo YD, Mun SR, Ji CH, Sung KW, Kang KY, Heo AJ, et al. N-terminal arginylation generates a bimodal degron that modulates autophagic proteolysis. Proc Natl Acad Sci U S A. 2018;115(12):E2716-E24.

287. Young AR, Chan EY, Hu XW, Kochl R, Crawshaw SG, High S, et al. Starvation and ULK1-dependent cycling of mammalian Atg9 between the TGN and endosomes. J Cell Sci. 2006;119(Pt 18):3888-900.

288. Yu SL, Melia TJ. The coordination of membrane fission and fusion at the end of autophagosome maturation. Curr Opin Cell Biol. 2017;47:92-8.

289. Yu WH, Cuervo AM, Kumar A, Peterhoff CM, Schmidt SD, Lee JH, et al. Macroautophagy--a novel Beta-amyloid peptide-generating pathway activated in Alzheimer's disease. J Cell Biol. 2005;171(1):87-98.

290. Zalckvar E, Berissi H, Mizrachy L, Idelchuk Y, Koren I, Eisenstein M, et al. DAP-kinase-mediated phosphorylation on the BH3 domain of beclin 1 promotes dissociation of beclin 1 from Bcl-XL and induction of autophagy. EMBO Rep. 2009;10(3):285-92.

291. Zhang C, Zhang W, Lu Y, Yan X, Yan X, Zhu X, et al. NudC regulates actin dynamics and ciliogenesis by stabilizing cofilin 1. Cell Res. 2016;26(2):239-53.

292. Zhang T, Cronshaw J, Kanu N, Snijders AP, Behrens A. UBR5-mediated ubiquitination of ATMIN is required for ionizing radiation-induced ATM signaling and function. Proc Natl Acad Sci U S A. 2014;111(33):12091-6.

293. Zhao YG, Sun L, Miao G, Ji C, Zhao H, Sun H, et al. The autophagy gene Wdr45/Wipi4 regulates learning and memory function and axonal homeostasis. Autophagy. 2015;11(6):881-90.

294. Zheng JX, Li Y, Ding YH, Liu JJ, Zhang MJ, Dong MQ, et al. Architecture of the ATG2B-WDR45 complex and an aromatic Y/HF motif crucial for complex formation. Autophagy. 2017;13(11):1870-83.

295. Zhou CQ, Ma KL, Gao RZ, Mu CL, Chen LB, Liu QQ, et al. Regulation of mATG9 trafficking by Src- and ULK1-mediated phosphorylation in basal and starvation-induced autophagy. Cell Res. 2017;27(2):184-201.

296. Zhou F, Wu Z, Zhao M, Murtazina R, Cai J, Zhang A, et al. Rab5-dependent autophagosome closure by ESCRT. J Cell Biol. 2019.

297. Zhuang X, Chung KP, Cui Y, Lin W, Gao C, Kang BH, et al. ATG9 regulates autophagosome progression from the endoplasmic reticulum in Arabidopsis. Proc Natl Acad Sci U S A. 2017;114(3):E426-E35.

Abbreviations

(−)IRE/DMT1: ferrous iron transporter without the iron response element

3-MA: 3-methyladenine

4EBP1: mammalian 4E-binding protein 1

AcCoA: Leu metabolite acetyl-coenzyme A

AIM/ LIR: ATG8-interacting motif/ LC3-interacting region

AMBRA1: mammalian VPS34 activator autophagy and beclin 1 regulator 1

AMPK: mammalian AMP-activated protein kinase

AP1: mammalian Adaptor protein 1, tetrameric clathrin-associated complex

APT1: aberrant pollen transmission 1

ARFIP: mammalian ADP-Ribosylation Factor Interacting Protein 1

ATE1: Arginyltransferase 1

BafA1: bafilomycin A1, specifically targets the vacuolar-type H+ -ATPase (V-ATPase) enzyme

BAG3: BCL2 associated athanogene 3

BAR: Bin/Amphiphysin/Rvs

BCL2: mammalian BCL2 Apoptosis Regulator

BECN1: ULK1 complex then phosphorylates beclin1

BPAN: beta-propeller protein-associated neurodegeneration

CAG: cytosine-adenine-guanine

CathD: Cathepsin D

CHMP: mammalian charged multivesicular body protein

CMA: chaperone-mediated autophagy

COPII: mammalian coat protein complex that initiates the budding process

ER: Endoplasmic Reticulum

ESCRT: endosomal sorting complexes required for transport

Fab1: yeast homolog of PIKfyve (Phosphatidylinositol-3-Phosphate/Phosphatidylinositol 5-Kinase, Type III)

FAK: focal adhesion kinase

FAME: familial adult myoclonic epilepsy

Fig4: yeast homolog of FIG4 Phosphoinositide 5-Phosphatase

FIP200: mammalian 200 kDa FAK Family Kinase-Interacting Protein

FKBP12: the mammalian 12-kDa FK506-binding protein

GABARAP: γ-aminobutyric acid receptor-associated protein

GABARAPL1: mammalian γ-aminobutyric acid receptor-associated protein-like 1

GATE-16: mammalian Golgi-associated ATPase enhancer of 16 kDa

GOLGA2: mammalian Golgin subfamily A member 2

GP: globus pallidus

HOPS: the homotypic fusion and protein sorting complex

IGRM: mammalian immunity-related GTPase family M protein, also known as interferon-inducible protein 1 (IFI1)

LDS: hydrophobic patch

LGG-1, LGG-2: Caenorhabditis elegans ortholog of human GABARAP and LC3 respectively

LKB1: mammalian liver kinase B1, also known as Serine/threonine kinase 11 (STK11).

LTR: Lysotracker red

LUV: large unilamellar vesicles

MAP1LC3/ LC3: mammalian Microtubule-associated protein 1A/1B-light chain 3

MFN1/2: human mitofusin-1/2

mLST8: mammalian lethal with Sec13 protein 8, also known as GβL

mTOR: mechanistic target Of rapamycin

MVB: multivesicular body

NBIA: X-linked dominant subtype of neurodegeneration with iron accumulation

NCOA4: nuclear receptor coactivator 4

NRBF2: mammalian nuclear receptor binding factor 2

Nt: N-terminal

p150: phosphoinositide-3-kinase regulatory subunit 4 Vps15

P62/SQSTM1, NDP52, NBR1, OPTN and TAXBP1

PABC: Poly-Adenylation Binding Protein

PE: phosphatidylethanolamine

PI(3,5)P2: Phosphatidylinositol 3,5-bisphosphate (PtdIns(3,5)P2)

PI3KC3: phosphatidylinositol 3-kinase class 3

PI4K: mammalian phosphatidylinositol 4 kinase

PI4P, PI5P:: phosphatidylinositol 4-phosphate and phosphatidylinositol 5-phosphate

PLEKHM1: pleckstrin homology domain-containing family M member 1

PM: plasma membrane

PMN: piecemeal of the nuclear

polyQ: homomeric polyglutamine

PROPPIN: mammalian β-propellers that bind phosphoinositide, also called WIPI

RAB1A: mammalian Ras-related protein Rab-1A

RAPTOR: mammalian regulatory-associated protein of mTOR

RMC1: Regulator of MON1-CCZ1 complex, component of the CCZ1-MON1 RAB7 guanine exchange factor (GEF).

S6K: mammalian ribosomal protein S6 kinase polypeptide 1

SCA: spinocerebellar ataxias

SENDA: static encephalopathy in childhood with neurodegeneration in adulthood

SH3GLB1: mammalian Endophilin-B1, also BIF-1.

SLC2A: mammalian SoLute Carrier Family 2 Member

SN: substantia nigra

SNAP29: Synaptosomal-associated protein 29

SNARE: Soluble NSF Attachment proteins (SNAP) Receptor

STX17: mammalian Syntaxin 17.

SUV: small unilamellar vesicles

TfR: transferrin receptor

TGN: Trans Golgi network, a part of the golgi apparatus in cells

TGOLN2: Trans-Golgi network integral membrane protein 2

TRAPIII: The transport protein particle, consists of trafficking protein particle complex (TRAPPC) 8,11 and 12.

TRAPPC5: mammalian trafficking protein particle complex 5

UBA: ubiquitin associated

UBR: ubiquitin recognin box

UDS: ubiquitin-docking site

UIM: ubiquitin-interacting motif

ULK: mammalian Unc-51 Like Autophagy Activating Kinase

Vac7, Vac14: Vacuolar segregation protein 7 and Vacuolar segregation protein 14, both components of PIKfyve protein kinase complex.

VAMP8: mammalian vesicle-associated membrane protein 8

VPS34: mammalian Vacuolar protein sorting 34, the only known mammalian Class III phosphatidylinositol 3-kinase

Vps4: vacuolar protein sorting-associated protein 4, yeast homolog of VPS4A,B.

WD40 repeat: a short structural motif of approximately 40 amino acids, often terminating in a tryptophan-aspartic acid (W-D) dipeptide.

WIPI: WD repeat domain phosphoinositide-interacting

YKT6: human Synaptobrevin homolog YKT6

Ymr1: yeast homolog of phosphoinositide 3-phosphatase

Ypt1: yeast homolog of Ras-related protein Rab-1